11311-1-F = RL-2216

Sensor and Simulation Notes
Note

February 1973

ON THE TRANSIENT WAVEFORMS RADIATED BY A RESISTIVELY LOADED LINEAR ANTENNA

Yu-Ping Liu, Dipak L. Sengupta and Chen-To Tai
The University of Michigan Radiation Laboratory
Department of Electrical and Computer Engineering
Ann Arbor, Michigan 48105

Abstract

The transient waveforms radiated by step voltage excited linear antennas, loaded non-uniformly and continuously with resistance, are investigated by numerical means. The input time varying excitations considered are step voltage, Gaussian pulse and gamma pulse types. Current distributions on the harmonically excited antenna are obtained as functions of frequency for different values of the loading. The transfer functions of the antenna and the spectral densities of the radiated waveforms are obtained as functions of frequency and the loading for two values of the antenna thickness and for different directions in space. Finally the time dependent radiated waveforms produced by the antenna are obtained by using fast Fourier inversion technique. The effects of the various antenna parameters on the radiated waveforms are also investigated. Some of the results are compared with available approximate analytical results.

TABLE OF CONTENTS

LIST OF FIGURE CAPTIONS

Figure 1: Amplitude of the current distribution along a non-reflectively loaded antenna. $\frac{L}{a} = 156$, $\frac{\omega L}{c} = 5\pi$, $r_o = 318$.

Figure 2: The phase variation of the current along a non-reflectively loaded antenna. $\frac{L}{a} = 156$, $\frac{\omega L}{c} = 5\pi$, $r_o = 318$.

Figure 3: The amplitude of the current distribution along the antenna as a function of the loading parameter. $\frac{L}{a} = 156$, $\frac{\omega L}{c} = 3\pi$.

Figure 4: The phase of the current distribution along the antenna as a function of the loading parameter. $\frac{L}{a} = 156$, $\frac{\omega L}{c} = 3\pi$.

Figure 5: The amplitude and phase of the current distribution along a non-reflectively loaded antenna for two different frequencies. $\frac{L}{a} = 156$, $r_o = 600$.

Figure 6(a): Amplitude and phase of $\tilde{f}_\theta(\frac{\pi}{2}, \omega)$ as functions of normalized frequency with r_o as the parameter. $\frac{L}{a} = 156$.

Figure 6(b): Amplitude and phase of $\tilde{f}_\theta(\frac{\pi}{3}, \omega)$ as functions of normalized frequency with r_o as the parameter. $\frac{L}{a} = 156$.

Figure 6(c): Amplitude and phase of $\tilde{f}_\theta(\frac{\pi}{4}, \omega)$ as functions of normalized frequency with r_o as the parameter. $\frac{L}{a} = 156$.

Figure 6(d): Amplitude and phase of $\tilde{f}_\theta(\frac{\pi}{6}, \omega)$ as functions of normalized frequency with r_o as the parameter. $\frac{L}{a} = 156$.

Figure 7(a): Amplitude and phase of $\tilde{f}_\theta(\frac{\pi}{2}, \omega)$ as functions of normalized frequency with r_o as the parameter. $\frac{L}{a} = 100$.

Figure 7(b). Amplitude and phase of $\tilde{f}_\theta(\frac{\pi}{3}, \omega)$ as functions of normalized frequency with r_o as the parameter. $\frac{L}{a} = 100$.

Figure 7(c): Amplitude and phase of $\tilde{f}_\theta(\frac{\pi}{4}, \omega)$ as functions of normalized frequency with r_o as the parameter. $\frac{L}{a} = 100.$

Figure 7(d): Amplitude and phase of $\tilde{f}_\theta(\frac{\pi}{6}, \omega)$ as functions of normalized frequency with r_o as the parameter. $\frac{L}{a} = 100.$

Figure 8(a): Envelope of $\left|\tilde{e}_\theta(\frac{\pi}{2}, \omega)\right|$ as a function of normalized frequency with r_o as the parameter. $\frac{L}{a} = 156.$

Figure 8(b): Envelope of $\left|\tilde{e}_\theta(\frac{\pi}{3}, \omega)\right|$ as a function of normalized frequency with r_o as the parameter. $\frac{L}{a} = 156.$

Figure 8(c): Envelope of $\left|\tilde{e}_\theta(\frac{\pi}{4}, \omega)\right|$ as a function of normalized frequency with r_o as the parameter. $\frac{L}{a} = 156.$

Figure 8(d): Envelope of $\left|\tilde{e}_\theta(\frac{\pi}{6}, \omega)\right|$ as a function of normalized frequency with r_o as the parameter. $\frac{L}{a} = 156.$

Figure 9(a): Envelope of $\left|\tilde{e}_\theta(\frac{\pi}{2}, \omega)\right|$ as a function of normalized frequency with r_o as the parameter. $\frac{L}{a} = 100.$

Figure 9(b): Envelope of $\left|\tilde{e}_\theta(\frac{\pi}{3}, \omega)\right|$ as a function of normalized frequency with r_o as the parameter. $\frac{L}{a} = 100.$

Figure 9(c): Envelope of $\left|\tilde{e}_\theta(\frac{\pi}{4}, \omega)\right|$ as a function of normalized frequency with r_o as the parameter. $\frac{L}{a} = 100.$

Figure 9(d): Envelope of $\left|\tilde{e}_\theta(\frac{\pi}{6}, \omega)\right|$ as a function of normalized frequency with r_o as the parameter. $\frac{L}{a} = 100.$

Figure 10(a): $e_\theta(\frac{\pi}{2}, t)$ as a function of t/τ with r_o as the parameter. $\tau = 3.33$ ns, $T = 20.94$ ns and $\frac{L}{a} = 156.$

Figure 10(b): $e_\theta(\frac{\pi}{3}, t)$ as a function of t/τ with r_o as the parameter. $\tau = 3.33$ ns, $T = 20.94$ ns and $\frac{L}{a} = 156.$

Figure 10(c): $e_\theta(\frac{\pi}{4}, t)$ as a function of t/τ with r_o as the parameter. $\tau = 3.33$ ns, $T = 20.94$ ns and $\frac{L}{a} = 156$.

Figure 10(d): $e_\theta(\frac{\pi}{6}, t)$ as a function of t/τ with r_o as the parameter. $\tau = 3.33$ ns, $T = 20.94$ ns and $\frac{L}{a} = 156$.

Figure 11(a): $e_\theta(\frac{\pi}{2}, t)$ as a function of t/τ with r_o as the parameter. $\tau = 3.33$ ns, $T = 20.94$ ns and $\frac{L}{a} = 100$.

Figure 11(b): $e_\theta(\frac{\pi}{3}, t)$ as a function of t/τ with r_o as the parameter. $\tau = 3.33$ ns, $T = 20.94$ ns and $\frac{L}{a} = 100$.

Figure 11(c): $e_\theta(\frac{\pi}{4}, t)$ as a function of t/τ with r_o as the parameter. $\tau = 3.33$ ns, $T = 20.94$ ns and $\frac{L}{a} = 100$.

Figure 11(d): $e_\theta(\frac{\pi}{6}, t)$ as a function of t/τ with r_o as the parameter. $\tau = 3.33$ ns, $T = 20.94$ ns and $\frac{L}{a} = 100$.

Figure 12: t_o/τ as a function of r_o with θ as the parameter. $\tau = 3.33$ ns, $T = 20.94$ ns; ———— $\frac{L}{a} = 156$, - - - - - - - $\frac{L}{a} = 100$.

Figure 13: Early time behavior of $e_\theta(\theta, t)$ as a function of time. $\tau = 3.33$ ns, $T = 20.94$ ns, $r_o = 480$, $\frac{L}{a} = 156$. ———— numerical; - - - - - - - asymptotic results of Latham and Lee.

(List of Figure Captions from Appendix A)

Figure A-1: Division of the antenna into N-sections.

Figure A-2: Real (I_r) and imaginary (I_c) parts of the current distribution on uniformly loaded dipole. $L = \pi/2$, $\Omega = 9.92$, $\phi_i = 2\lambda r^i/\eta_0$.

Figure A-3: Current distribution on non-reflectively loaded monopole. $\Omega = 11.5$, $\omega L/c = 2\pi$, $\psi\alpha = 5.3$.

Figure A-4: Current distribution on exponentially loaded monopole. $\Omega = 11.5$, $\psi\alpha = 5.3$, $\omega L/c = 2\pi$.

Figure A-5: Phase variation of the current along the antenna.

Figure A-6: Current distribution on non-reflectively loaded antenna. $\Omega = 11.5$, $kL = 5\pi$, $\psi\alpha = 5.3$, $R_s(z) = 60\,\psi\alpha/L - |z|$.

Figure A-7: Phase variation of the current along the non-reflectively loaded antenna. $\Omega = 11.5$, $kL = 5\pi$, $\psi\alpha = 5.3$, $R_s(z) = 60\,\psi\alpha/L - |z|$.

Figure A-8: Transfer function $f_\theta(\theta;\omega)$ of the non-reflectively loaded antenna. $\Omega = 11.5$, $kL = 5\pi$, $\psi\alpha = 5.3$, $R_s(z) = 60\,\psi\alpha/L - |z|$.

Figure A-9: Amplitude of the current distribution on resistively loaded dipole antenna as a function of loading. $\Omega = 11.5$, $kL = 5\pi$, $\psi\alpha$ variable.

Figure A-10a: Amplitude of the current distribution $|I(z,\omega)|$ vs z/L on the loaded antenna with $kL(=\omega L/c)$, as the parameter, $C = 60 \times 4$.

Figure A-10b: Amplitude of the current distribution $|I(z,\omega)|$ vs z/L on the loaded antenna with $kL\,(=\omega L/c)$, as the parameter, $C = 60 \times 5$.

Figure A-10c: Amplitude of the current distribution $|I(z,\omega)|$ vs z/L on the loaded antenna with $kL\,(=\omega L/c)$, as the parameter, $C = 60 \times 8$.

Figure A-10d: Amplitude of the current distribution $|I(z,\omega)|$ vs z/L on the loaded antenna with $kL\,(=\omega L/c)$, as the parameter, $C = 60 \times 10$.

Figure A-11a: Magnitude and phase of the transfer function $\tilde{f}_\theta(\pi/2\omega)$, of the loaded antenna in the direction $\theta = \pi/2$ as a function of $kL = (\omega L/c)$ for different loading. $C = 60 \times 4$.

Figure A-11b: Magnitude and phase of the transfer function $\tilde{f}_\theta(\pi/2,\omega)$ of the loaded antenna in the direction $\theta = \pi/2$ as a function of $kL = (\omega L/c)$ for different loading. $C = 60 \times 5$.

Figure A-11c: Magnitude and phase of the transfer function $\tilde{f}_\theta(\pi/2,\omega)$ of the loaded antenna in the direction $\theta = \pi/2$ as a function of $kL = (\omega L/c)$ for different loading. $C = 60 \times 8$.

Figure A-11d: Magnitude and phase of the transfer function $\tilde{f}_\theta(\pi/2, \omega)$ of the loaded antenna in the direction $\theta = \pi/2$ as functions of $kL = (\omega L/c)$ for different loading. $C = 60 \times 10$.

Figure A-12a: Magnitude and phase of the transfer function $\tilde{f}_\theta(\pi/3, \omega)$ of the loaded antenna in the direction $\theta = \pi/3$ as functions of $kL = (\omega L/c)$ for different loading. $C = 60 \times 4$.

Figure A-12b: Magnitude and phase of the transfer function $\tilde{f}_\theta(\pi/3, \omega)$ of the loaded antenna in the direction $\theta = \pi/3$ as functions of $kL = (\omega L/c)$ for different loading. $C = 60 \times 5$.

Figure A-12c: Magnitude and phase of the transfer function $\tilde{f}_\theta(\pi/3, \omega)$ of the loaded antenna in the direction $\pi = \pi/3$ as functions of $kL = (\omega L/c)$ for different loading. $C = 60 \times 8$.

Figure A-12d: Magnitude and phase of the transfer function $\tilde{f}_\theta(\pi/3, \omega)$ of the loaded antenna in the direction $\theta = \pi/3$ as functions of $kL = (\omega L/c)$ for different loading. $C = 60 \times 10$.

Figure A-13a: Magnitude and phase of the transfer function $\tilde{f}_\theta(\pi/4, \omega)$ of the loaded antenna in the direction of $\theta = \pi/4$ as functions of $kL = (\omega L/c)$ for different loading. $C = 60 \times 4$.

Figure A-13b: Magnitude and phase of the transfer function $\tilde{f}_\theta(\pi/4, \omega)$ of the loaded antenna in the direction $\theta = \pi/4$ as functions of $kL = (\omega L/c)$ for different loading. $C = 60 \times 4$.

Figure A-13c: Magnitude and phase of the transfer function $\tilde{f}_\theta(\pi/4, \omega)$ of the loaded antenna in the direction $\theta = \pi/4$ as functions of $kL (= \omega L/c)$ for different loading. $C = 60 \times 8$.

Figure A-13d: Magnitude and phase of the transfer function $\tilde{f}_\theta(\pi/4, \omega)$ of the loaded antenna in the direction $\theta = \pi/4$ as functions of $kL (= \omega L/c)$ for different loading. $C = 60 \times 10$.

Figure A-14a: Magnitude and phase of the transfer function $\tilde{f}_\theta(\pi/6, \omega)$ of the loaded antenna in the direction $\theta = \pi/6$ as functions of $kL = (\omega L/c)$ for different loading. $C = 60 \times 4$.

Figure A-14b: Magnitude and phase of the transfer function $\tilde{f}_\theta(\pi/6, \omega)$ of the loaded antenna in the direction $\theta = \pi/6$ as functions of $kL = (\omega L/c)$ for different loading. $C = 60 \times 5$.

Figure A-14c: Magnitude and phase of the transfer function $\tilde{f}_\theta(\pi/6, \omega)$ of the loaded antenna in the direction $\theta = \pi/6$ as functions of $kL = (\omega L/c)$ for different loading. $C = 60 \times 8$.

Figure A-14d: Magnitude and phase of the transfer function $\tilde{f}_\theta(\pi/6, \omega)$ of the loaded antenna in the direction $\theta = \pi/6$ as functions of $kL = (\omega L/c)$ for different loading. $C = 60 \times 10$.

Figure A-15a: $\left|\tilde{e}_\theta(\pi/2, \omega)\right|$ vs $\omega L/c$ for the loaded antenna excited by a Gaussian pulse with $\sigma = 0.471$ ns.

Figure A-15b: $e_\theta(\pi/2, t)$ vs t for the loaded antenna excited by a Gaussian pulse with $\sigma = 0.471$ ns.

Figure A-16a: $\left|\tilde{e}_\theta(\pi/2, \omega)\right|$ vs $\omega L/c$ for the loaded antenna excited by a Guassian pulse with $\sigma = 1$ ns.

Figure A-16b: $e_\theta(\pi/2, t)$ vs t for the loaded antenna excited by a Gaussian pulse with $\sigma = 1$ ns.

Figure A-17: $e_\theta(\pi/2, t)$ vs t and $\left|\tilde{e}_\theta(\pi/2, \omega)\right|$ vs $\omega L/c$ for the loaded antenna excited by a Gaussian pulse with $\sigma = 3.33$ ns.

Figure A-18a: $\left|\tilde{e}_\theta(\pi/3, \omega)\right|$ vs $\omega L/c$ for the loaded antenna excited by a Gaussian pulse with $\sigma = 0.471$ ns.

Figure A-18b: $e_\theta(\pi/3, t)$ vs t for the loaded antenna excited by a Gaussian pulse with $\sigma = 0.471$ ns.

Figure A-19a: $\left|\tilde{e}_\theta(\pi/4, \omega)\right|$ vs $\omega L/c$ for the loaded antenna excited by a Gaussian pulse with $\sigma = 0.471$ ns.

Figure A-19b: $e_\theta(\pi/4, t)$ vs t for the loaded antenna excited by a Gaussian pulse with $\sigma = 0.471$ ns.

Figure A-20a: $\left|\tilde{e}_\theta(\pi/6, \omega)\right|$ vs $\omega L/c$ for the loaded antenna excited by a Gaussian pulse with $\sigma = 0.471$ ns.

Figure A-20b: $e_\theta(\pi/6, t)$ vs t for the loaded antenna excited by a Gaussian pulse with $\sigma = 0.471$ ns.

Figure A-21: Gamma pulse with $d = 1.7 \times 10^9$/sec obtained from Fast Fourier Transform program.

Figure A-22a: $\left|\tilde{e}_\theta(\pi/2, \omega)\right|$ vs $\omega L/c$ for the loaded antenna excited by a gamma pulse with $d = 1.7 \times 10^9$/sec.

Figure A-22b: $e_\theta(\pi/2, t)$ vs t for the loaded antenna excited by a gamma pulse with $d = 1.7 \times 10^9$/sec.

Figure A-23a: $\left|\tilde{e}_\theta(\pi/3, \omega)\right|$ vs $\omega L/c$ for the loaded antenna excited by a gamma pulse with $d = 1.7 \times 10^9$/sec.

Figure A-23b: $e_\theta(\pi/3, t)$ vs t for the loaded antenna excited by a gamma pulse with $d = 1.7 \times 10^9$/sec.

Figure A-24a: $\left|\tilde{e}_\theta(\pi/4, \omega)\right|$ vs $\omega L/c$ for the loaded antenna excited by a gamma pulse with $d = 1.7 \times 10^9$/sec.

Figure A-24b: $e_\theta(\pi/4, t)$ vs t for the loaded antenna excited by a gamma pulse with $d = 1.7 \times 10^9$/sec.

Figure A-25a: $\left|\tilde{e}_\theta(\pi/6, \omega)\right|$ vs $\omega L/c$ for the loaded antenna excited by a gamma pulse. $C = 60 \times 4$, $d = 1.7 \times 10^9$/sec.

Figure A-25b: $e_\theta(\pi/6, t)$ vs t for the loaded antenna excited by a gamma pulse $C = 60 \times 4$, $d = 1.7 \times 10^9$/sec.

(List of Figure Captions from Appendix B)

Figure B-1a: Far field waveform in the broadside direction. $\sigma = 1$ ns; $\tau = 3.33$ ns; $\psi = 5$.

Figure B-1b: Far field waveform in the broadside direction. $\sigma = 1$ ns; $\tau = 3.33$ ns; $\psi = 8$.

Figure B-2a: Far field waveform in the broadside direction. $\sigma = 0.471$ ns; $\tau = 3.33$ ns; $\psi = 5$.

Figure B-2b: Far field waveform in the broadside direction. $\sigma = 0.471$ ns; $\tau = 3.33$ ns; $\psi = 8$.

Figure B-3a: Far field waveform in the direction $\theta = \pi/6$. $\sigma = 1$ ns; $\tau = 3.33$ ns; $\psi = 8$.

Figure B-3b: Far field waveform in the direction $\theta = \pi/4$. $\sigma = 1$ ns; $\tau = 3.33$ ns; $\psi = 8$.

Figure B-3c: Far field waveform in the direction $\theta = \pi/3$. $\sigma = 1$ ns; $\tau = 3.33$ ns; $\psi = 8$.

Figure B-4a: Far field waveform in the direction $\theta = \pi/6$. $\sigma = 0.471$ ns; $\tau = 3.33$ ns; $\psi = 8$.

Figure B-4b: Far field waveform in the direction $\theta = \pi/4$. $\sigma = 0.471$ ns; $\tau = 3.33$ ns; $\psi = 8$.

Figure B-4c: Far field waveform in the direction $\theta = \pi/3$. $\sigma = 0.471$ ns; $\tau = 3.33$ ns; $\psi = 8$.

I

INTRODUCTION

The transient far field waveforms radiated by linear antennas, loaded non-uniformly and continuously with resistance, are investigated in the present technical note. The antennas considered are finite length thin cylinders excited symmetrically by unit slice generators having unit step function type of time dependence. Emphasis is given here to a specific type of resistive loading in which the amount of loading increases continuously towards the antenna end points where it becomes infinitely large.

Resistively loaded long and thin dipoles may be used as simulators (RES) to radiate intense electromagnetic pulses of desirable shapes. Basic design considerations and limitations of pulse radiating long dipoles have been discussed by Baum[1,2]. In any pulse radiating finite antenna, the reflection effects at the antenna end points produce undesirable features and distortions in the radiated waveforms. One way to reduce such distortions is to attenuate the outward traveling current waves on the antenna to an insignificant amount by the time they reach the end points. A possible method of obtaining this is to load the antenna with resistance; reactive loading being frequency sensitive is ruled out from the wave distortion point of view. It is also clear from physical considerations that uniform resistive loading is incapable of eliminating the wave reflections at the antenna end points although it may reduce the effects of such reflections to a certain extent. It has been shown by Wu and King[3] and by Baum[4] that with a special type of non-uniform resistive loading it is possible to obtain a reflection free antenna, i.e., the antenna sustains only single outward traveling current wave. As discussed by Baum[4], such an antenna may be used to radiate intense electromagnetic pulses of desirable shape. The motivation of the present research has been to investigate and obtain quantitative results for the various effects of the resistive loading on the transient radiation from such an antenna.

II

BACKGROUND

Rigorous analytical solutions of similar time dependent boundary value problems are extremely difficult, if not impossible, and are available only for some highly restricted cases. Wu[5] and Morgan[6] have derived theoretical expressions for the transient current distribution on unloaded infinitely long linear antennas excited by a step voltage across an infinitesimal center gap. Brundell[7] treated analytically the more general problem of determining the fields anywhere in space for a step excited unloaded dipole. Transient radiated fields for unloaded and uniformly loaded infinite linear antennas with similar excitations have been discussed theoretically by Latham and Lee[8,9]. The waveforms radiated by a Gaussian pulse excited infinitely long dipole have been obtained numerically by Harrison and King[10]. The time dependent far fields radiated by unloaded and uniformly loaded finite linear antennas with Gaussian pulse excitation have been obtained by Bennett and Auckenthaler[11] by applying direct time domain numerical analysis. Transients in step voltage excited unloaded cylindrical antennas have been investigated both theoretically and experimentally by Schmitt[12]. Schmitt's theoretical time domain radiated waveforms are of limited value because of the fact that he arbitrarily truncated the frequency domain results at $kL \simeq 5$, where 2L is the length of the antennas and $k = \frac{\omega L}{c}$ is the free space propagation constant. By applying the moment methods in the time domain Sayre[13] obtained the waveforms radiated by unloaded and loaded dipoles for step excitation. Taylor and his group[14,15] obtained by numerical means some results of limited application for the case of discretely loaded linear antennas excited by step voltage. Transient waveforms radiated by discretely loaded linear antennas with step excitation have also been studied numerically by Merewether[16,17].

Transient waveforms radiated by a non-uniformly loaded finite linear

antenna with step voltage excitation have first been investigated analytically by Baum[4] who used the transmission line model for the antenna. The transmission line model simplifies considerably the analytical investigation of the antenna and led to the development of the special non-reflective loading which significantly improves the radiated waveform[4]. However, because of the basic approximations involved the results obtained from the transmission line model are rather approximate.

In the following sections we investigate numerically the waveforms radiated by a step voltage excited linear antenna which is continuously and non-uniformly loaded with resistance along its length. At first the radiation fields produced by the harmonically excited antenna are obtained. The far field waveforms produced by the step voltage excited antenna are then obtained numerically with the help of Fast Fourier Inversion technique. The effects of the loading and other physical parameters of the antenna on the radiated waveforms are also studied in detail.

Numerical investigations of the waveforms radiated by similar antennas with short pulse excitations and analytical results for the Gaussian pulse excitations were discussed in our two previous reports. In view of their limited accessibility,and also for completeness, these two reports are included here as Appendices A and B without any significant editing.

III

BASIC RELATIONS

Let us assume that a linear antenna of length 2L be aligned along the z-axis of a rectangular coordinate system with the origin located at the center of the antenna and that it is excited by a unit slice generator located at the origin. The far electric field produced by such an antenna is directed entirely in the θ-direction. In the time harmonic case the far electric field is given by the following:

$$F = \tilde{F}_\theta(r, \theta, \omega)\, e^{j\omega t} \quad , \tag{1}$$

where,

$$\tilde{F}_\theta(r, \theta, \omega) = \frac{j\omega\eta_o \sin\theta}{4\pi c} \frac{e^{-j\frac{\omega}{c}r}}{r} \int_{-L}^{L} \tilde{I}(z', \omega)\, e^{j\frac{\omega}{c}z'\cos\theta}\, dz', \tag{2}$$

$\eta_o = \sqrt{\frac{\mu_o}{\epsilon_o}}$ is the intrinsic impedance of free space,

$c = \frac{1}{\sqrt{\mu_o \epsilon_o}}$ is the velocity of light in free space,

ω is the radian frequency of excitation,

r, θ, ϕ are the spherical polar coordinates of the far field point with the origin located at the center of the antenna,

$\tilde{I}(z', \omega)$ is the current distribution on the antenna due to the harmonically time dependent unit slice generator.

In Eq. (2), $\tilde{F}_\theta(r, \theta, \omega)$ is the time independent far electric field produced by the antenna. For convenience we define the antenna transfer function in the following manner:

$$\tilde{f}_\theta(\theta, \omega) = r\tilde{F}_\theta(r, \theta, \omega)\, e^{j\frac{\omega}{c}r}$$

$$= \frac{j\omega\eta_o \sin\theta}{4\pi c} \int_{-L}^{L} \tilde{I}(z', \omega)\, e^{j\frac{\omega}{c}z'\cos\theta}\, dz' \quad . \tag{3}$$

Notice that in the transfer function given by Eq. (3) the dependence of the field amplitude on r as well as the phase shift suffered by the field in traveling from the antenna to the far field point are both suppressed. As a result of this all the field quantitites in our subsequent discussion will be independent of r.

Let the slice generator have arbitrary time dependence such that the input signal voltage in time is represented V(t). It is now assumed that V(t) is Fourier transformable. This means that the following relations hold:

$$\tilde{V}(\omega) = \int_{-\infty}^{\infty} V(t) e^{-j\omega t}\, dt \quad , \tag{4}$$

$$V(t) = \frac{1}{2\pi} \int_{-\infty}^{\infty} \tilde{V}(\omega) e^{j\omega t}\, d\omega \quad . \tag{5}$$

After making use of the linearity of the system along with the superposition theorem and the concepts of Fourier transform technique, it can be shown that the time dependent far field produced by the antenna excited by a unit slice generator signal V(t) is given by the following:

$$e_\theta(\theta, t) = \frac{1}{2\pi} \int_{-\infty}^{\infty} \tilde{f}_\theta(\theta, \omega)\tilde{V}(\omega) e^{j\omega t}\, d\omega$$

$$= \frac{1}{2\pi} \int_{-\infty}^{\infty} \tilde{e}_\theta(\theta, \omega) e^{j\omega t}\, d\omega \quad . \tag{6}$$

In Eq. (6) the quantity $\tilde{e}_\theta(\theta, \omega) = \tilde{f}_\theta(\theta, \omega)\tilde{V}(\omega)$ may be looked upon as the spectral density of the far field waveform. Notice that, by definition, $e_\theta(\theta, t)$ and $\tilde{e}_\theta(\theta, \omega)$ are related to each other by the following transform relationship:

$$\tilde{e}_\theta(\theta, \omega) = \tilde{f}(\theta, \omega)\tilde{V}(\omega)$$

$$= \int_{-\infty}^{\infty} e_\theta(\theta, t)\, e^{-j\omega t}\, dt \quad . \tag{7}$$

In the present problem the transient voltage at the δ-gap located at the center of the antenna is represented by

$$V(t) = f(t) \quad , \tag{8}$$

where,

$$f(t) = \begin{cases} 1/T \ , & 0 \leq t \leq T \\ 0 \ , & \text{otherwise} \end{cases} \tag{9}$$

For sufficiently large T (usually T = few times τ, where $\tau = \frac{L}{c}$ = the transit time on the antenna) the radiated waveforms may be identified with those radiated by the same antenna when excited by a unit step function voltage in time, i.e., $V(t) = U(t)$. For convenience of numerical computation, the rectangular pulse type of excitation has been used here to obtain the step voltage response from the antenna. With the input signal of the form given by Eqs. (8) and (9) we have,

$$\tilde{V}(\omega) = \frac{\sin \omega T/2}{\omega T/2}\, e^{-j\omega T/2} \tag{10}$$

as the spectrum of the input voltage signal.

As can be seen from the above, the first step in the analysis is the determination of the current distribution $\tilde{I}(z', \omega)$ on the antenna when it is excited by a harmonically time dependent unit slice generator. Let us assume that the an-

tenna is loaded with distributed resistance such that its internal impedance may be expressed as $r_s(z')$ ohms/meter for $0 \leq |z'| \leq L$. Under this condition it can be shown that the current distribution $I(z', \omega)$ on the antenna satisfies the following modified Hallén's integral equation:

$$\int_{-L}^{L} \tilde{I}(z', \omega) \frac{e^{-j\frac{\omega}{c}\left[(z-z')^2 + a^2\right]^{1/2}}}{4\pi\left[(z-z')^2 + a^2\right]^{1/2}} dz' = B\cos kz - \frac{j}{2\eta_o} \sin k|z| + \frac{j}{\eta_o}\int_0^z \tilde{I}(\xi, \omega) r_s(\xi) \sin k(z-\xi)\, d\xi \quad , \tag{11}$$

where,

$k = \frac{\omega}{c}$ is the propagation constant,

B is a constant to be determined from the end condition $\tilde{I}(\pm L, \omega) = 0$,

a is the radius of the antenna element.

IV

A NOTE ON THE LOADING

The antenna is assumed to be resistively loaded such that its internal impedance may be expressed as:

$$r_s(z') = \frac{r_o}{1-|z'|/L} \text{ ohms/meter}, \quad -L \leq z' \leq L \ , \qquad (12)$$

where $r_o = r_s(0)$ ohms/meter and is referred to as the loading parameter. Eq. (12) predicts that the internal resistance of the antenna increases continuously from the value r_o at the input end to infinity at the antenna end points. The rationale behind this particular type of resistive loading is as follows. It is known[3] that for a linear antenna loaded according to Eq. (12) there exists a critical value of r_o, depending on the thickness parameter $\Omega = 2\ell n \frac{2L}{a}$ of the antenna, for which the loaded antenna excited by a harmonic slice generator sustains a single wave of current traveling in the direction of increasing z', i.e., from the generator towards both ends of the antenna. In other words, for this type of loading there is no reflected wave on the antenna traveling in the opposite direction. For this reason the antenna loaded according to (12) and with this critical value of r_o is sometimes referred to as the reflectionless antenna. Baum[4] arrived at the same conclusion from his transmission line analysis of the same antenna. For r_o less than the above critical value the antenna stops being reflectionless and sustains a standing wave type of current distribution. From theoretical considerations Shen and Wu[18] have found that for r_o larger than the critical r_o the antenna sustains a progressive wave of current whose distribution may be expressed as a hypergeometric function. Our previous numerical investigation of the problem (Appendix A) essentially confirmed the above observations. In the present study we investigate in detail

the effects of the variation of the loading parameter r_o on the transient far field waveforms radiated by the antenna.

V

BRIEF OUTLINE OF THE NUMERICAL METHOD USED

As mentioned in Section II we have used numerical techniques to obtain the solution of the problem outlined in Section III. Detailed discussion of the numerical methods is given in Appendix A. In this section we give only a brief outline of the numerical techniques used to obtain the various quantities.

Standard numerical techniques[19,20] are used to solve Eq. (11) for $\tilde{I}(z', \omega)$. For this purpose the integral equation (11) is reduced by moment methods to the following set of N simultaneous algebraic equations:

$$\sum_{n=1}^{N} \int_{\Delta z_n} \tilde{I}(z', \omega)\, G(z_j, z')\, dz'$$

$$= B \cos \cdot kz_j - \frac{j}{2\eta_o} \sin k|z_j|$$

$$+ \frac{j}{\eta_o} \sum_{n}{}' \int_{\Delta z_n} \tilde{I}(z', \omega)\, r_s(z') \sin k(z_j - z')\, dz' \quad , \qquad (13)$$

$$j = 1, 2, \ldots\ldots, N,$$

where,

$$G(z_j, z') = \frac{e^{-jk\left[(z_j - z')^2 + a^2\right]^{1/2}}}{4\pi\left[(z_j - z')^2 + a^2\right]^{1/2}} \qquad (14)$$

$$\sum_{n}{}' = \begin{cases} -\sum_{n=j}^{N/2}, & \text{for } j \le \frac{N}{2}, \\ \sum_{n=\frac{N}{2}+1}^{j}, & \text{for } j > \frac{N}{2}, \end{cases} \qquad (15)$$

and it is assumed that N is an even number and $z' \epsilon \Delta z_n$. Eq. (13) implies that the antenna of length 2L is divided into N sections, the numbering of the sections increasing from 1 to N along the antenna length from -L to L.

It is now necessary to make an appropriate approximation to the current distribution $\tilde{I}(z')$ (for simplicity we use the notation $\tilde{I}(z')$ for $\tilde{I}(z', \omega)$) in each of the sections Δz_n. We make the following quadratic approximation to the unknown current in each section:

$$\tilde{I}(z') = A_n + B_n(z' - z_n) + C_n(z' - z_n)^2 \quad , \quad \text{for } z' \epsilon \Delta z_n \quad ,$$
$$= 0 \quad , \quad \text{otherwise,} \tag{16}$$

where A_n, B_n, C_n are the three unknown constants. These constants are determined by requiring that the continuations of $\tilde{I}(z')$ expression given by Eq. (16) into the centers of the adjacent sections give the appropriate current values there. After evaluating the constants it can be shown (Appendix A) that the current in each section is given by the following recurrence relation:

$$\tilde{I}(z') = I_{n-1} X_n(z') + I_n Y_n(z') + I_{n+1} Z_n(z') \quad , \quad z' \epsilon \Delta z_n \quad , \tag{17}$$

where,

$$X_n(z') = -\frac{z' - z_n}{2\Delta z} + \frac{(z' - z_n)^2}{2\Delta z^2} \quad , \quad z' \epsilon \Delta z_n \tag{18}$$

$$Y_n(z') = 1 - \frac{(z' - z_n)^2}{\Delta z^2} \quad , \quad z' \epsilon \Delta z_n \tag{19}$$

$$Z_n(z') = \frac{z' - z_n}{2\Delta z} + \frac{(z' - z_n)^2}{2\Delta z^2} \quad , \quad z' \epsilon \Delta z_n \tag{20}$$

$\tilde{I}(z_n) = I_n$ etc.,

Δz is the length of each section,

$n \neq 1, N.$

For the two end sections Δz_1 and Δz_N the currents are given by the following (Appendix A):

$$\tilde{I}(z') = I_1 Y'_1(z') + I_2 Z'_1(z') \quad , \quad \text{for } z' \epsilon \Delta z_1 \quad , \tag{21}$$

$$\tilde{I}(z') = I_N Y'_N(z') + I_{N-1} X'_N(z') \quad , \quad \text{for } z' \epsilon \Delta z_N \quad , \tag{22}$$

where,

$$Y'_1(z') = 1 + \frac{(z'-z_1)^2}{\Delta z} - 2\frac{(z'-z_1)^2}{\Delta z^2} \quad , \quad \text{for } z' \epsilon \Delta z_1 \quad , \tag{23}$$

$$Z'_1(z') = \frac{(z'-z_1)}{3\Delta z} + \frac{2(z'-z_1)^2}{3\Delta z^2} \quad , \quad \text{for } z' \epsilon \Delta z_1 \quad , \tag{24}$$

$$Y'_N(z') = 1 - \frac{(z'-z_N)}{\Delta z} - \frac{2(z'-z_N)^2}{\Delta z^2} \quad , \quad \text{for } z' \epsilon \Delta z_N \tag{25}$$

$$X'_N(z') = -\frac{(z'-z_N)}{3\Delta z} + \frac{2(z'-z_N)^2}{3\Delta z^2} \quad , \quad \text{for } z' \epsilon \Delta z_N \quad . \tag{26}$$

After substituting Eqs. (17)-(26) into Eq. (13) we obtain a set of N simultaneous algebraic equations involving the N unknown current coefficients $I_1, I_2, \ldots, I_N$. The extra unknown constant B is now determined by applying the end condition $\tilde{I}(L, \omega) = 0$. By using Taylor series expansion for the currents at the centers of the last four sections and retaining four terms in the series, we obtain the following extra equation:

$$-5I_{N-3} + 21I_{N-2} - 35I_{N-1} + 35I_N = 0 \quad . \tag{27}$$

We now have N+1 equations for the N+1 unknowns and the system of equations are solved by usual matrix methods for $I_1, I_2, \ldots, I_N$ and B.

The transfer function $\tilde{f}_\theta(\theta, \omega)$ given by Eq. (3) can now be evaluated numerically with the help of the following relation:

$$\tilde{f}_\theta(\theta, \omega) = j\frac{\omega\eta_o \sin\theta}{4\pi c} \sum_{n=1}^{N} I_n e^{j\frac{\omega}{c} z_n \cos\theta} \Delta z_n \quad , \tag{28}$$

where we have used the notation $\tilde{I}(z_n, \omega) = I_n$ and $z' = z_n$ is the coordinate of the center of the section Δz_n.

The spectral density $\tilde{e}_\theta(\theta, \omega)$ of the radiated waveforms is obtained by using Eqs. (7), (10) and (28). Finally the time dependent radiated waveform $e_\theta(\theta, t)$ is obtained by carrying out the integral given by Eq. (6) with the help of Fast Fourier Inversion technique.

During the numerical computation the antenna of length 2L has been divided into N equal length sections. Time domain results have been obtained for L = 1 meter so that the antenna is 2 meters long. The frequency domain calculations have been truncated at the highest frequency f_o such that $\Delta z = \frac{2L}{N} \simeq \frac{\lambda_o}{6}$, where λ_o is the free space wavelength corresponding to f_o. In the next two sections we discuss the various results obtained.

VI

CURRENT DISTRIBUTION $\tilde{I}(z, \omega)$

It is instructive to study how the loading effects the current distribution on the harmonically excited antenna. Figures 1 and 2 show the amplitude and the phase distribution, respectively, of the time independent current on the linear antenna of length $2L = 5\lambda$, $\frac{L}{a} \simeq 156$ and $r_o \simeq 318$. Under these conditions the antenna approximately satisfies the non-reflecting criterion[3,4,21]. The approximate theories of Wu and King[3] and Baum[4] predict the existence of a pure traveling wave of current with linearly decaying amplitude distribution on the antenna. The results shown in Fig. 1 indicate that the amplitude distribution of current may be considered to be approximately linear except near the feed region where it is significantly different. The linear variation of phase in Fig. 2 indicates the existence of a pure traveling wave of current in the antenna.

Figures 3 and 4 show the amplitude and the phase distribution of the current on the harmonically excited antenna of length $2L = 3\lambda$, $\frac{L}{a} = 156$ and for different values of the loading parameter r_o. For $r_o < 318$, the reflection effects on the current distribution become appreciable; the results for $r_o = 120$ clearly indicate that the antenna sustains a standing wave type of current distribution. For $r_o > 318$, the amplitude distribution of the current resembles an exponentially decaying function and the phase distribution, although not linear, is progressive along the length of the antenna. In this sense it is proper to say that for r_o larger than the critical value of the loading parameter (i.e., larger than 318 in this case) the antenna maintains its non-reflecting properties, but it supports a progressive wave of current. It should be noted that the critical value of the loading parameter r_o is different for an antenna with different value of $\frac{L}{a}$.

For a given non-reflecting antenna with $\frac{L}{a} = 156$, $r_o = 600$, the amplitude and phase of $\tilde{I}(z, \omega)$ are shown in Fig. 5 for two values of frequency ω such

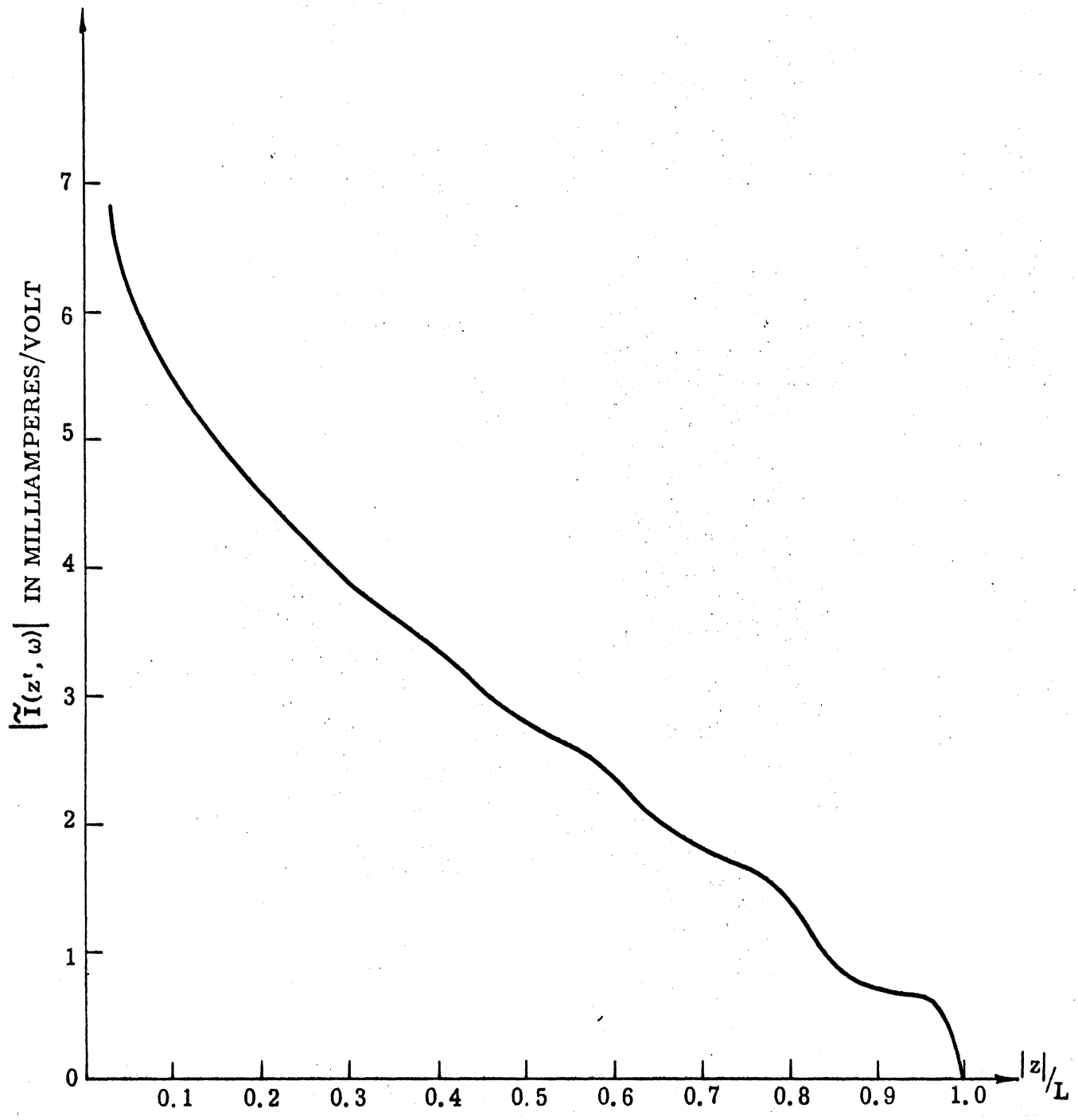

Figure 1: Amplitude of the current distribution along a non-reflectively loaded antenna. $\frac{L}{a} = 156$, $\frac{\omega L}{c} = 5\pi$, $r_o = 318$.

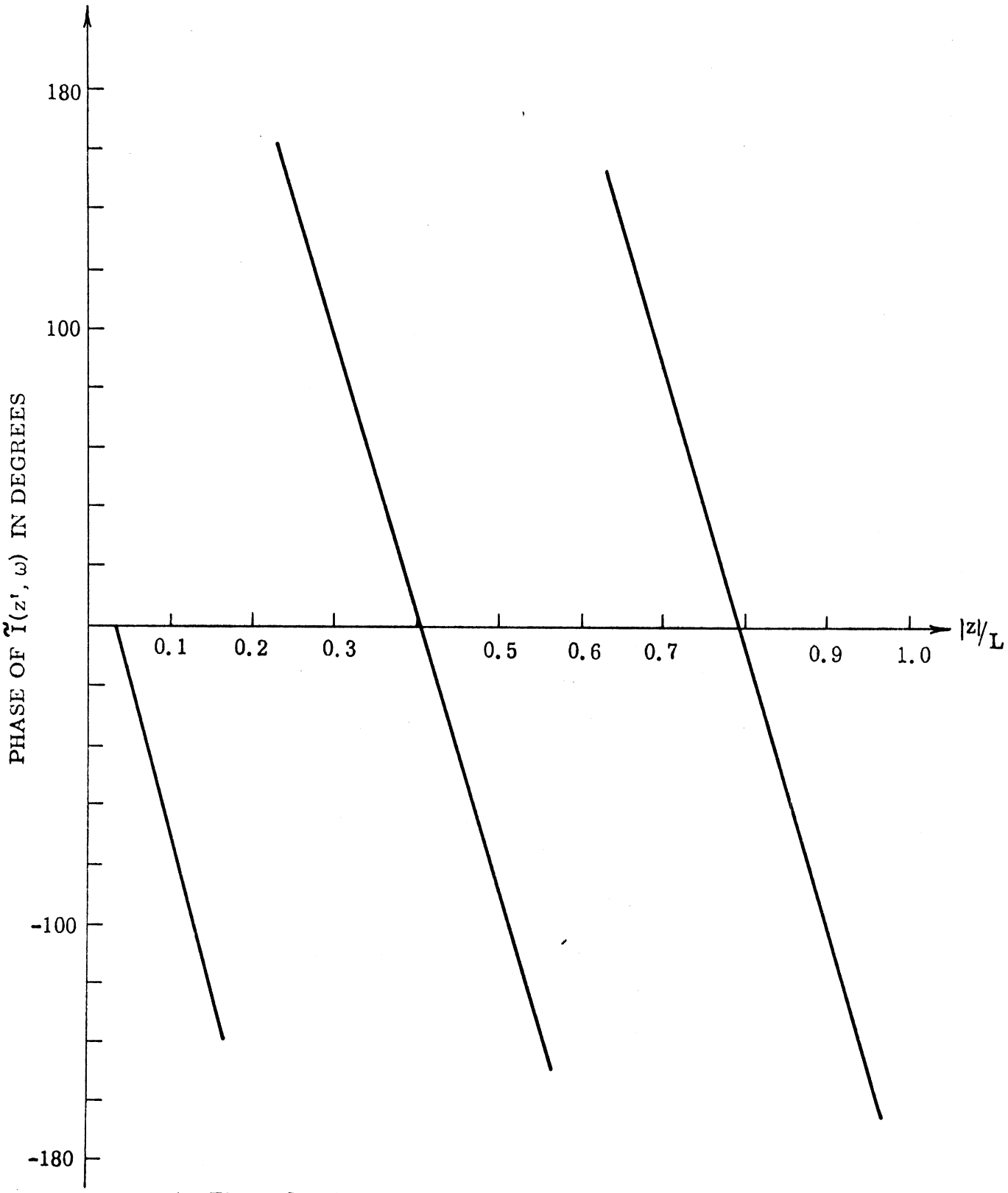

Figure 2: The phase variation of the current along a non-reflectively loaded antenna. $\frac{L}{a} = 156$, $\frac{\omega L}{c} = 5\pi$, $r_o = 318$.

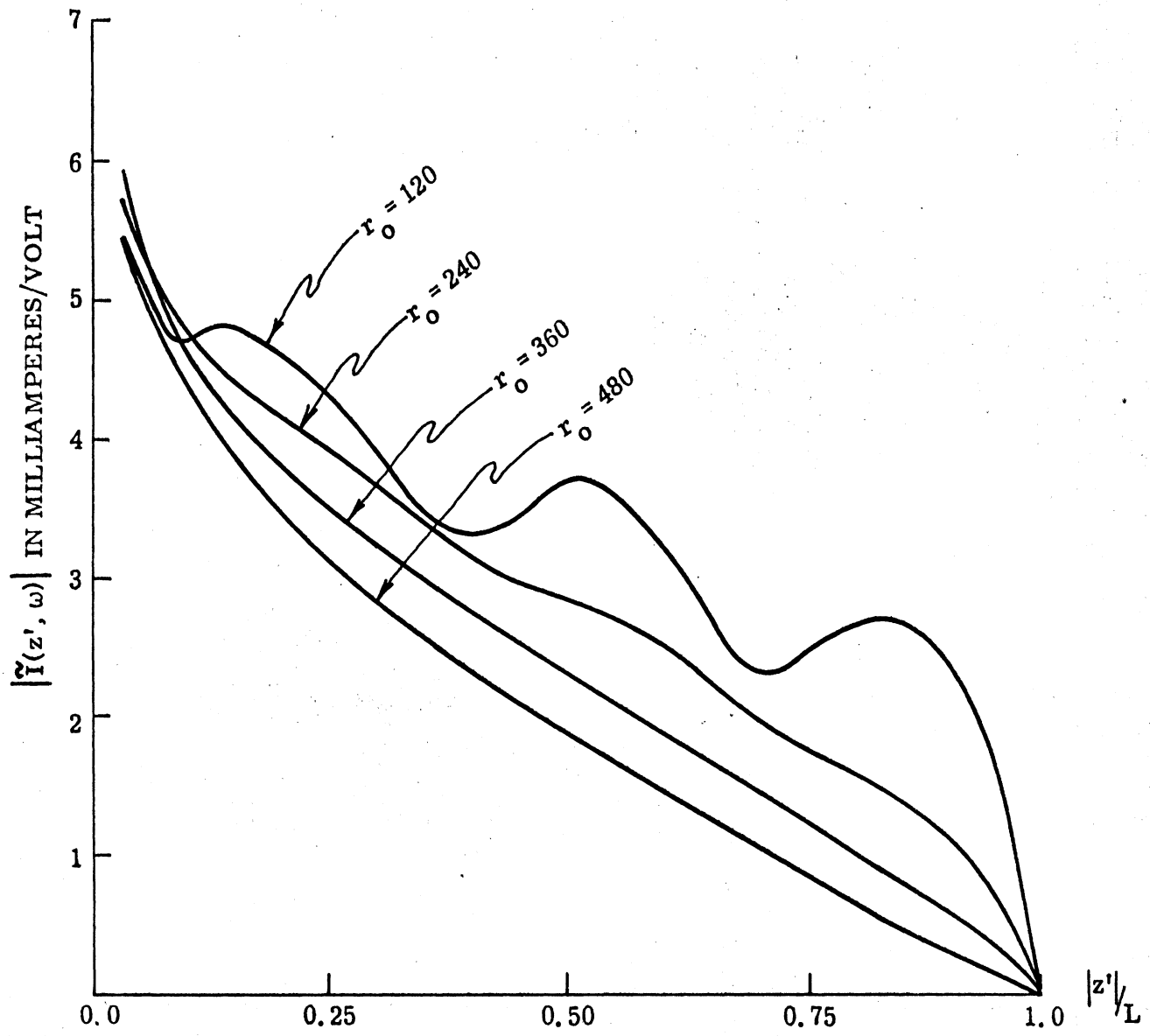

Figure 3: The amplitude of the current distribution along the antenna as a function of the loading parameter. $\frac{L}{a} = 156$, $\frac{\omega L}{c} = 3\pi$.

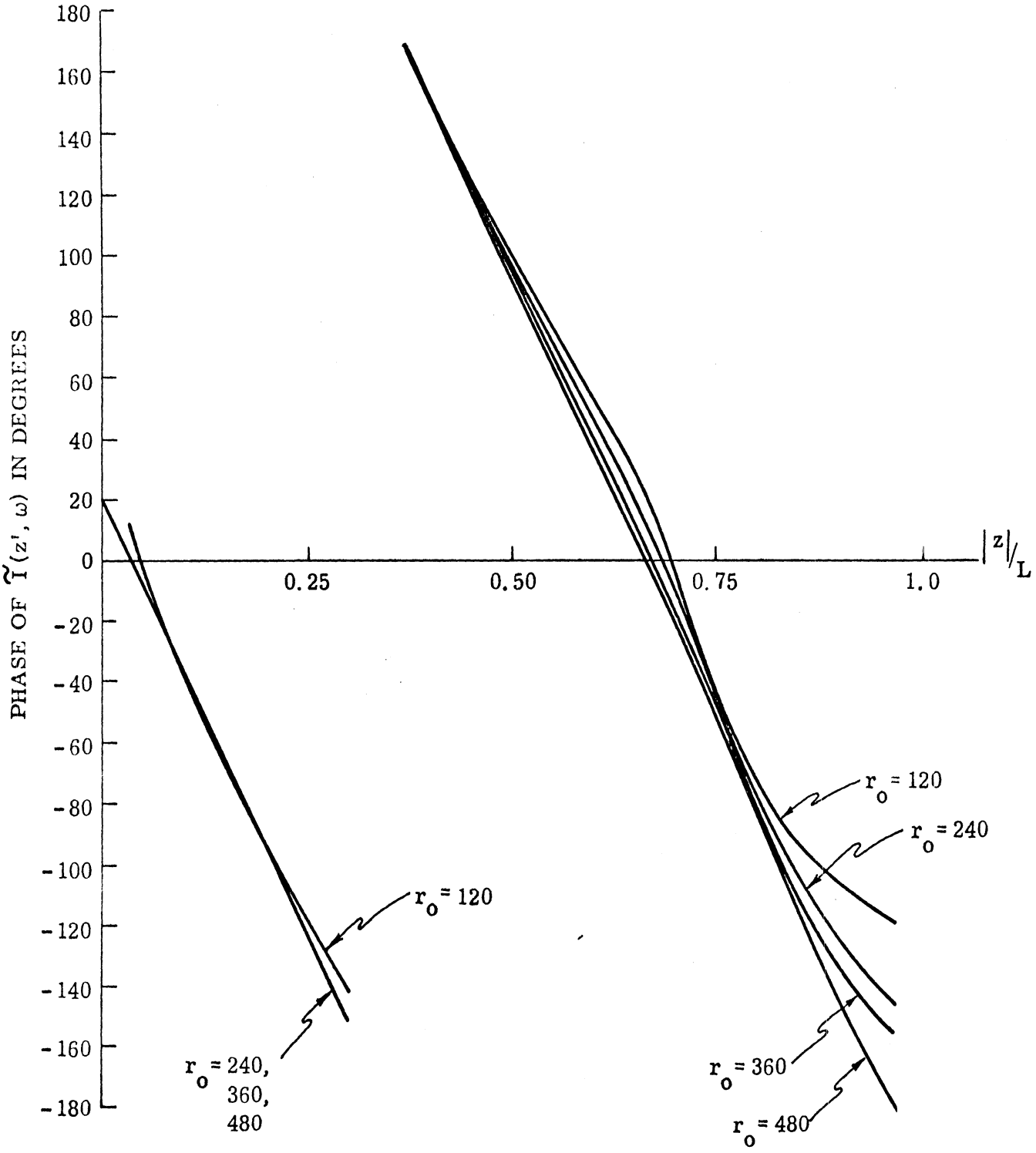

Figure 4: The phase of the current distribution along the antenna as a function of the loading parameter. $\frac{L}{a} = 156$, $\frac{\omega L}{c} = 3\pi$.

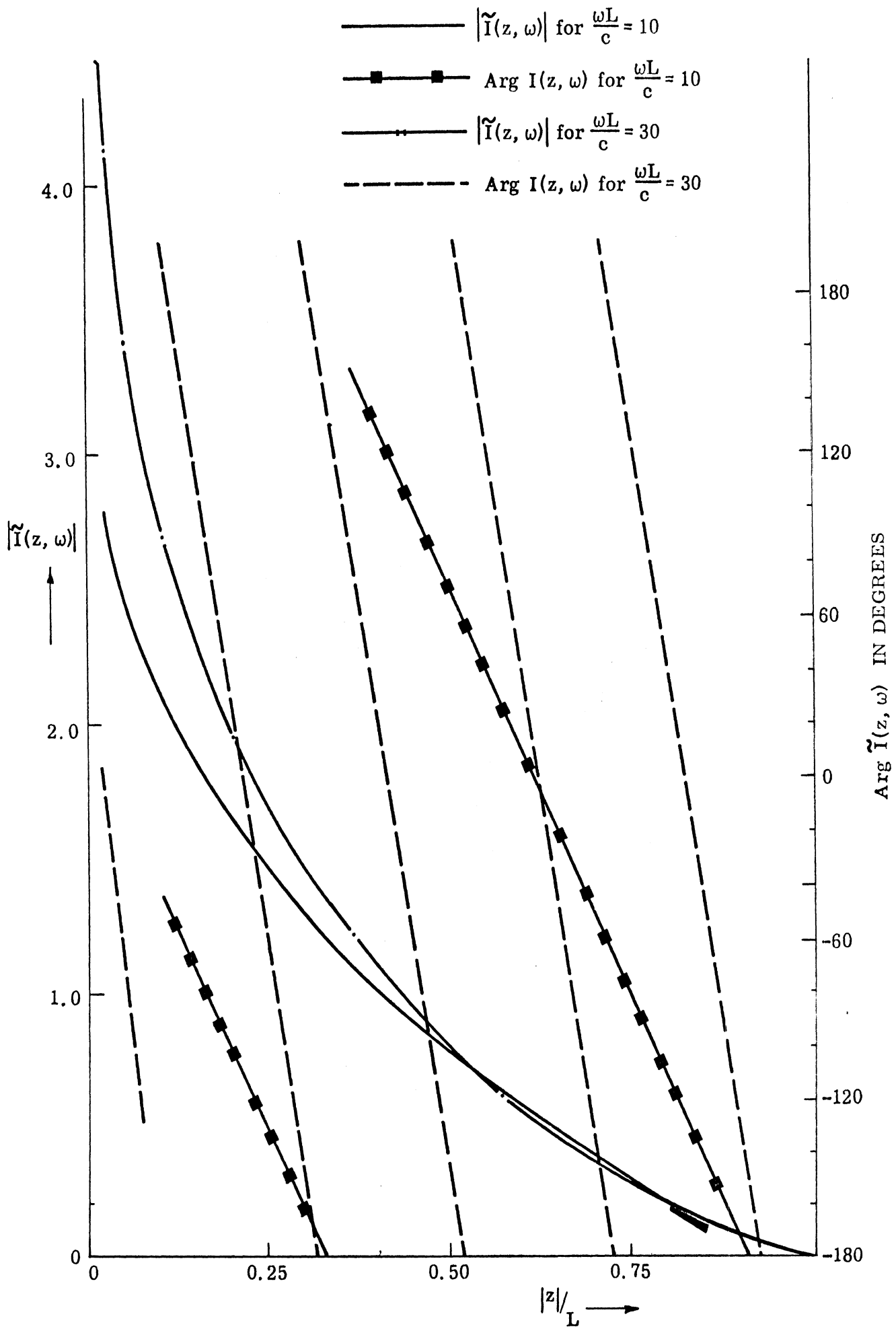

Figure 5: The amplitude and phase of the current distribution along a non-reflectively loaded antenna for two different frequencies. $\frac{L}{a} = 156$, $r_o = 600$.

that $\frac{\omega L}{c} = 10$ and $\frac{\omega L}{c} = 30$. It is found that the antenna retains its non-reflecting characteristics within the range of frequencies considered in Fig. 5.

VII

TRANSFER FUNCTION OF THE ANTENNA $\tilde{f}_\theta(\theta, \omega)$

In this section the magnitude and phase of the transfer function of the antenna are given as functions of $\omega L/c$ and for different values of the loading parameter r_o. Figure 6 a gives the variations of the magnitude and phase of $\tilde{f}_\theta(\theta, \omega)$ in the broadside direction ($\theta = \pi/2$) of the antenna of length 2L and $\frac{L}{a} = 156$ and for three values of the loading parameter. Similar results are shown in Figs. 6 b-d for the same antenna and for three different directions. The corresponding results for an antenna of length 2L and $\frac{L}{a} = 100$ are shown in Figs. 7 a-d.

In all the curves, $\left|f_\theta(\theta, \omega)\right|$ approaches zero as ω approaches zero which is consistent with the fact that there is no radiation at zero frequency. For higher frequencies the mean value of $\left|f_\theta(\theta, \omega)\right|$ tends to increase with an increase of frequency. In general, the mean value of the phase of $\tilde{f}_\theta(\theta, \omega)$ appears to decrease rapidly for small values of $\omega L/c$ and then assumes a constant value.

In each case for $r_o = 240$ both the amplitude and phase of $\tilde{f}_\theta(\theta, \omega)$ oscillate with $\omega L/c$. With increase of r_o these oscillations are smoothed out. It is interesting to observe that the oscillations in the amplitude and phase of $\tilde{f}_\theta(\theta, \omega)$ appear to be smoothed out for $r_o \geq$ the critical loading parameter.

The increase of the parameter $\frac{L}{a}$ tends to increase the amount of oscillation in the curves.

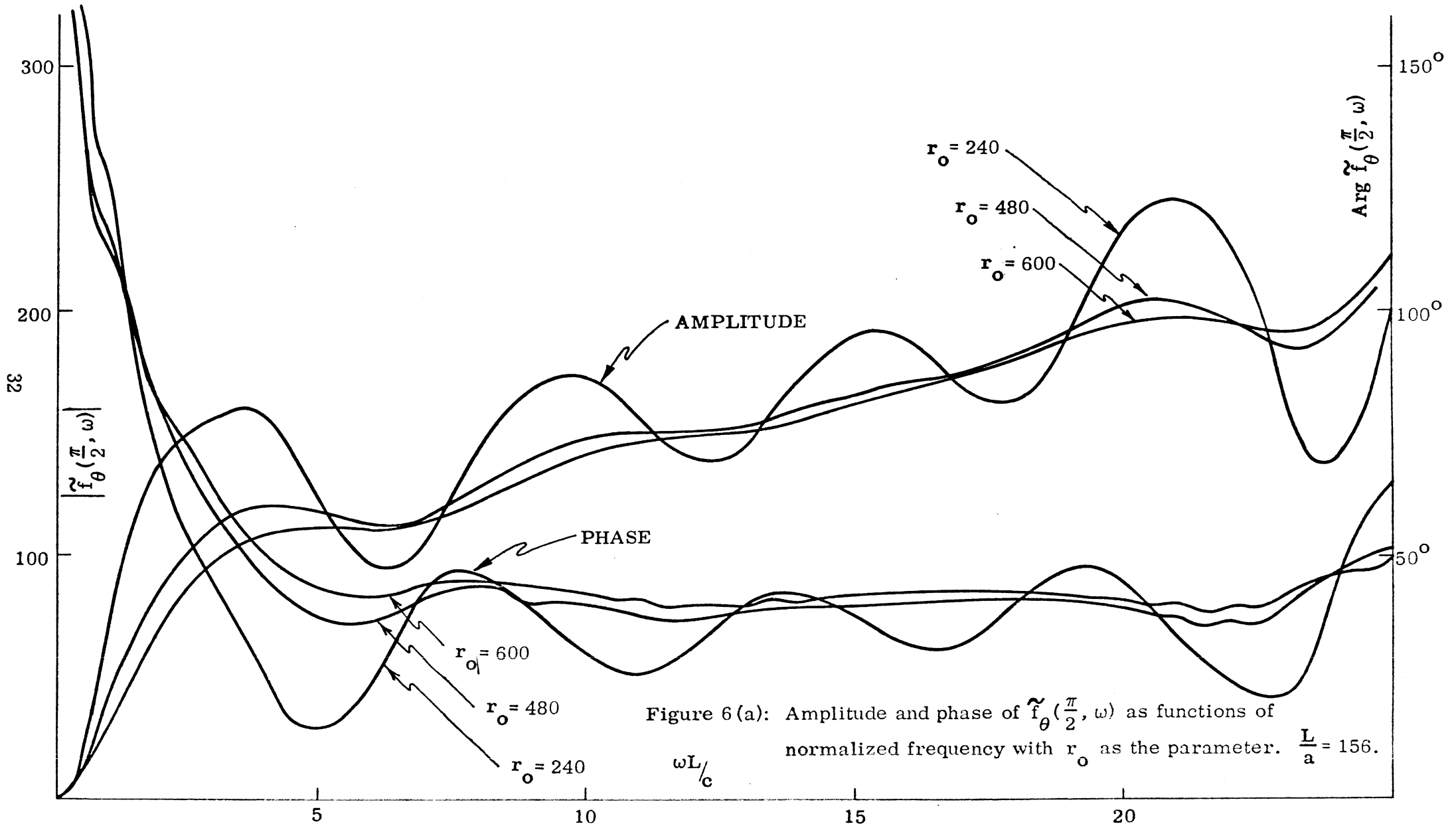

Figure 6(a): Amplitude and phase of $\tilde{f}_\theta(\frac{\pi}{2}, \omega)$ as functions of normalized frequency with r_o as the parameter. $\frac{L}{a} = 156$.

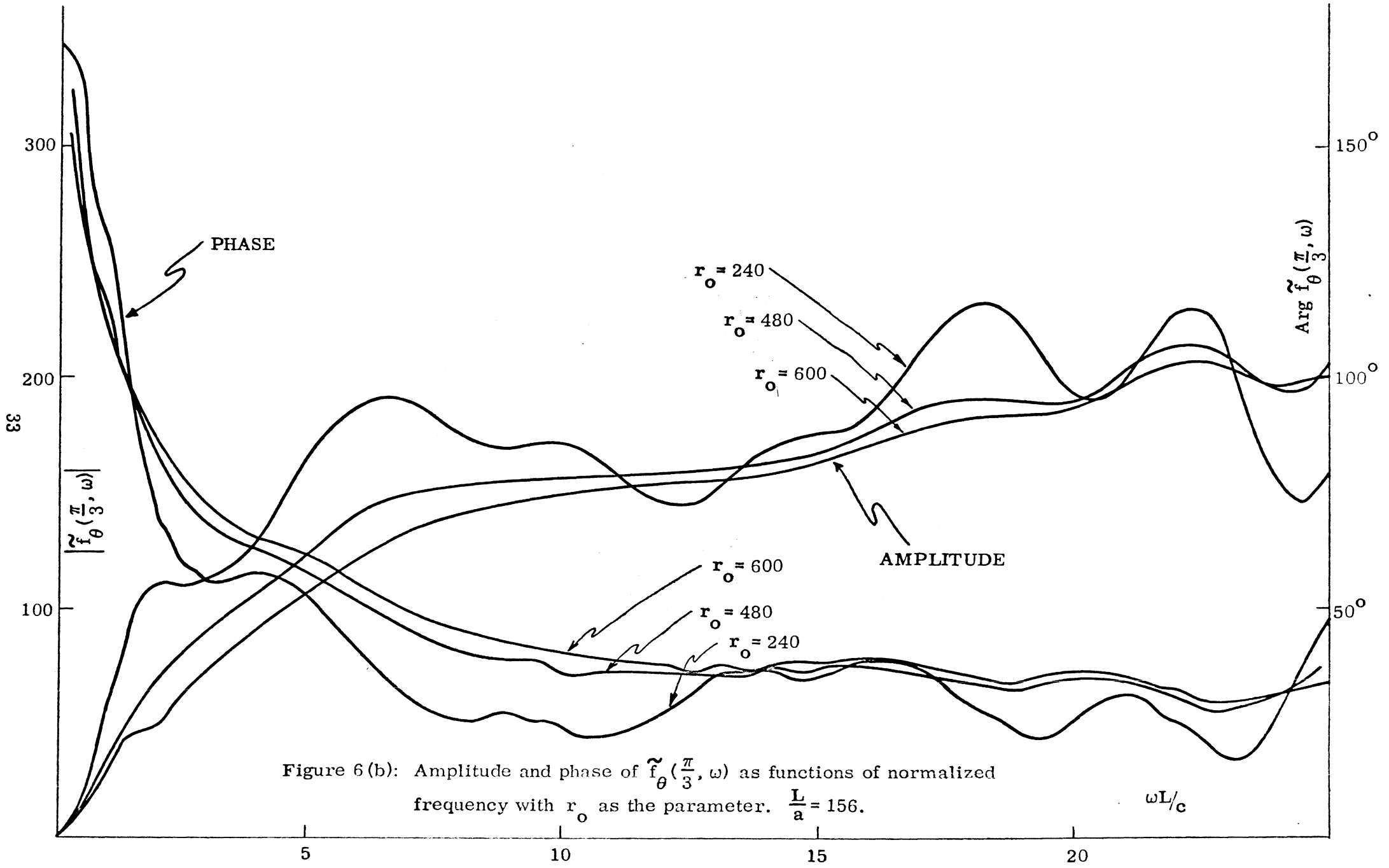

Figure 6(b): Amplitude and phase of $\tilde{f}_\theta(\frac{\pi}{3}, \omega)$ as functions of normalized frequency with r_o as the parameter. $\frac{L}{a} = 156$.

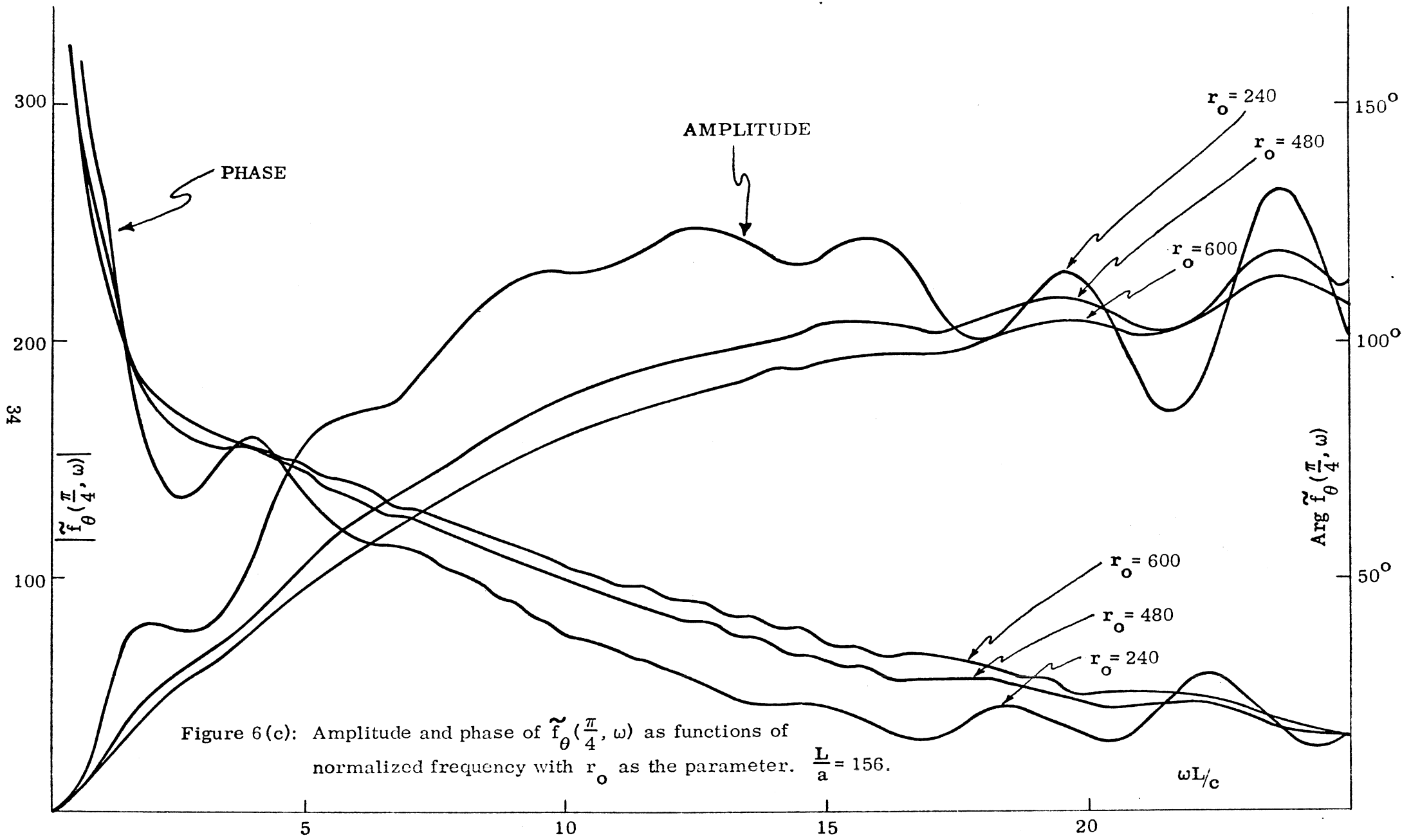

Figure 6(c): Amplitude and phase of $\tilde{f}_\theta(\frac{\pi}{4}, \omega)$ as functions of normalized frequency with r_o as the parameter. $\frac{L}{a} = 156$.

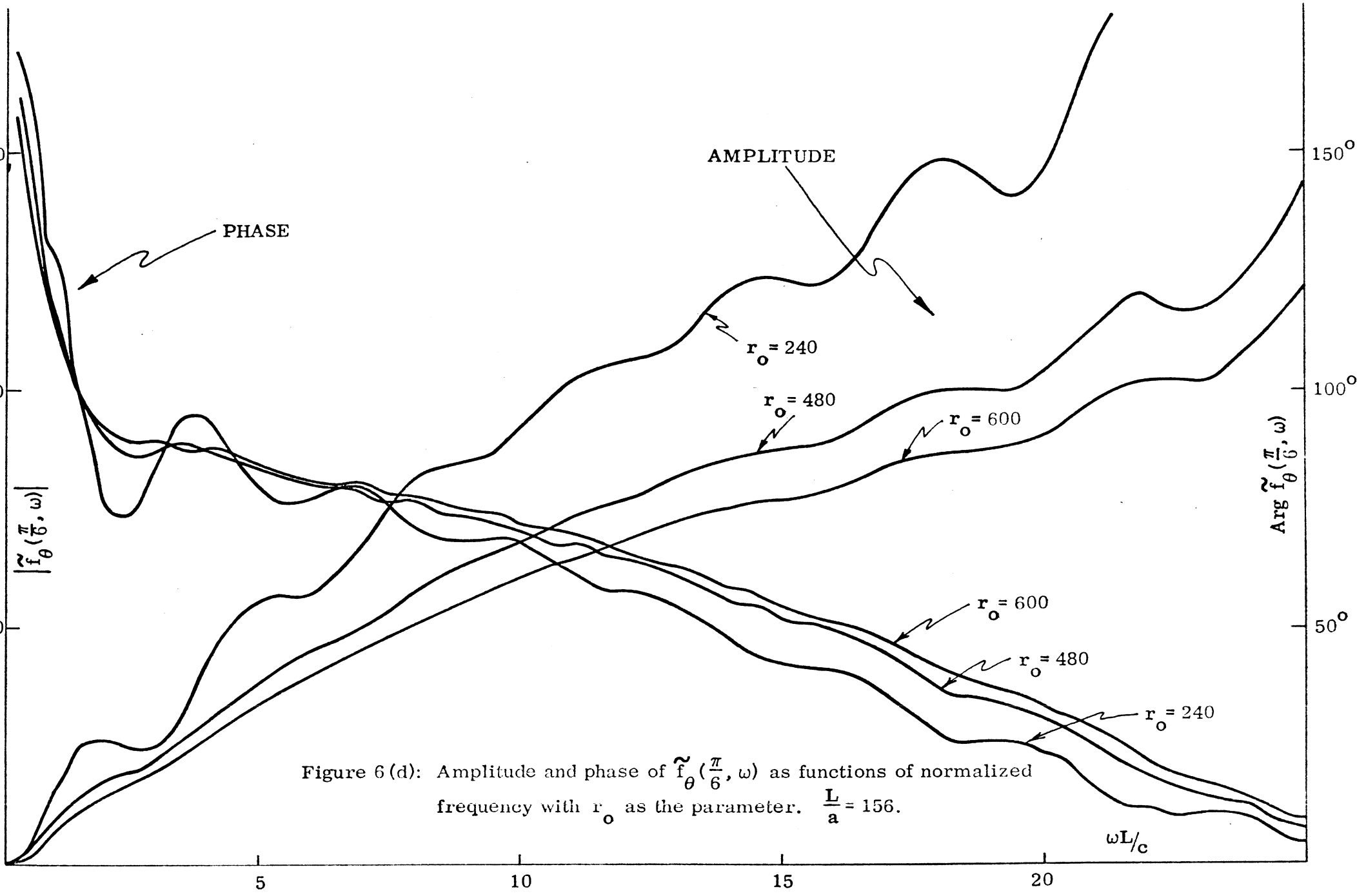

Figure 6 (d): Amplitude and phase of $\tilde{f}_\theta(\frac{\pi}{6}, \omega)$ as functions of normalized frequency with r_o as the parameter. $\frac{L}{a} = 156$.

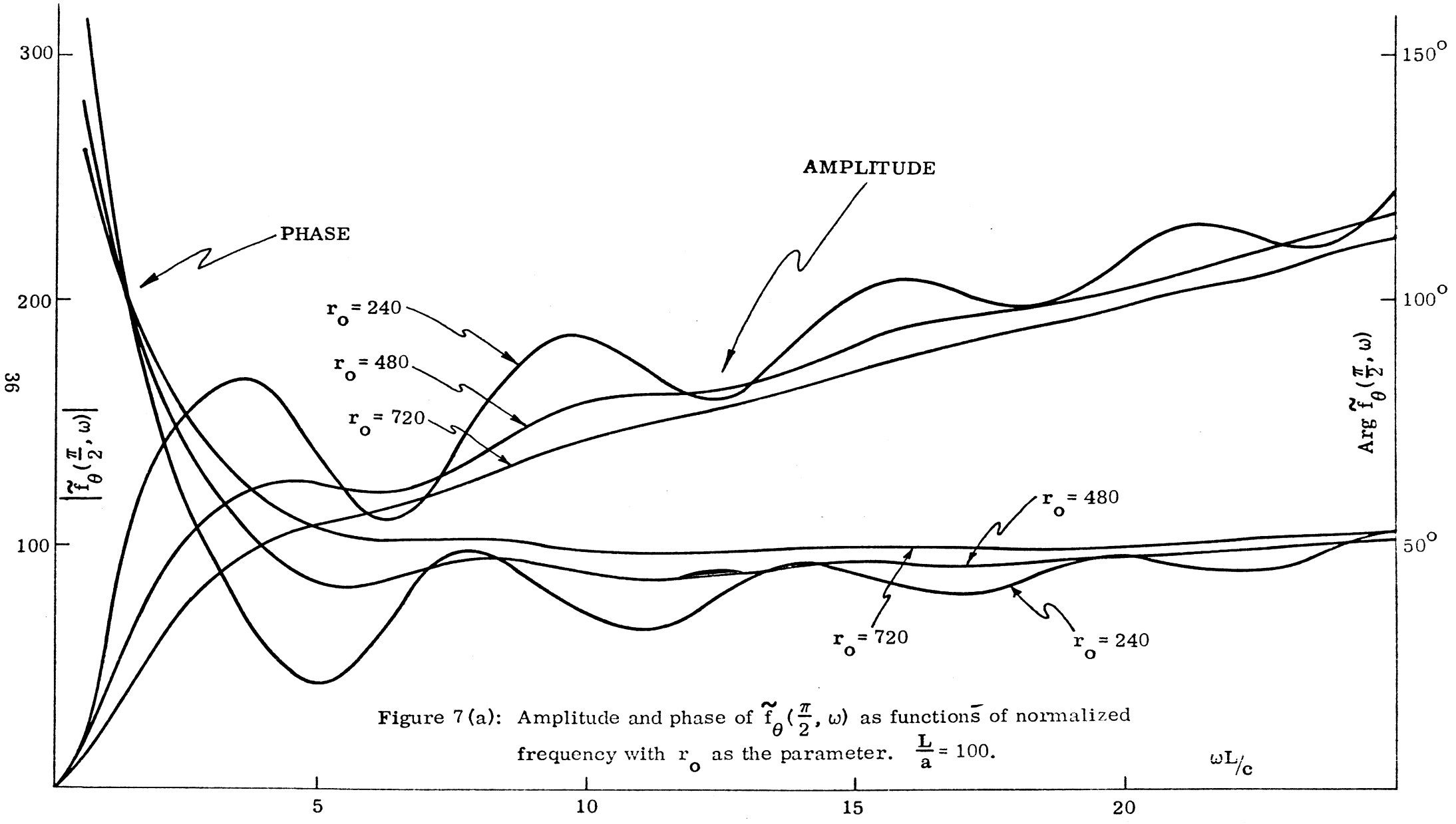

Figure 7(a): Amplitude and phase of $\tilde{f}_\theta(\frac{\pi}{2}, \omega)$ as functions of normalized frequency with r_o as the parameter. $\frac{L}{a} = 100$.

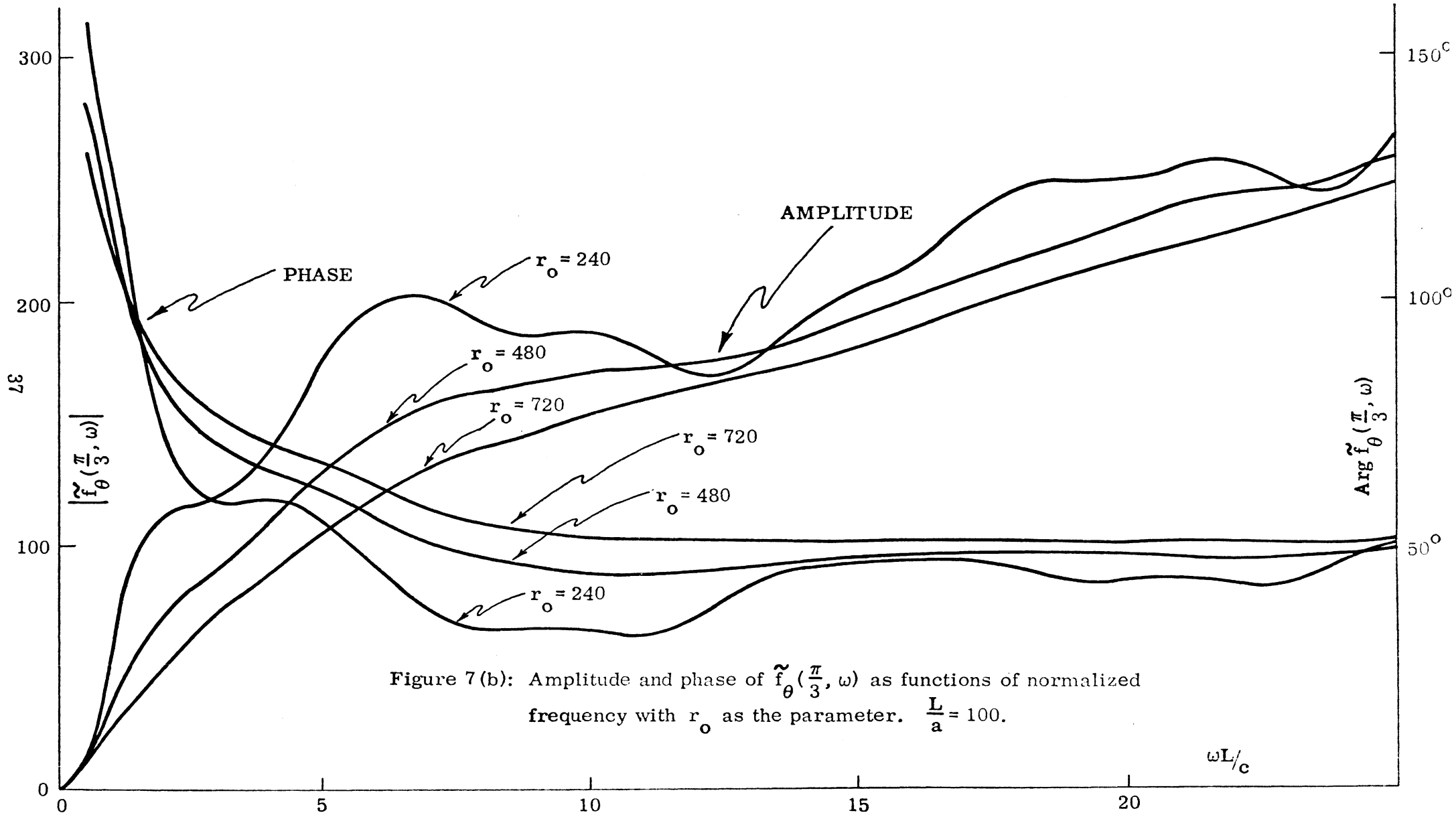

Figure 7 (b): Amplitude and phase of $\tilde{f}_\theta(\frac{\pi}{3}, \omega)$ as functions of normalized frequency with r_o as the parameter. $\frac{L}{a} = 100$.

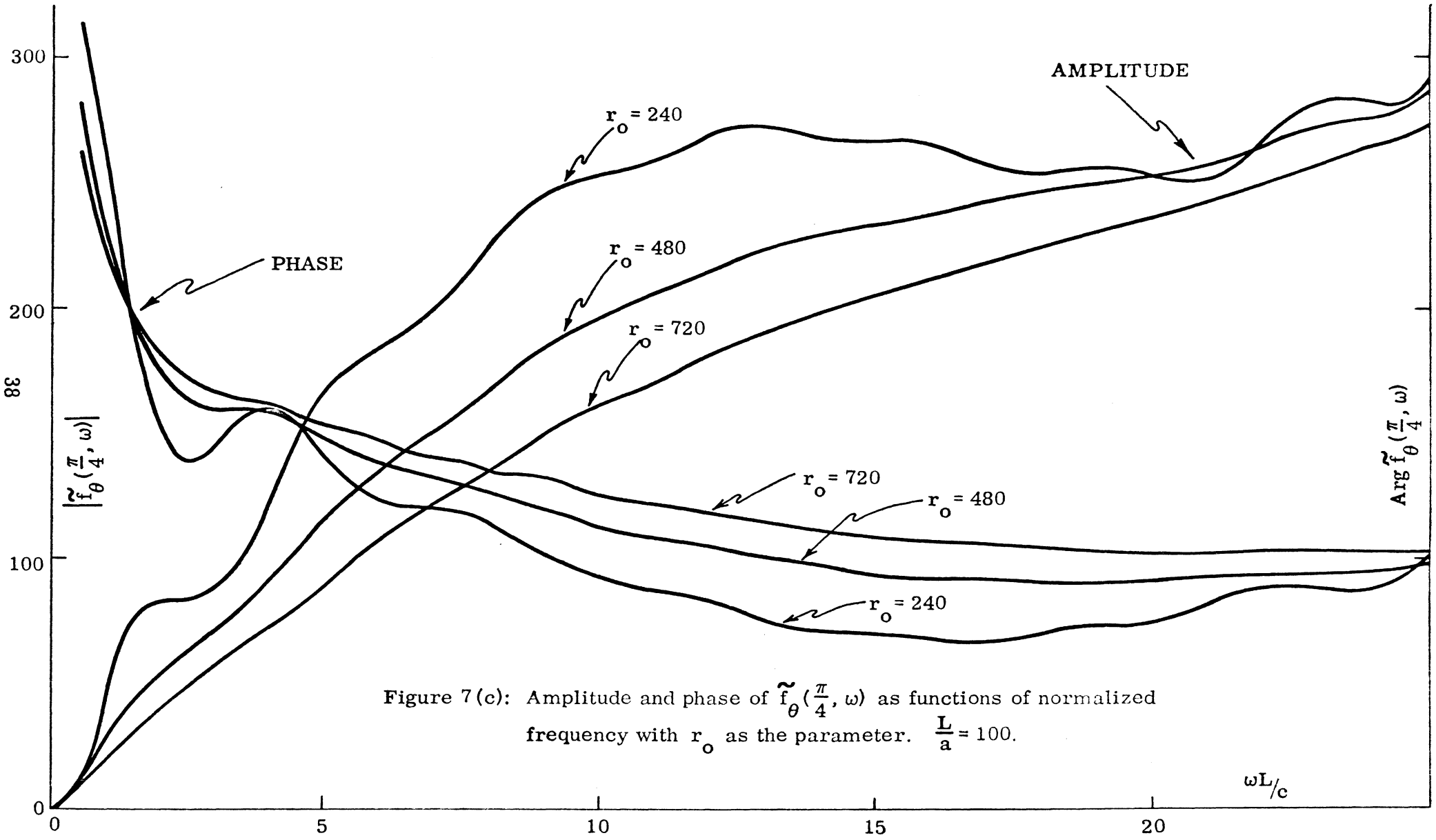

Figure 7(c): Amplitude and phase of $\tilde{f}_\theta(\frac{\pi}{4}, \omega)$ as functions of normalized frequency with r_o as the parameter. $\frac{L}{a} = 100$.

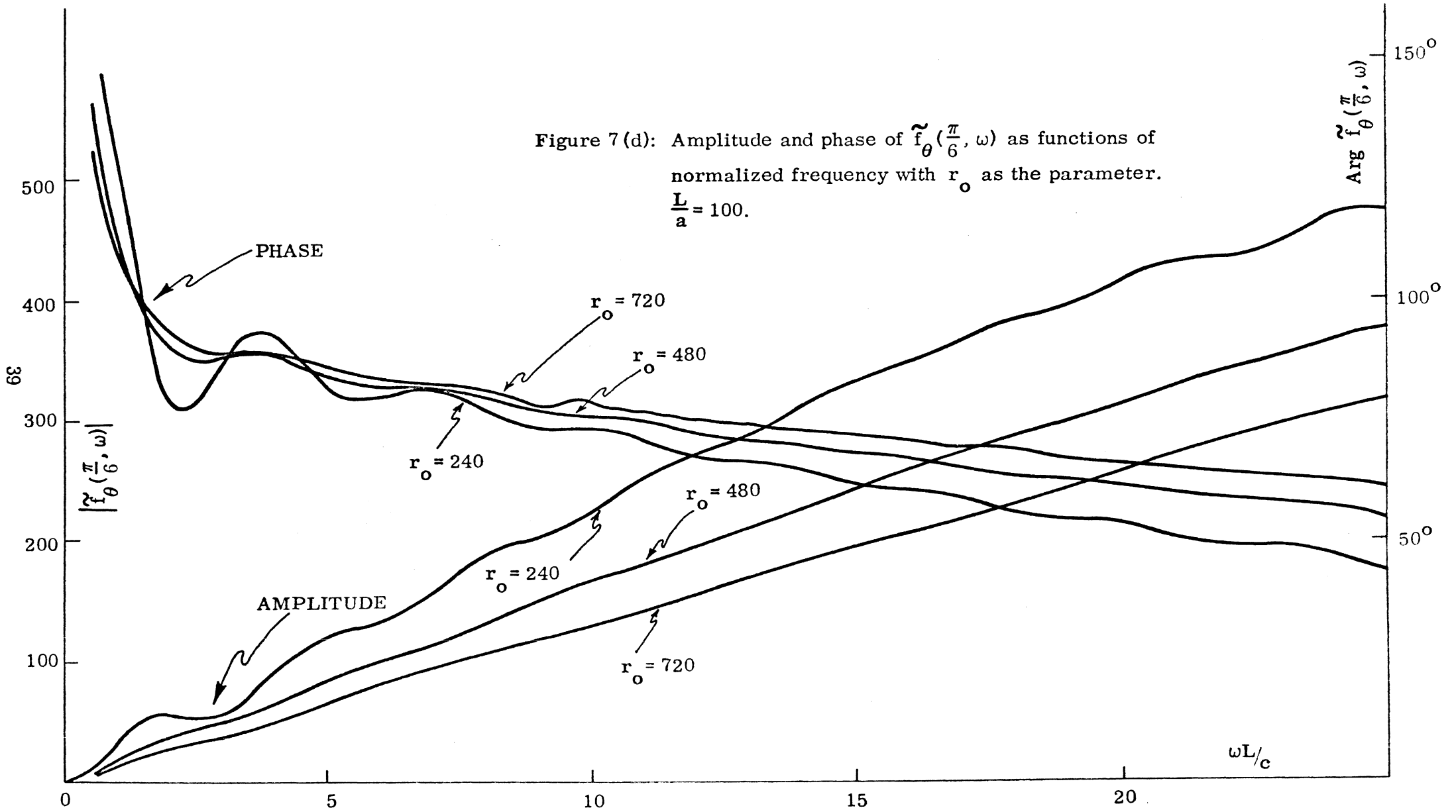
Figure 7 (d): Amplitude and phase of $\tilde{f}_\theta(\frac{\pi}{6}, \omega)$ as functions of normalized frequency with r_o as the parameter. $\frac{L}{a} = 100$.
PHASE
AMPLITUDE
$r_o = 720$
$r_o = 480$
$r_o = 240$
$r_o = 480$
$r_o = 240$
$r_o = 720$
$|\tilde{f}_\theta(\frac{\pi}{6}, \omega)|$
Arg $\tilde{f}_\theta(\frac{\pi}{6}, \omega)$
500
400
300
200
100
39
150°
100°
50°
0
5
10
15
20
$\omega L/c$

VIII

SPECTRAL DENSITY $\tilde{e}_\theta(\theta, \omega)$

The spectral densities $\tilde{e}_\theta(\theta, \omega)$ of the transient waveforms radiated by the step voltage excited antenna under various conditions are discussed in the present section. For three given values of r_o and $\frac{L}{a} = 156$, Figs. 8 a-d show the envelope of $|\tilde{e}_\theta(\theta, \omega)|$ vs. $\omega L/c$ for four values of the observation angle θ. It is found from Fig. 8 that in general the envelope of $|\tilde{e}_\theta(\theta, \omega)|$ vs. $\omega L/c$ has a dominant peak at the low frequency end for all values of θ and r_o. After the initial peak $|\tilde{e}_\theta(\theta, \omega)|$ decays at first rapidly and then slowly with increase of $\omega L/c$. Depending on the values of r_o and θ there also appear some minor peaks in $|\tilde{e}_\theta(\theta, \omega)|$ for large values of $\omega L/c$. For the purpose of discussing the behavior of $|\tilde{e}_\theta(\theta, \omega)|$ let us define the frequency regions larger and smaller than the frequency where the initial peak appears as the high and low frequency regions, respectively. Critical study of the results shown in Fig. 8 reveals the following observations:

(a) As θ decreases away from the broadside direction $\theta = 90^o$, the low frequency content of $|\tilde{e}_\theta(\theta, \omega)|$ decreases and the high frequency content decreases. Also for a given loading, as θ decreases the amplitude of the initial peak decreases. For a given r_o, the position of the initial peak appears to be independent of θ. As θ decreases from 90^o the minor peaks in $\tilde{e}_\theta(\theta, \omega)$ become appreciable.

(b) As r_o increases, the low frequency content of $|\tilde{e}_\theta(\theta, \omega)|$ and the initial peak in $|\tilde{e}_\theta(\theta, \omega)|$ decreases significantly. The rate of decrease of $|\tilde{e}_\theta(\theta, \omega)|$ in the high frequency end appears to be almost independent of r_o.

(c) In the broadside direction the position of the initial peak in $|\tilde{e}_\theta(\theta, \pi/2)|$ increases with an increase in the loading parameter r_o. For example, from Fig. 8 a it is found that the initial peaks are located at $\omega L/c \simeq 1.56$, 2.4 and

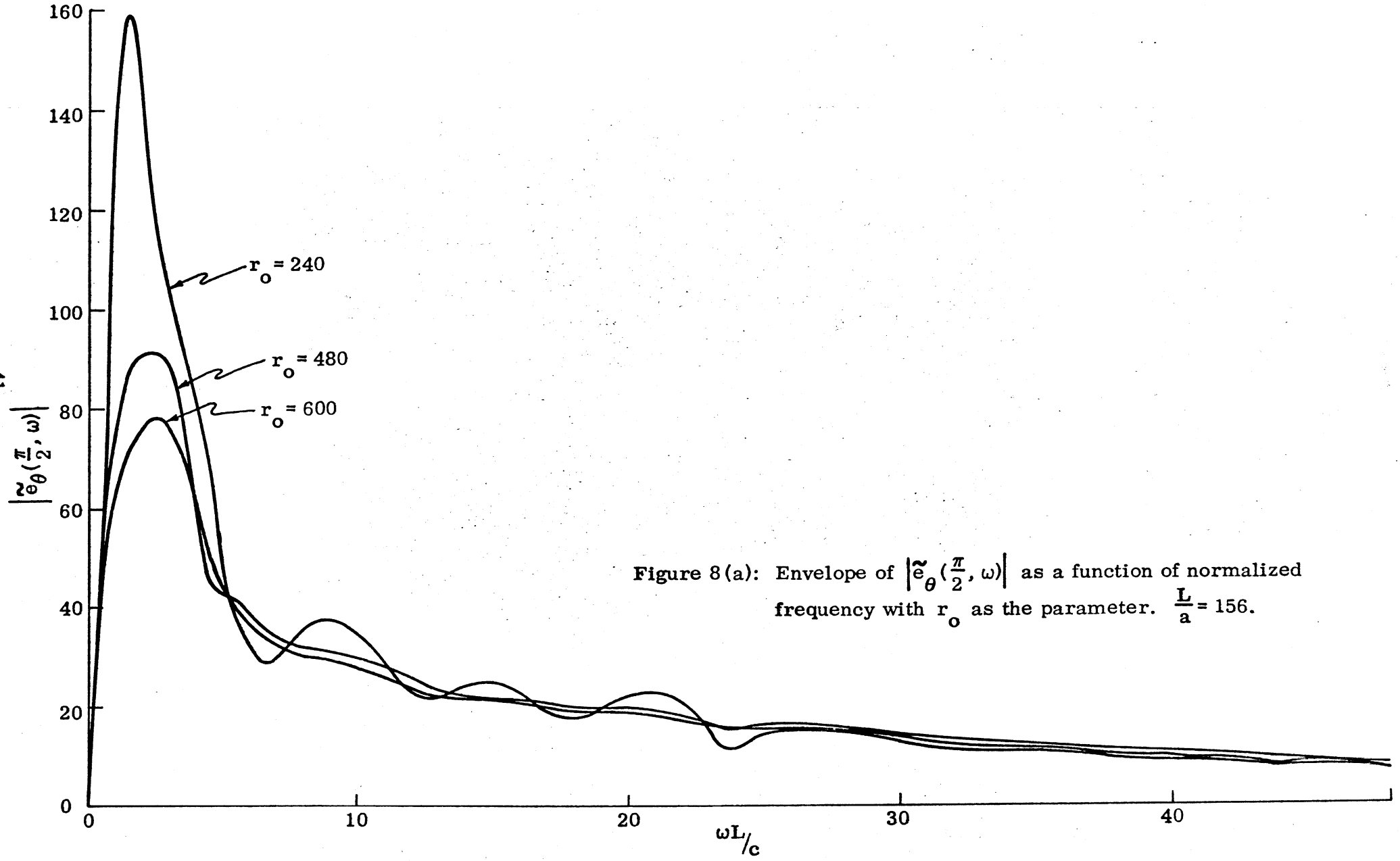

Figure 8(a): Envelope of $\left|\tilde{e}_\theta(\frac{\pi}{2}, \omega)\right|$ as a function of normalized frequency with r_o as the parameter. $\frac{L}{a} = 156$.

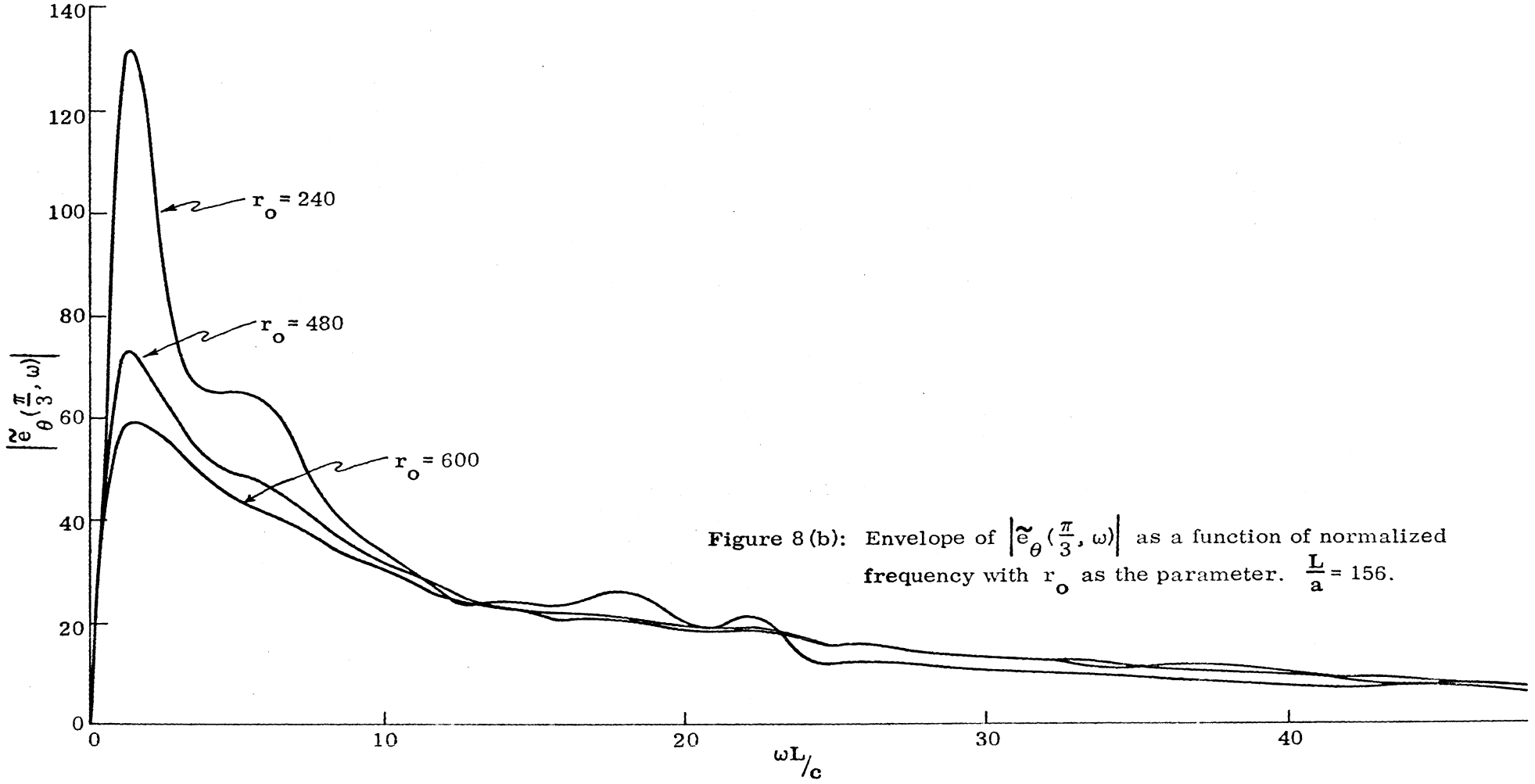

Figure 8 (b): Envelope of $\left|\tilde{e}_\theta(\frac{\pi}{3}, \omega)\right|$ as a function of normalized frequency with r_o as the parameter. $\frac{L}{a} = 156$.

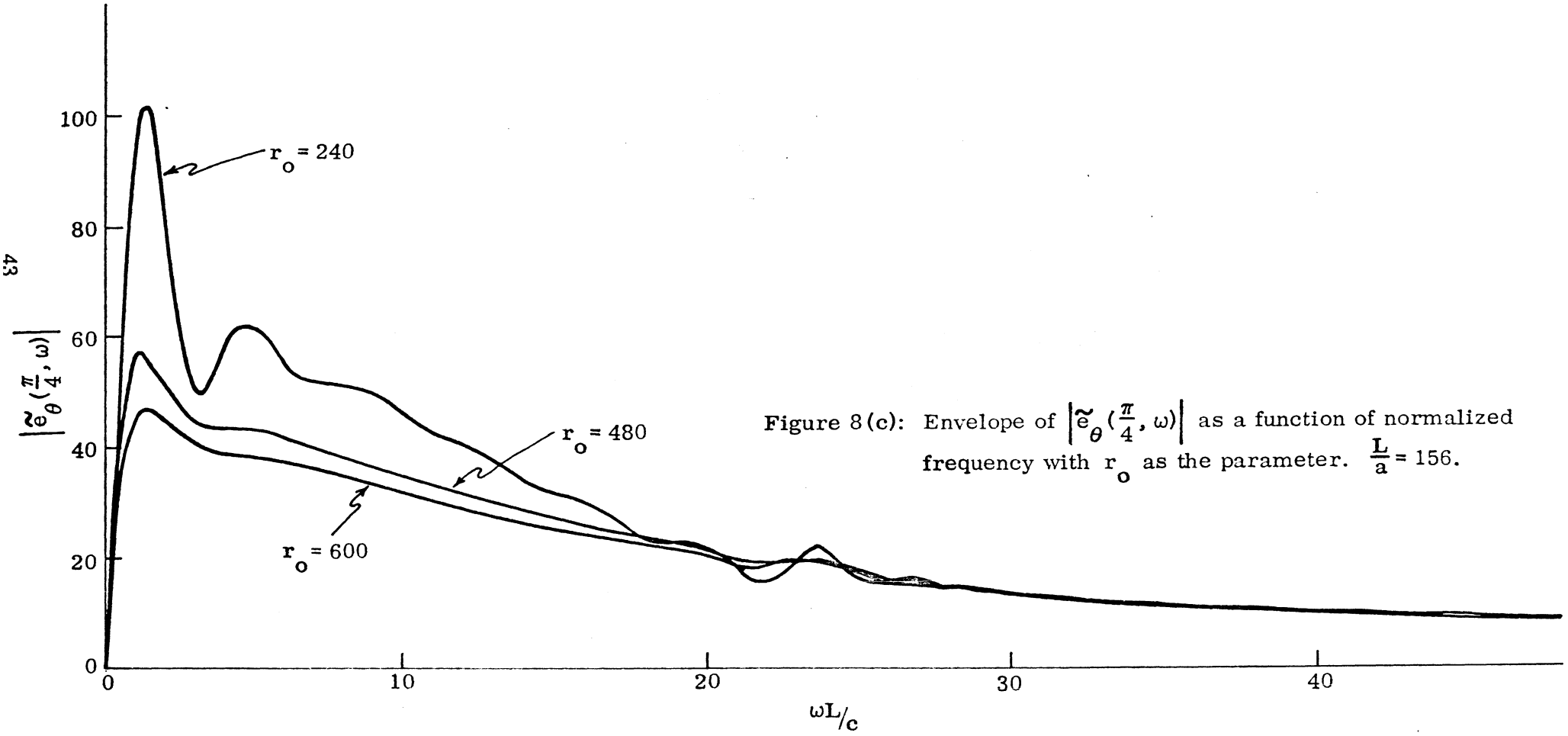

Figure 8(c): Envelope of $\left|\tilde{e}_\theta(\frac{\pi}{4}, \omega)\right|$ as a function of normalized frequency with r_o as the parameter. $\frac{L}{a} = 156$.

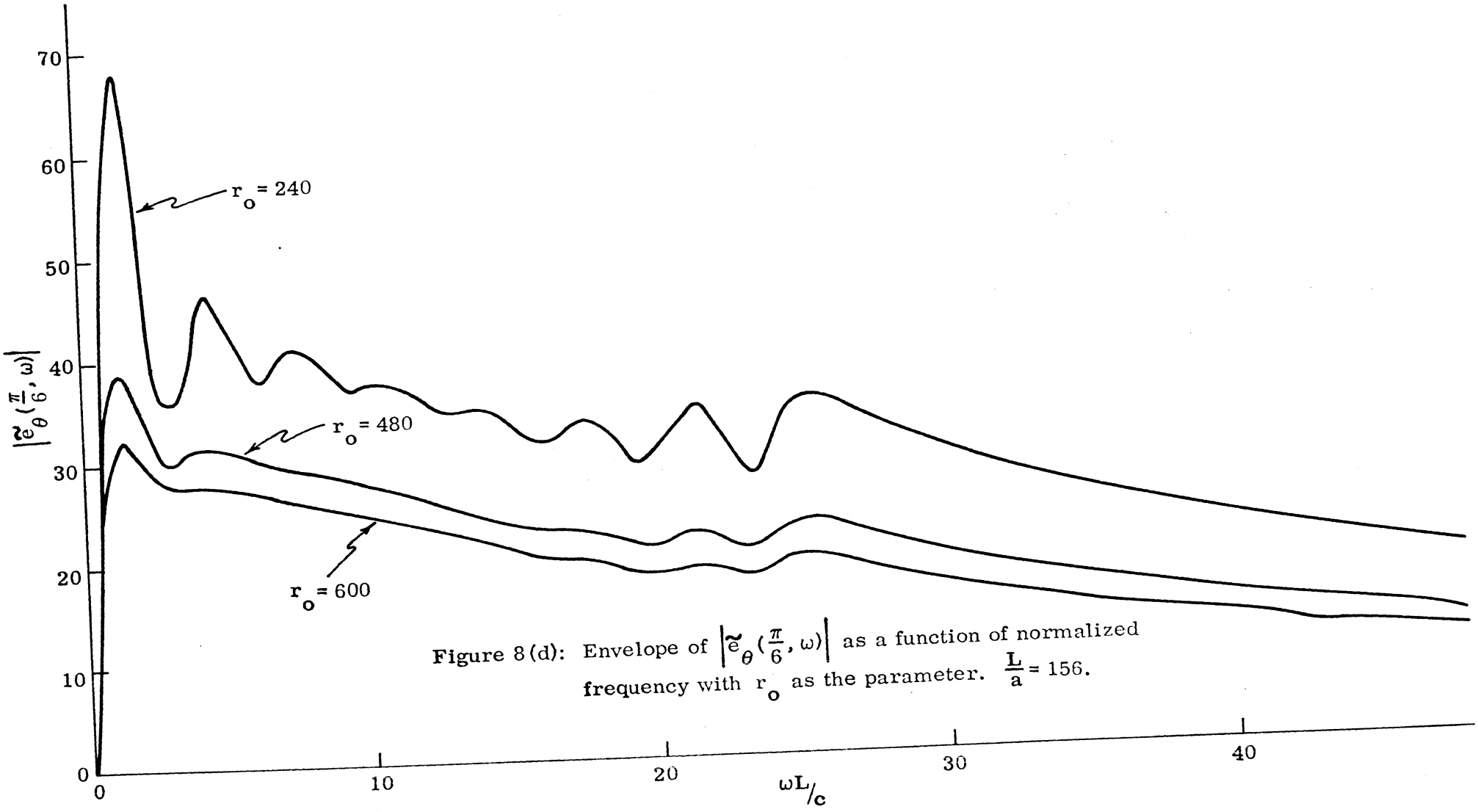

Figure 8(d): Envelope of $\left|\tilde{e}_\theta(\frac{\pi}{6}, \omega)\right|$ as a function of normalized frequency with r_o as the parameter. $\frac{L}{a} = 156$.

2.6 for $r_o = 240$, 480 and 600, respectively.

The above observations will have implications in the corresponding time dependent waveforms. Figures 9 a-d show the corresponding results for the antenna with $\frac{L}{a} = 100$. The general behavior of these results is similar to that of the results shown in Fig. 8. On comparing the results of Figs. 8 and 9 it is found that the decrease of $\frac{L}{a}$ tends to make the minor peaks in $|\tilde{e}_\theta(\theta, \omega)|$ less pronounced.

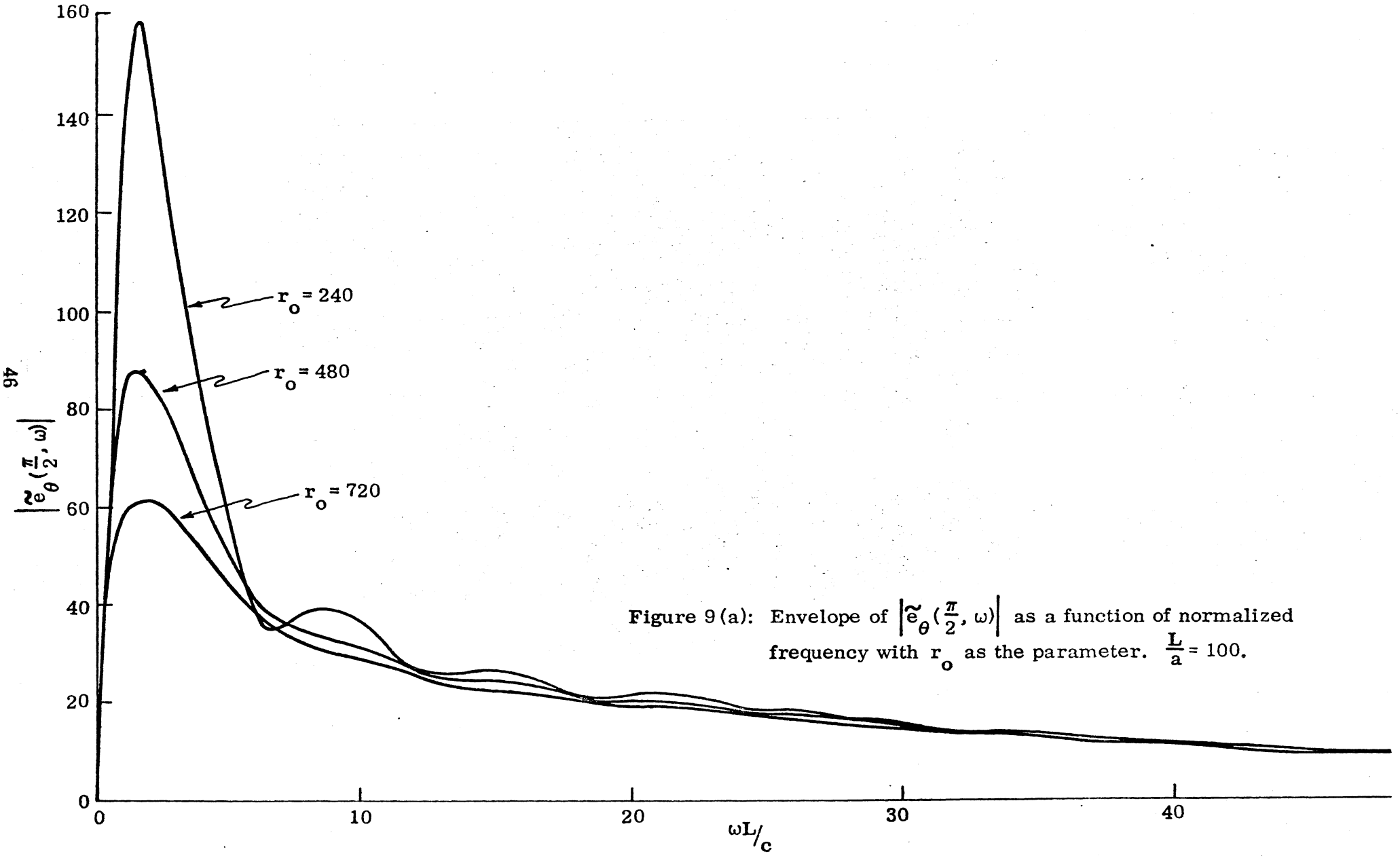

Figure 9(a): Envelope of $\left|\tilde{e}_\theta(\frac{\pi}{2}, \omega)\right|$ as a function of normalized frequency with r_o as the parameter. $\frac{L}{a} = 100$.

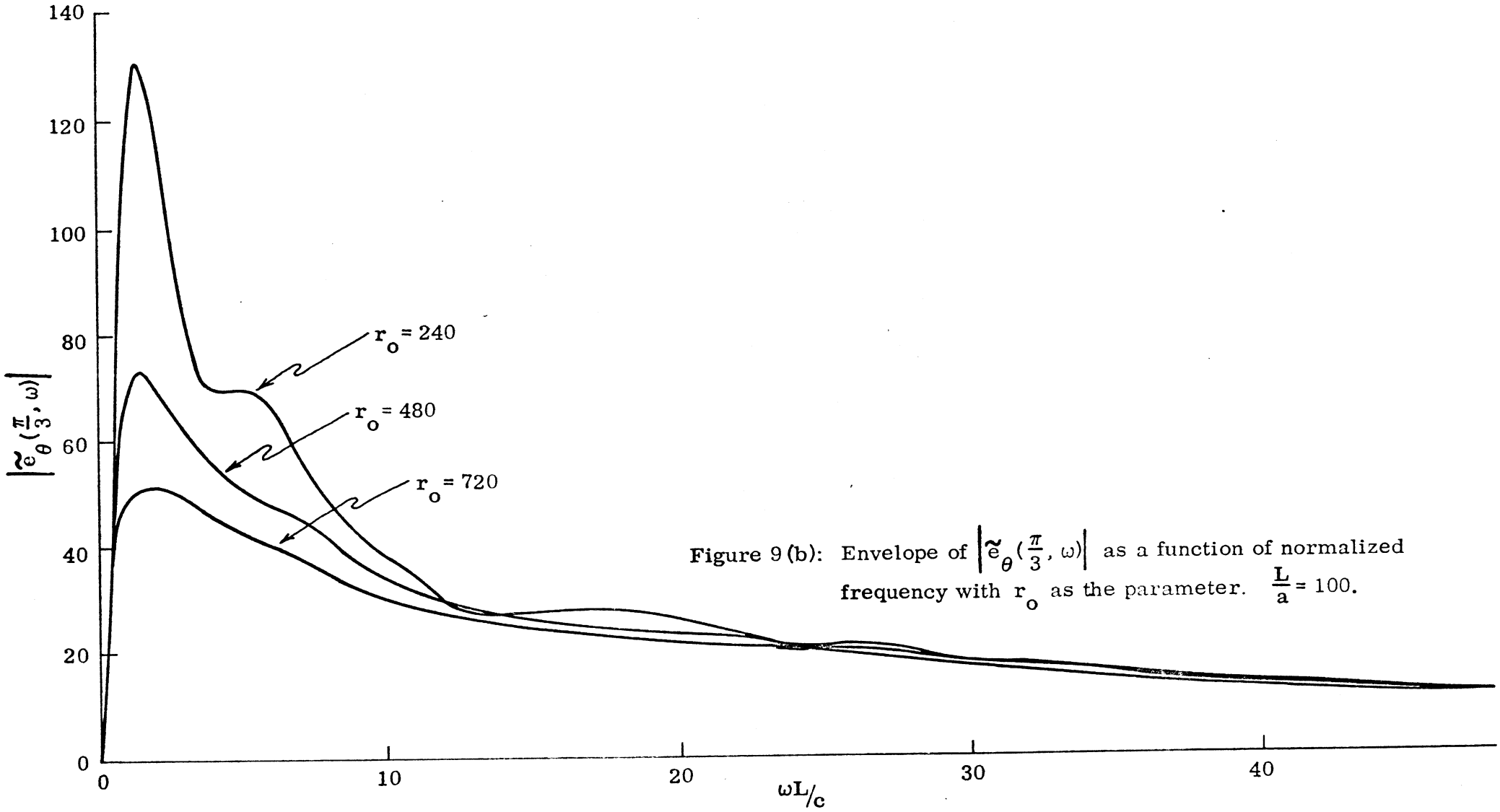

Figure 9 (b): Envelope of $\left|\tilde{e}_\theta(\frac{\pi}{3}, \omega)\right|$ as a function of normalized frequency with r_o as the parameter. $\frac{L}{a} = 100$.

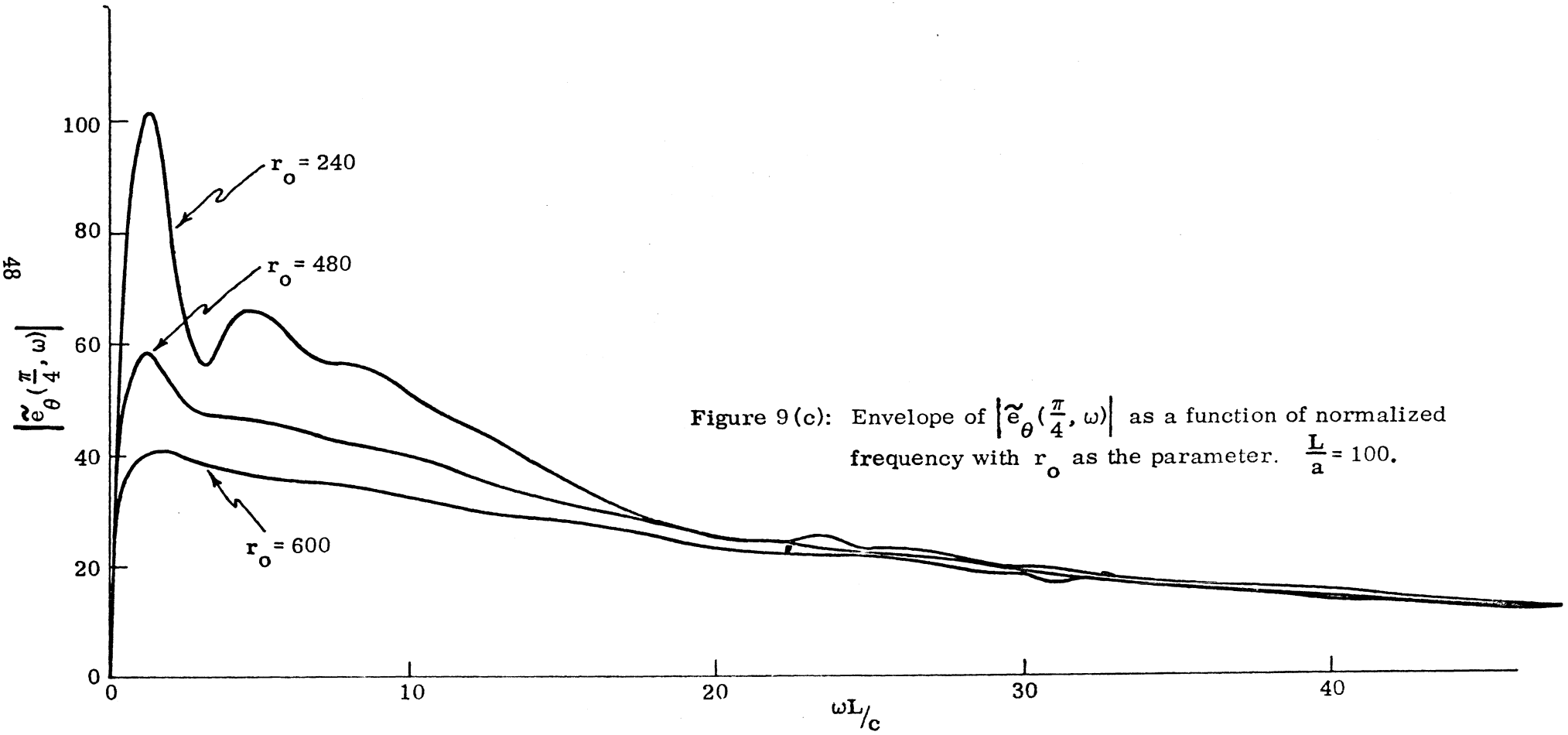

Figure 9(c): Envelope of $\left|\tilde{e}_\theta(\frac{\pi}{4}, \omega)\right|$ as a function of normalized frequency with r_o as the parameter. $\frac{L}{a} = 100$.

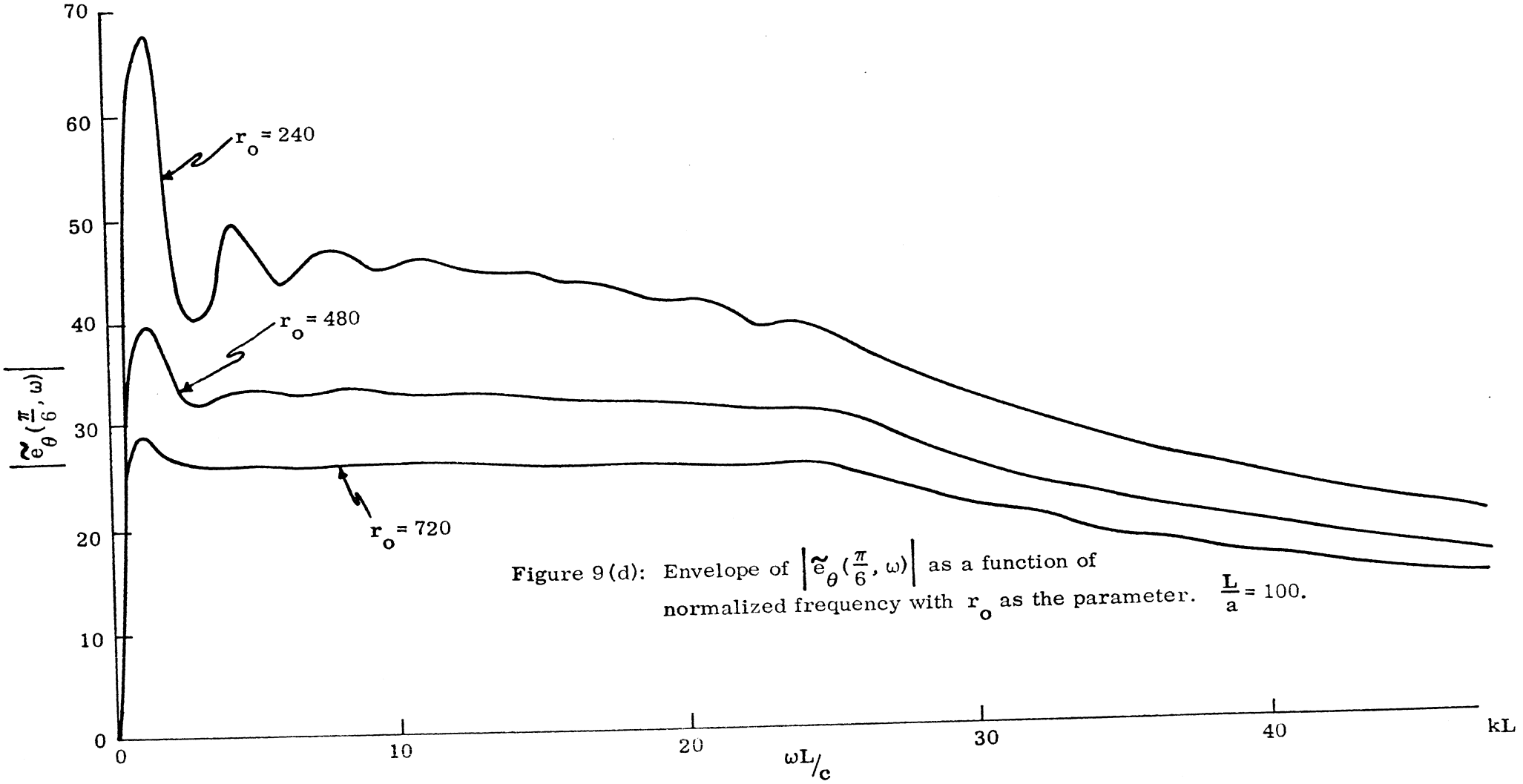

Figure 9(d): Envelope of $\left|\tilde{e}_\theta(\frac{\pi}{6}, \omega)\right|$ as a function of normalized frequency with r_o as the parameter. $\frac{L}{a} = 100.$

IX

TIME DEPENDENT RADIATED WAVEFORM $e_\theta(\theta, t)$

Figures 10 a-d and 11 a-d show the time dependent waveforms in different directions radiated by loaded linear antennas for $\frac{L}{a} = 156$ and 100, respectively, and for various values of the loading parameter r_o. In each case $L = 1$ meter so that $\tau = 3.33$ ns and the width of the input rectangular voltage pulse $T = 20.94$ ns. It has been found that for $T \gtrsim 3\tau$, the time dependent radiated waveforms due to the discontinuities at the two ends of the input pulse do not interfere with each other. Hence, the results shown here for $T = 20.94$ ns may be identified with the transient waveforms radiated by the antenna for step voltage excitation.

The undulations in the waveform for $r_o = 240$ (for example, Fig. 10 a) are attributed to the existence of reflected current waves on the antenna. In general, the existence of reflection effects causes the waveform to cross the zero axis more than once, as can be seen in the $r_o = 240$ waveform in Fig. 10 a. For $r_o >$ the critical value, the radiated waveform has only one zero crossing. It has been found that for a given angle θ, the increase of r_o has the following effects on the radiated waveforms:

(i) decreases the initial amplitude $e_\theta(\theta, t)$. This conclusion is based on the numerical sense. In the asymptotic results obtained from analytical studies it is found[9] that $e_\theta(\theta, t) \propto \frac{1}{\sqrt{t}}$ as $t \to 0$.

(ii) increases the rate of decay of $e_\theta(\theta, t)$ after the initial rise,

(iii) decreases the first zero crossing time t_o and consequently decreases the pulse width,

(iv) decreases the amplitude $e_\theta(\theta, t)$ for $t > {}^{t_o}/_{\tau}$.

For a given value of the loading parameter r_o, the decrease of the observation angle θ from the broadside direction ($\theta = {}^{\pi}/_{2}$) has the following effects on the radiated waveforms:

(i) increases the rate of decrease of $e_\theta(\theta, t)$ from its initial amplitude and decreases the zero crossing time t_o. Consequently, the pulse width decreases,

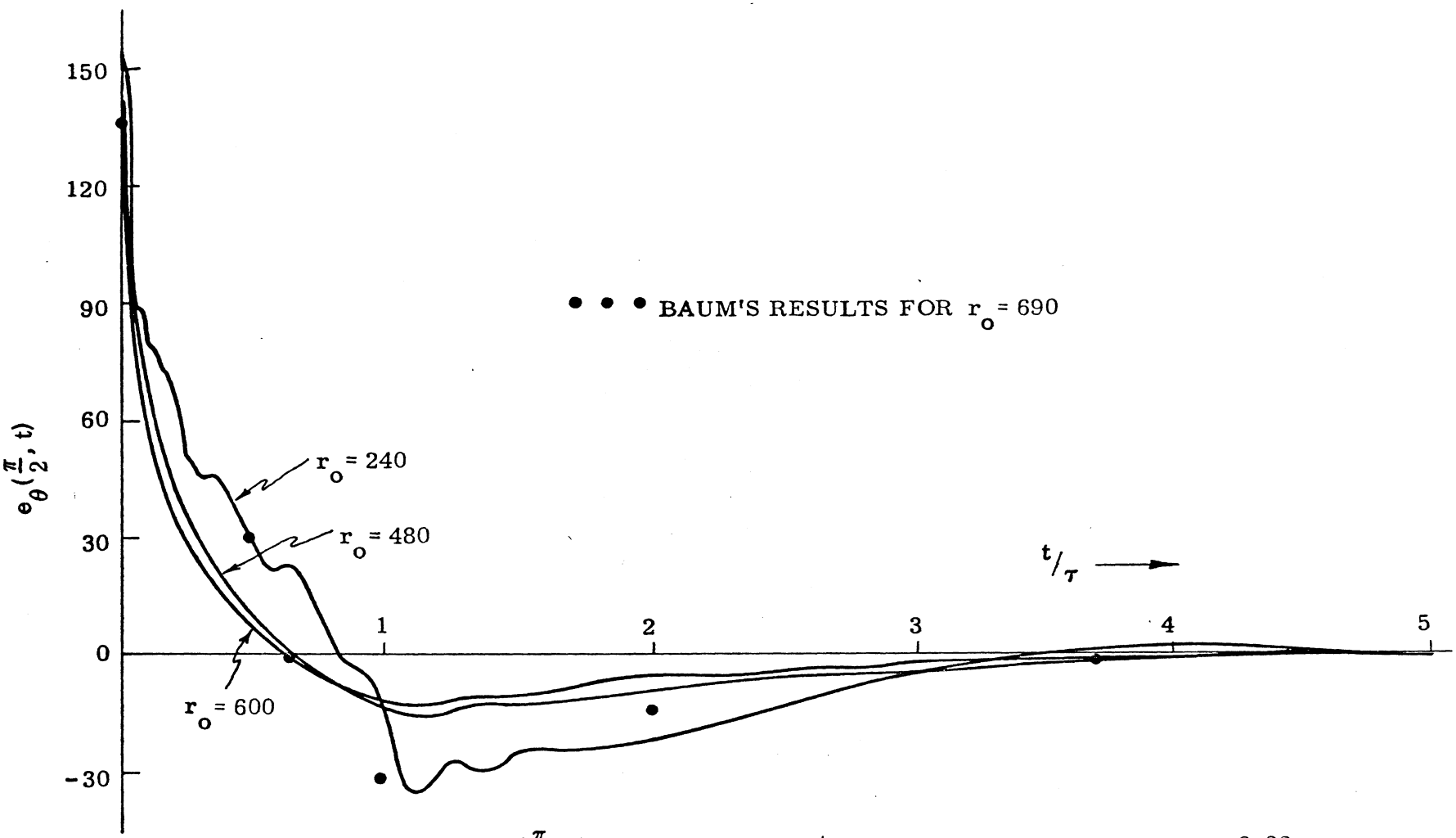

Figure 10(a): $e_\theta(\frac{\pi}{2}, t)$ as a function of t/τ with r_o as the parameter. $\tau = 3.33$ ns, $\frac{T}{\tau} \sim 6$ and $\frac{L}{a} = 156$.

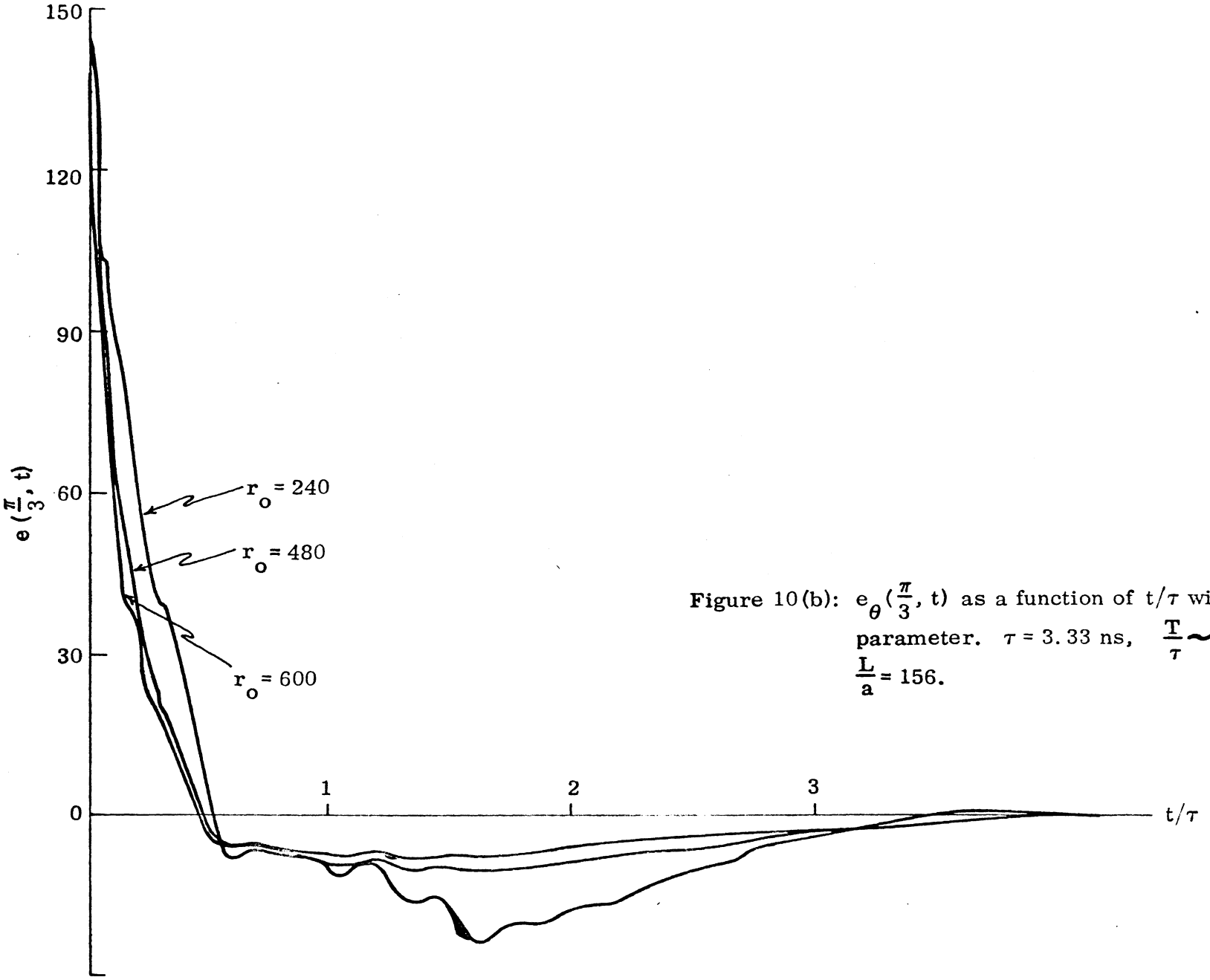

Figure 10(b): $e_\theta(\frac{\pi}{3}, t)$ as a function of t/τ with r_o as the parameter. $\tau = 3.33$ ns, $\frac{T}{\tau} \sim 6$ and $\frac{L}{a} = 156$.

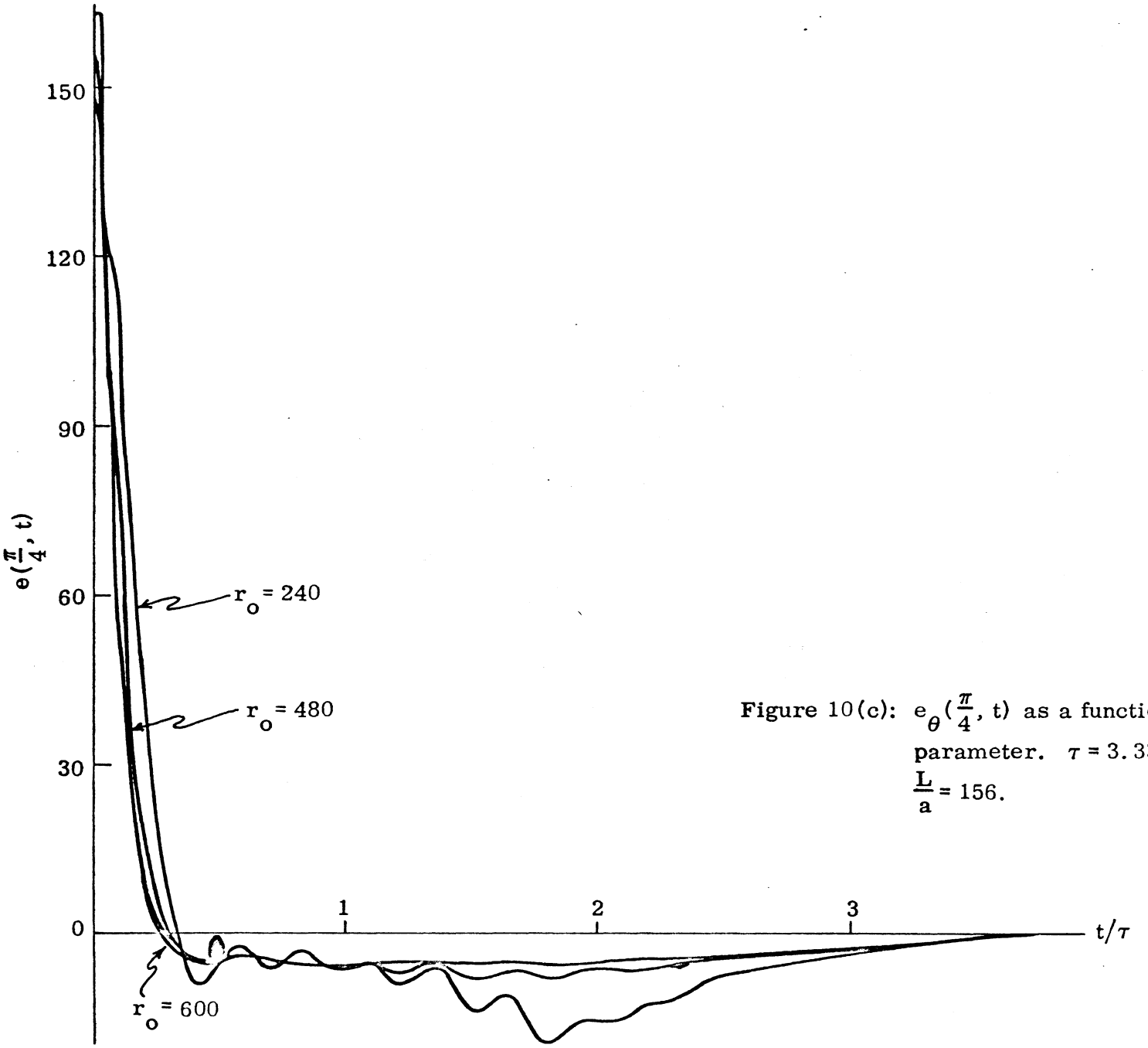

Figure 10(c): $e_\theta(\frac{\pi}{4}, t)$ as a function of t/τ with r_o as the parameter. $\tau = 3.33$ ns, $\frac{T}{\tau} \sim 6$ and $\frac{L}{a} = 156$.

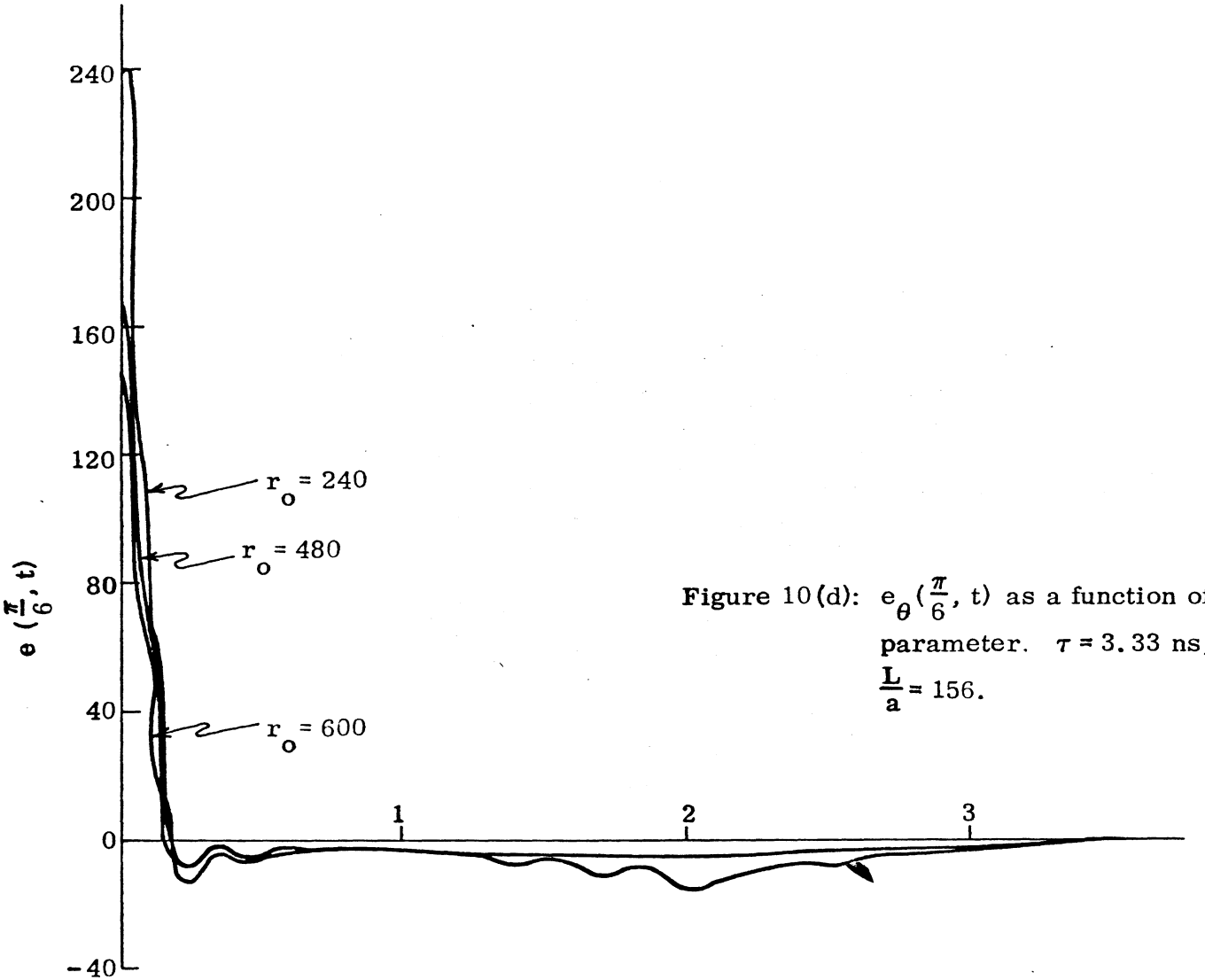

Figure 10(d): $e_\theta(\frac{\pi}{6}, t)$ as a function of t/τ with r_o as the parameter. $\tau = 3.33$ ns, $\frac{T}{\tau} \sim 6$ and $\frac{L}{a} = 156$.

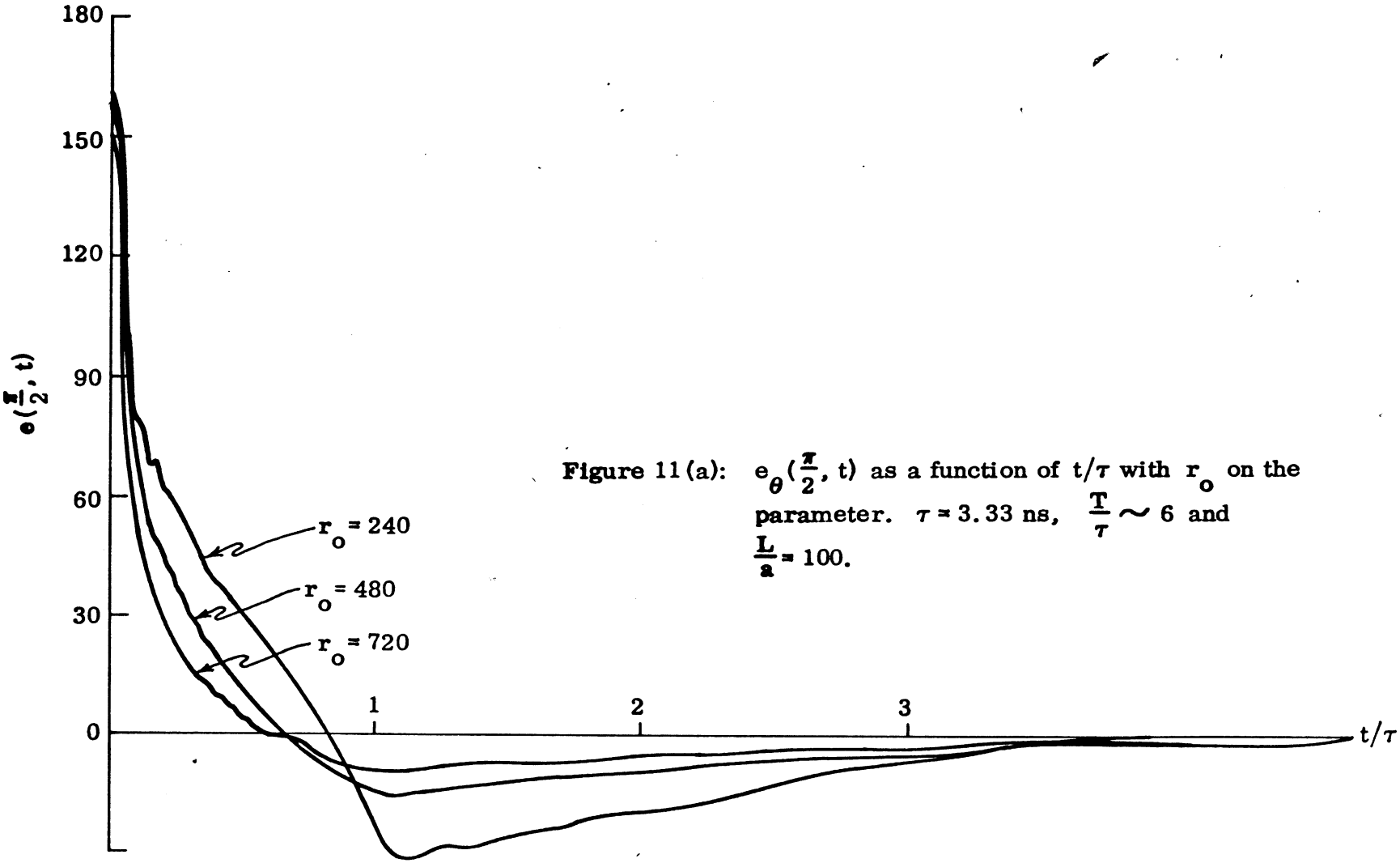

Figure 11 (a): $e_\theta(\frac{\pi}{2}, t)$ as a function of t/τ with r_o on the parameter. $\tau = 3.33$ ns, $\frac{T}{\tau} \sim 6$ and $\frac{L}{a} = 100$.

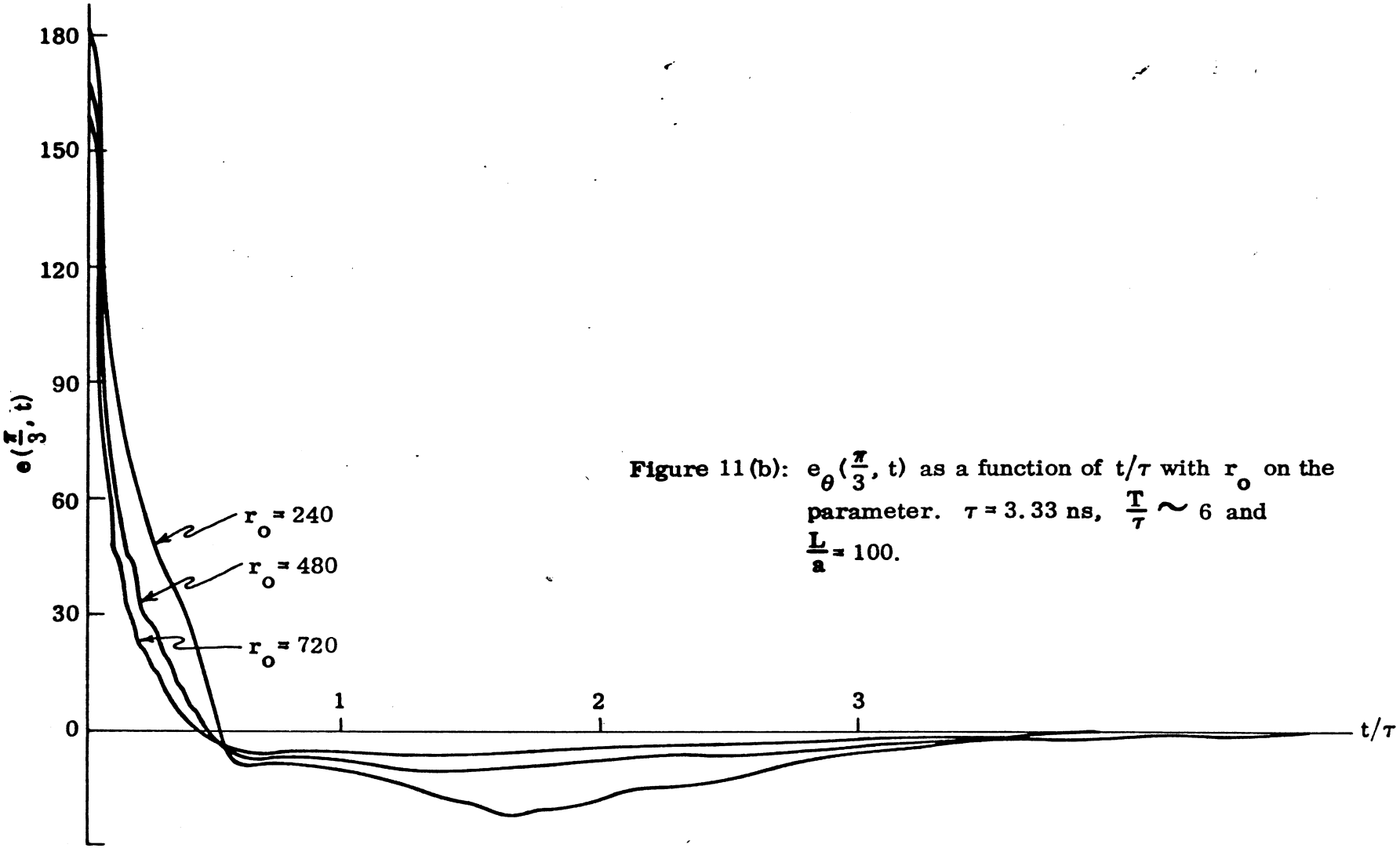

Figure 11(b): $e_\theta(\frac{\pi}{3}, t)$ as a function of t/τ with r_o on the parameter. $\tau = 3.33$ ns, $\frac{T}{\tau} \sim 6$ and $\frac{L}{a} = 100$.

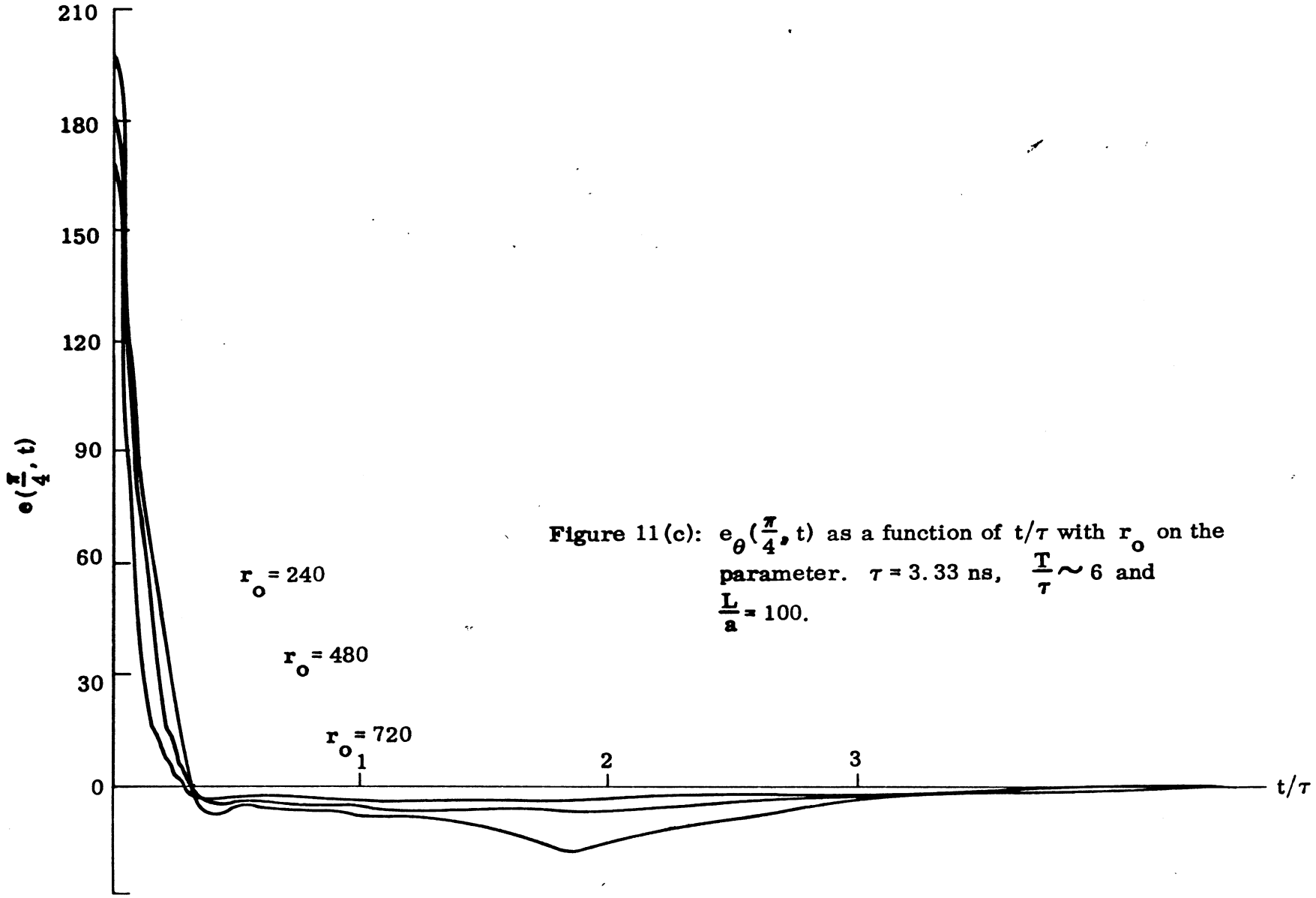

Figure 11(c): $e_\theta(\frac{\pi}{4}, t)$ as a function of t/τ with r_o on the parameter. $\tau = 3.33$ ns, $\frac{T}{\tau} \sim 6$ and $\frac{L}{a} = 100$.

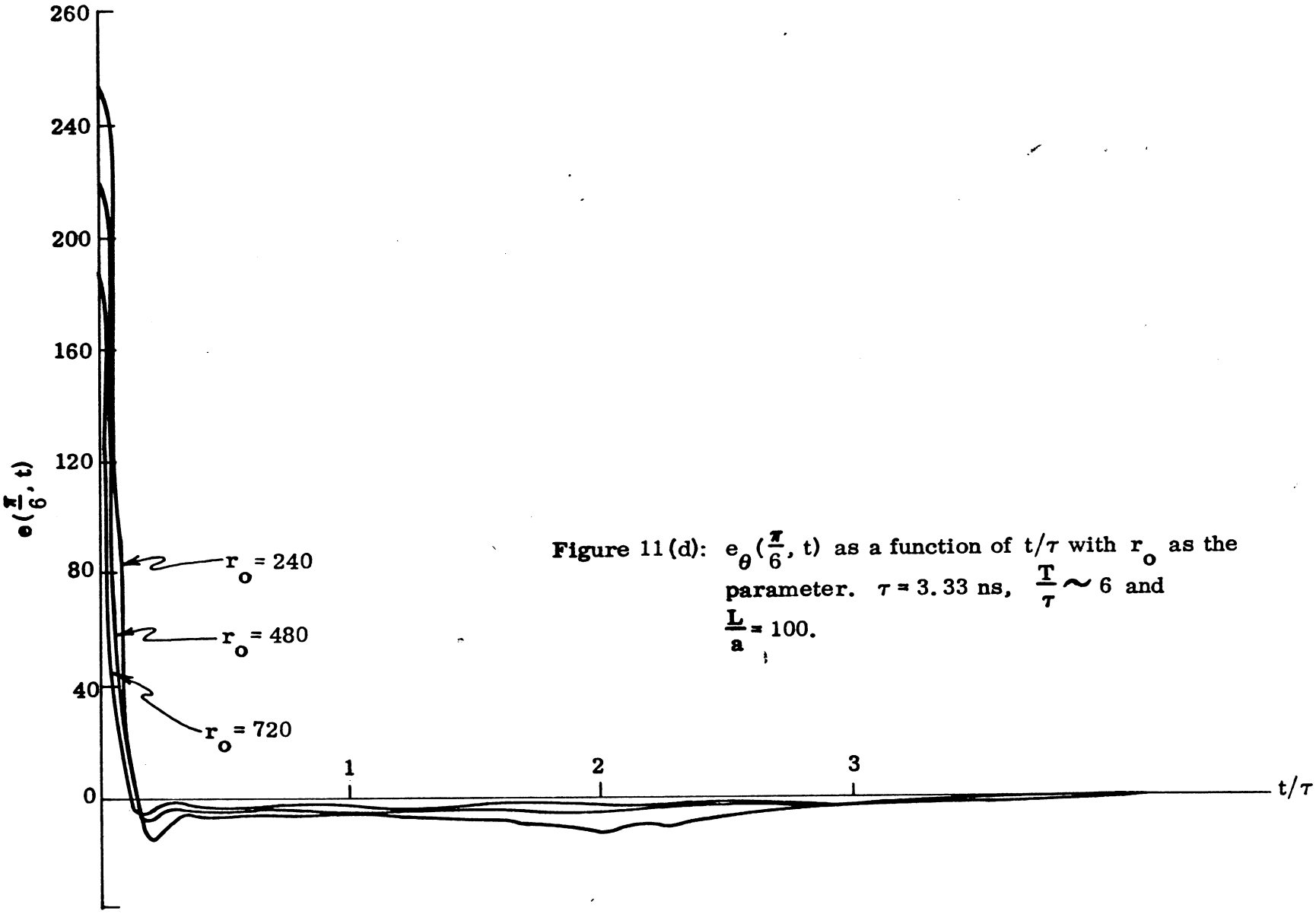

Figure 11 (d): $e_\theta(\frac{\pi}{6}, t)$ as a function of t/τ with r_o as the parameter. $\tau = 3.33$ ns, $\frac{T}{\tau} \sim 6$ and $\frac{L}{a} = 100$.

(ii) the initial amplitude of $e_\theta(\theta, t)$ increases.

The shape of the waveform radiated by a non-reflecting antenna can be adjusted by adjusting the zero-crossing time t_o. For this purpose it is of interest to study the variation of t_o as a function of the various physical parameters of the antenna. Figure 12 shows the normalized zero crossing time as a function of loading with the observation angle θ as the parameter. Notice that results are shown for values of $\frac{L}{a} = 156$ and 100. As far as the zero crossing time is concerned, it is found from Fig. 12 that the decrease of θ has similar effects of t_o as the increase of r_o, i.e., t_o decreases with a decrease of θ. In the broadside direction, t_o is found to decrease with the decrease of $\frac{L}{a}$. In this direction the spread between the t_o values, for the two values of $\frac{L}{a}$ shown, increases with an increase of r_o.

It is interesting to compare the time dependent waveform obtained by numerical means with that obtained by analytical means from the transmission line model of the same antenna as done by Baum[4]. For comparison the waveform produced by the loaded antenna with $r_o = 690$ are superimposed in Fig. 10a. It appears from Fig. 10a that the transmission line model predicts slightly slower decay of $e_\theta(\pi/2, t)$ for $t < t_o$ than our values. For $t > t_o$, the approximate model predicts a higher value of $e_\theta(\pi/2, t)$. These discrepancies may be attributed to the fact that the transmission line model assumes a linearly decaying current amplitude distribution on the antenna. Our numerical investigation indicates that the amplitude of the current distribution of the antenna is, in general, approximately exponentially decaying.

The early time behavior of $e_\theta(\theta, t)$ is compared with Latham and Lee's asymptotic results for uniformly loaded infinite dipole antennas. It is assumed that the infinite dipole antenna is loaded uniformly in such a manner that the internal impedance of the antenna is r_o ohms per meter. We compare the early time behavior of the waveform radiated by this infinite antenna with that

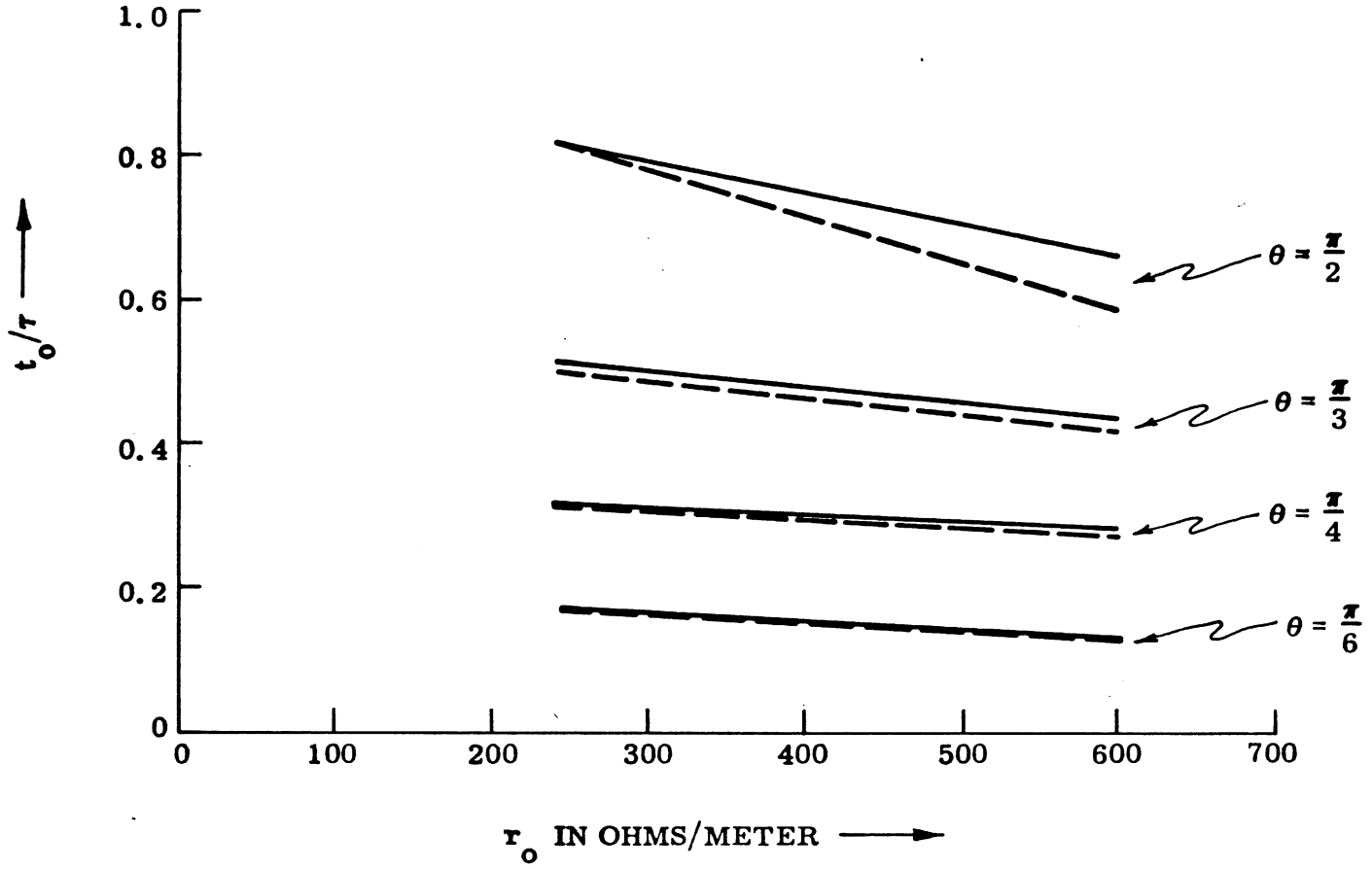

Figure 12: t_o/τ as a function of r_o with θ as the parameter. $\tau = 3.33$ ns, $T = 20.94$ ns;
——— $\frac{L}{a} = 156$, ----- $\frac{L}{a} = 100$.

of the waveform produced by the non-reflectively loaded finite antenna for $t \ll \tau$. It is assumed that the paramater 'a' is the same for both antennas. The results are shown in Fig. 13 which indicates that the Latham and Lee theory predicts faster decay of $e_\theta(\theta, t)$ for early times. With the assumption that the antenna is loaded uniformly with r_o, the decay rate of the field for early times should have been slower. This discrepancy indicates that the nonuniformly loaded finite antenna may not be approximated by a uniformly loaded infinite antenna for $t \ll \tau$.

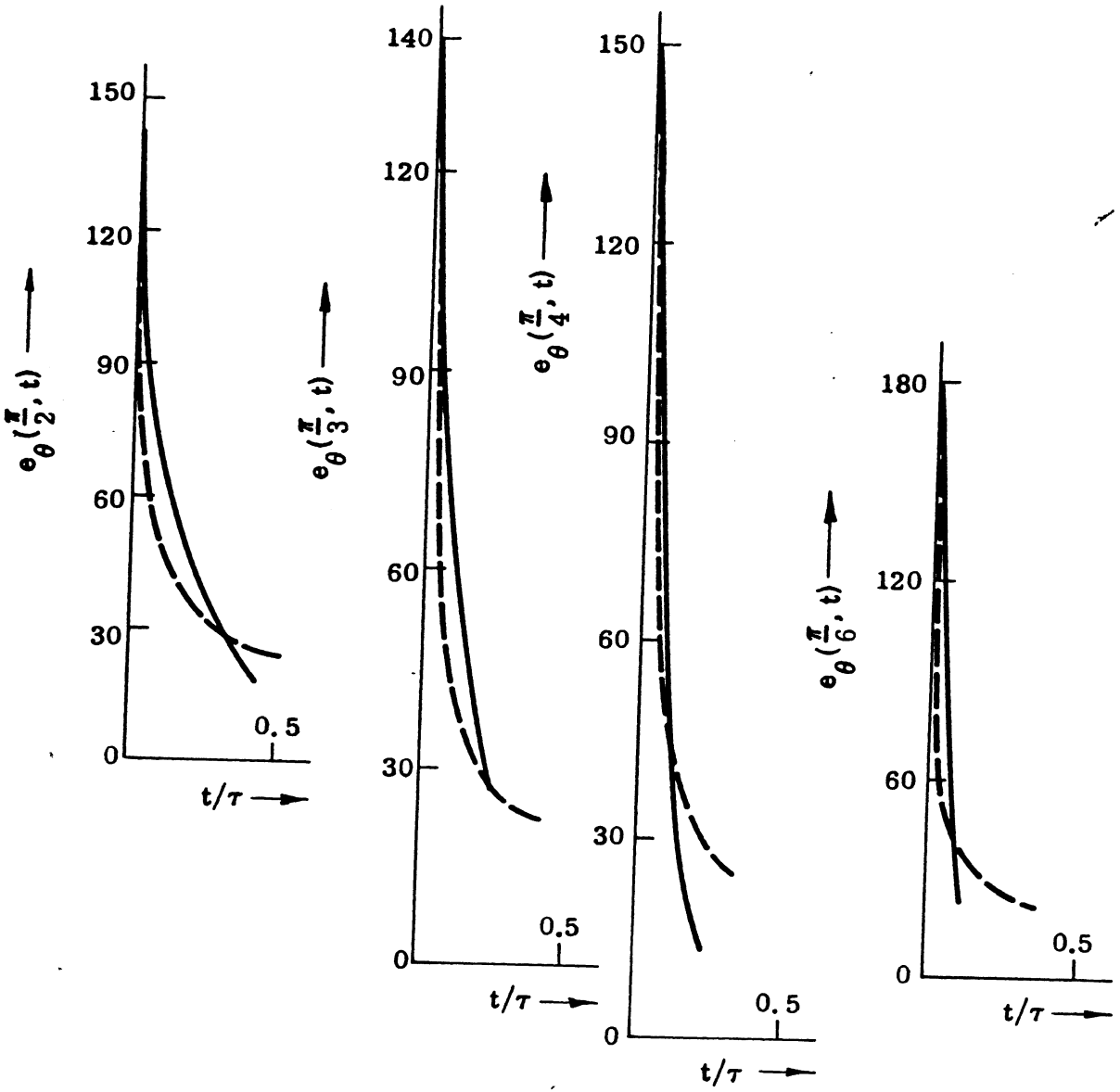

Figure 13: Early time behavior of $e_\theta(\theta, t)$ as a function of time. $\tau = 3.33$ ns, $T = 20.94$ ns, $r_o = 480$, $\frac{L}{a} = 156$. ——— numerical; -------- asymptotic results of Latham and Lee.

X

CONCLUSIONS

Transient waveforms radiated by a step voltage excited resistively loaded linear antenna have been investigated by numerical means. Results have been obtained in different observation angles from the antenna and for different values of the loading parameter. It has been found that for an antenna of given $\frac{L}{a}$ ratio there exists a critical value of the loading parameter. If the loading parameter is equal to or larger than the critical value, the antenna becomes non-reflecting. The waveform produced by the non-reflectively loaded antenna shows only one zero crossing. The zero crossing time as well as the radiated pulse width depends upon the loading parameter and the observation angle. It is hoped that these observations may be found useful in designing a pulse radiating dipole antenna.

It would be interesting to compare our time dependent results with those obtained by the singularity expansion method (SEM). In particular, the relationship of the critical loading parameter with the natural resonant frequency (or frequencies) of the antenna should be investigated.

APPENDIX A

NUMERICAL INVESTIGATION OF WAVEFORMS RADIATED BY A PULSE EXCITED RESISTIVELY LOADED LINEAR ANTENNA

ABSTRACT

The waveforms of the radiation field produced by non-uniformly resistance-loaded finite linear antenna excited by pulse signals are investigated by numerical means. The antenna model considered is a thin cylinder loaded symmetrically and continuously with resistance and is assumed to be excited symmetrically by a slice generator supplying a time dependent signal of arbitrary shape.

Current distributions and the transfer functions of the antenna are obtained as functions of frequency for different values of the loading. Spectral density of the radiated waveform produced by the antenna is obtained as a function of frequency for two different types of input pulse and for different values of loading and widths of input pulse. Finally the radiated waveforms produced by the antenna for the particular input pulse are obtained by using Fast Fourier inversion technique. Far field waveforms are obtained in $\theta = \pi/2$, $\pi/3$, $\pi/4$, $\pi/6$ directions and for different values of the loading. Three selected values of the ratio of the input pulse width to the transit time on the antenna have been used for a Gaussian pulse, while one specific ratio value has been used for a Gamma pulse. pulse.

APPENDIX A

1. INTRODUCTION

The waveforms of the radiation field produced by non-uniformly resistance-loaded finite linear antennas excited by pulse signals are investigated in the present Appendix. The antenna model considered is a thin cylinder loaded symmetrically and continuously with resistance. Emphasis is given to a specific type of loading in which the amount of loading increases continuously towards the antenna end-points. The antenna is excited symmetrically by a slice generator supplying short pulse type time dependent signals.

Analytical solution of such a boundary value problem is extremely difficult. A similar problem with step input excitation has been analyzed by Baum[4] from the transmission line point of view. Analytic results for both unloaded and uniform resistively loaded antennas with step excitations are given by Latham and Lee[9a, 9b] only for cases when the antenna lengths are infinite. Bennett and Auckenthaler[11] reported some results for uniformly loaded finite linear antennas obtained by applying numerical technique directly in the time domain. By applying the moment methods in the time domain Sayre[13] obtained results for unloaded and uniformly loaded linear antennas of finite length. Taylor and his group[14, 15] obtained some results of limited application by numerical means for the case of discretely loaded linear antennas.

In the present Appendix our approach to the problem has been numerical. At first the radiation field produced by the antenna excited by harmonically time dependent slice generators are obtained numerically as a function of frequency. The far field waveforms produced by the pulse excited antenna are then obtained numerically with the help of Fast Fourier Inversion technique.

2. METHODS OF ANALYSIS

In this section we give a brief discussion of the method of analysis and also define a few terms that will be used throughout. Let us assume that the linear antenna of length 2L be aligned along the z-axis of a rectangular coordinate system with origin located at the center of the antenna and that it is excited by a slice generator located at the origin. In the harmonically time dependent case the voltage signal supplied to the antenna by the unit strength slice generator may be represented by $e^{j\omega t}$ volts, where ω is the radian frequency. Let the current distribution on the antenna due to this source be $I(z, \omega)e^{j\omega t}$. The far electric field produced by the antenna under such conditions, will have only a θ-component and may be written formally as follows:

$$F = \tilde{F}_{\theta}(r, \omega)\, e^{j\omega t} \quad , \tag{A.1}$$

where,

$$\tilde{F}_{\theta}(r, \omega) = \frac{j\eta_o \omega \sin\theta}{c\, 4\pi} \frac{e^{-jkr}}{r} \int_{-L}^{L} I(z', \omega)\, e^{jkz' \cos\theta}\, dz' \quad . \tag{A.2}$$

where,

$\eta_o = \sqrt{\frac{\mu_o}{\epsilon_o}}$ = intrinsic impedance of free space,

$c = \frac{1}{\sqrt{\mu_o \epsilon_o}}$ = velocity of light in free space,

$k = \frac{\omega}{c}$ = propagation constant in free space,

(r, θ, ϕ) = the spherical coordinates.

Let the slice generators have arbitrary time dependence such that the input signal voltage envelope in time is represented by $V(t)$. It is now assumed that $V(t)$ is Fourier transformable i.e.

$$V(t) \longleftrightarrow \tilde{V}(\omega) \tag{A.3}$$

which means that the following relations are true,

$$\tilde{V}(\omega) = \int_{-\infty}^{\infty} V(t)\, e^{-j\omega t}\, dt \quad , \tag{A.4}$$

$$V(t) = \frac{1}{2\pi} \int_{-\infty}^{\infty} \tilde{V}(\omega)\, e^{j\omega t}\, d\omega \quad . \tag{A.5}$$

Assuming the linearity of the entire system and using the superposition theorem, it can be shown that the far field produced by the antenna when excited by a slice generator having arbitrary time dependence is given by the following expression:

$$E_\theta\left(r,\ t - \frac{r}{c}\right) = \frac{1}{2\pi} \int_{-\infty}^{\infty} \tilde{F}_\theta(r, \omega)\, \tilde{V}(\omega)\, e^{j\omega t}\, d\omega \quad . \tag{A.6}$$

Notice that E_θ, as given by Eq. (6) is dependent on the parameter r, and also that it is delayed in time with respect to the input by $\frac{r}{c}$ which is the retarded time taken by the signal to reach the far field point from the antenna. It is found convenient sometimes to remove both of these effects from the final result. This can be done as follows.

Let us define a quantity $\tilde{f}_\theta$ which is related to $\tilde{F}_\theta$ in the following manner:

$$\tilde{f}_\theta(\theta, \omega) = r\, \tilde{F}_\theta(r, \omega)\, e^{+j\frac{\omega}{c}r}$$

$$= \frac{j\eta_o \omega \sin\theta}{c\ 4\pi} \int_{-L}^{L} I(z', \omega)\, e^{jkz'\cos\theta}\, dz' \, . \tag{A.7}$$

Similarly we can remove the dependence of r and $\frac{r}{c}$ from Eq. (A.6) and define the following modified field quantity produced by the antenna excited by arbitrary

time dependent input signals:

$$e_\theta(\theta, t) = \frac{1}{2\pi} \int_{-\infty}^{\infty} r\tilde{F}_\theta(r, \omega)\, e^{j\frac{\omega}{c}r}\, \tilde{V}(\omega)\, e^{j\omega t}\, d\omega$$

$$= \frac{1}{2\pi} \int_{-\infty}^{\infty} \tilde{f}_\theta(\theta, \omega)\, \tilde{V}(\omega)\, e^{j\omega t}\, d\omega \quad . \tag{A.8}$$

Thus, formally if the field $\tilde{f}_\theta(\theta, \omega)$ produced by harmonically time dependent excitation of unit strength is known, then the field produced by any other time dependent signal can be obtained with the help of Eq. (A.8). Of course, it is assumed that the time dependent signal must have a Fourier transform.

From the analogy with signal transmission through linear system, we shall call $\tilde{f}_\theta(\theta, \omega)$ given by Eq. (A.7) as the frequency response or the transfer function of the antenna and $\tilde{e}_\theta(\theta, \omega) = \tilde{f}_\theta(\theta, \omega)\, \tilde{V}(\omega)$ as the spectral density function of the radiated signal for arbitrary time dependent input signal. Note that according to this definition $e_\theta(\theta, t)$ and $\tilde{e}_\theta(\theta, \omega)$ constitute a Fourier transform pair, i.e.

$$e_\theta(\theta, t) \leftrightarrow \tilde{e}_\theta(\theta, \omega) \tag{A.9}$$

3. BRIEF OUTLINE OF THE REPORT

It can be seen from Eq. (A.8) that the knowledge of the transfer function of the antenna under consideration is necessary for obtaining the waveform radiated by the antenna for arbitrary signal input. Equation (A.7) indicates that the current distribution $I(z, \omega)$ on the antenna for the harmonic time dependent excitation must be known so that $\tilde{f}_\theta(\theta, \omega)$ may be evaluated. In the following sections we at first determine the current distribution $I(z, \omega)$. This is done by numerically solving a modified form of Hallen's integral equation appropriate for the antenna

under consideration. The transfer function $\tilde{f}_\theta(\theta, \omega)$ is then obtained by numerically evaluating Eq. (A.7). The spectral density function $\tilde{e}_\theta(\theta, \omega)$ is obtained by multiplying the transfer function by the Fourier spectrum of the input signal. Finally the waveform of the radiated signal is obtained by numerically evaluating Eq. (A.8) with the help of Fast Fourier Inversion technique. Two input waveforms have been assumed in this work. They are the Gaussian and gamma pulse represented by

$$V_1(t) = e^{-t^2/2\sigma^2} \tag{A.10a}$$

$$V_2(t) = t\, e^{-dt} U(t) \tag{A.10b}$$

where the constants parameter σ and $1/d$ are proportional to the width of the input pulse and $U(t)$ is the unit step function. The Fourier spectra corresponding to the signals given above are, respectively,

$$\tilde{V}_1(\omega) = \sqrt{2\pi}\ \sigma\, e^{-\omega^2\sigma^2/2} \tag{A.11a}$$

$$\tilde{V}_2(\omega) = \frac{1}{(j\omega + d)^2} \tag{A.11b}$$

4. INTEGRAL EQUATION FOR THE CURRENT DISTRIBUTION $I(z, \omega)$.

In this section we discuss briefly the integral equation for the current distributions on thin cylindrical antennas continuously loaded with resistance. As before we consider a linear antenna of length $2L$ oriented along the z-axis of the Cartesian coordinate system such that $z = 0$ is at the center of the antenna. Assuming azimuthally independent excitation, Hallen's integral equation for the current distribution on a linear antenna excited by harmonically time dependent slice generator of unit strength is given by:

$$\int_{-L}^{L} I(z', \omega)\, G(z, z')\, dz' = B \cos kz - j/\eta_o \int_0^z E_{sz}(\xi) \sin k(z-\xi)\, d\xi \tag{A.12}$$

where, E_{sz} is the electric field on the surface of the antenna due to the induced currents. $G(z, z')$ is the free space Green's function and B is a constant to be determined from the end condition $I(\pm L) = 0$, a is the radius of the antenna element and ϵ_o is the free space permittivity. Since the dipole is electrically thin, i.e., $\frac{a}{\lambda} < 0.01$, we can assume the current to be located at the axis of the antenna. This implies that the Green's function is approximately given by:

$$G(z, z') = \frac{e^{-jk\left[(z-z')^2 + a^2\right]^{1/2}}}{4\pi\left[(z-z')^2 + a^2\right]^{1/2}} \tag{A.13}$$

If the antenna is loaded with distributed resistance $R_s(z)$ ohms/meter, then the total tangential electrical field on the surface of the antenna is given by:

$$E_z(z) = I(z, \omega) R_s(z) = E_{oz}(z) + E_{sz}(z) \tag{A.14}$$

where $E_{oz}(z)$ is the field due to the externally impressed source. In the present case the external source is assumed to be a unit slice generator with harmonic time dependence, i.e.,

$E_{oz}(z) = \delta(z)$, where $\delta(z)$ is the Dirac delta function.

Under these conditions, the integral equation for the current distribution on a symmetrically loaded linear antenna is given by:

$$\int_{-L}^{L} I(z', \omega) \frac{e^{-jk\left[(z-z')^2 + a^2\right]^{1/2}}}{4\pi\left[(z-z')^2 + a^2\right]^{1/2}} dz'$$

$$= B \cos kz - \frac{j}{2\eta_o} \sin k|z| +$$

$$+ j\frac{1}{\eta_o}\int_0^z I(\xi,\omega)\, R_s(\xi) \sin k(z-\xi)\, d\xi \qquad (A.15)$$

Eq.(A.15) is the desired integral equation for the current distribution on the loaded antenna when excited by slice generator of unit strength having harmonic time dependence $e^{j\omega t}$.

In the next section Eq.(A.15) will be solved numerically for some assumed values of $R_s(z)$. The loading function of special importance to us is of the form:

$$R_s(z) = \frac{C}{L-|z|} \qquad (A.16)$$

Note that according to the previous notation of Eq. (12), $r_o = C/L$. For some special value of C, the above loading gives rise to a pure outward traveling wave at a specific frequency on the antenna as discussed by Wu and King[9]. For this reason the antenna with this special loading is sometimes referred to as the reflectionless antenna. Baum[1] arrived at the same conclusion from his transmission line model analysis of this antenna. We shall consider in detail the effects of the loading of the type given by Eq. (A.16) for various values of C including the value corresponding to the reflectionless case.

5. EVALUATION OF THE CURRENT DISTRIBUTION $I(z, \omega)$.

Standard numerical technique[19] is used to solve Eq. (A.15) for $I(z, \omega)$. For this purpose the integral equation is reduced by moments method to the following set of N simultaneous algebraic equations:

$$\sum_{n=1}^{N} \int_{\Delta z_n} I(z', \omega)\, G(z_j, z')\, dz'$$

$$= B \cos k z_j - \frac{j}{2\eta_o} \sin k|z_j|$$

$$+ j/\eta_o \sum_n{}' \int_{\Delta z_n} I(z', \omega) R_s(z') \sin k(z_j - z') \, dz'$$

$$j = 1, 2, \ldots, N \qquad \text{(A.17)}$$

where the summation on the r.h.s. of Eq. (A.17) is interpreted as:

$$\sum_n{}' = - \sum_{n=j}^{N/2} \quad , \quad \text{for } j \leq N/2$$

$$= \sum_{n = N/2 + 1}^{j} \quad \text{for } j > N/2 \qquad \text{(A.18)}$$

and it is assumed that N is an even number and $z' \in \Delta z_n$. Eq. (A.17) implies that the antenna of length 2L is divided into N sections, the numbering of the sections increasing from 1 to N along the antenna length from -L to L as shown in Fig. A-1.

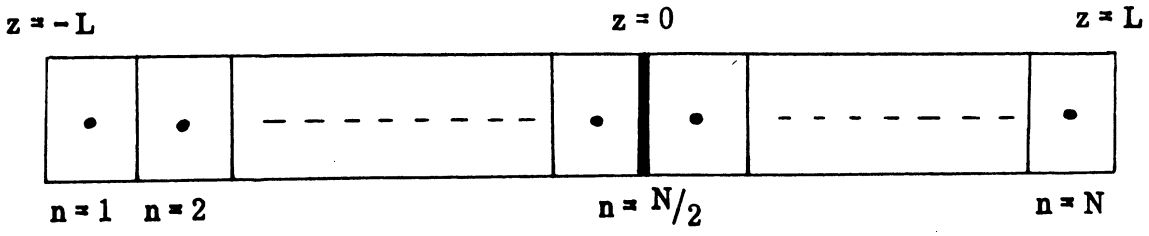

FIG. A-1: Division of the antenna into N-sections.

It remains now to make an appropriate approximation to the current distribution $I(z')$ in each of the sections Δz_n. When the antenna length is small

electrically the usual pulse approximation[20] to the current in each section provides sufficient accuracy. Since our preliminary results have been obtained by this method we give here a brief discussion of the appropriate expressions used in this method.

Pulse Approximation Expressions

In this method the unknown current in each section is assumed to be a rectangular pulse, i.e.,

$$\begin{aligned} I(z') &= I_n \qquad z' \in \Delta z_n \qquad n = 1, 2, \ldots, N \\ &= 0 \qquad \text{elsewhere} \end{aligned} \tag{A.19}$$

Using Eq. (A.19) it can be shown that the general integral equation given by Eq. (A.15) can be transformed into the following N simultaneous equations:

$$\sum_{n=1}^{N} I_n \int_{\Delta z_n} G(z_j, z')\, dz' = B \cos k z_j - \frac{j}{2\eta_0} \sin k(z_j) + j/\eta_0 \sum_{n}{}' I_n \int_{\Delta z_n} R_s(\xi) \sin k(z_j - \xi)\, d\xi \,, \tag{A.20}$$

$$j = 1, 2, \ldots, N$$

where the meaning the summation $\sum_{n}{}'$ is as explained before. In general the unknown current $I(z)$ and the unknown constant B are complex quantities. Let us assume:

$$\left.\begin{aligned} I(z) &= I_R(z) + jI_C(z) \\ B &= B_R + jB_C \end{aligned}\right\} \tag{A.21}$$

Separating Eq. (A. 20) into real and imaginary parts we obtain:

$$\sum_{n=1}^{N} I_{R_n} \int_{\Delta z_n} \frac{\cos k\left[(z_j - z')^2 + a^2\right]^{1/2}}{4\pi\left[(z_j - z')^2 + a^2\right]^{1/2}} dz' - B_R \cos k z_j$$

$$\mp {}^{1}/_{\eta_o} \sum_{n} I_{C_n} \int_{\Delta z_n} R_s(\xi) \sin k(z_j - \xi)\, d\xi$$

$$+ \sum_{n=1}^{N} I_{C_n} \int_{\Delta z_n} \frac{\sin k\left[(z_j - z')^2 + a^2\right]^{1/2}}{4\pi\left[(z_j - z')^2 + a^2\right]^{1/2}} dz' = 0 \qquad \text{(A.22)}$$

$$\sum_{n=1}^{N} I_{C_n} \int_{\Delta z_n} \frac{\cos k\left[(z_j - z')^2 + a^2\right]^{1/2}}{4\pi\left[(z_j - z')^2 + a^2\right]^{1/2}} dz' - B_C \cos k z_j$$

$$\pm {}^{1}/_{\eta_o} \sum_{n} I_{R_n} \int_{\Delta z_n} R_s(\xi) \sin k(z_j - \xi)\, d\xi$$

$$- \sum_{n=1}^{N} I_{R_n} \int_{\Delta z_n} \frac{\sin k\left[(z_j - z')^2 + a^2\right]^{1/2}}{4\pi\left[(z_j - z')^2 + a^2\right]^{1/2}} dz'$$

$$= -\frac{1}{2\eta_o} \sin k|z_j| \quad , \qquad \text{(A.23)}$$

where the upper (lower) sign is used for $j \leq N/2$ $(j > N/2)$ respectively. The above sets of equations along with the end conditions have been solved numerically for the unknown currents. The results will be discussed later. Pulse approximation method provides farily accurate results for small antenna lengths. However, if the antenna length is long electrically, to obtain sufficiently accurate results, N must be chosen very large. Hence to obtain accurate results without taxing the computer capability a different type of approximation should be used. In the next section we discuss such a method.

Quadratic Approximation Expressions

As mentioned before, when the antenna length is large, the computer capability makes it inappropriate to use the pulse approximation method. For the present problem of resistively loaded linear antenna, it is known from theoretical considerations[1, 9] that the current amplitude decreases linearly towards the ends of the antenna.

For this reason, we make the following quadratic approximation to the unknown current in each section:

$$\begin{aligned} I(z') &= A_n + B_n(z'-z_n) + C_n(z'-z_n)^2 \quad , \qquad \text{for } z' \in \Delta z_n \\ &= 0 \, , \qquad\qquad\qquad \text{otherwise,} \end{aligned} \tag{A.24}$$

where A_n, B_n, C_n are three unknown constants. These constants are determined by requiring that the continuation of $I(z')$ expressions given by Eq. (A.24) into the centers of the adjacent sections give the appropriate current values there. Thus we obtain the following:

$$\left.\begin{aligned} I(z_n) &= I_n = A_n \\ I(z_{n-1}) &= I_{n-1} = A_n + B_n(z_{n-1}-z_n) + C_n(z_{n-1}-z_n)^2 \\ I(z_{n+1}) &= I_{n+1} = A_n + B_n(z_{n+1}-z_n) + C_n(z_{n+1}-z_n)^2 \end{aligned}\right\} \tag{A.25}$$

After eliminating A_n, B_n, C_n from Eq. (A.5) with the help of the relations given by Eq. (A.6) we obtain the following recurrence relation for the current in each section:

$$I(z') = I_{n-1} X_n(z') + I_n Y_n(z') + I_{n+1} Z_n(z') \quad , \quad \text{for } z' \epsilon \Delta z_n \qquad (A.26)$$

where

$$X_n(z') = -\frac{z' - z_n}{2\Delta z} + \frac{(z' - z_n)^2}{2\Delta z^2} \quad , \quad z' \epsilon \Delta z_n \qquad (A.27)$$

$$Y_n(z') = 1 - \frac{(z' - z_n)^2}{\Delta z^2} \quad , \quad z' \epsilon \Delta z_n \qquad (A.28)$$

$$Z_n(z') = \frac{z' - z_n}{2\Delta z} + \frac{(z' - z_n)^2}{2\Delta z^2} \quad , \quad z' \epsilon \Delta z_n \quad . \qquad (A.29)$$

where it has been assumed that each subsection is of equal length Δz. In view of the fact that in Eq.(A.26) the value of the current in section Δz_n is related to the currents I_{n+1}, I_{n-1} in the centers of the adjacent sections Δz_{n+1} and Δz_{n-1} respectively, the current values at the center and hence the entire two end sections Δz_1 and Δz_N should be treated separately. For this purpose we make use of the two sets of current coefficients I_{-L}, I_1, I_2 and I_{N-1}, I_N, I_L for obtaining the currents in the sections Δz_1 and Δz_N respectively. Using these two sets of current coefficients we obtain the following from Eq. (A.24) to determine the currents in the two end sections:

$$I(z') = I_1 Y_1'(z') + I_2 Z_1'(z') \quad , \quad \text{for } z' \epsilon \Delta z_1 \qquad (A.30)$$

$$I(z') = I_N Y_N'(z') + I_{N-1} X_N'(z') \quad , \quad \text{for } z' \epsilon \Delta z_N \quad , \qquad (A.31)$$

where,

$$Y_1'(z') = 1 + \frac{(z' - z_1)}{\Delta z} - 2\frac{(z' - z_1)^2}{\Delta z^2} \quad , \qquad z' \epsilon \Delta z_1 \quad , \qquad \text{(A.32)}$$

$$Z_1'(z') = \frac{(z' - z_1)}{3\Delta z} + \frac{2(z' - z_1)^2}{3\Delta z^2} \quad , \qquad z' \epsilon \Delta z_1 \quad , \qquad \text{(A.33)}$$

$$Y_N'(z') = 1 - \frac{z' - z_N}{\Delta z} - \frac{2(z' - z_N)^2}{\Delta z^2} \quad , \qquad z' \epsilon \Delta z_N \quad , \qquad \text{(A.34)}$$

$$X_N'(z') = -\frac{(z' - z_N)}{3\Delta z} + \frac{2(z' - z_N)^2}{3\Delta z^2} \quad , \qquad z' \epsilon \Delta z_N \quad . \qquad \text{(A.35)}$$

After substituting Eqs. (A.26)–(A.35) into Eq. (A.17) the following set of N simultaneous equations are obtained:

$$I_1\left[\int_{\Delta z_1} Y_1'(z')G(z', z_j)\,dz' + \int_{\Delta z_2} X_2(z')G(z', z_j)\,dz'\right]$$

$$+ I_2\left[\int_{\Delta z_1} Z_1'(z')G(z', z_j)\,dz' + \int_{\Delta z_2} Y_2(z')G(z', z_j)\,dz' + \int_{\Delta z_3} X_3(z')G(z', z_j)\,dz'\right]$$

$$+ \sum_{n=3}^{N-2} I_n\left[\int_{\Delta z_{n-1}} Z_{n-1}(z')G(z', z_j)dz' + \int_{\Delta z_n} Y_n(z')G(z', z_j)dz' + \int_{\Delta z_{n+1}} X_{n+1}(z')G(z', z_j)dz\right.$$

$$+ I_{N-1}\left[\int_{\Delta z_{N-2}} Z_{N-2}(z')G(z', z_j)\,dz' + \int_{\Delta z_{N-1}} Y_{N-1}(z')G(z', z_j)\,dz' + \right.$$

$$\left. + \int_{\Delta z_N} X_N'(z')G(z', z_j)\,dz'\right] +$$

$$+ I_N \left[\int_{\Delta z_N} Y'_N(z')G(z', z_j)dz' + \int_{\Delta z_{N-1}} Z_{N-1}(z')G(z', z_j)\,dz' \right]$$

$$= B \cos k z_j - \frac{j V_o}{2\eta_o} \sin k|z_j| + \frac{j\omega\epsilon}{k} \left\{ H_{1,j} I_1 \left[\int_{\Delta z_1} Y'_1(z')F(z')dz' + \int_{\Delta z_2} X_2(z')F(z')dz' \right] \right.$$

$$+ H_{2j} I_2 \left[\int_{\Delta z_1} Z'_1(z')F(z')dz' + \int_{\Delta z_2} Y_2(z')F(z')dz' + \int_{\Delta z_3} X_3(z')F(z')dz' \right]$$

$$+ \sum_{n=3}^{N/2} H_{n,j} I_n \left[\int_{\Delta z_{n-1}} Z_{n-1}(z')F(z')dz' + \int_{\Delta z_n} Y_n(z')F(z')dz' \right.$$

$$\left. \left. + \int_{\Delta z_{n+1}} X_{n+1}(z')F(z')dz' \right] \right\}, \quad \text{for } j \leq N/2$$

$$+ {}^{j}/_{\eta_o} \left\{ \sum_{n=\frac{N}{2}+1}^{j} H_{n,j} I_n \left[\int_{\Delta z_{n-1}} Z_{n-1}(z')F(z')dz' + \int_{\Delta z_n} Y_{n+1}(z')F(z')dz' + \int_{\Delta z_{n+1}} X_{n+1}(z')F(z')dz' \right] \right.$$

$$+ H_{N-1,j} I_{N-1} \left[\int_{\Delta z_{N-2}} Z_{N-2}(z')F(z')dz' + \int_{\Delta z_{N-1}} Y_{N-1}(z')F(z')dz' \right.$$

$$\left. + \int_{\Delta z_N} X'_N(z')F(z')dz' \right]$$

$$\left. + H_{N,j} I_N \left[\int_{\Delta z_{N-1}} Z_{N-1}(z')F(z')dz' + \int_{\Delta z_N} Y'_N(z')F(z')dz' \right] \right\}, \quad \text{(A.36)}$$

for $j > N/2$,

j (as the subscript) $= 1, 2, 3, \ldots, N$

where

$$H_{m,j} \begin{cases} 1, & \text{for } j \geq m \\ 0, & \text{for } j < m \end{cases}$$

$$F(z') = \frac{C}{L-|z'|} \sin k(z_j - z') \quad . \tag{A.37}$$

The above is a set of N algebraic equations involving the N unknown current coefficients $I_1, I_2, \ldots, I_N$ and the extra unknown constant B which is to be determined by applying the end condition $I(-L) = 0$. By using Taylor's expansion for the currents at the centers of the first three sections we obtain the following:

$$I(z_1) = I_1 = (z_1+L)I'(-L) + \frac{(z_1+L)^2}{2} I''(-L) \quad , \tag{A.38}$$

$$I(z_2) = I_2 = (z_2+L)I'(-L) + \frac{(z_2+L)^2}{2} I''(-L) \quad , \tag{A.39}$$

$$I(z_3) = I_3 = (z_3+L)I'(-L) + \frac{(z_3+L)^2}{2} I''(-L) \quad , \tag{A.40}$$

where we have already used the fact $I(-L) = 0$. The derivative terms in (A.38)-(A.40) can be eliminated and we obtain the following extra equation:

$$3I_3 - 10I_2 + 15I_1 = 0 \quad . \tag{A.41}$$

Thus Eqs. (A.36) and (A.41) constitute a set of N+1 equations for the N+1 unknowns (i.e., $I_1, I_2, \ldots, I_N$, B). The system can now be solved by standard means.

If the end condition is applied at the other end of the antenna, i.e. $I(+L) = 0$, then the following equations should be used instead of Eq. (A.41):

$$15I_N - 10I_{N-1} + 3I_{N-2} = 0 \quad . \tag{A.42}$$

Eqs. (A.41) and (A.42) will be referred to as the 3-point end condition formula. In order to estimate the accuracy of the results, computation has also been done by using 4-point and 2-point end condition expressions. These have been obtained by applying the end condition $I(+L) = 0$ and retaining 4 and 2 terms in the Taylor's expansion respectively. The relevant expressions for these two cases are:

$$-5I_{N-3} + 21I_{N-2} - 35I_{N-1} + 35I_N = 0 \quad , \tag{A.43}$$

$$3I_N - I_{N-1} = 0 \quad . \tag{A.44}$$

The above completes the theoretical discussion on the numerical procedure to be followed in the determination of the current distribution for the loaded linear antenna.

6. EVALUATION OF THE TRANSFER FUNCTION $\tilde{f}_\theta(\theta, \omega)$

In the previous section we discussed the numerical method of obtaining the current distribution $I(z, \omega)$ on the antenna for the harmonic time dependence case. After introducing the sampled values of $I(z, \omega)$ in Eq. (A.7), $f_\theta(\theta, \omega)$ is obtained numerically with the help of the following equation:

$$\tilde{f}_\theta(\theta, \omega) = j\frac{\omega\eta_o}{c} \cdot \frac{\sin\theta}{4\pi} \sum_n I_n e^{j\frac{\omega}{c} z_n \cos\theta} \Delta z_n \quad , \tag{A.45}$$

where we have used the notation $I(z_n) = I_n$ and $z' = z_n$ is the coordinate at the center of the section Δz_n. The pulse approximation is good for transfer function calculation because the current distribution is linear as mentioned before.

7. PRELIMINARY NUMERICAL RESULTS

In this section we discuss briefly some preliminary numerical results

obtained for a few simple cases. The motivation behind this section has been mainly to ascertain the correctness and accuracy of the numerical technique used for later investigation.

7.1 Uniformly Loaded Antenna $L = \lambda/2$.

For the case of uniformly loaded dipole of total length $2L = \lambda$, there is no variation of loading along the antenna, i.e., $R_s(z) = r^i$ ohms/meter. Fig. A-2 shows the real and imaginary parts of the current distribution on a uniformly loaded dipole for two values of r^i. These results have been obtained by using Eqs. (21)-(23) with $N = 30$. In Fig. A-2 we have used the notation $\phi_i = 2\lambda r^i/\eta_o$ where λ is the wavelength and η_o is the intrinsic impedance of free space. The results shown here compare very well with those of King, et. al.[12]. Thus it proves the correctness of the computation followed here.

7.2 Non-Reflecting Loaded Case $L = \lambda$.

Here consider a one wavelength long linear antenna non-uniformly loaded according to Eq. (A. 16). The radius a of the antenna element is chosen such that $\Omega = 2\ell n\frac{2L}{a} = 11.5$. This value of Ω is chosen so that our results may be compared with some available published results. Wu and King[3] predicted from theoretical considerations that a purely outgoing traveling wave of current is sustained on the antenna loaded according to Eq. (A. 16) provided the constant C is chosen to be equal to $60\,\psi\alpha$ with $\psi\alpha = 5.3$. In other words the antenna considered in this section is loaded as follows:

$$R_s(z) = \frac{60\,\psi\alpha}{L - |z|} \quad , \tag{A.46}$$

with $\psi\alpha = 5.3$ (Note: in this notation, $r_o = 60\,\psi\alpha/L$). The $\psi\alpha$ notation is used here to correspond to that used in Wu and King[9]. Figure A-3 gives the amplitude of the current distribution on the antenna as obtained by numerical computation using pulse approximation with $N = 30$. The current distributions obtained for the same antenna by Taylor[23] and Shen[18] are also shown in Figure A-3 for compari-

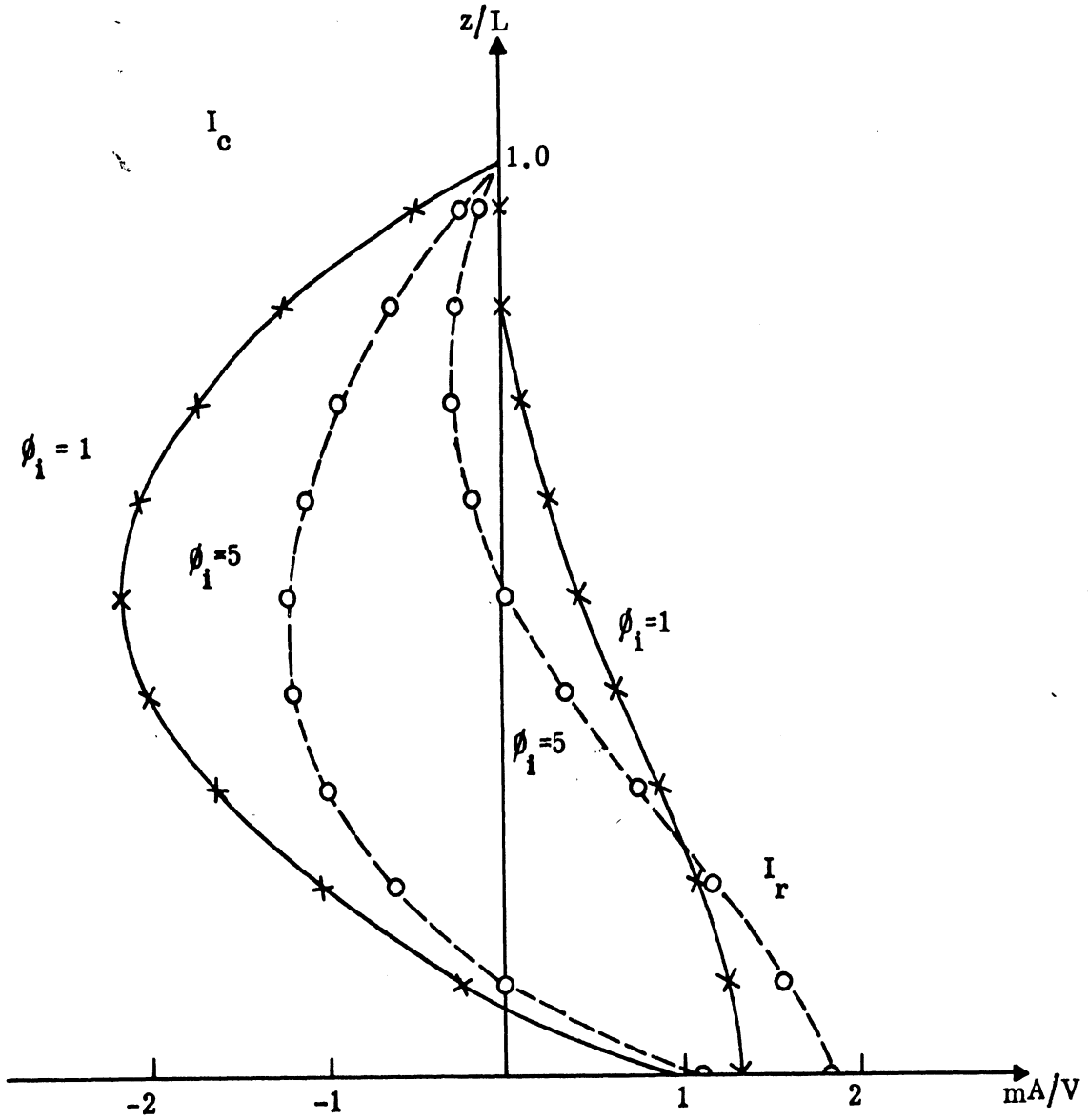

FIG. A-2: Real (I_r) and imaginary (I_c) parts of the current distribution on uniformly loaded dipole. $L=\pi/2$, $\Omega=9.92$, $\phi_i = 2\lambda r^i/\eta_0$.

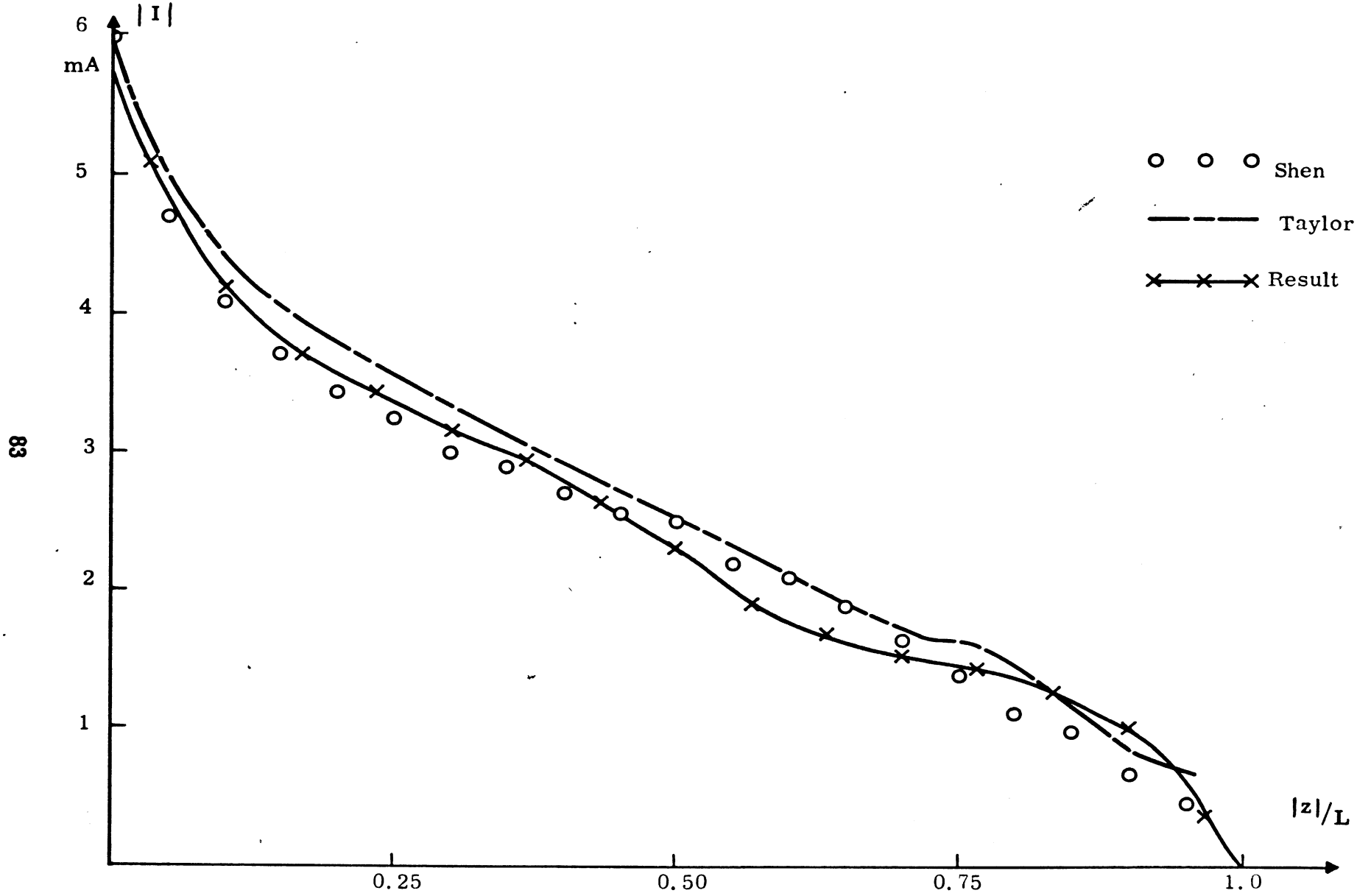

FIG. A-3: Current distribution on non-reflectively loaded monopole. $\Omega = 11.5$, $\omega L/c = 2\pi$, $\psi\alpha = 5.3$.

son. The results of Shen have been obtained experimentally and those of Taylor have been obtained by numerical solution of Pocklington integral equation for the current distribution. Figure A-3 indicates that our computed results agree fairly well with Shen's experimental values.

7.3 Exponentially Loaded Case

Fig. A-4 shows the current distributions on a one wavelength long monopole loaded exponentially. The loading function used is

$$R_s(z) = c' e^{\alpha |z|} , \qquad (A.47)$$

where c' is a constant and α is another constant which determines the rate of loading. In order to compare the results of Fig. A-4 with those of Fig. A-3 the constant c' is chosen to be $c' = 604\alpha = 60 \times 5.3$. Fig. A-4 shows the current distributions obtained numerically with the help of Eqs. (A.21)-(A.23) with $N = 30$ for two cases with $\alpha = 2.2$ and $\alpha = -2.2$. The case with $\alpha = 2.2$ corresponds approximately to Shen's[18] and it clearly shows the existence of a traveling wave type of current distribution. For $\alpha = -2.2$, the loading decreases towards the end and the current distribution obtained is of standing wave nature.

7.4 Phase Distribution of the Current

Fig. A-5 shows the phase variations of the current along the length of the antenna for the different non-uniformly loaded cases considered above. The progressive linear variations of phase for the non-reflecting case indicates the existence of a pure traveling wave of current in the antenna. It is interesting to observe from Fig. A-4 that for the exponentially loaded case with $c' = 60 \times 5.3$, $\alpha = 2.2$ the antenna may be considered to be approximately non-reflecting. This observation may have significant implications for theoretical analysis of such antennas. No such conclusion can be made from the phase variation for the exponentially loaded antenna with $\alpha = -2.2$.

7.5 Results for a Long Antenna $2L = 5\lambda$

In the previous sections numerical results have been given for an antenna

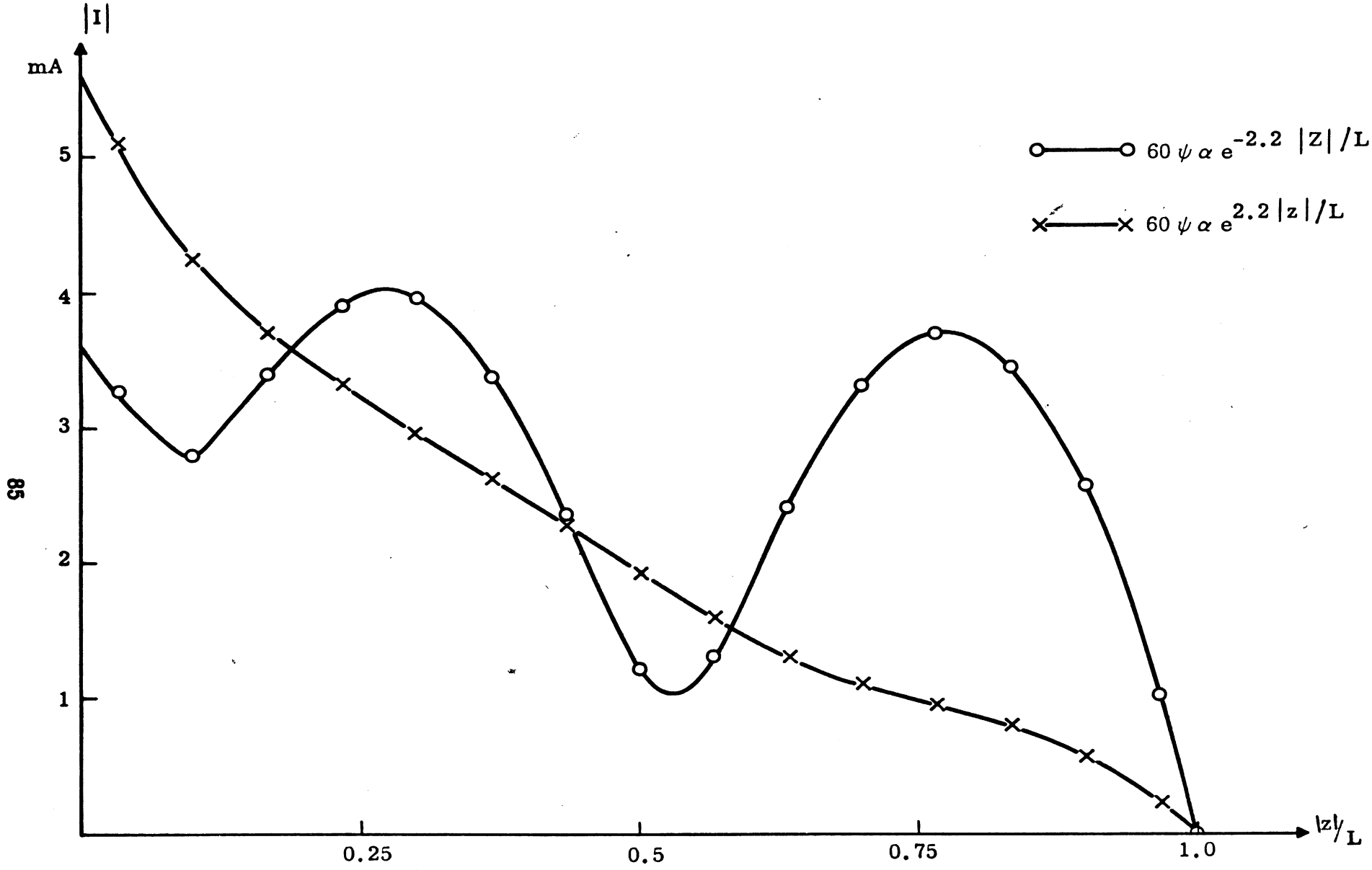

FIG. A-4: Current distribution on exponentially loaded monopole. $\Omega = 11.5$, $\psi\alpha = 5.3$, $\omega L/c = 2\pi$.

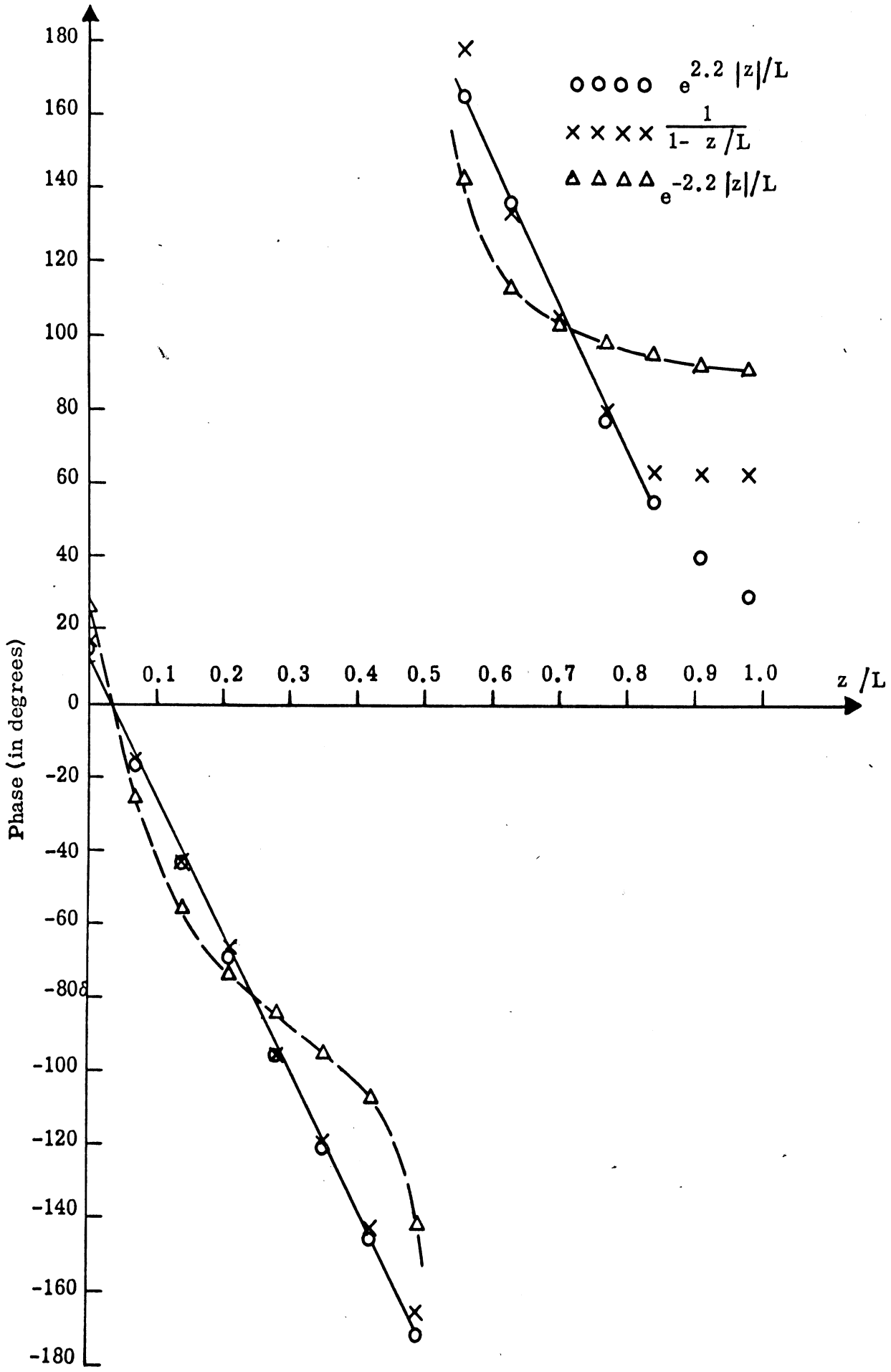

FIG. A-5: Phase variation of the current along the antenna.

having total length $2L = 2\lambda$. During the process of obtaining the transfer function of the antenna as a function of frequency, the effective length of the antenna becomes very large at the high frequency end. The computer capacity as well as the accuracy of the numerical results restrict the highest frequency for which the transfer function can be evaluated. For long antennas, the computer program should be modified for retaining satisfactory accuracy of the results without taxing the computer. For small antenna length the usual pulse approximation for the current in each section Δz_n provides sufficient accuracy as has been found in the previous sections. As discussed in Section 4, for long antennas we use the quadratic approximation to the current during the numerical evaluation of the current. We study the accuracy of this procedure in this section. In addition to this we also investigate the use of 4-, 3- and 2-point end conditions for the long antenna case. The results of a sample computation done for the case with $2L = 5\lambda$ with different values of the loading parameter in Eq. (A. 16) are discussed in the present section.

Figs. A-6 -- A-8 show the current amplitude distribution, the current phase distribution and the transfer function respectively of the non-reflecting loaded linear antenna of length $2L = 5\lambda$ with the loading parameter $C = 60 \times 5.3$. All these curves have been obtained by using Eqs.(A. 36) with $N = 30$. In each case the results obtained by using 4-, 3- and 2-point end condition expressions are also shown in Figs. A-5 — A-7. It can be seen from Figs. A-5 — A-7 that the results are not appreciably different among the three cases. However, near the end of the antenna the results are found to differ with each other slightly. From a study of Figs. A-5 and A-6, in particular, the phase variation near the end of the antenna as shown in Fig. A-6 it is concluded that the 4-point end condition expression given by Eq. (A. 43) is more accurate and hence should be used during the numerical computation of the transfer function of the antenna for high frequencies. Figure A-9 shows the amplitude of the current distribution on the antenna as a function of the loading parameter $C = 60\psi\alpha$ obtained by Eq. (A. 36) with $N = 30$ and the 4-point end condition.

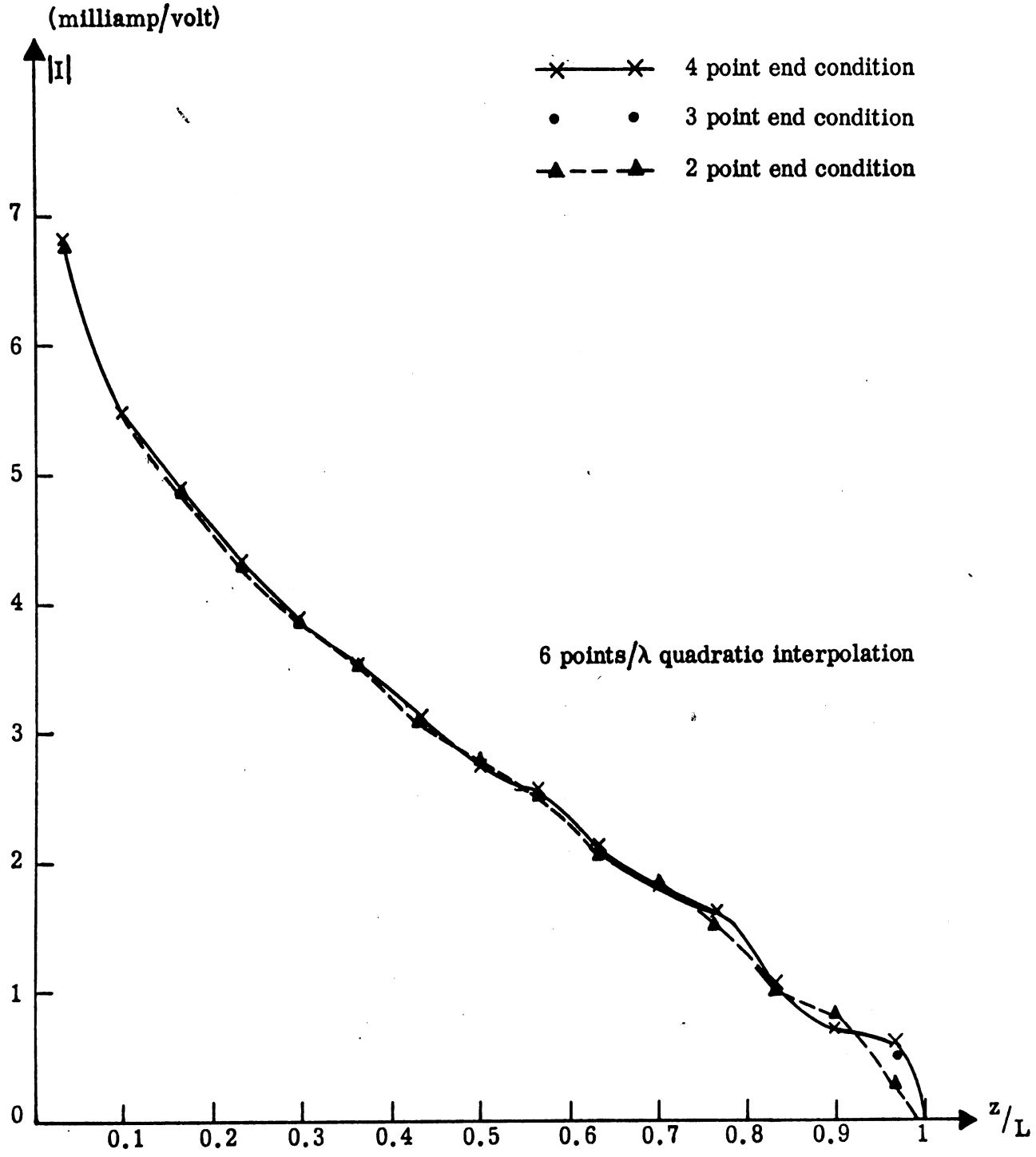

FIG. A-6: Current distribution on non-reflectively loaded antenna, $\Omega = 11.5$ $kL = 5\pi$, $\psi\alpha = 5.3$, $R_s(z) = 60\,\psi\alpha/L - |z|$.

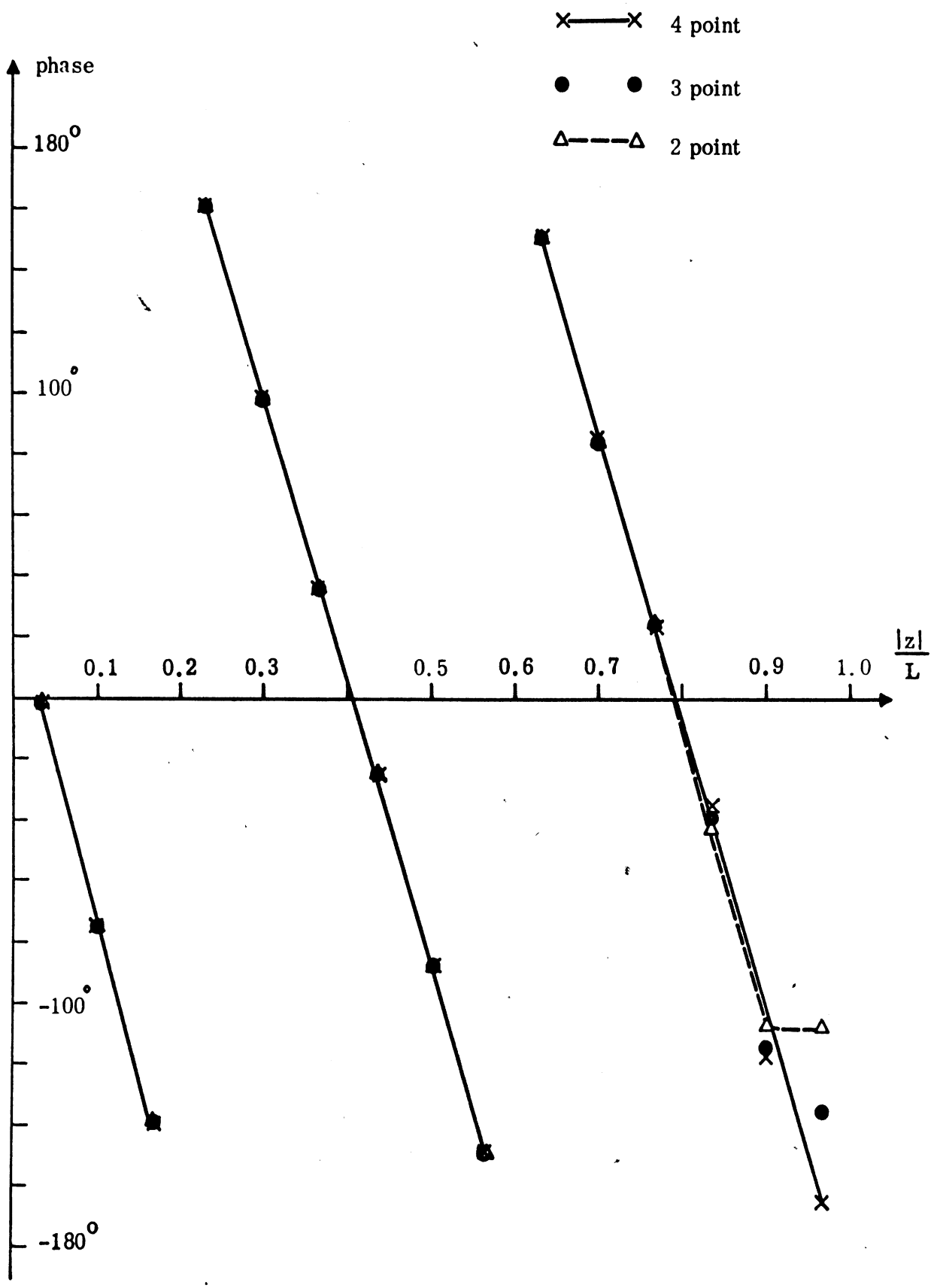

FIG. A-7: Phase variation of the current along the non-reflectively loaded antenna, $\Omega = 11.5$, $kL = 5\pi$, $\psi/\alpha = 5.3$, $R_s(z) = 60\psi/\alpha/L - |z|$.

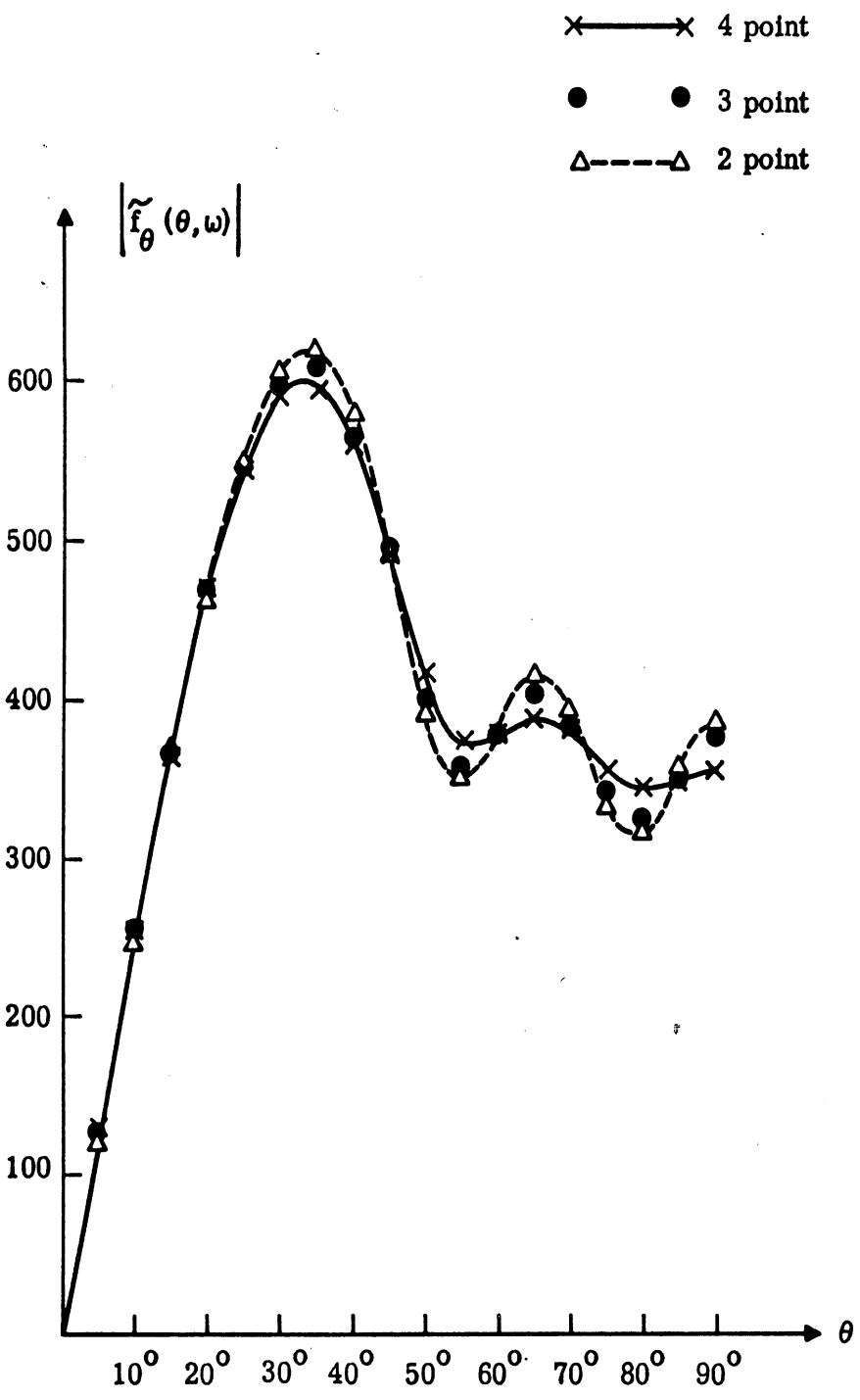

FIG. A-8: Transfer function $\tilde{f}_\theta(\theta,\omega)$ of the non-reflectively loaded antenna. $\Omega = 11.5$, $kL = 5\pi$, $\psi\alpha = 5.3$, $R_s(z) = 60\psi\alpha/L - |z|$.

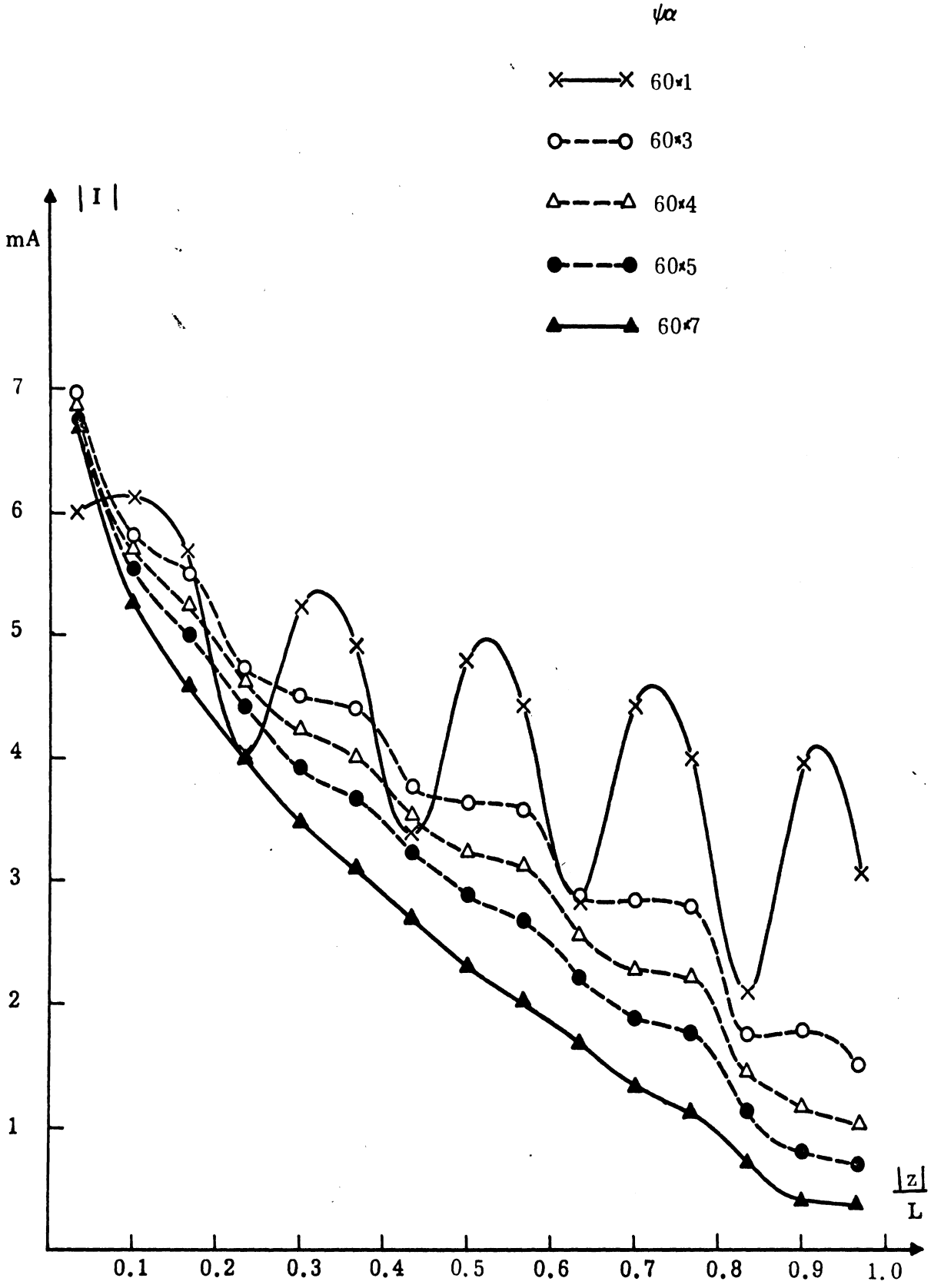

FIG. A-9: Amplitude of the current distribution on resistively loaded dipole antenna as a function of loading. $\Omega = 11.5$, $kL = 5\pi$, $\psi\alpha$ variable.

It is interesting to observe here that on the basis of King's work, the expansion factor ψ is a fixed value for one particular size and frequency. That means only at this specific value of loading ($60\psi\alpha$) and specific frequency, we can have a reflectionless current wave on the antenna. For $C < 60 \times 5$, the reflection effects on the current distribution become quite appreciable as expected. While $C > 60 \times 7$, Fig. A-9 tells us the nonreflective nature. The higher value of loading on the antenna supresses the small amount of reflection that occurs due to the use of a value of ψ slightly different from the specific value referred to above.

On the basis of the results given in this section, we have decided to use the 4-point end-condition expression during the numerical computation. Six subsections per wavelength to divide the antenna is required to guarantee the accuracy.

8. CURRENT DISTRIBUTION $I(z, \omega)$ ON THE LOADED ANTENNA

In this section we give the numerical results obtained for the amplitude of the current distribution $I(z, \omega)$ for the harmonically excited loaded antenna. The loading used is of the form given by Eq. (A.16) with C variable. Figures A-10a-A-10d show the amplitude of the current distribution on the antenna with antenna length as parameter for different values of the loading.

The amplitude of the current in general increases as the frequency is increased. The value of the magnitude at the same frequency is surpressed by the higher loading as expected. The current distribution is not strictly linear as those of the transmission line found by Baum. It is due to the factor ψ which is a function of the thickness ratio of the antenna and the frequency used. So it is not possible to excite a traveling current wave for all frequencies on an antenna of fixed size.

9. TRANSFER FUNCTION OF THE LOADED ANTENNA $\tilde{f}_\theta(\theta, \omega)$.

In this section the magnitude and phase of the transfer function of the antenna are given as functions of $\omega L/c$ for different values of the loading parameter C.

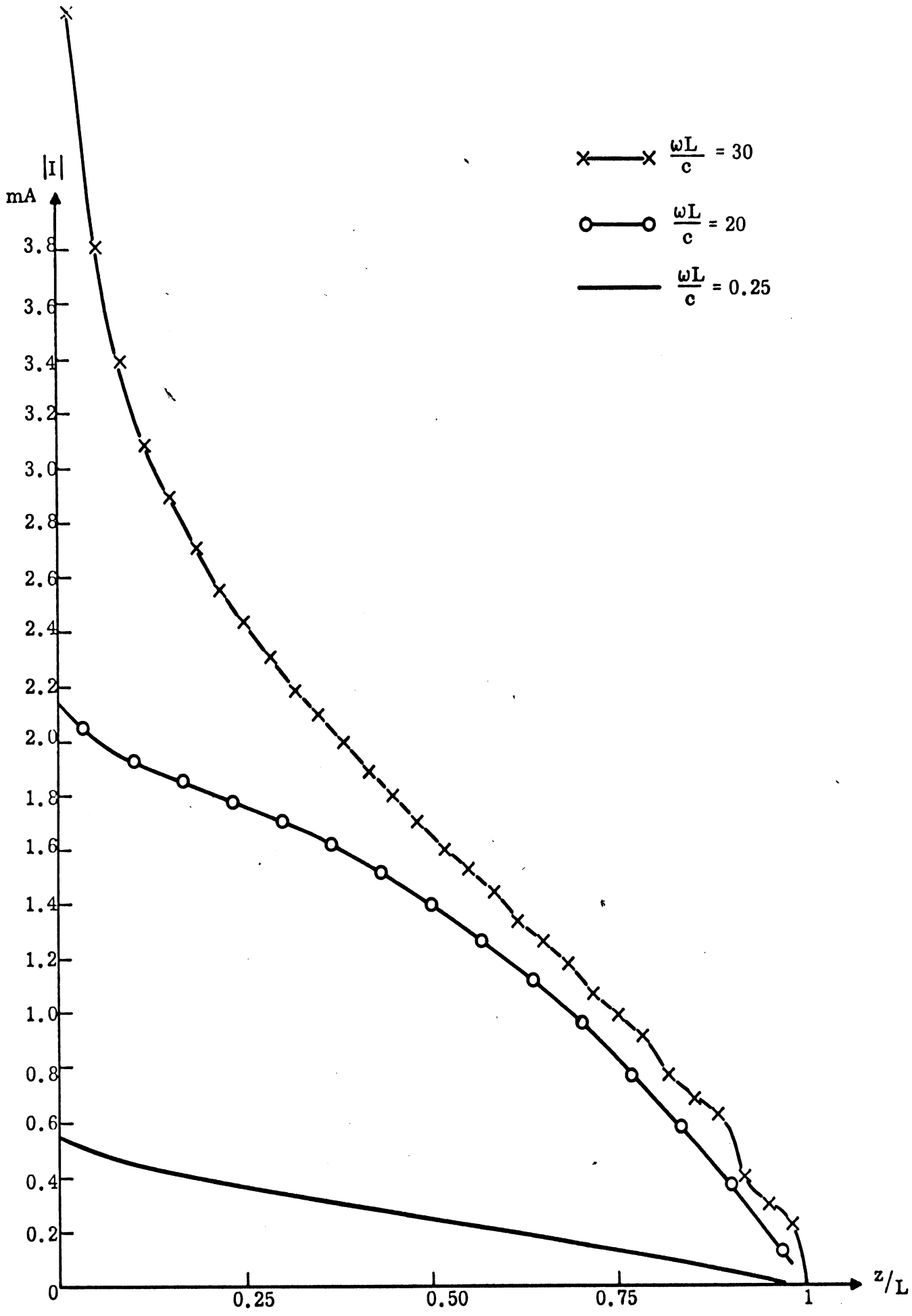

FIG. A-10a: Amplitude of the current distribution $|I(z,\omega)|$ vs z/L on the loaded antenna with kL (= ωL/c), as the parameter, C = 60 x 4.

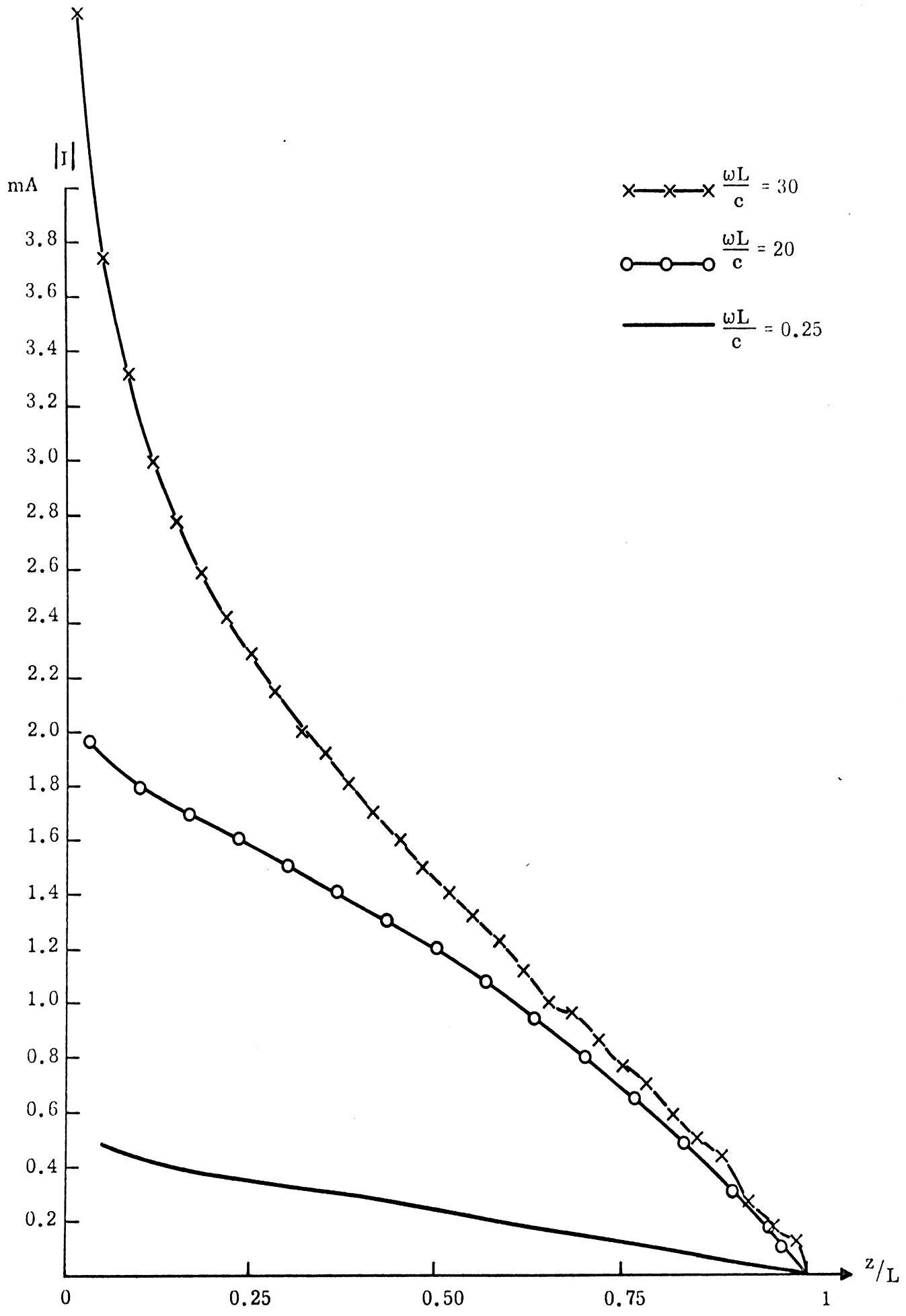

FIG. A-10b: Amplitude of the current distribution $|I(z,\omega)|$ vs. z/L on the loaded antenna with $kL\ (= \omega L/c)$, as the parameter $C = 60 \times 5$.

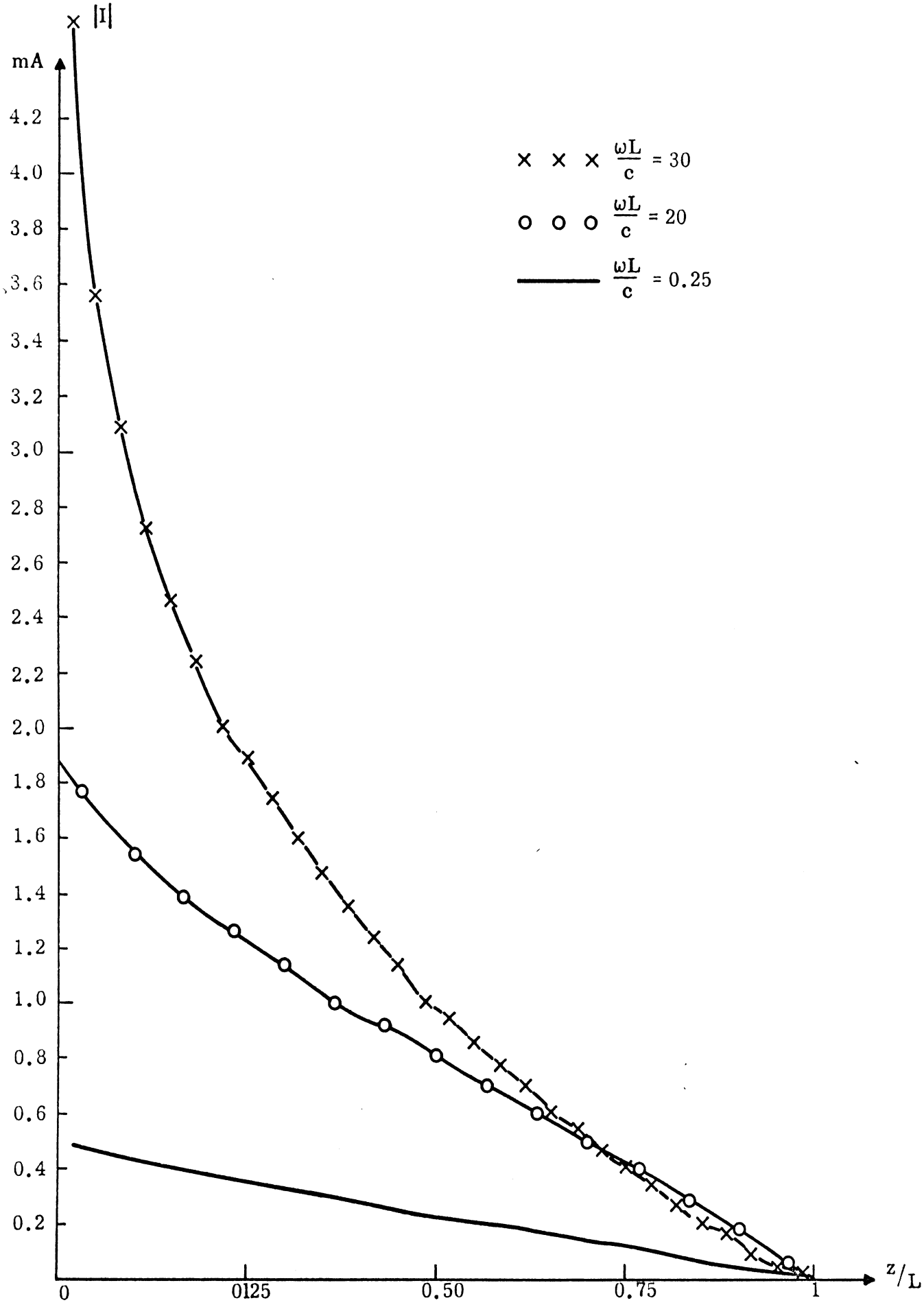

FIG. A-10c: Amplitude of the current distribution $|I(z,\omega)|$ vs z/L on the loaded antenna with kL (= ωL/c), as the parameter. C = 60 x 8.

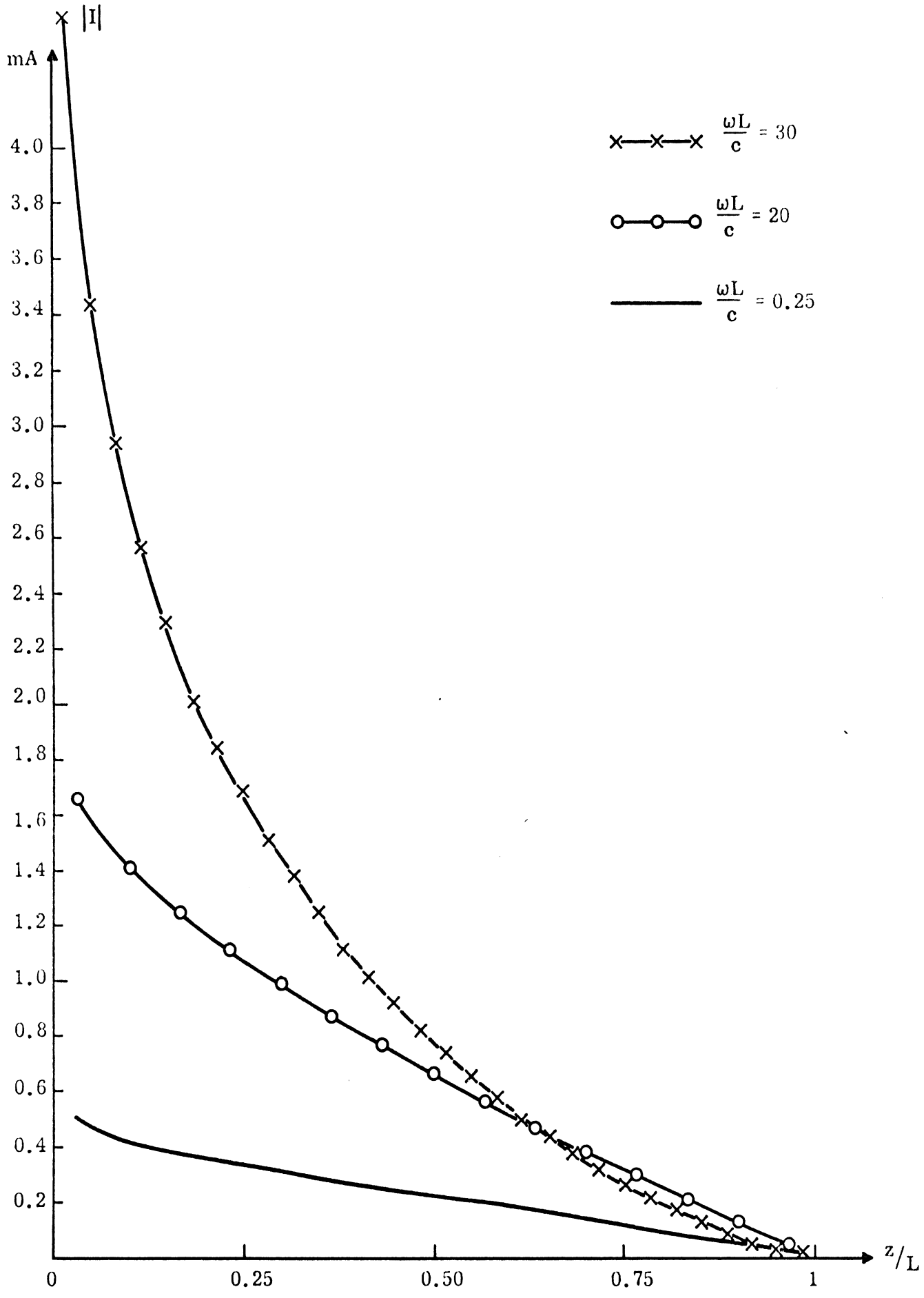

FIG. A-10d: Amplitude of the current distribution $|I(z,\omega)|$ vs z/L on the loaded antenna with $kL = \omega L/c$), as the parameter. C = 60 x 10.

These have been obtained numerically with the help of Eq. (A.45) and the sampled values of the current distributions discussed in the previous section. Figures A-11a-A-11d give the variations of the magnitude and phase of the transfer function in the broadside direction ($\theta = \pi/2$) of the antenna and for four values of the loading parameter c. Similar results are given for $\theta = \pi/3$, $\theta = \pi/4$, $\theta = \pi/6$ in Figs. A-12 -- A-14 respectively. Each figure contains four different values of the loading factor C. In all the curves shown, $|\tilde{f}_\theta(\theta, \omega)|$ approaches zero as ω approaches zero, which corresponds to the fact that there is no radiation at zero frequency. For higher frequencies, $|\tilde{f}_\theta(\theta, \omega)|$ appears to be an oscillating function and tends to decrease with increase of the frequency. The phase of $\tilde{f}_\theta(\theta, \omega)$ falls steadily to a positive constant. Wu and King[3] proved that the asympotatic value of the transfer function is a constant. However, within the range of the computations covered here the transfer function in Figs. A-11 -- A-14 does not reach its asymptotic value especially for $\theta = \pi/6$. For an unloaded thin linear antenna, we know that the transfer function would be zero for $L = n\lambda$ at the broadside direction (where n is an integer) when the current is sinusoidal. Fig. A-11a shows that the values at $kL = 2\pi$, 4π, 6π, 8π are minimal. For higher values of C, the loading reduces the ringing which is due to the reflection from the end.

It is appropriate to mention here that the impulse response of the antenna may be obtained by numerically carrying out the inverse Fourier transform. However, the data for $\tilde{f}_\theta(\theta, \omega)$ obtained so far is not sufficient to get reasonably good results. Taylor[14] has shown that the transfer function reaches its asymptotic value at a certain frequency which is beyond the value $\omega L/c = 25$ considered here.

10. NUMERICAL RESULTS

In this section we discuss the numerical results for two different shapes of voltage input. Spectral density is obtained by multiplying the transfer function with the input pulse spectrum. The waveform of the radiated signal is then

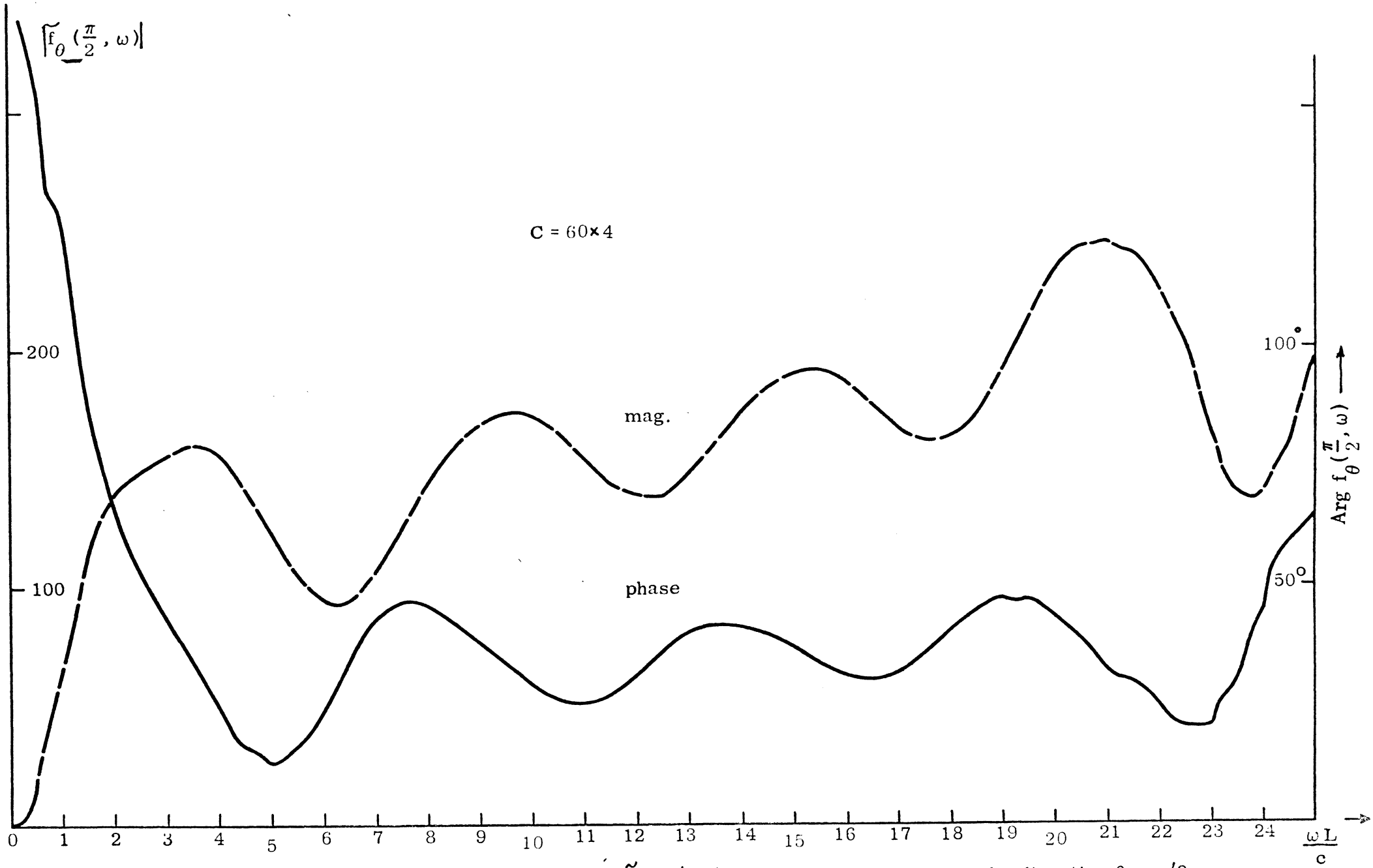

FIG. A-11a: Magnitude and phase of the transfer function $\tilde{f}_\theta(\pi/2\,\omega)$, of the loaded antenna in the direction $\theta = \pi/2$ as a function of $kL = (\omega L/c)$ for different loading. ■C = 60 x 4.

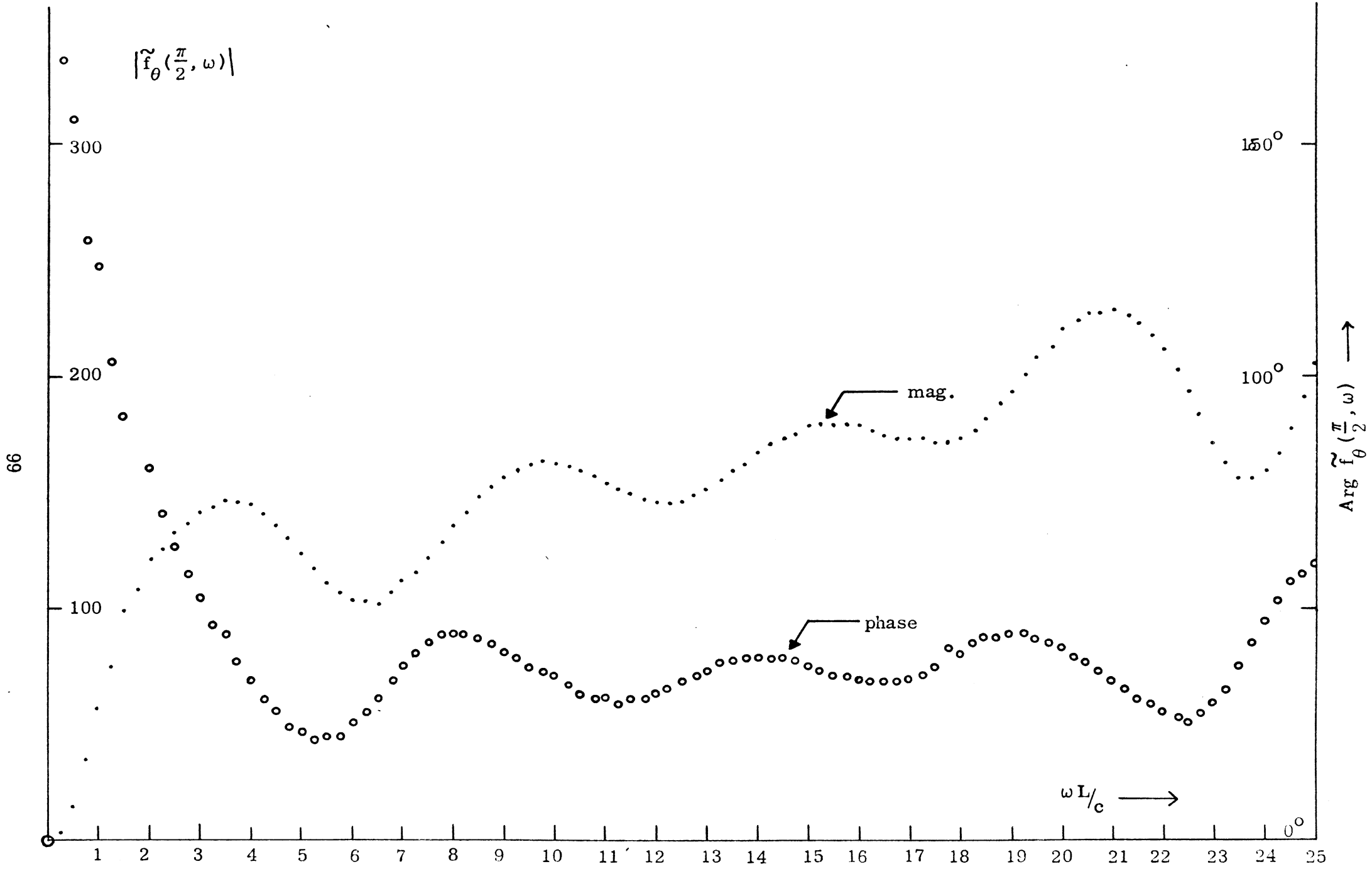

FIG. A-11b: Magnitude and phase of the transfer function $\tilde{f}_\theta(\pi/2, \omega)$ of the loaded antenna in the direction $\theta = \pi/2$ as a function of $kL = (\omega l/c)$ for different loading. C = 60 x 5.

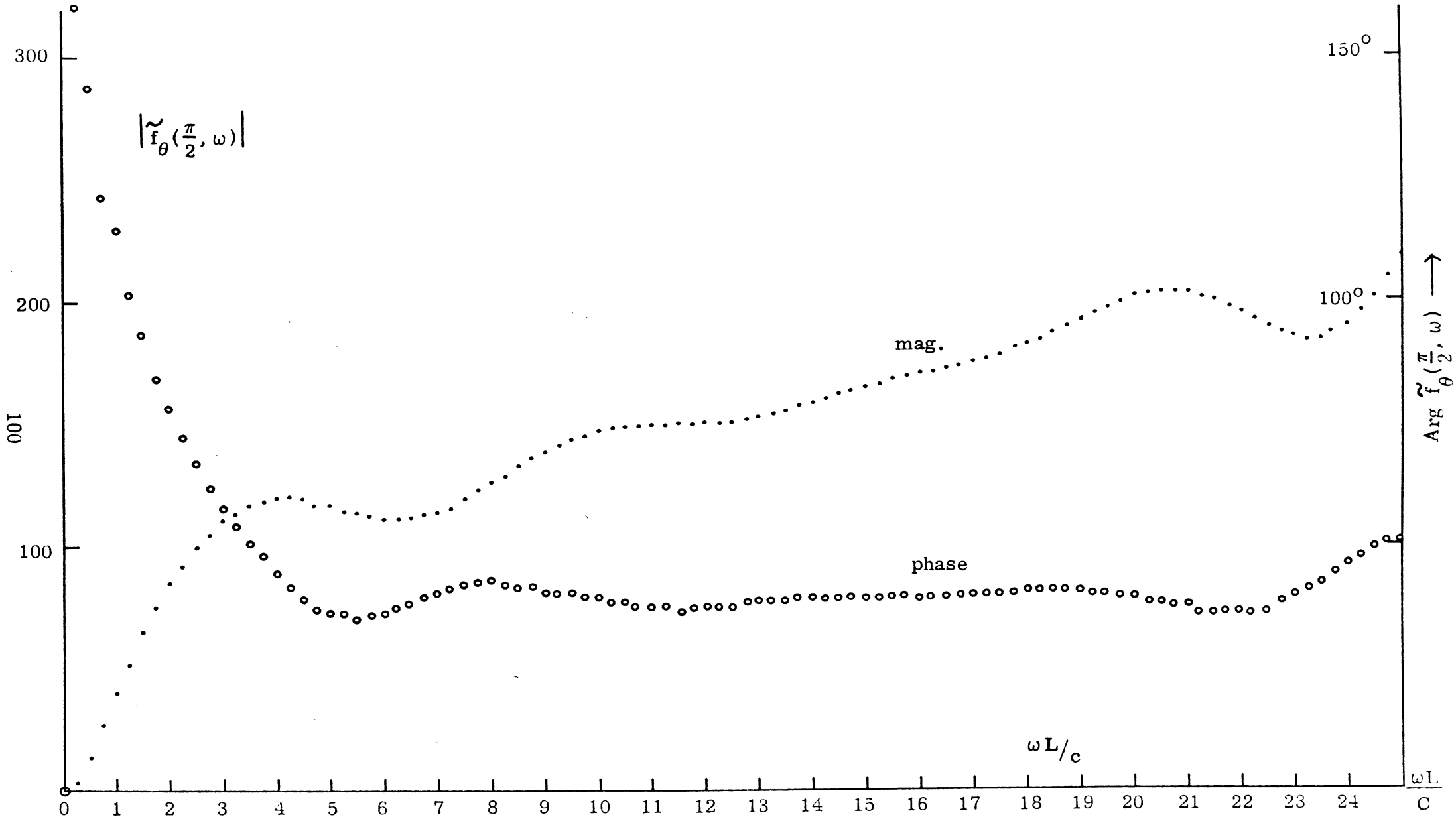

FIG. A-11c: Magnitude and phase of the transfer function $\tilde{f}_\theta(\pi/2, \omega)$ of the loaded antenna in the direction $\theta = \pi/2$ as a function of $kL = (\omega L/c)$ for different loading. C = 60 x 8.

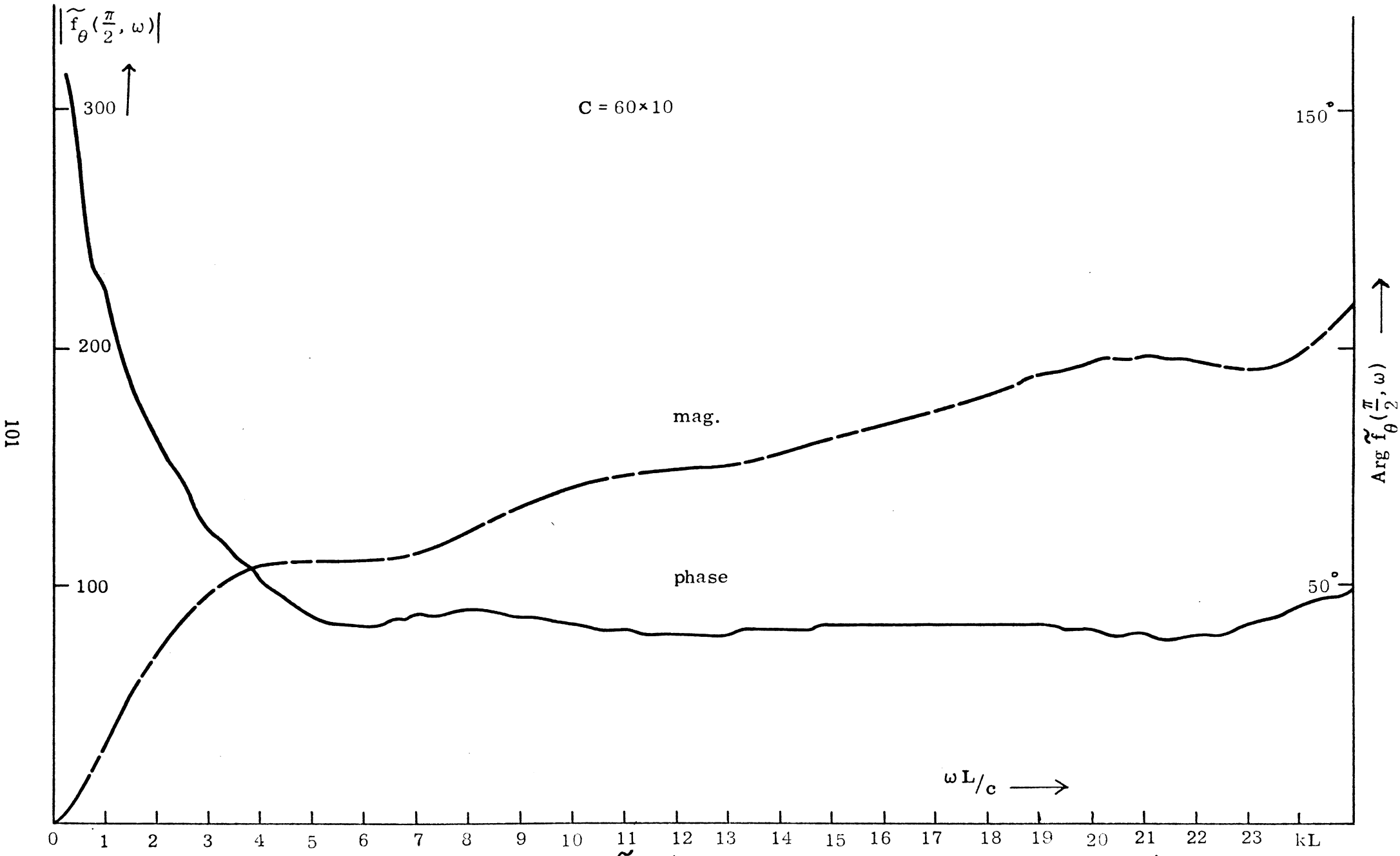

FIG. A-11d: Magnitude and phase of the transfer function $\widetilde{f}_\theta(\pi/2, \omega)$ of the loaded antenna in the direction $\theta = \pi/2$ as functions of $kL = (\omega L/c)$ for different loading. C = 60 x 10.

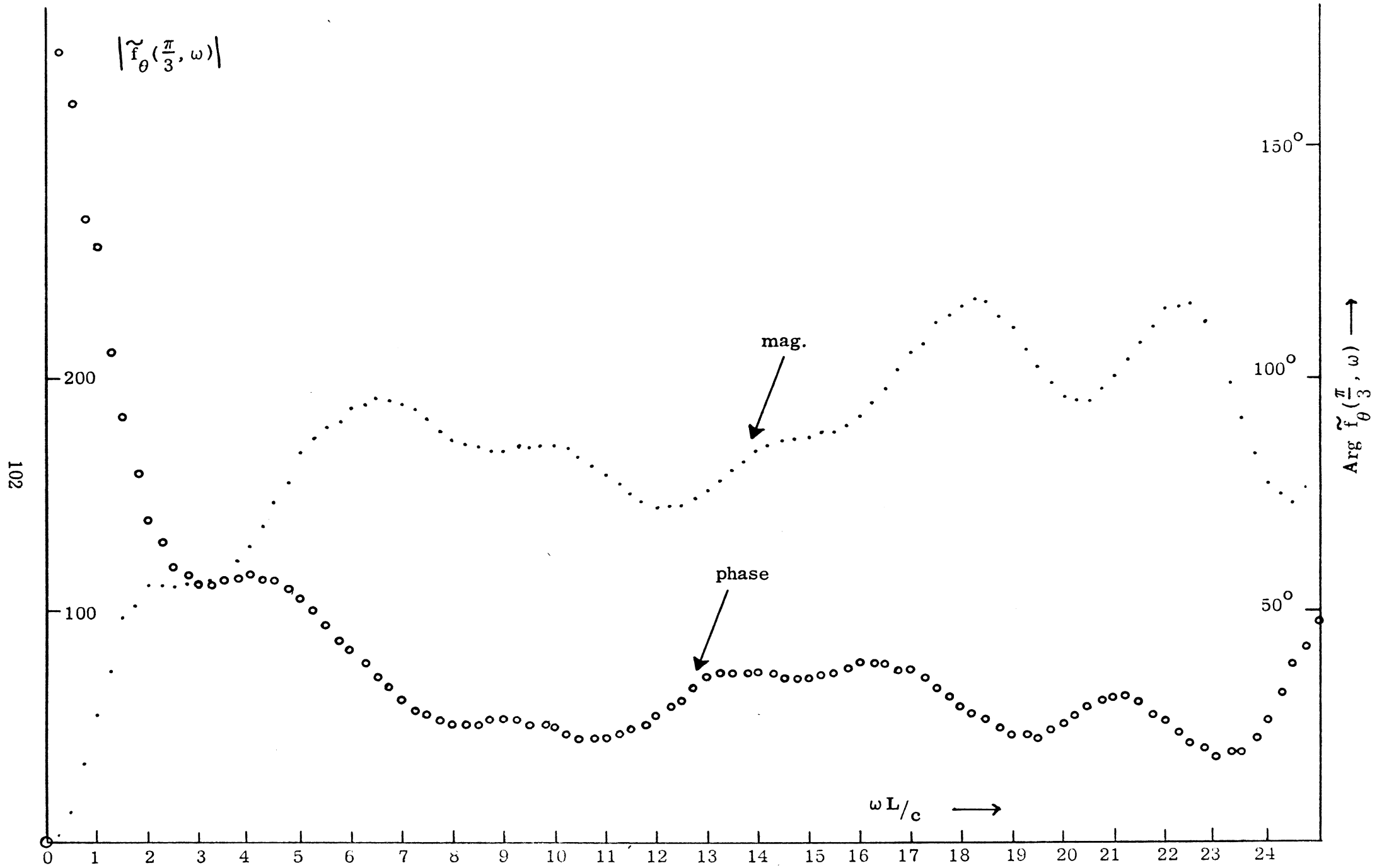

FIG. A-12a: Magnitude and phase of the transfer function $\tilde{f}_\theta(\pi/3, \omega)$ of the loaded antenna in the direction $\theta = \pi/3$ as functions of kL (= $\omega L/c$) for different loading. C = 60 x 4.

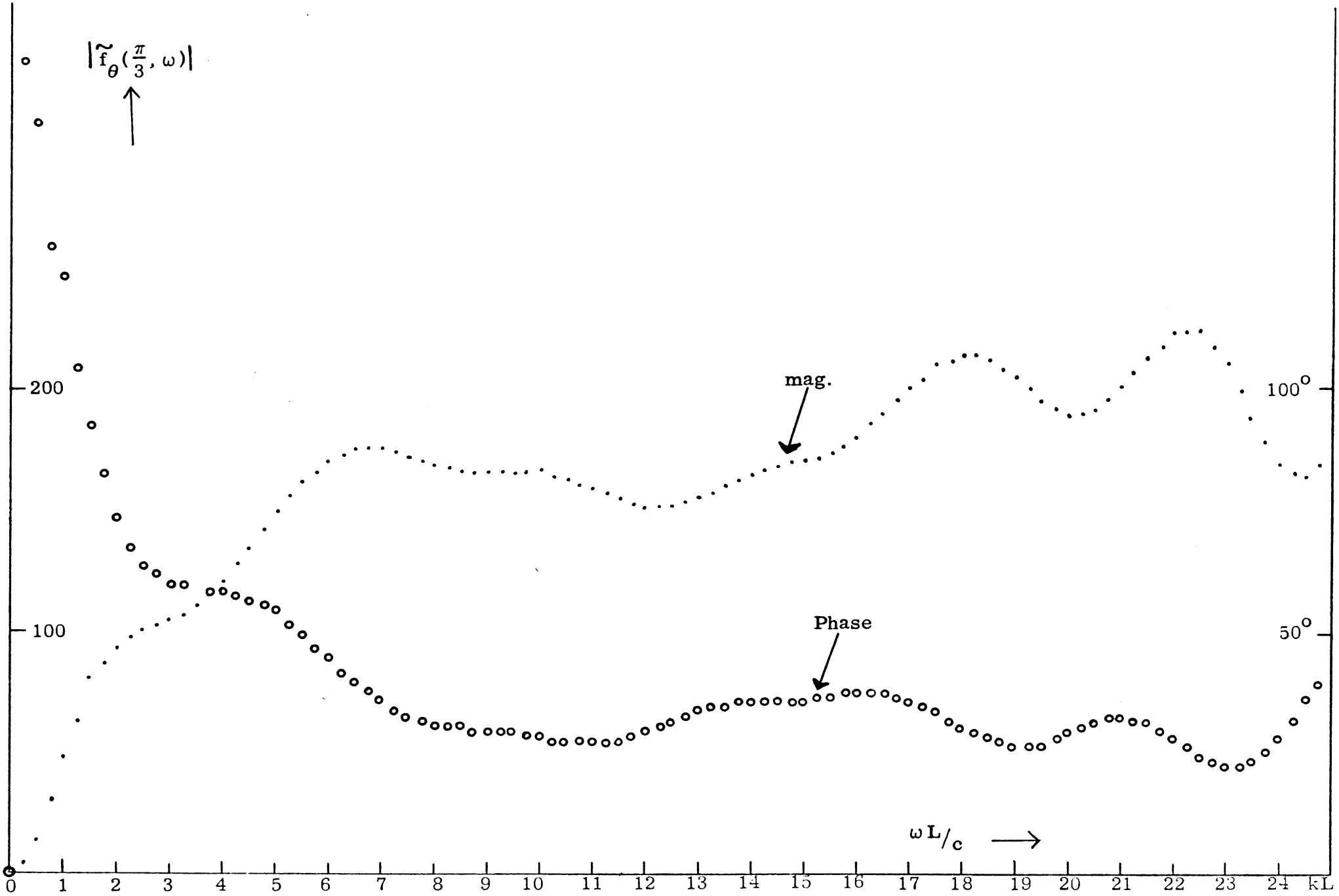

FIG. A-12b: Magnitude and phase of the transfer function $\tilde{f}_\theta(\pi/3, \omega)$ of the loaded antenna in the direction $\theta = \pi/3$ as functions of kL ($= \omega L/c$) for different loading. C = 60 x 5.

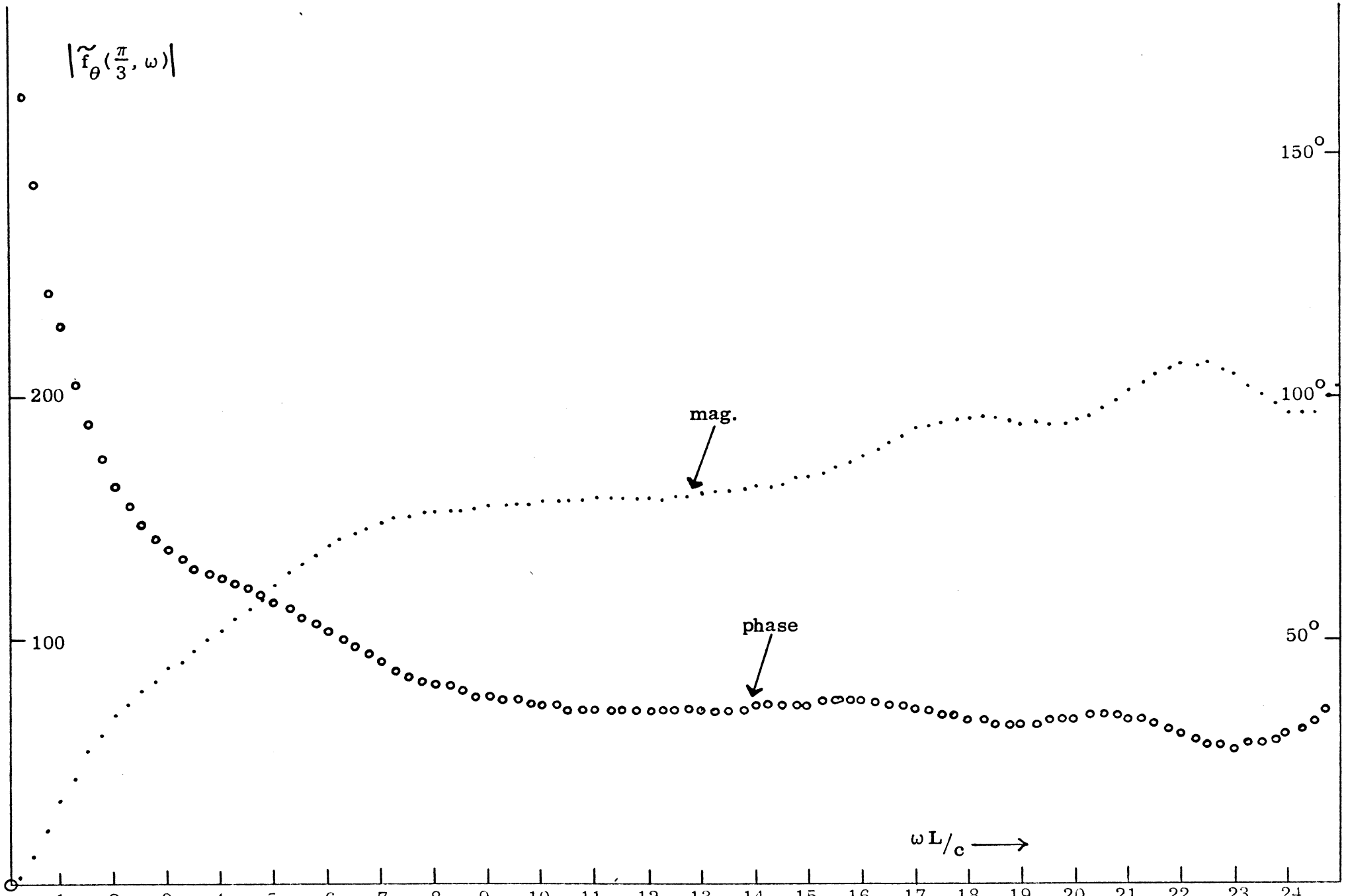

FIG. A-12c: Magnitude and phase of the transfer function $\tilde{f}_\theta(\pi/3, \omega)$ of the loaded antenna in the direction $\pi = \pi/3$ as functions of kL ($= \omega L/c$) for different loading. C = 60 x 8.

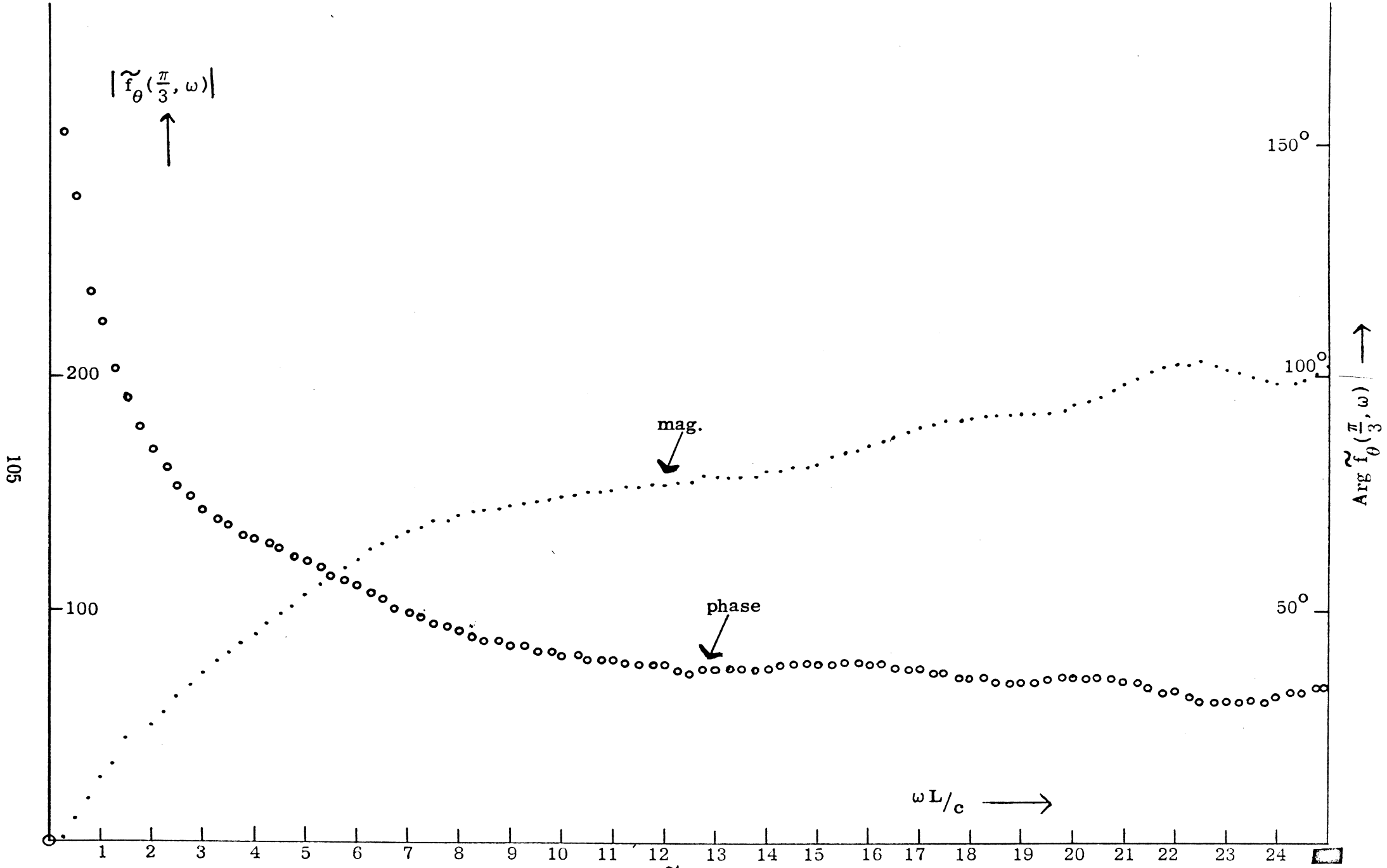

FIG. A-12d: Magnitude and phase of the transfer function $\tilde{f}_\theta(\pi/3, \omega)$ of the loaded antenna in the direction $\theta = \pi/3$ as functions of $kL(= \omega L/c)$ for different loading. C = 60 x 10.

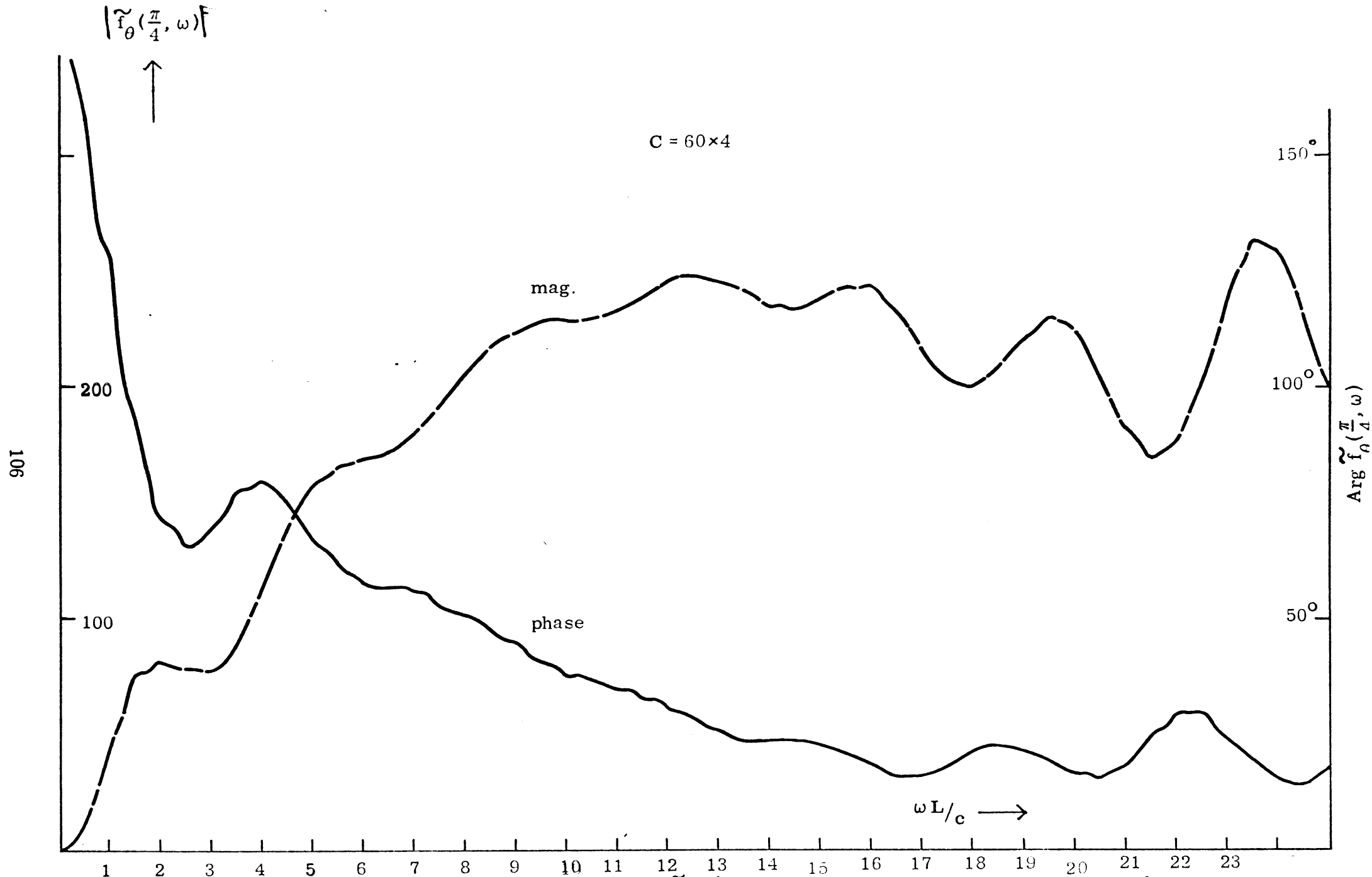

FIG. A-13a: Magnitude and phase of the transfer function $\tilde{f}_\theta(\pi/4, \omega)$ of the loaded antenna in the direction of $\theta = \pi/4$ as function of kL ($= \omega L/c$) for different loading. C = 60 x 4.

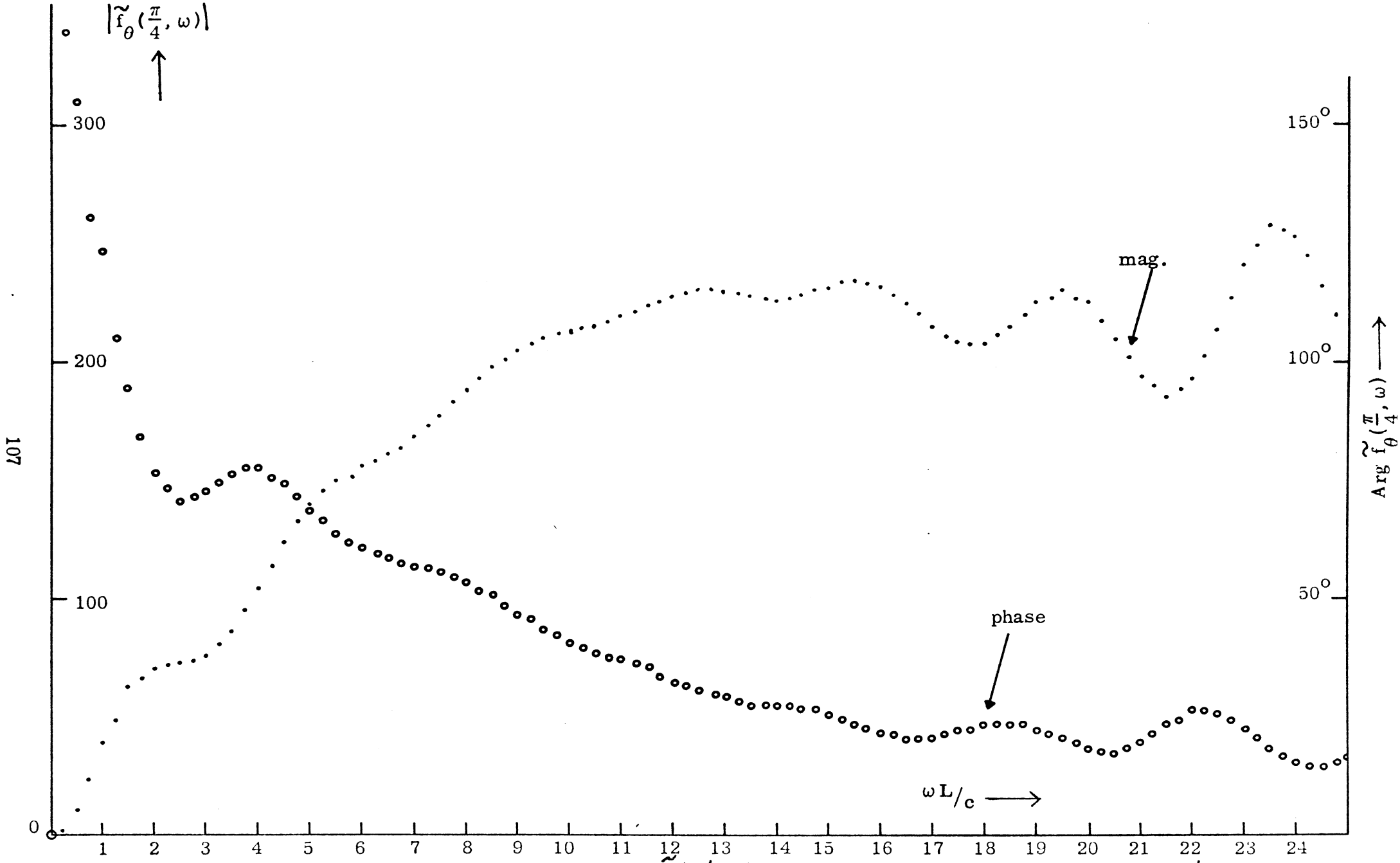

FIG. A-13b: Magnitude and phase of the transfer function $\tilde{f}_\theta(\pi/4, \omega)$ of the loaded antenna in the direction $\theta = \pi/4$ as functions of kL (= $\omega L/c$) for different loading. C = 60 x 4.

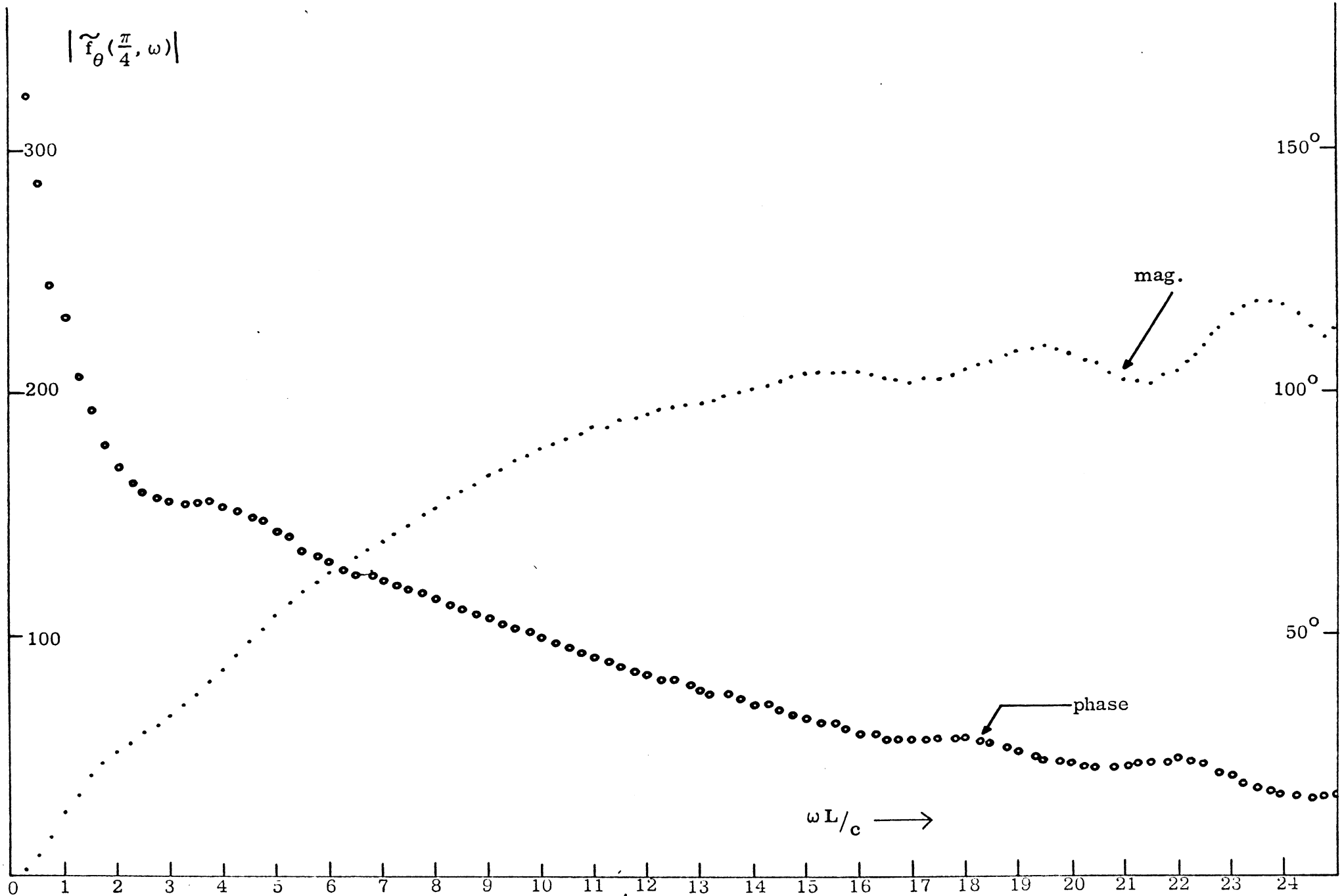

FIG. A-13c: Magnitude and phase of the transfer function $\tilde{f}_\theta(\pi/4, \omega)$ of the loaded antenna in the direction $\theta = \pi/4$ as functions of kL (= $\omega L/c$) for different loading. C = 60 x 8.

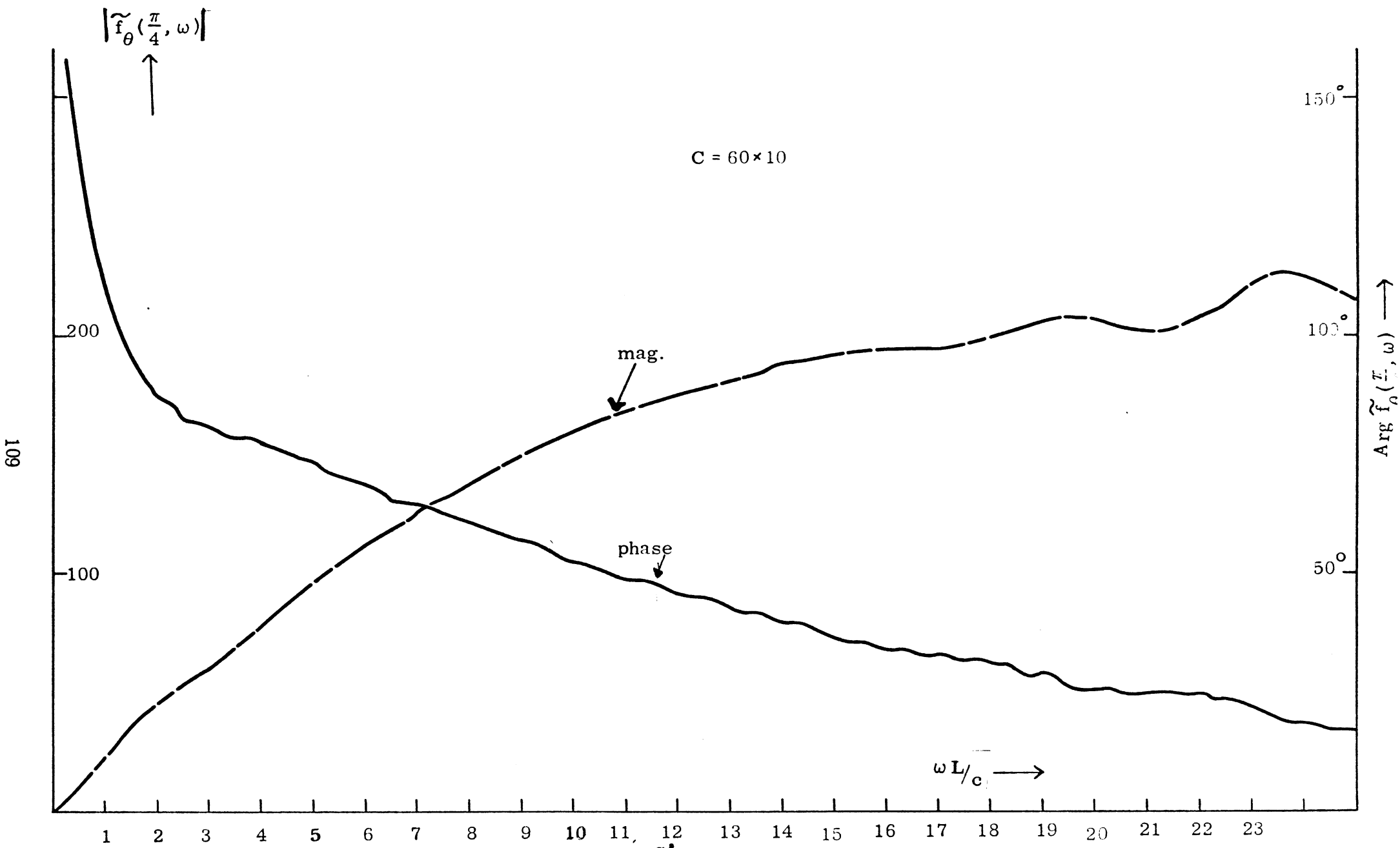

FIG. A-13d: Magnitude and phase of the transfer function $\tilde{f}_\theta(\pi/4, \omega)$ of the loaded antenna in the direction $\theta = \pi/4$ as function of $kL(= \omega L/c)$ for different loading. C = 60 x 10.

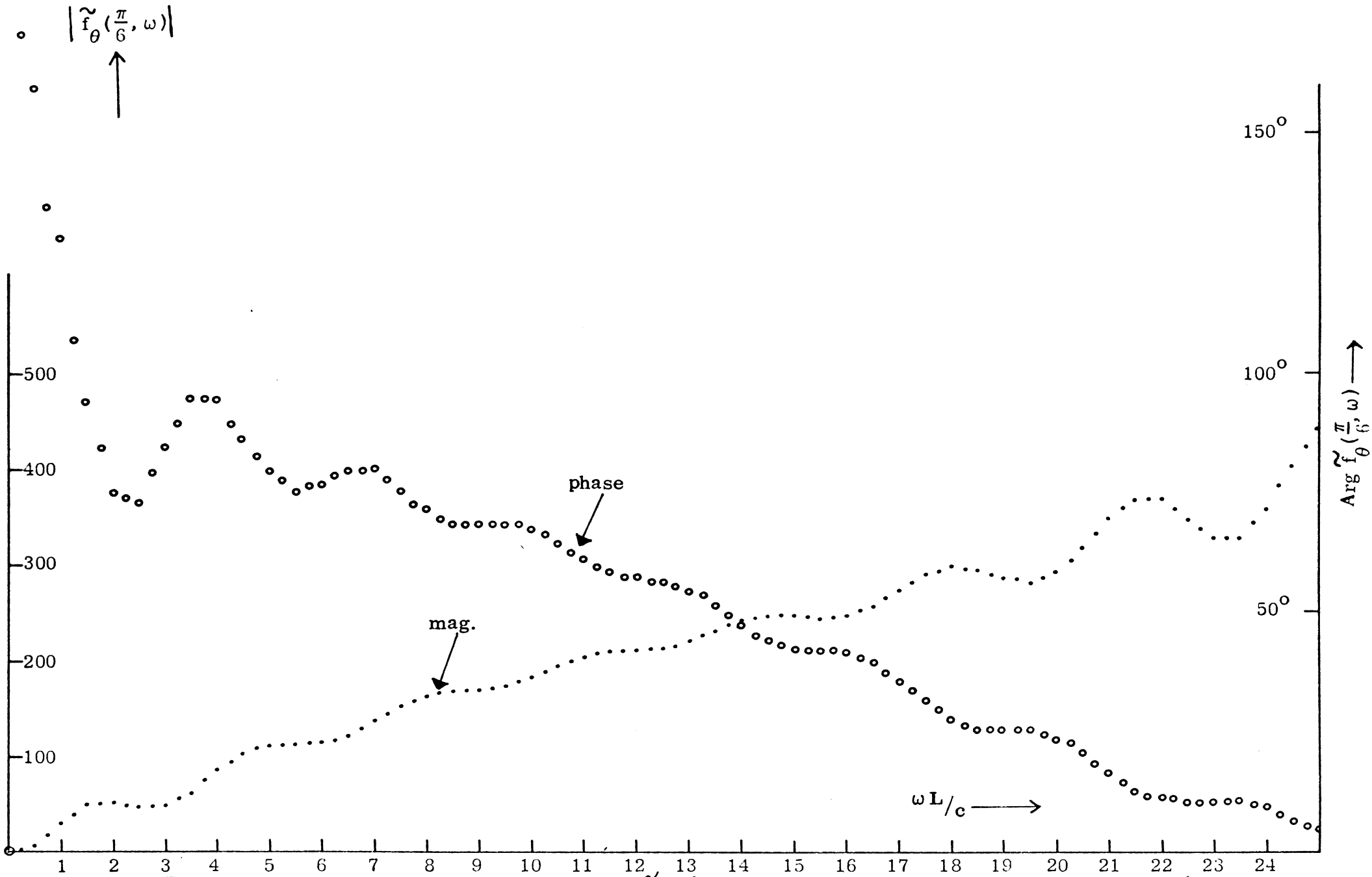

FIG. A-14a: Magnitude and phase of the transfer function $\tilde{f}_\theta(\pi/6,\omega)$ of the loaded antenna in the direction $\theta = \pi/6$ as function of kL (= $\omega L/c$) for different loading. C = 60 x 4.

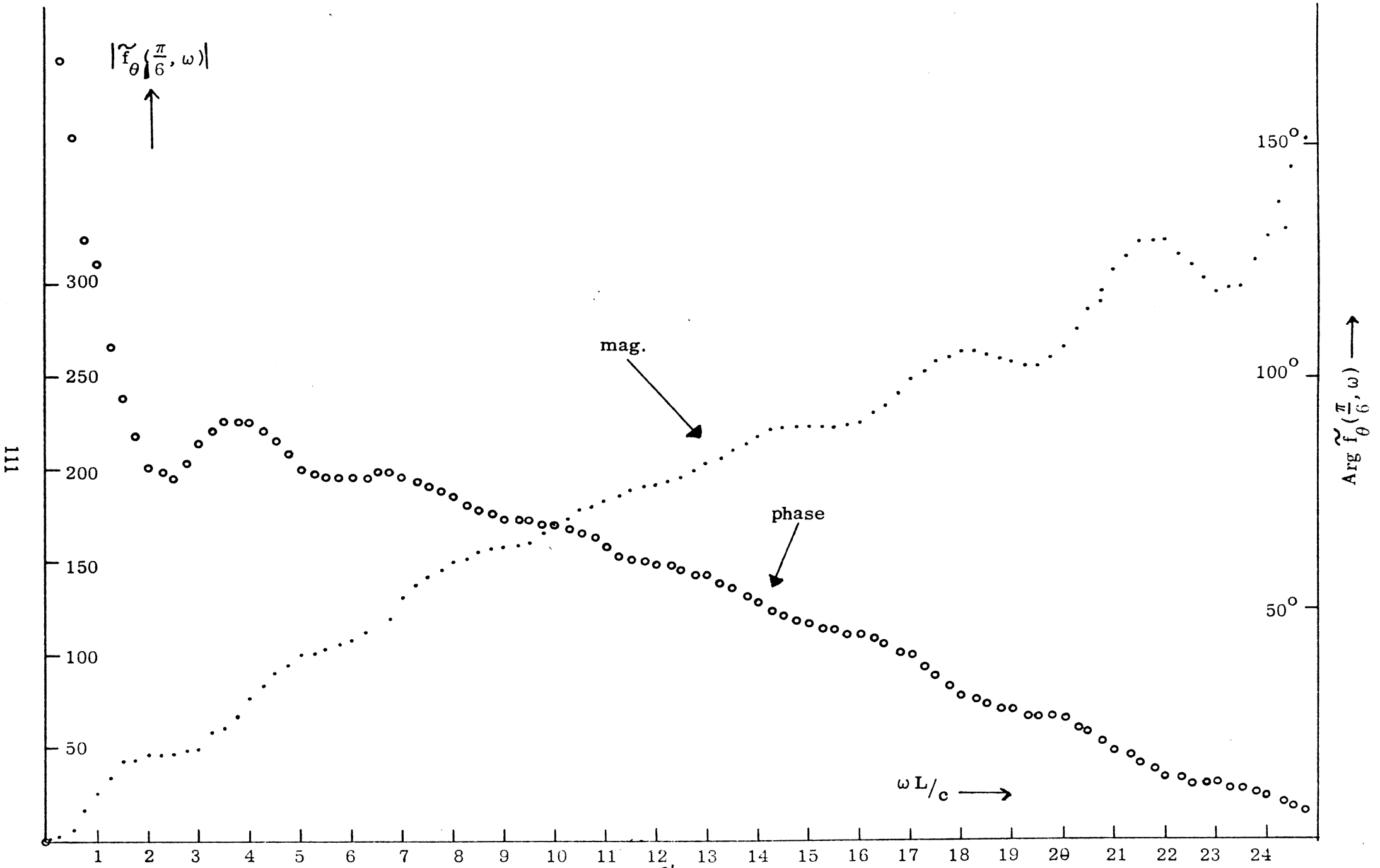

FIG. A-14b: Magnitude and phase of the transfer function $\tilde{f}_\theta(\pi/6, \omega)$ of the loaded antenna in the direction $\theta = \pi/6$ as function of kL ($= \omega L/c$) for different loading. C = 60 x 5.

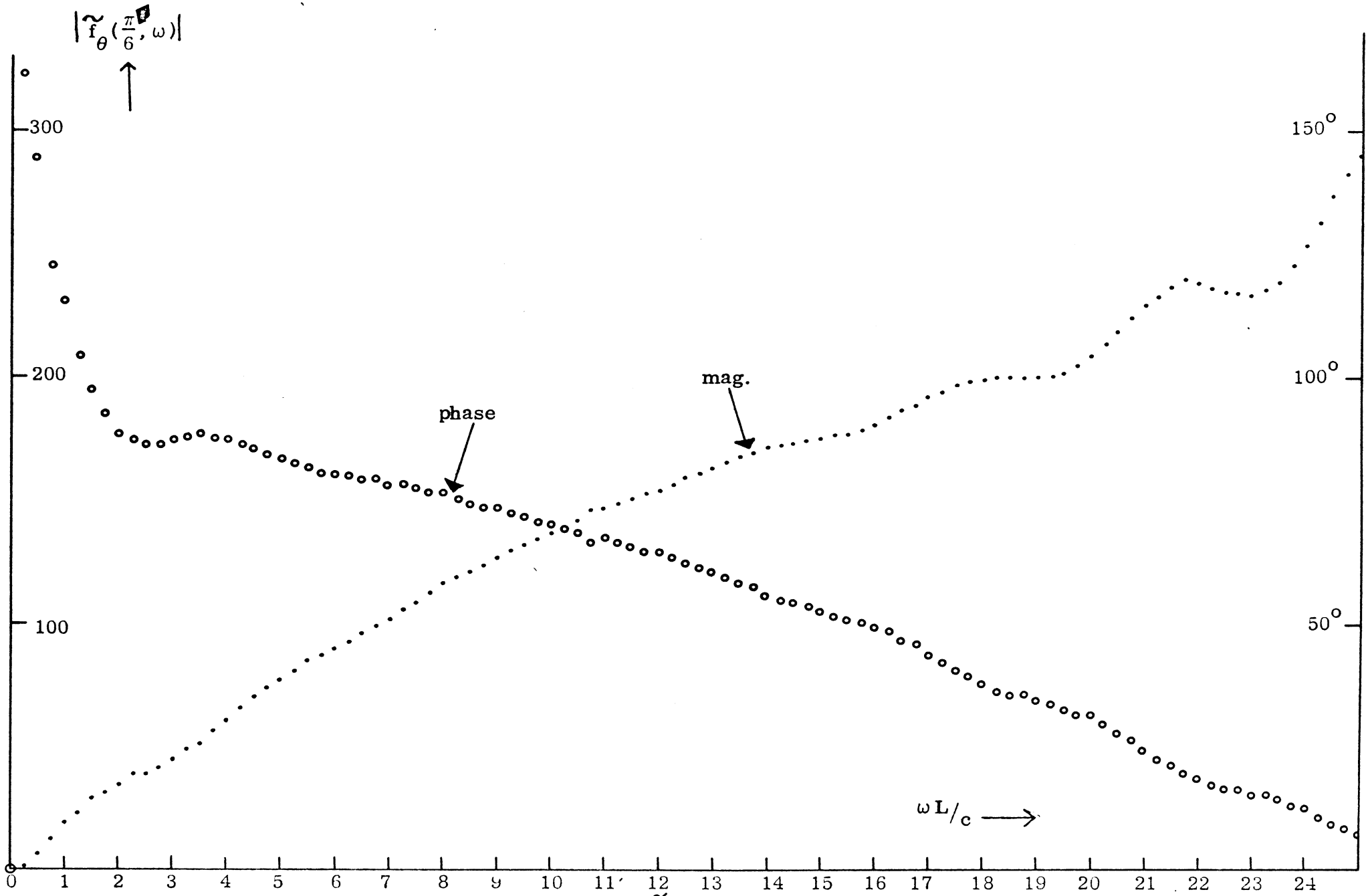

FIG. A-14c: Magnitude and phase of the transfer function $\tilde{f}_\theta(\pi/6, \omega)$ of the loaded antenna in the direction $\theta = \pi/6$ as function of kL ($= \omega L/c$) for different loading. C = 60 x 8.

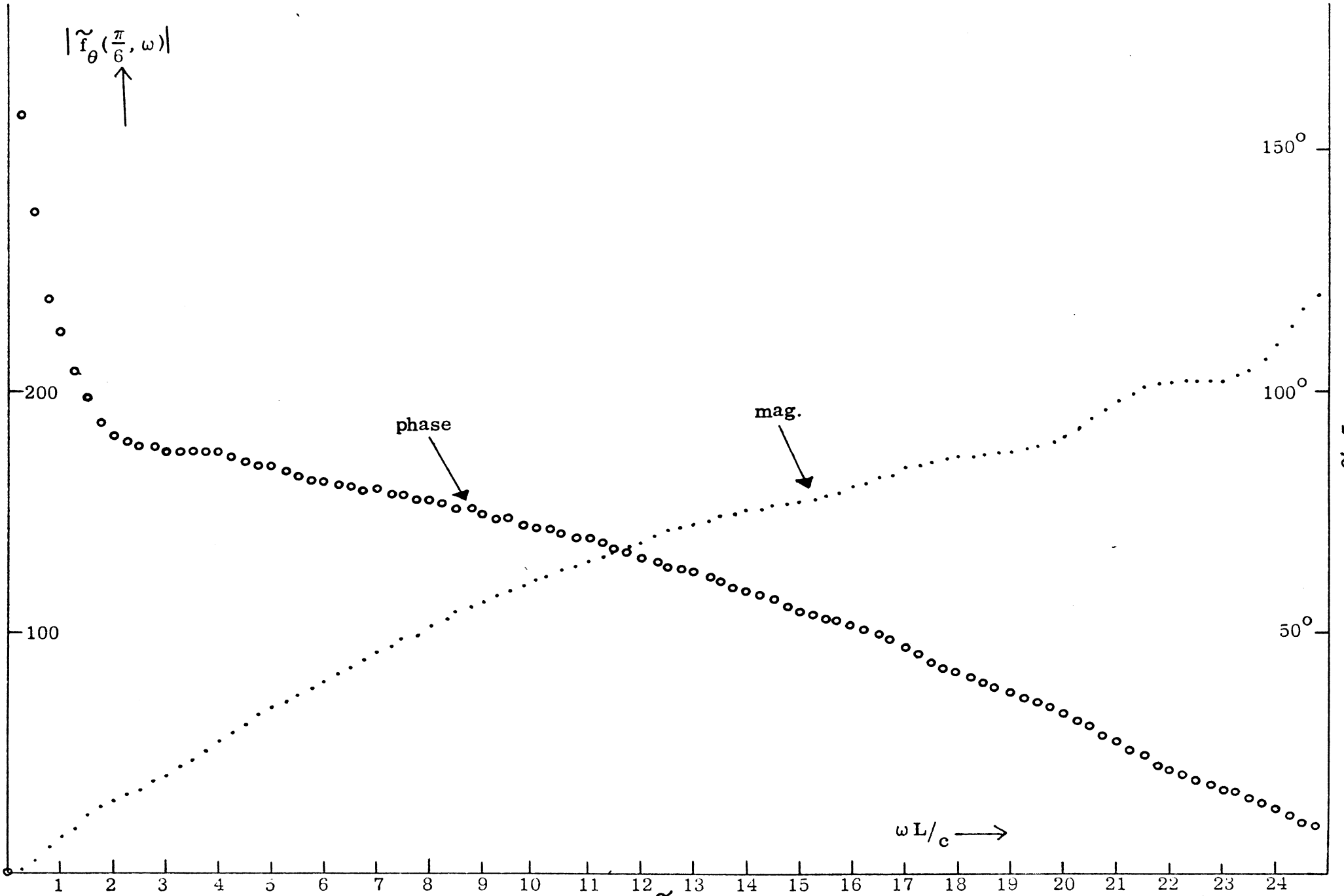

FIG. A-14d: Magnitude and phase of the transfer function $\tilde{f}_\theta(\pi/6, \omega)$ of the loaded antenna in the direction $\theta = \pi/6$ as function of kL (= $\omega L/C$) for different loading. C = 60 x 10

obtained by using Fast Fourier inversion technique.

10.1 Spectral Density $\tilde{e}_\theta(\theta, \omega)$ and the Time Domain Solution $e_\theta(\theta, t)$ of the Radiated Field Excited by Gaussian Type Pulse

In this section, results are given for the spectral density $\tilde{e}_\theta(\theta, \omega)$ and the time domain solution $\tilde{e}_\theta(\theta, t)$ excited by a Gaussian pulse input. The form of the input pulse and its Fourier transform are given by Eqs. (A.10a) and (A.11a). For the time domain results shown here, the antenna length is taken to be $L = 1$ meter. This implies that the transit time on the antenna for centerfed case is $\tau = L/c = 3.33$ nanosecond. The radius a of the antenna element is chosen such that $\Omega = 2 \ell n \frac{2L}{a} = 11.5$ in all cases.

The spectral density $\tilde{e}_\theta(\theta, \omega)$ of the radiated waveform shown here has been obtained by multiplying the transfer function of the antenna by the Fourier spectrum density function of the input signal. The waveform $e_\theta(\theta, t)$ of the radiation field produced by the antenna excited by the Gaussian signal has been obtained by numerically carrying out the integral in Eq. (A.8) with the aid of Fast Fourier inversion technique.

The results shown here have been calculated in the directions $\theta = \pi/2$, $\pi/3$, $\pi/4$ and $\pi/6$ from the antenna, where $\theta = \pi/2$ corresponds to the broadside direction. Three different values of the width of the Gaussian pulse have been considered for $\theta = \pi/2$, while only a narrow pulse has been obtained for the other directions. These pulses are chosen such that the spectral density will converge to zero at high frequencies. Four different values of the loading constant are used in each case. Figs. A-15—A-17 show $|\tilde{e}(\pi/2, \omega)|$ versus kL and $e_\theta(\pi/2, t)$ versus t for these cases with $\sigma = 0.471$ n sec., 1 n sec., 3.33 n sec. respectively. From the frequency domain results, we observe that for a wider pulse only the low frequency portion of the transfer function is responsible for the overall response. For example, when $\sigma = 3.33$ n sec., we only have to consider the frequency spectrum up to $kL = 3.5$ as shown in Fig. A-17. For a narrow pulse, a wider frequency domain of the antenna transfer function has to be considered. However, if the width of the pulse is too narrow, then the computing time re-

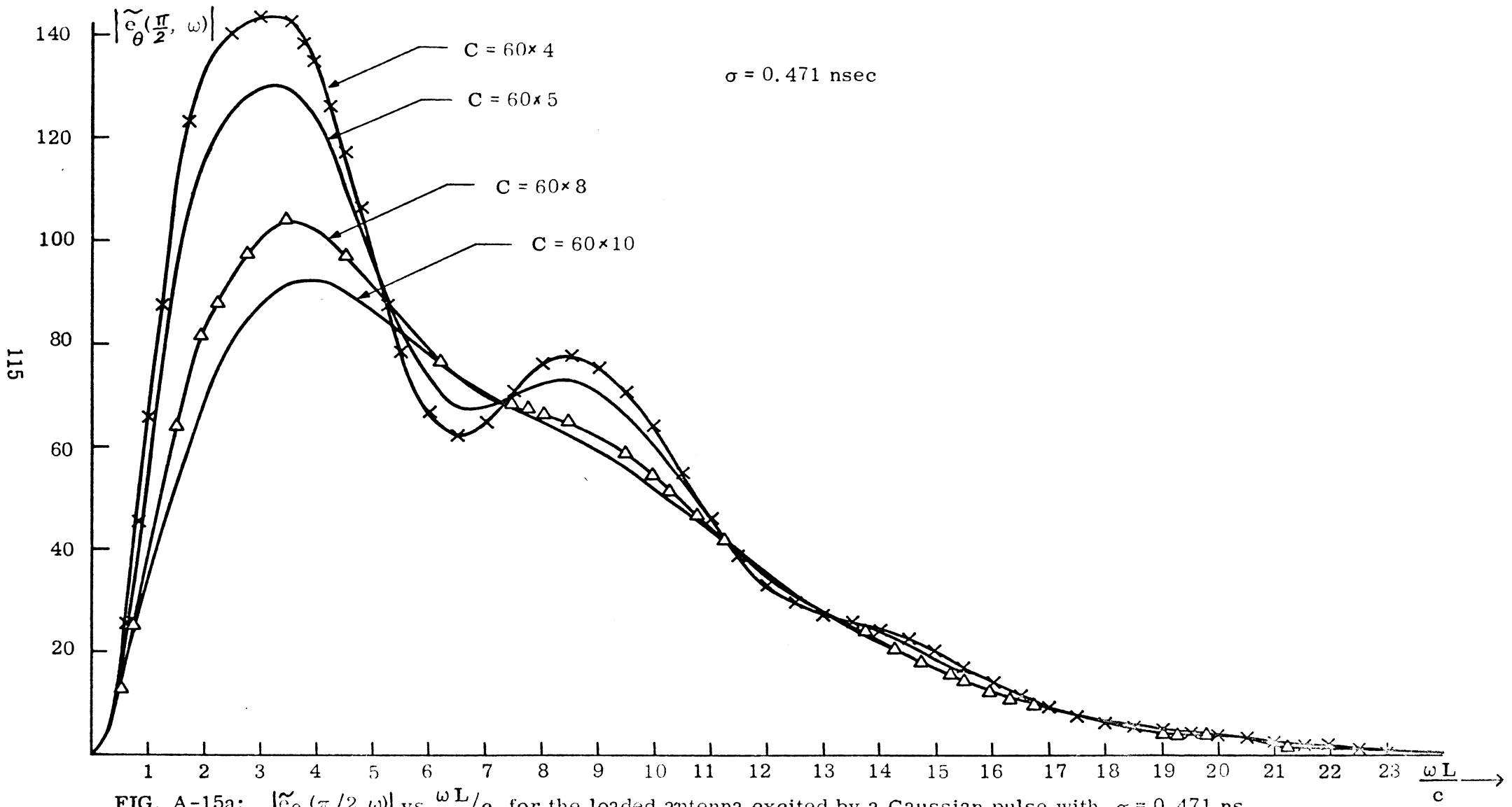

FIG. A-15a: $|\tilde{e}_\theta(\pi/2, \omega)|$ vs $\omega L/c$ for the loaded antenna excited by a Gaussian pulse with $\sigma = 0.471$ ns.

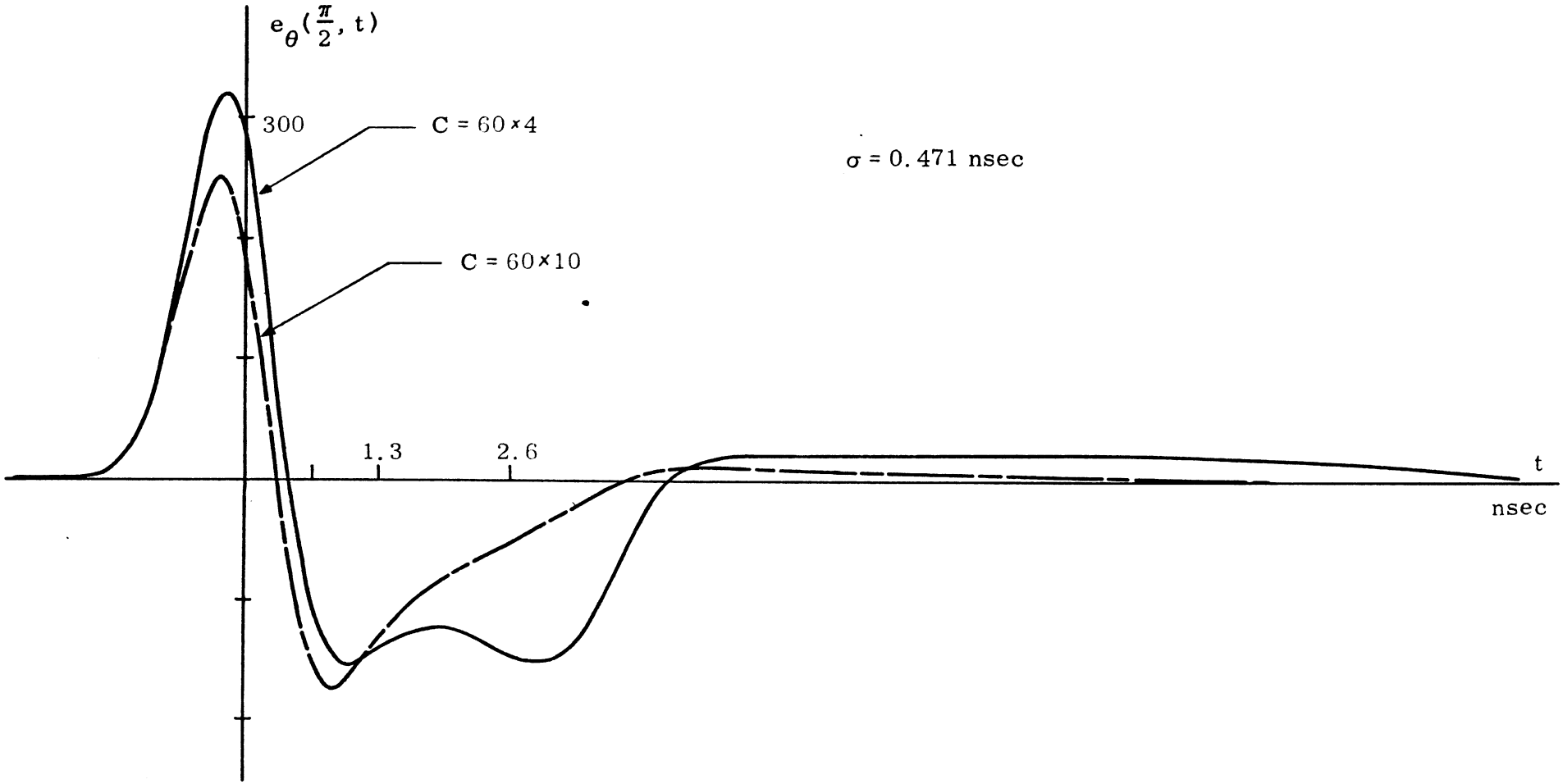

FIG. A-15b: $e_\theta(\pi/2, t)$ vs t for the loaded antenna excited by a Gaussian pulse with $\sigma = 0.471$ ns.

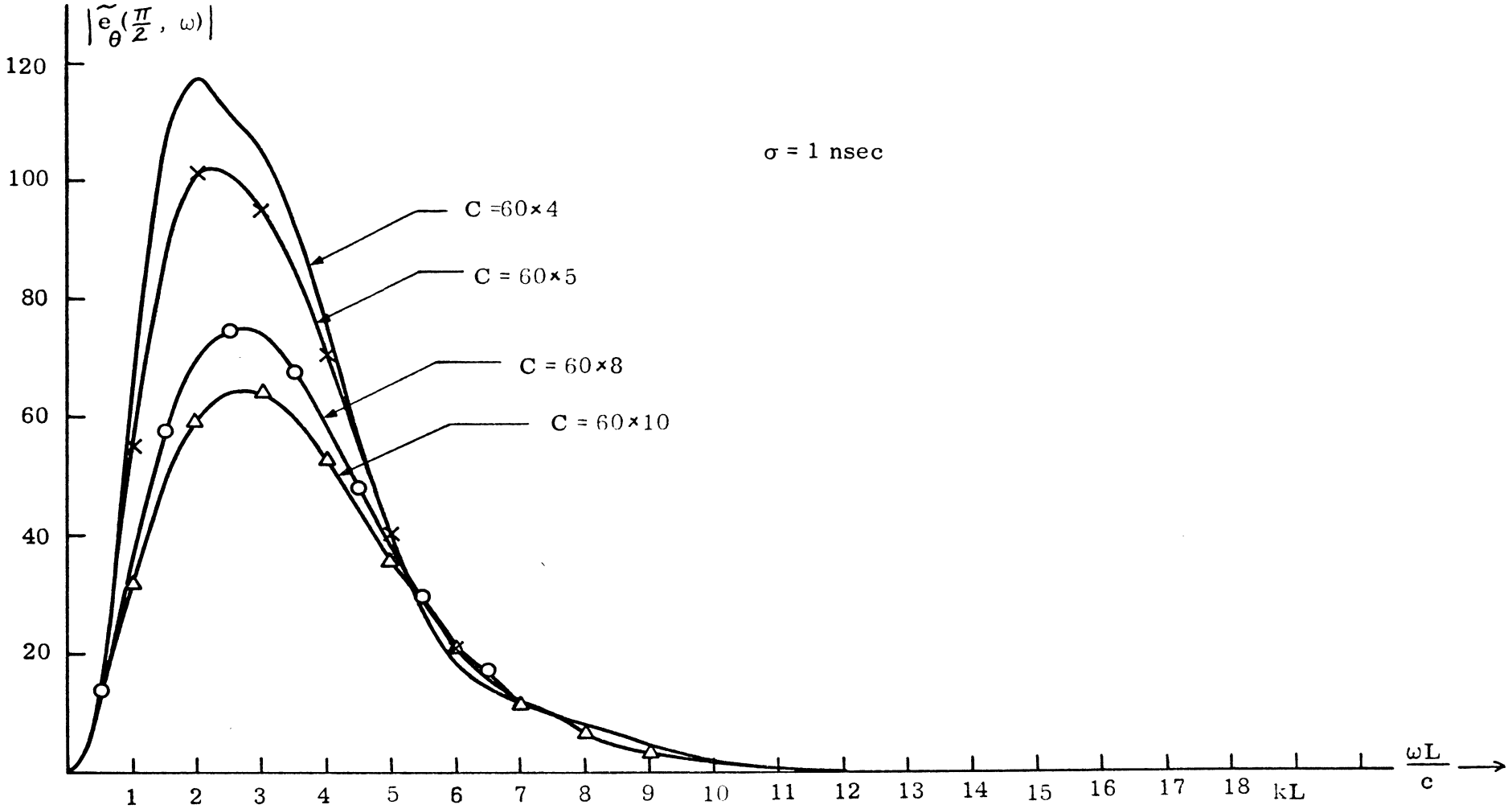

FIG. A-16a: $|e_\theta(\pi/2, \omega)|$ vs $\omega L/c$ for the loaded antenna excited by a Gaussian pulse. σ = 1 ns.

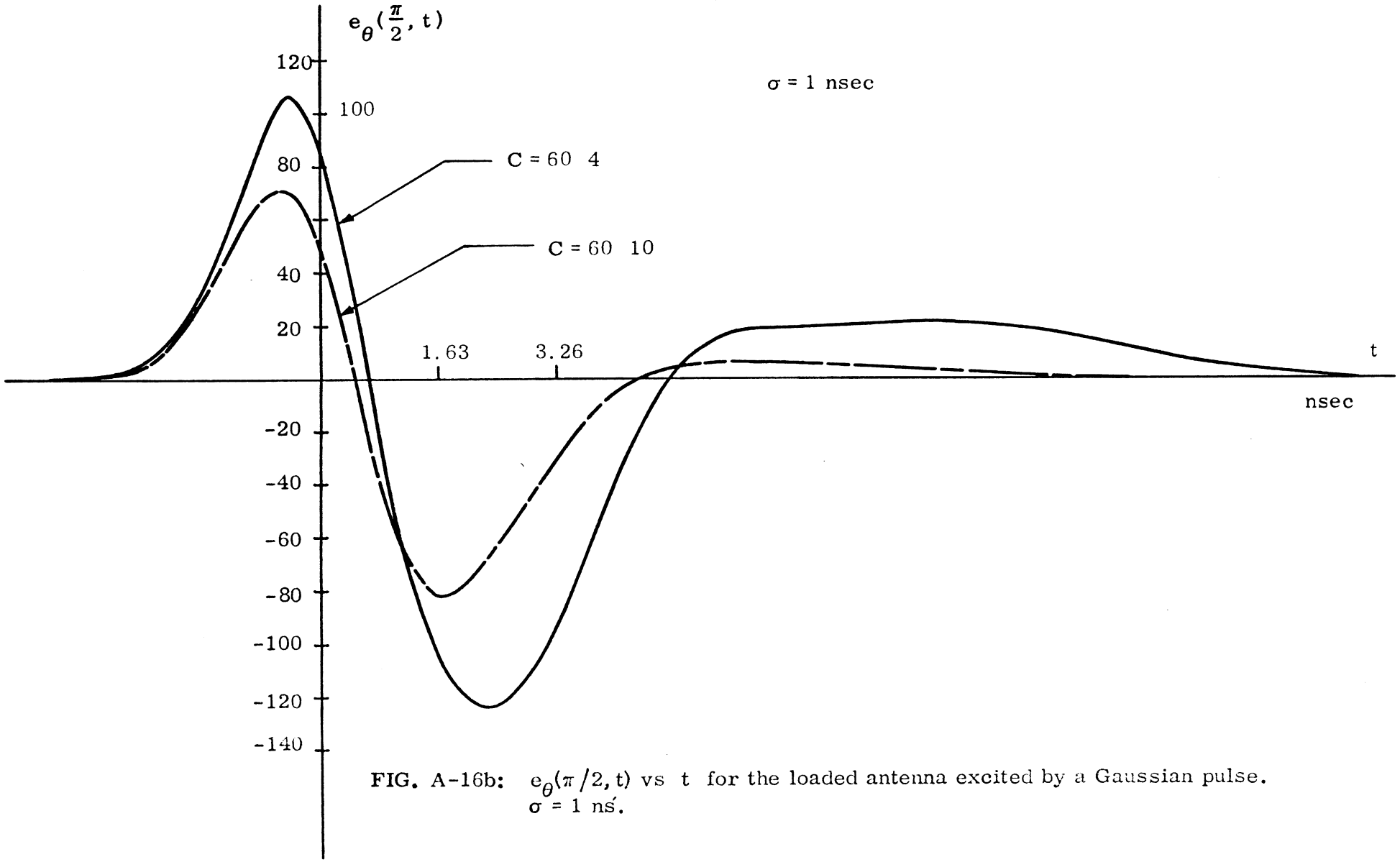

FIG. A-16b: $e_\theta(\pi/2, t)$ vs t for the loaded antenna excited by a Gaussian pulse. σ = 1 ns.

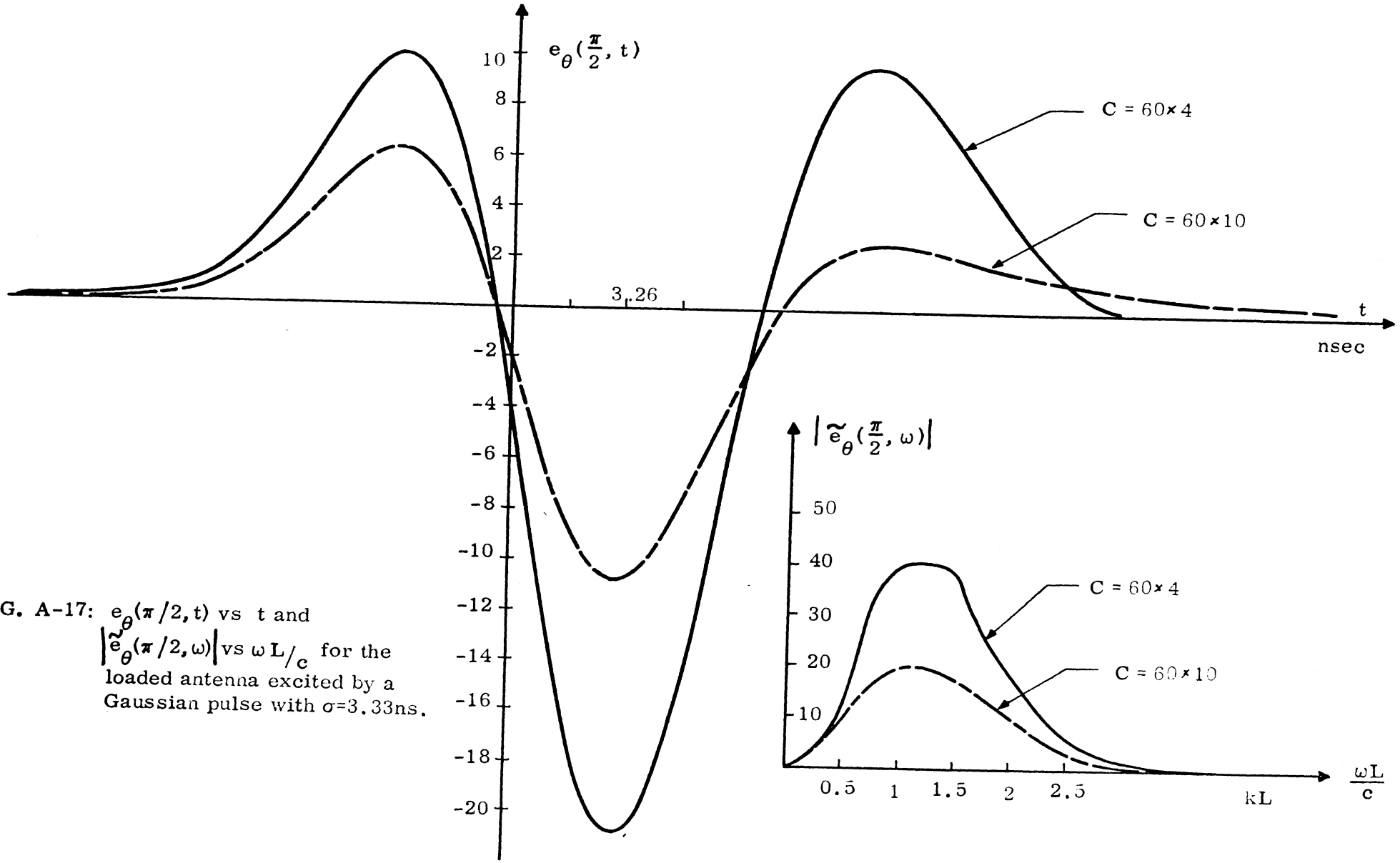

FIG. A-17: $e_\theta(\pi/2, t)$ vs t and $|\tilde{e}_\theta(\pi/2, \omega)|$ vs $\omega L/c$ for the loaded antenna excited by a Gaussian pulse with σ=3.33ns.

quired becomes excessive. For practical consideration of the computing time, we we have chosen $\sigma = 0.471$ n sec. such that the upper frequency spectrum limit corresponds to $kL = 25$.

Fig. A-15a shows $|e_\theta(\pi/2, \omega)|$ for $\sigma = 0.471$ n sec. For values of $C = 60 \times 4$ and $C = 60 \times 5$, the ringing phenomenon enters the picture. For C exceeds 60×8 the ringing disappears.

From the time domain results shown in Fig. A-15b, it appears that the initial part of the waveform represents predominantly the time derivative of the input Gaussian pulse. The general shape of the waveform depends on the radio σ/τ as expected. It is also seen that after the second zero crossing, $e(\pi/2, t)$ remains positive for all positive values of t and the magnitude decreases with the increasing C of the resistive loading.

Corresponding results are shown in Figs. A-18 — A-20 for three other directions with $\sigma = 0.471$ n sec. and for four different resistive loading. The general characteristics are similar to those discussed above. Due to the difference of the path length, the reflection occurs at different frequencies $|\tilde{e}_\theta(\theta, \omega)|$. The strength of the far field is maximum at $\theta = \pi/2$ and decreases as θ deviates from the broadside direction. In every case, the effect of loading in general reduces or eliminates the ringing.

10.2 Spectral Density $\tilde{e}_\theta(\theta, \omega)$ and the Time Domain Solution $e_\theta(\theta, t)$ of the Radiated Field Excited by a Gamma Pulse

In this section, we consider an input voltage function represented by a Gamma pulse. The equations which define this pulse and its transform are given by Eqs. (A. 10b) and (A. 11b). Unlike the Gaussian pulse, the Gamma pulse is defined here for positive values of t only.

The spectral density $\tilde{e}_\theta(\theta, \omega)$ shown here, again, has been obtained by multiplying the transfer function of the antenna with the Fourier Spectrum of the input signal. Then Fast Fourier inversion technique is used as before.

The results shown in Figs. A-22 — A-25, correspond to one particular pulse width

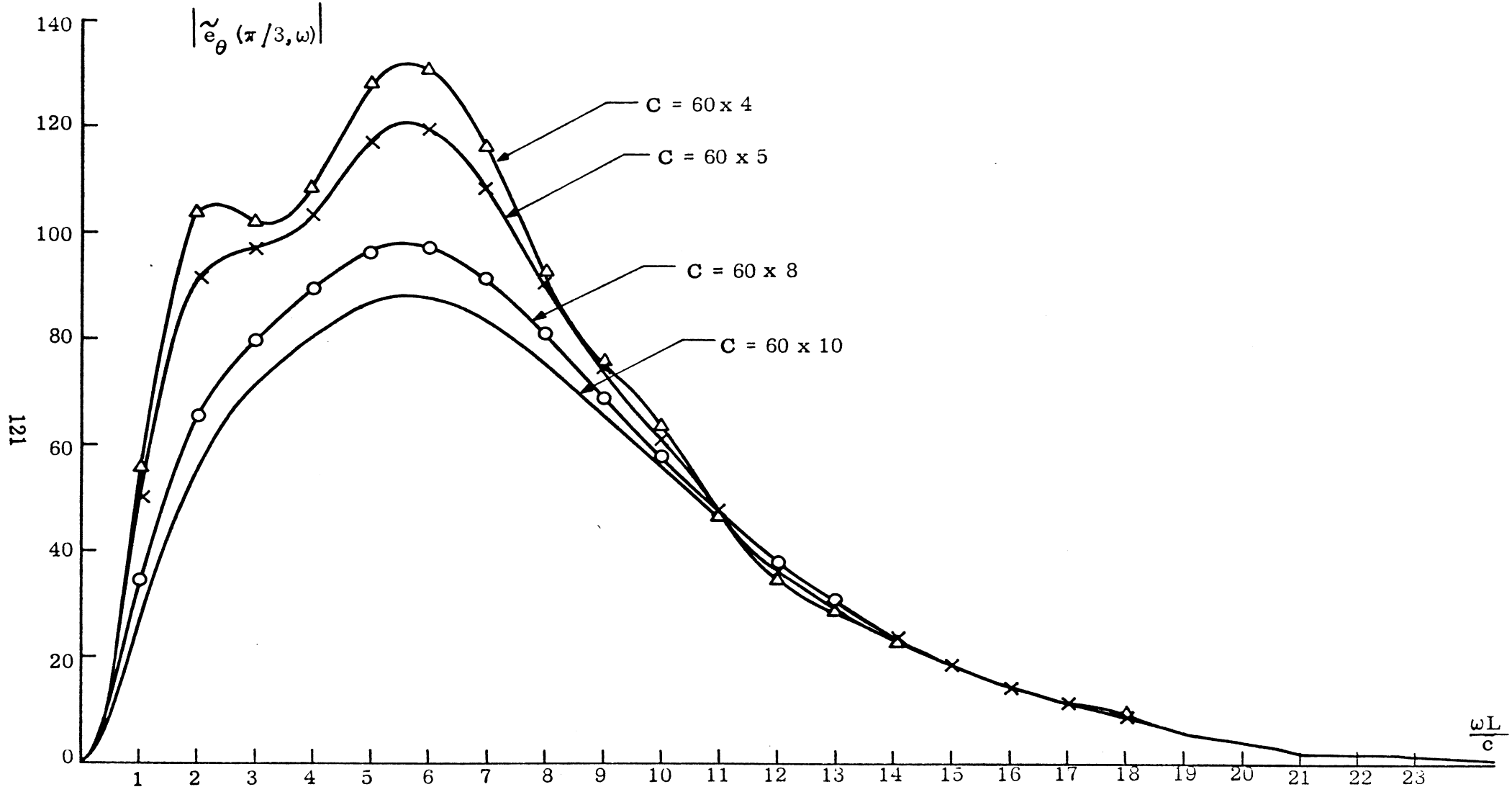

FIG. A-18a: $|\tilde{e}_\theta(\pi/3,\omega)|$ vs $\omega L/c$ for the loaded antenna excited by a Gaussian pulse with $\sigma = 0.471$ ns.

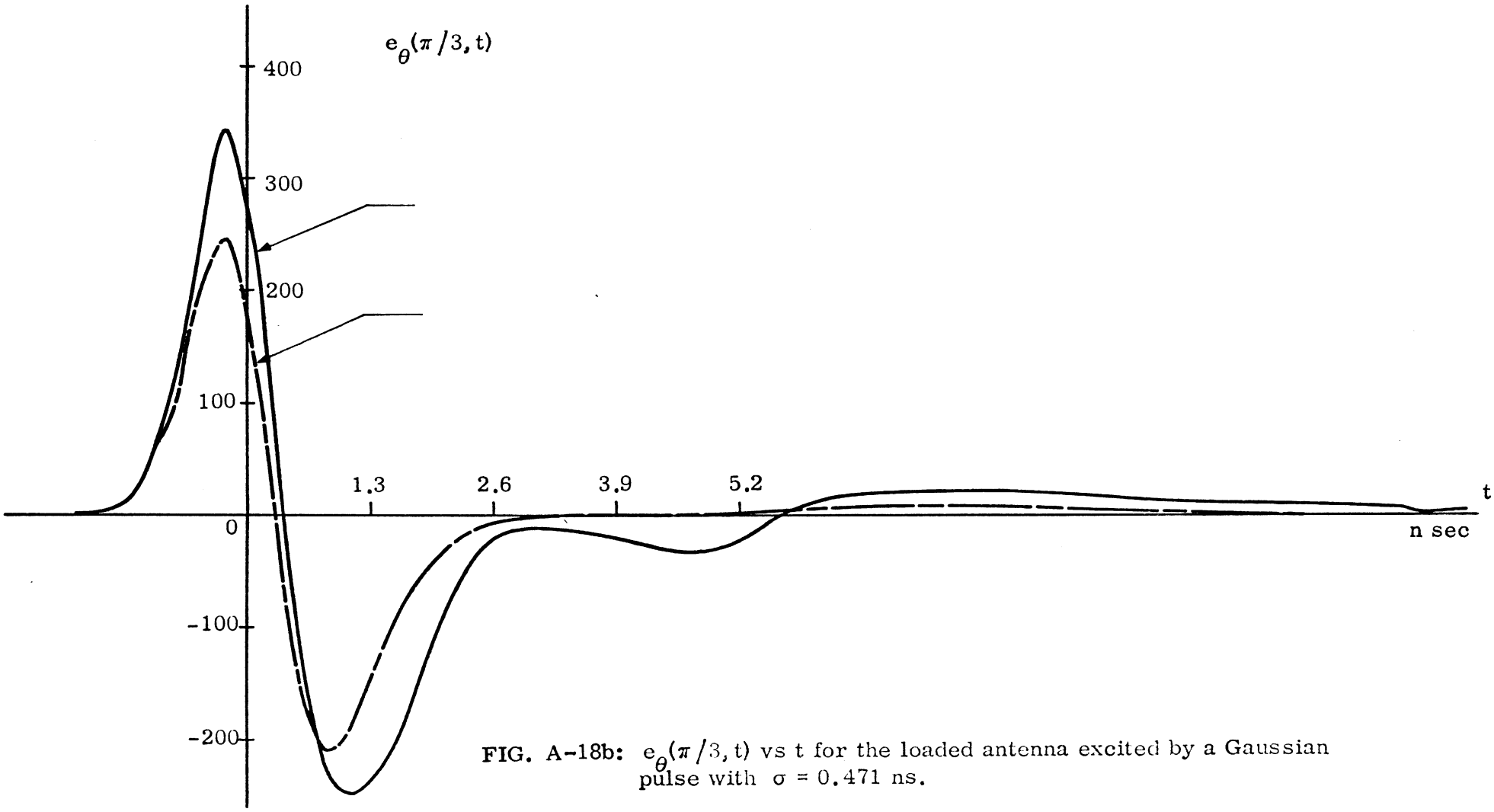

FIG. A-18b: $e_\theta(\pi/3, t)$ vs t for the loaded antenna excited by a Gaussian pulse with $\sigma = 0.471$ ns.

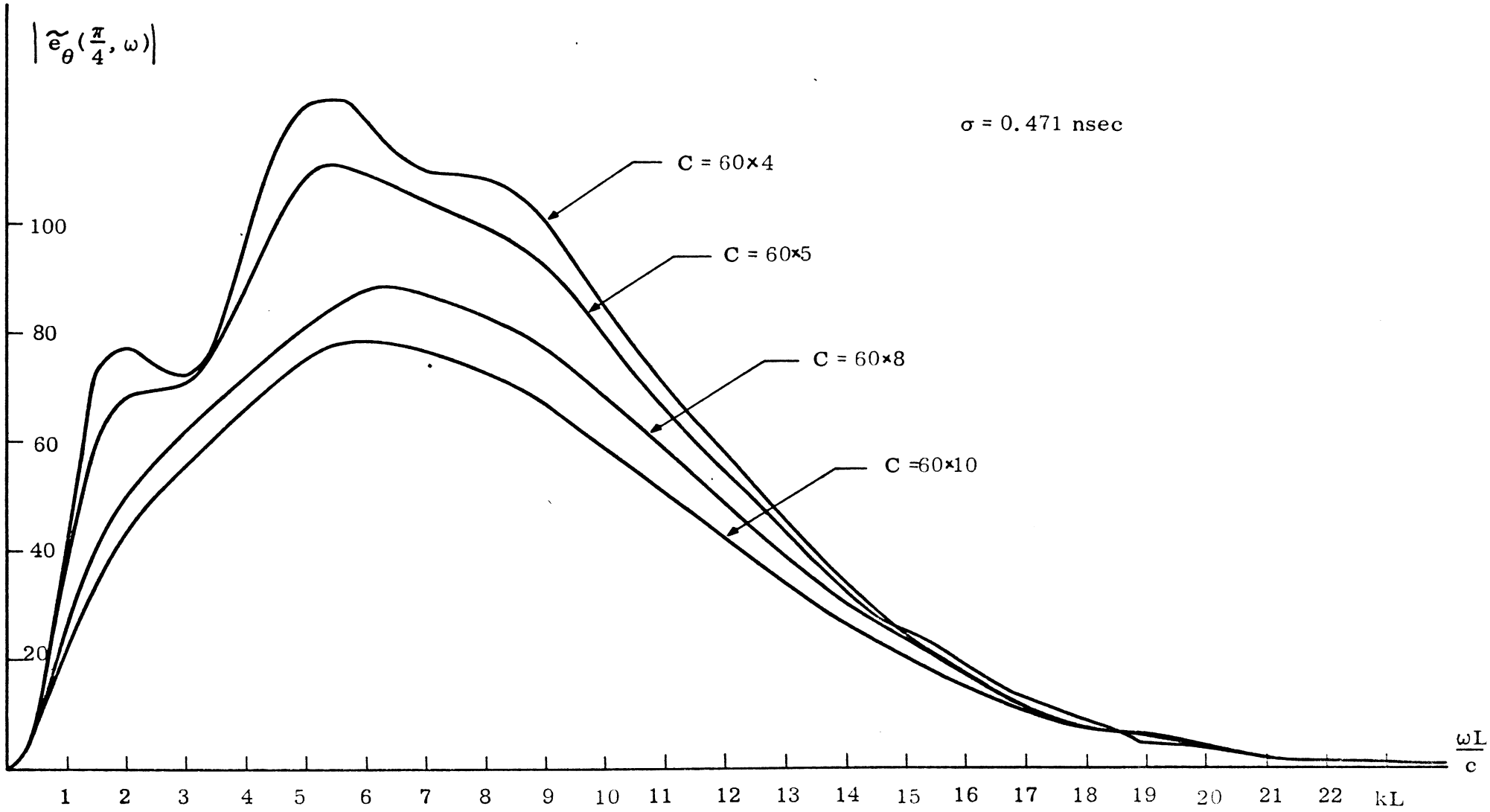

FIG. A-19a: $|\tilde{c}_\theta(\pi/4, \omega)|$ vs $\omega L/c$ for the loaded antenna excited by a Gaussian pulse with $\sigma = 0.471$ ns.

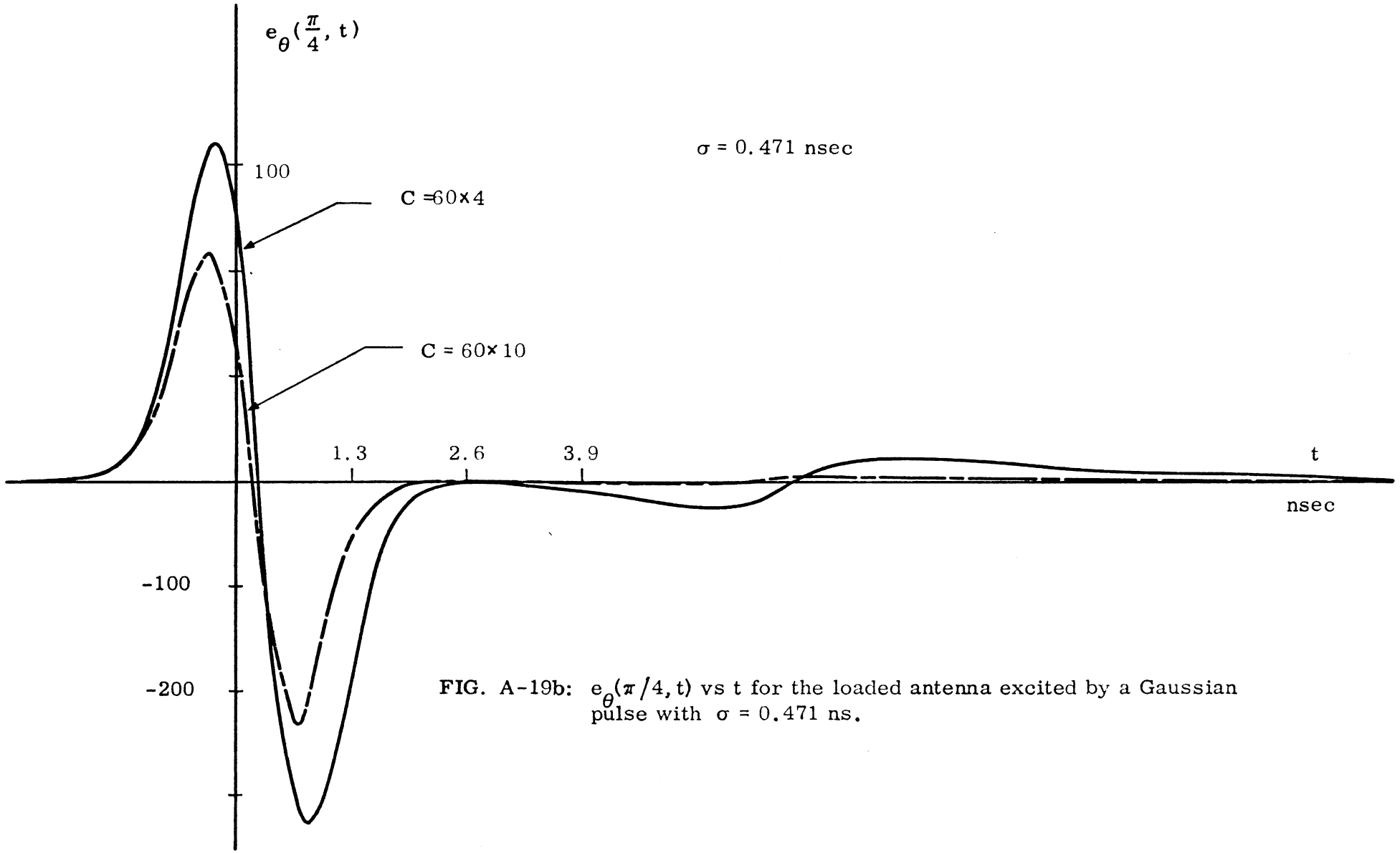

FIG. A-19b: $e_\theta(\pi/4, t)$ vs t for the loaded antenna excited by a Gaussian pulse with σ = 0.471 ns.

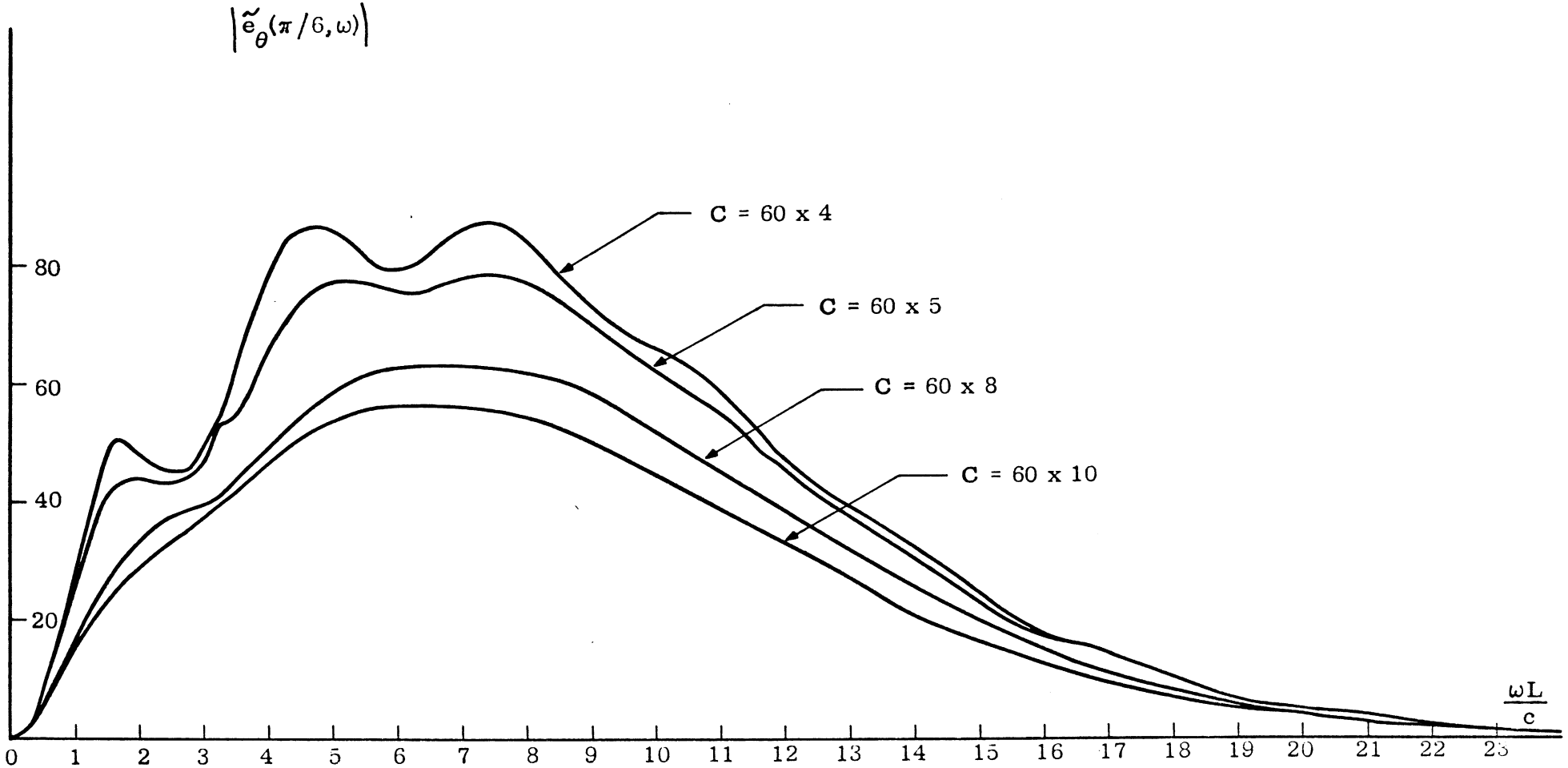

FIG. A-20a: $\left|\tilde{e}_\theta(\pi/6,\omega)\right|$ vs $\omega L/c$ for the loaded antenna excited by a Gaussian pulse with $\sigma = 0.471$ ns.

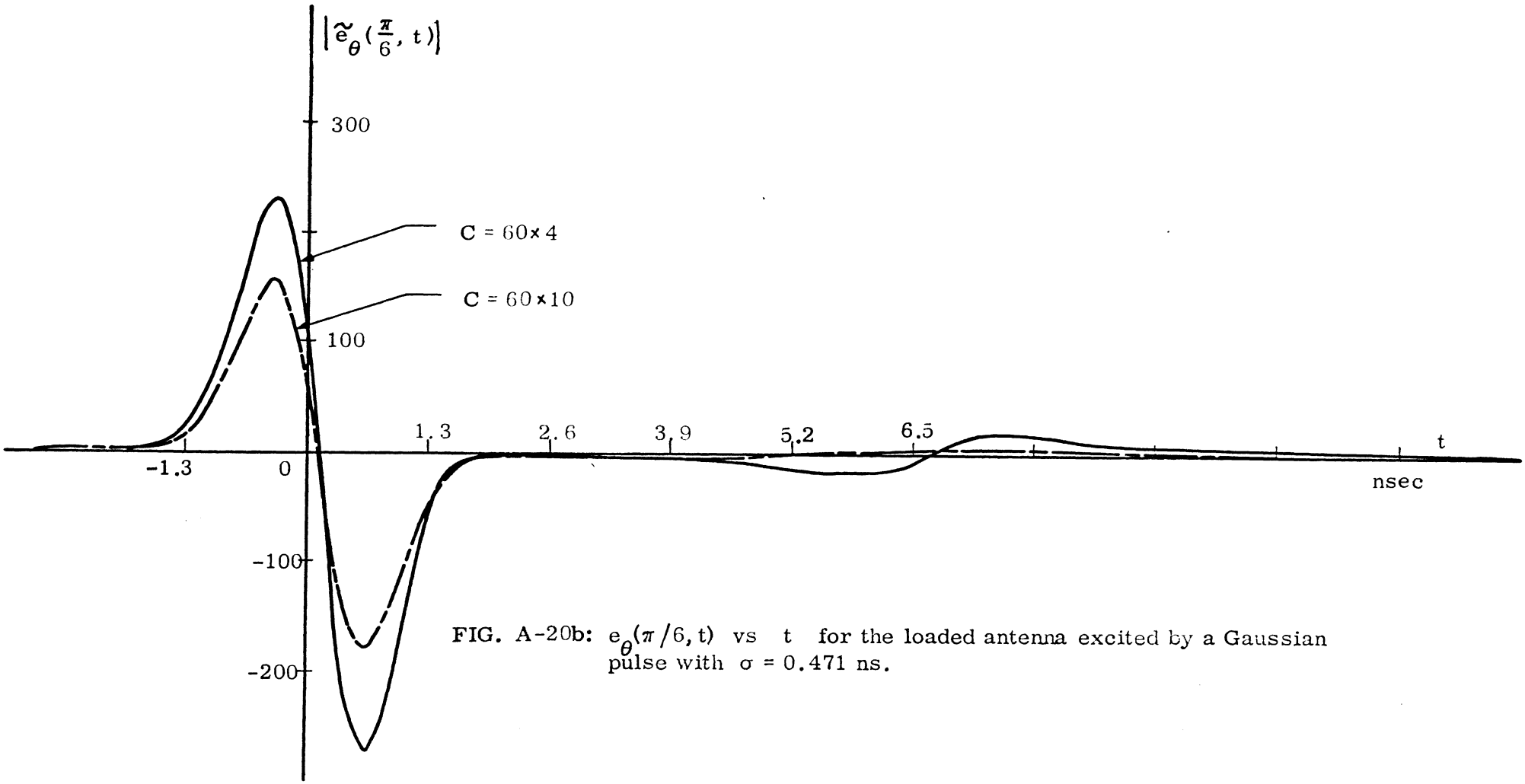

FIG. A-20b: $e_\theta(\pi/6, t)$ vs t for the loaded antenna excited by a Gaussian pulse with $\sigma = 0.471$ ns.

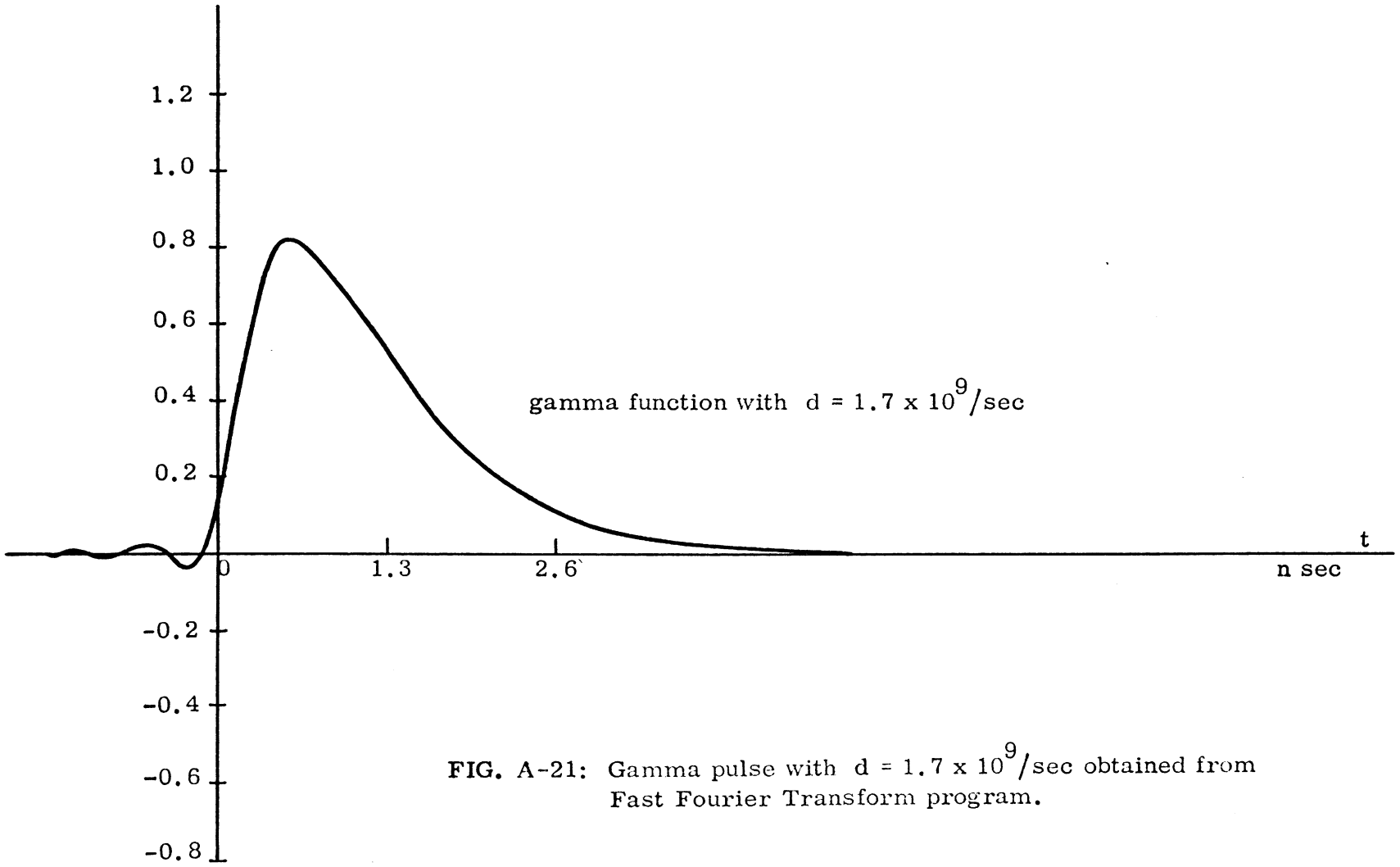

FIG. A-21: Gamma pulse with $d = 1.7 \times 10^9$/sec obtained from Fast Fourier Transform program.

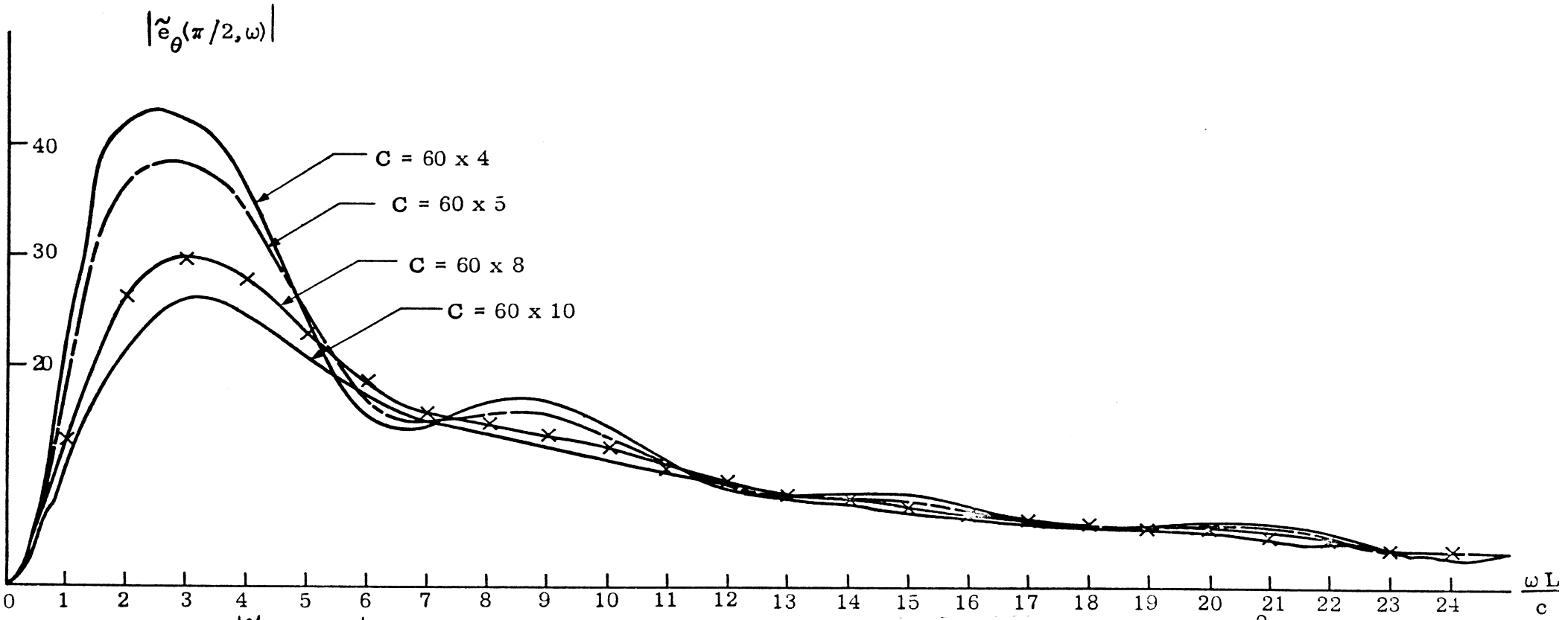

FIG. A-22a: $|\tilde{e}_\theta(\pi/2,\omega)|$ vs $\omega L/c$ for the loaded antenna excited by a gamma pulse with $d = 1.7 \times 10^9$/sec.

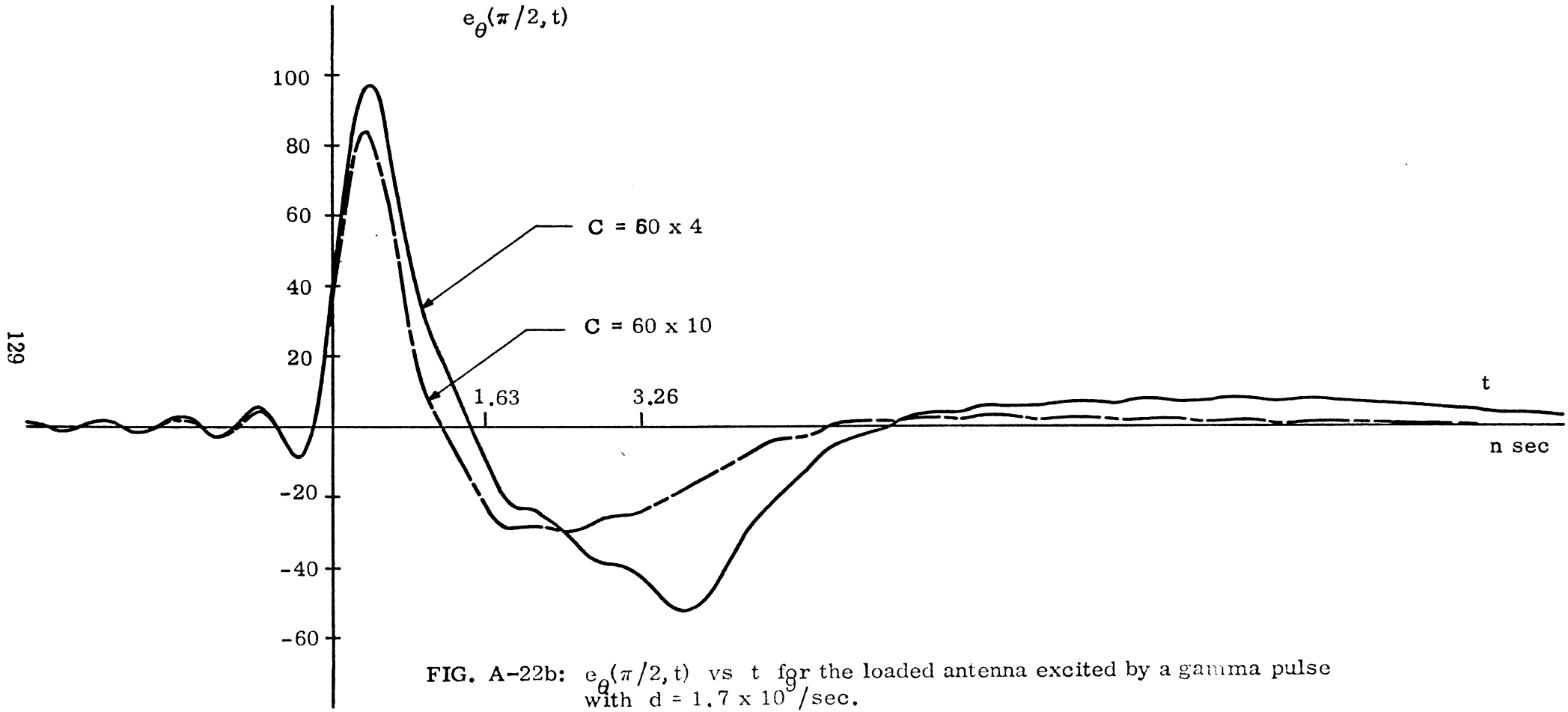

FIG. A-22b: $e_\theta(\pi/2, t)$ vs t for the loaded antenna excited by a gamma pulse with $d = 1.7 \times 10^9$/sec.

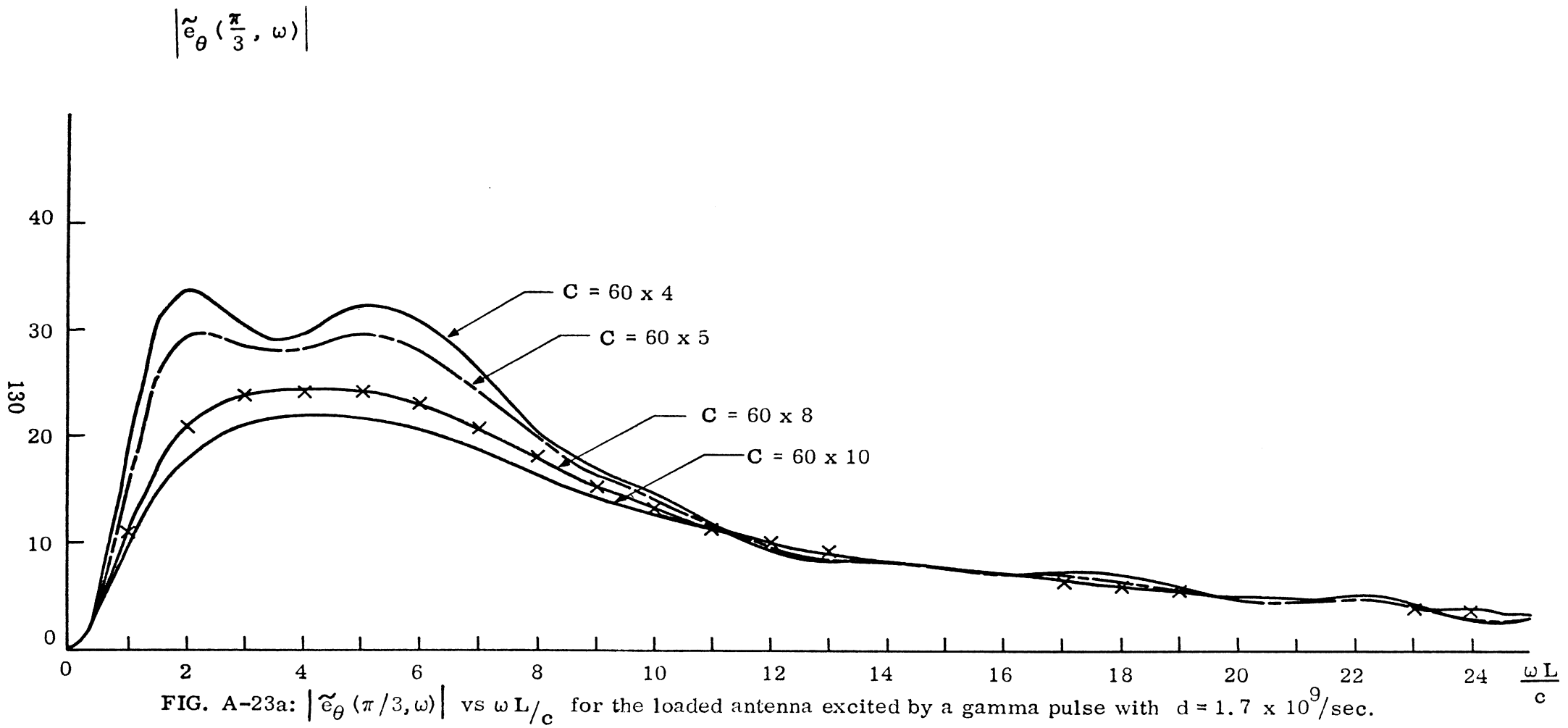

FIG. A-23a: $\left|\tilde{e}_\theta(\pi/3, \omega)\right|$ vs $\omega L/c$ for the loaded antenna excited by a gamma pulse with $d = 1.7 \times 10^9/\text{sec}$.

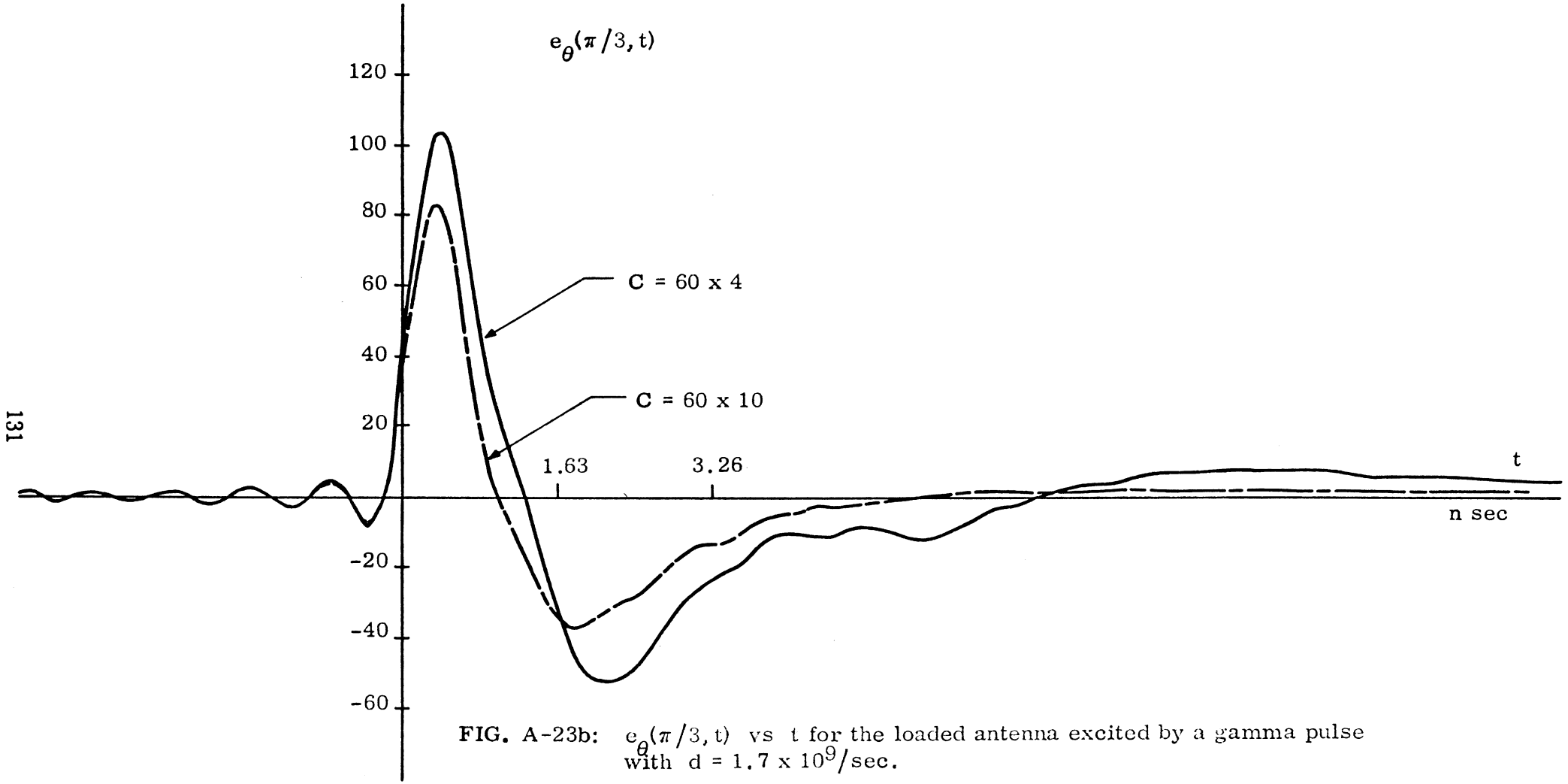

FIG. A-23b: $e_\theta(\pi/3, t)$ vs t for the loaded antenna excited by a gamma pulse with d = 1.7×10^9/sec.

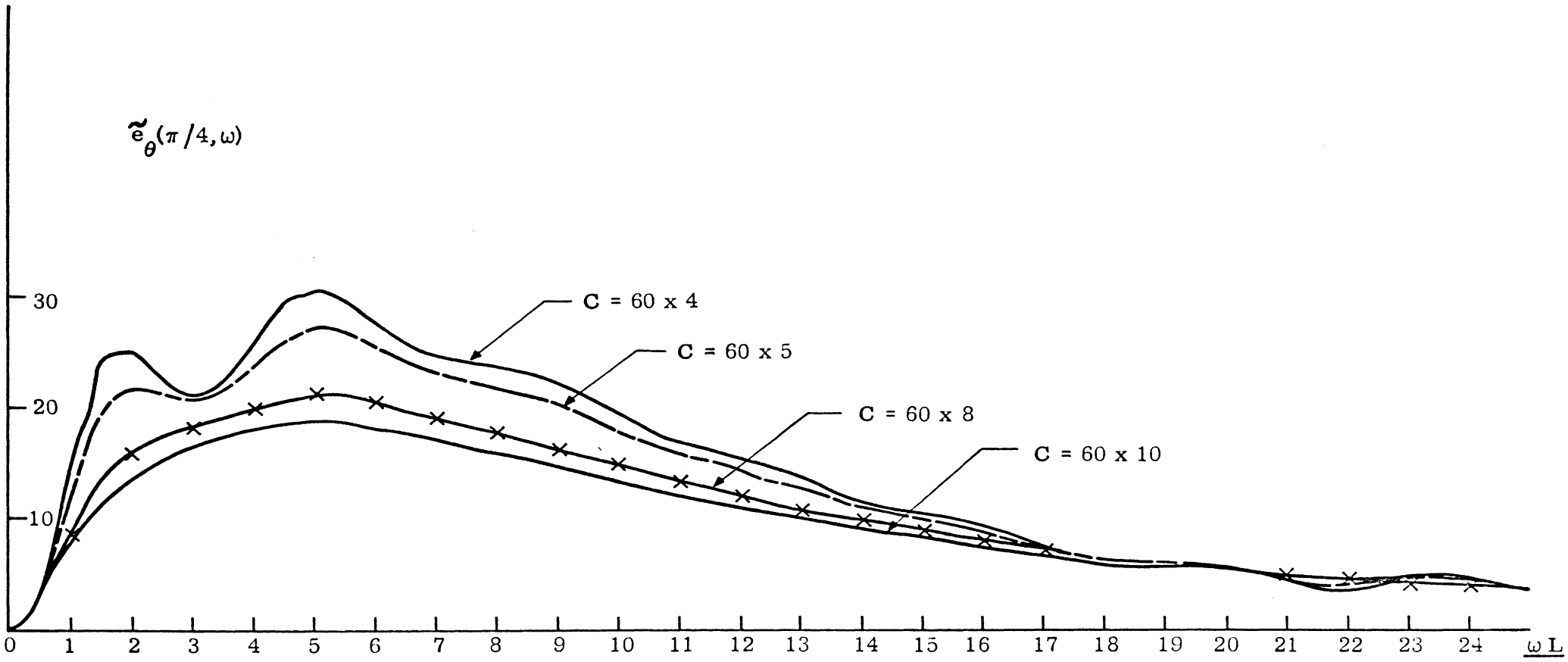

FIG. A-24a: $\left|\tilde{e}_\theta(\pi/4,\omega)\right|$ vs $\omega L/c$ for the loaded antenna excited by a gamma pulse with $d = 1.7 \times 10^9$/sec.

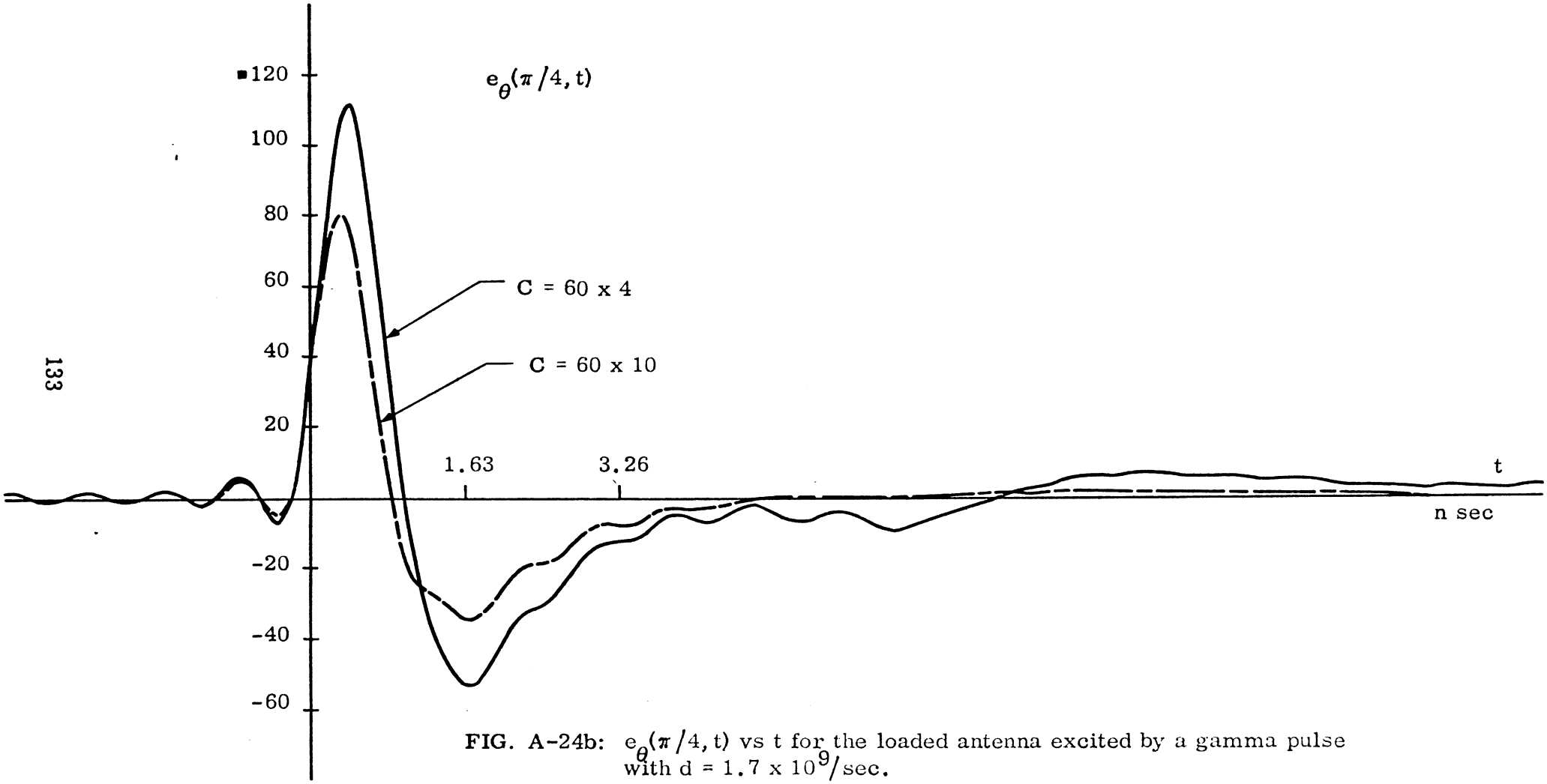

FIG. A-24b: $e_\theta(\pi/4, t)$ vs t for the loaded antenna excited by a gamma pulse with d = 1.7×10^9/sec.

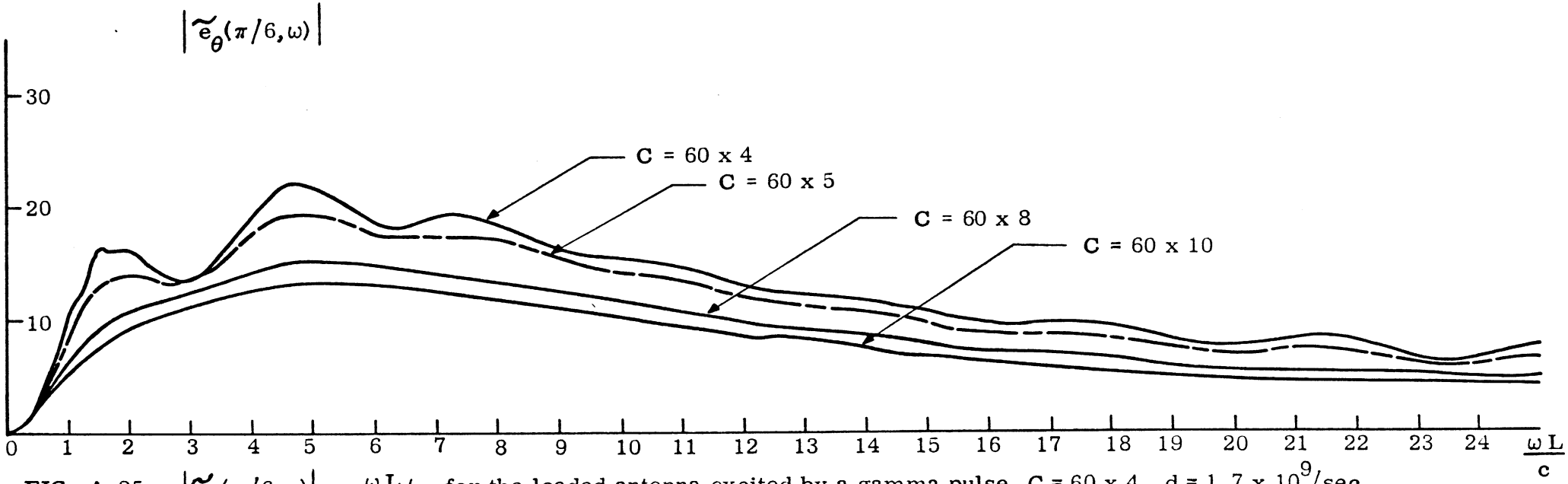

FIG. A-25a: $|\tilde{e}_\theta(\pi/6,\omega)|$ vs $\omega L/c$ for the loaded antenna excited by a gamma pulse C = 60 x 4, d = 1.7 x 10^9/sec.

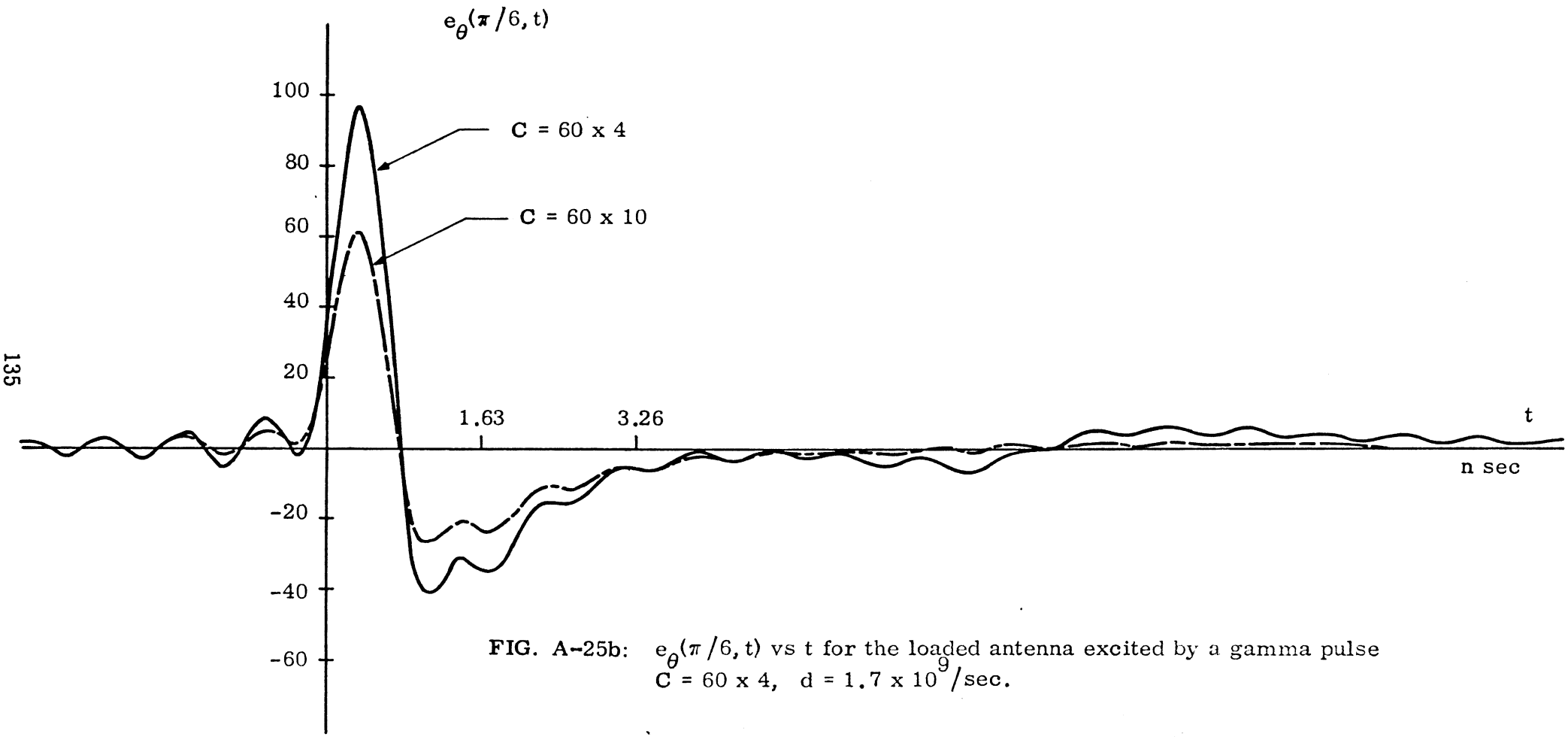

FIG. A-25b: $e_\theta(\pi/6, t)$ vs t for the loaded antenna excited by a gamma pulse $C = 60 \times 4$, $d = 1.7 \times 10^9$/sec.

at four different directions. For each direction in space, four values of loading have been considered. The width d of the gamma pulse is chosen to be 1.7×10^9 / sec. which approximates the same width as that of a Gaussian pulse with $\sigma = 0.47$. Figure A-21 shows the input gamma pulse reproduced by using the Fast Fourier inversion program. This computation is to show the round-off error involved in the F. F. T. program for sharply rising pulse. The truncation of the high frequency portion of the spectrum also induces error. The error results in the oscillating portion for negative value of t and the shift of the starting point to the left instead of at zero. Similar error would be introduced in computing the time domain solutions based on gamma pulse input.

Since gamma pulse does not converge to zero as fast as Gaussian pulse, the spectral density shows small oscillation at high frequencies as shown in Figs. A-22--A-25. The truncation of a gamma pulse also introduces a larger error than that of a Gaussian at the same truncation frequency. Except for these minor variations, the general behavior of the time domain solution presented previously for the Gaussian pulse also applies to the gamma pulse.

11. CONCLUSION

The waveform of the far-zone field radiated by a non-uniform resistively loaded linear antenna excited by a voltage pulse has been investigated by numerical means. Results have been obtained for a Gaussian pulse with three different pulse width and for one particular gamma pulse at four directions of observation. Various values of the loading parameter have been considered.

In general, the resultant waveform corresponds to the convolution of the harmonic response and the input signal. The initial portion of the resultant wave however, appears to be proportional to time derivative of the input signal.

The result shows that the amplitude of the current distribution on the harmonically excited antenna is almost linear, being independent of the loading resis-

tance when the latter exceeds certain value. The phase of the current represents the characteristics of a traveling wave. Thus, the analysis of Baum[1] based on the transmission line model appears to be a valid description of the current for a resistively loaded antenna too. Our study also verifies the work of Wu and King[3] who examined the problem only for one particular loading at a single frequency. In the broadside direction, the waveform exhibits a compression in pulse width as the loading resistance is increased. No general trend is observed in other directions.

For a Gaussian pulse, our numerical results check very well with the analytical solution which indicates that the computing program has been properly executed. To simulate practical problems, we have considered the excitation to be presented by gamma pulse. In general, much of the result obtained using the Gaussian pulse also applies to the gamma pulse. One significant difference concerns the computing error involved in the two cases. For a gamma pulse, the truncation error appears to be prominent. As a whole, it appears that a "critical" damping can be achieved when the loading resistance attains a certain sufficiently high value, corresponding to $C \geq 60 \times 10$.

APPENDIX B

ANALYTICAL INVESTIGATION OF WAVEFORMS RADIATED BY A RESISTIVELY LOADED LINEAR ANTENNA EXCITED BY A GAUSSIAN PULSE

ABSTRACT

The far field waveforms radiated by linear antennas loaded non-uniformly and continuously with resistance are investigated analytically. The antennas considered are symmetrical and excited at the centers by slice generators having Gaussian pulse type of time dependence. Expressions have been developed for the far field waveforms produced by such antennas in any direction. The analytic results have been compared with those obtained by direct numerical means. The general agreement between the two results has been found to be satisfactory. It is thus concluded that the various expressions given may be used to study the behavior of waveforms radiated by a resistively loaded linear antenna excited by Gaussian pulse type signals.

1. INTRODUCTION

The present report discusses analytically the far field waveforms produced by symmetrical linear antennas loaded non-uniformly and continuously with resistance. The antennas considered are thin cylinders and excited at the centers by slice generators having Gaussian pulse type of time dependence. Emphasis is given here to a specific type of loading in which the amount of loading increases continuously towards the antenna end-points.

Direct numerical investigation of such a problem has been discussed in Appendix A. Here we derive theoretical expressions for the waveforms produced by the loaded linear antenna excited by Gaussian pulse type time dependent signals. Fourier transform technique is utilized in obtaining the final time dependent results. Numerical results are obtained by computing the various expressions derived. These results are then compared with those obtained by direct numerical means.

2. BASIC RELATIONS

Let us assume that the linear antenna of length 2 L be aligned along the z-axis of a rectangular coordinate system with the origin located at the center of the antenna and that it is excited by a slice generator located at the origin. The far electric field produced by the antenna when excited by a harmonically time dependent slice generator of unit strength consists of only a θ-component and is given by the following expression:

$$F = \tilde{F}_{\theta}(r, \theta, \omega)\, e^{j\omega t} \quad , \tag{B.1}$$

where,

$$\tilde{F}(r, \theta, \omega) = \frac{j\omega\eta_o \sin\theta}{4\pi c} \frac{e^{-j\frac{\omega}{c}r}}{r} \int_{-L}^{L} \tilde{I}(z', \omega)\, e^{j\frac{\omega}{c}z'\cos\theta}\, dz' \quad , \tag{B.2}$$

$\eta_o = \sqrt{\frac{\mu_o}{\epsilon_o}}$ is the intrinsic impedance of free space,

$c = \frac{1}{\sqrt{\mu_o \epsilon_o}}$ is the velocity of light in free space,

r, θ, ϕ are the spherical polar coordinates of the far field point with origin located at the center of the antenna,

$\tilde{I}(z', \omega)$ is the current distribution on the antenna due to the harmonically time dependent slice generator.

$\tilde{F}_\theta(r, \theta, \omega)$ is the time independent far electric field produced by the antenna and may be looked upon as the transfer function of the antenna. For convenience we define the following modified form for the antenna transfer function:

$$\tilde{f}_\theta(\theta, \omega) = r\tilde{F}_\theta(r, \theta, \omega)\, e^{i\frac{\omega}{c}r}$$

$$= \frac{j\omega\eta_o \sin\theta}{4\pi c} \int_{-L}^{L} \tilde{I}(z', \omega)\, e^{j\frac{\omega}{c}z'\cos\theta}\, dz' \quad , \tag{B.3}$$

Notice that in the modified transfer function given by Eq. (B.3), the dependence on the factor r as well as the phase shift suffered by the signal in traveling from the antenna to the field point are both suppressed.

Let the time waveform of the input voltage signal be given by:

$$V(t) = e^{-t^2/2\sigma^2} \quad , \tag{B.4}$$

where σ is proportional to the width of the input Gaussian pulse. The Fourier transform $\tilde{V}(\omega)$ of $V(t)$ is obtained as follows:

$$\tilde{V}(\omega) = \int_{-\infty}^{\infty} V(t)\, e^{-j\omega t}\, dt = \sqrt{2\pi}\,\sigma\, e^{-\omega^2\sigma^2/2} \quad . \tag{B.5}$$

By making use of the linearity of the system along with superposition theorem and the concepts of Fourier transform technique, it can be shown that the modified time dependent far field produced by the antenna excited by a Gaussian voltage pulse is given by the following:

$$e_\theta(\theta, t) = \frac{1}{2\pi}\int_{-\infty}^{\infty} \tilde{e}_\theta(\theta, \omega)\, e^{j\omega t}$$

$$= \frac{1}{2\pi}\int_{-\infty}^{\infty} \tilde{f}_\theta(\theta, \omega)\, \tilde{V}(\omega)\, e^{j\omega t} \quad . \tag{B.6}$$

In Eq. (B.6) the quantity $\tilde{e}_\theta(\theta, \omega) = \tilde{f}_\theta(\theta, \omega)\tilde{V}(\omega)$ may be looked upon as the spectral density of the far field wave. Notice that by definition $e_\theta(\theta, t)$ and $\tilde{e}_\theta(\theta, \omega)$ are related to each other by the following transform relationship

$$\tilde{e}_\theta(\theta, \omega) = \int_{-\infty}^{\infty} e_\theta(\theta, t)\, e^{-j\omega t}\, dt$$

$$= \tilde{f}_\theta(\theta, \omega)\, \tilde{V}(\omega) \quad . \tag{B.7}$$

3. TRANSFER FUNCTION OF THE ANTENNA $\tilde{f}_\theta(\theta, \omega)$.

In this section we discuss the evaluation of the modified transfer function of the antenna as given by Eq. (B.3). To obtain $\tilde{f}_\theta(\theta, \omega)$ it is necessary to know the current distribution $\tilde{I}(z, \omega)$ on the antenna excited by the harmonically time dependent unit slice generator.

Let the antenna be resistively loaded in the following fashion:

$$r_s(z) = \frac{C}{L - |z|} \text{ ohms/meter} \quad , \tag{B.8}$$

where C is a constant expressed in ohms. For some special value of C, the loaded linear antenna sustains a pure outward traveling wave of current for the time harmonic case[3,4,24]. In particular, for the non-reflecting case the necessary loading is,

$$r_s(z) = \frac{\eta_o \psi}{2\pi} \frac{1}{L-|z|} \tag{B.9}$$

which means that the constant $C = \frac{\eta_o \psi}{2\pi}$, where ψ is obtained from the expansion parameter as defined by King and Wu[2].(Note: in this notation $r_o = C/L$). As discussed in the references cited, the current distribution on the antenna loaded according to Eq. (B.8) and excited by a harmonically time dependent unit slice generator is given by:

$$\tilde{I}(z,\omega) = \frac{2\pi}{\eta_o \psi} \left[\frac{j\omega L/c}{1+j\omega L/c}\right] \left[1 - \frac{|z|}{L}\right] e^{-j\frac{\omega}{c}|z'|} . \tag{B.10}$$

We shall not go into more discussion of the current distribution on the antenna. The parameter ψ in Eq. (B.10) is very slowly varying function[3] of ω and will be assumed from now on that ψ is a constant for an antenna of given length L and $\Omega = 2\ell n \frac{2L}{a}$, where a is the radius of the antenna element. For the non-reflecting case[5] $\psi \simeq 5.3$. Thus Eq. (B.10) gives the complete description of the current distribution on the non-reflectively loaded linear antenna excited by a harmonically time dependent slice generator of unit strength.

After introducing Eq. (B.10) into Eq. (B.3) the following expression is obtained for the antenna transfer function:

$$\tilde{f}_\theta(\theta,\omega) = \frac{\sin\theta}{2\psi} \frac{(j\omega\tau)(j\omega\tau)}{1+j\omega\tau} \times$$

$$\times \int_{-1}^{1} (1-|\nu|)\, e^{-j\omega\tau|\nu|}\, e^{j\omega\tau\nu\cos\theta}\, d\nu , \tag{B.11}$$

where,

$\tau = \frac{L}{c}$ = is the transit time of the signal on the antenna.

The integral involved in Eq. (B.11) can be carried out in closed form and is given by the following:

$$\int_{-1}^{1} (1-|\nu|)\, e^{-j\omega\tau|\nu|} e^{j\omega\tau\nu\cos\theta}\, d\nu$$

$$= \frac{1}{j\omega\tau(1-\cos\theta)}\left[\frac{e^{-j\omega\tau(1-\cos\theta)}-1}{j\omega\tau(1-\cos\theta)}+1\right]$$

$$+ \frac{1}{j\omega\tau(1+\cos\theta)}\left[\frac{e^{-j\omega\tau(1+\cos\theta)}-1}{j\omega\tau(1+\cos\theta)}+1\right] \quad . \qquad \text{(B.12)}$$

After introducing Eq. (B.12) into Eq. (B.11) we obtain the complete expression for the antenna transfer function $\tilde{f}_\theta(\theta,\omega)$.

4. SPECTRAL DENSITY OF THE FAR FIELD WAVEFORM: $\tilde{e}_\theta(\theta,\omega)$.

In this section we obtain the spectral density function $\tilde{e}_\theta(\theta,\omega)$ for the antenna when excited by a Gaussian pulse. This is done by making use of Eqs. (B.5), (B.7) (B.11) and (B.12) and the final result is given by the following expression:

$$\tilde{e}_\theta(\theta,\omega) = \frac{\sigma}{\psi}\sqrt{\frac{\pi}{2}}\,\sin\theta\,\frac{(j\omega\tau)(j\omega\tau)}{1+j\omega\tau}\,e^{-\sigma^2\omega^2/2}$$

$$\times\left[\frac{1}{j\omega\tau}\,\frac{1}{1-\cos\theta}\left\{\frac{e^{-j\omega\tau(1-\cos\theta)}-1}{(j\omega\tau)(1-\cos\theta)}+1\right\}\right. \qquad \text{(B.13)}$$

$$\left. + \frac{1}{j\omega\tau}\,\frac{1}{1+\cos\theta}\left\{\frac{e^{-j\omega\tau(1+\cos\theta)}-1}{(j\omega\tau)(1+\cos\theta)}+1\right\}\right] \quad .$$

In particular, in the broadside direction of the antenna $\theta = \pi/2$ and we obtain the following simplified expression for the spectral density of the far field waveform:

$$\tilde{e}_\theta\left(\frac{\pi}{2}, \omega\right) = \sqrt{2\pi}\,\frac{\sigma}{\psi}\, e^{-\sigma^2\omega^2/2}\,\frac{(j\omega\tau)\,(j\omega\tau)}{1+j\omega\tau}\;x$$

$$x\left[\frac{1}{j\omega\tau} - \frac{1}{j\omega\tau}\,\frac{\sin\omega\tau/2}{\omega\tau/2}\, e^{-j\omega\tau/2}\right] \quad . \tag{B.14}$$

All the important frequency domain results pertinent to the antenna may be obtained from Eq. (B.13). It is useful to investigate the high and low frequency behavior of $\tilde{e}_\theta(\theta, \omega)$ analytically. After studying the behavior of $\tilde{e}_\theta(\theta, \omega)$ as given by Eq. (13) in the low and high frequency limits it is found that

$$\tilde{e}_\theta(\theta, \omega) \sim \frac{\sigma}{\psi}\sqrt{\frac{\pi}{2}}\;(j\omega\tau)\;\sin\theta\; e^{-\sigma^2\omega^2/2} \quad , \quad \text{for } \omega\tau \ll 1 \tag{B.15}$$

$$\tilde{e}_\theta(\theta, \omega) \sim \frac{\sigma}{\psi}\sqrt{2\pi}\;\frac{1}{\sin\theta}\, e^{-\sigma^2\omega^2/2} \quad , \quad \text{for } \omega\tau \gg 1 \quad . \tag{B.16}$$

The above two relations indicate that for all $\theta \neq 0$, $\tilde{e}_\theta(\theta, \omega) \to 0$ as $\omega \to 0$ and ∞. After study Eq. (B.13) for θ 0 it is found that $e_\theta(\theta, \omega) = 0$. Thus it is concluded that for all values θ, the spectral density function tends to zero in both the low and high frequency limits.

5. EVALUATION OF THE FAR FIELD WAVEFORM $e_\theta(\theta, t)$.

After introducing Eq. (B.13) into Eq. (B.6) and some algebraic manipulations the far field waveform can be written in the following form:

$$e_\theta(\theta, t) = \frac{\sigma}{\psi}\sqrt{\frac{\pi}{2}}\;\sin\theta\left[I(\nu, t) + I(\nu', t)\right] \quad , \tag{B.17}$$

where

$$I(\nu, t) = \frac{1}{2\pi} \int_{-\infty}^{\infty} e^{-\sigma^2 \omega^2/2} \frac{(j\omega\tau)(j\omega\tau)}{1 + j\omega\tau} \left[\frac{1}{j\omega\tau\nu} + \frac{e^{-j\omega\tau\nu} - 1}{(j\omega\tau)^2 \nu^2} \right] e^{j\omega\tau} d\omega \quad , \quad (B.18)$$

$$\left.\begin{aligned} \nu &= 1 - \cos\theta \\ \nu' &= 1 + \cos\theta \end{aligned}\right\} . \quad (B.19)$$

The integral in Eq. (B.18) may be carried out by applying the convolution theorem. For this purpose it has been found convenient to write Eq. (B.18) in the following form:

$$I(\nu, t) = I_1(\nu, t) + I_2(\nu, t) \quad . \quad (B.20)$$

where,

$$I_1(\nu, t) = \frac{1}{2\pi} \int_{-\infty}^{\infty} e^{-\sigma^2 \omega^2/2} \frac{(j\omega\tau)(j\omega\tau)}{1 + j\omega\tau} \frac{1}{j\omega\tau\nu} e^{j\omega\tau} d\omega \quad , \quad (B.21)$$

$$I_2(\nu, t) = \frac{1}{2\pi} \int_{-\infty}^{\infty} e^{-\sigma^2 \omega^2/2} \frac{(j\omega\tau)(j\omega\tau)}{1 + j\omega\tau} \frac{e^{-j\omega\tau\nu} - 1}{(j\omega\tau)^2 \nu^2} e^{j\omega\tau} d\omega \quad . \quad (B.22)$$

Let us consider the integral given by Eq. (B.21) first. It can be shown that $I_1(\nu, t)$ can be written as follows:

$$I_1(\nu, t) = I_1'(\nu, t) + I_1''(\nu, t) \quad , \quad (B.23)$$

where,

$$I_1'(\nu, t) = \frac{1}{\nu\tau} \frac{1}{2\pi} \int_{-\infty}^{\infty} (j\omega) \frac{1}{\frac{1}{\tau^2} + \omega^2} e^{-\sigma^2 \omega^2/2} e^{j\omega\tau} d\omega \quad , \quad (B.24)$$

$$I_1''(\nu, t) = -\tau \frac{\partial I_1'(\nu, t)}{\partial t} \quad . \quad (B.25)$$

We now make use of the following two Fourier transform relations:[25]

$$e^{-t^2/2\sigma^2} \longleftrightarrow 2\pi\sigma e^{-\omega^2\sigma^2/2} \quad , \tag{B.26}$$

$$\pi\tau e^{-t/\tau} \longleftrightarrow \frac{1}{\frac{1}{\tau^2}+\omega^2} \quad . \tag{B.27}$$

After using the relations (B.26) and (B.27) and making use of the convolution theorem Eq.(B.24) can be transformed into the following form:

$$I_1'(\nu,t) = \sqrt{\frac{\pi}{2}}\,\frac{1}{\sigma\nu}\,\frac{\partial}{\partial t}\int_{-\infty}^{\infty} e^{-(t-\alpha)^2/2\sigma^2}\, e^{-|\alpha|/\tau}\, d\alpha \quad . \tag{B.28}$$

From Eq.(B.25) we obtain $I_1''(\nu, t)$ as follows:

$$I_1''(\nu, t) = -\sqrt{\frac{\pi}{2}}\,\frac{\tau}{\sigma\nu}\,\frac{\partial^2}{\partial t^2}\int_{-\infty}^{\infty} e^{-(t-\alpha)^2/2\sigma^2}\, e^{-|\alpha|/\tau}\, d\alpha \quad . \tag{B.29}$$

Before evaluating the integrals in Eqs. (B.28) and (B.29) we discuss the integral $I_2(\nu, t)$ given by Eq. (B.22). It has been found convenient to write $I_2(\nu, t)$ in the following form:

$$I_2(\nu, t) = I_{21}(\nu, t) - I_{21}(\nu, t-\tau\nu) \tag{B.30}$$

where,

$$I_{21}(\nu, t) = -\frac{1}{2\pi\nu^2}\int_{-\infty}^{\infty} \frac{e^{-\sigma^2\omega^2/2}}{1+j\omega\tau}\, e^{j\omega\tau}\, d\omega \tag{B.31}$$

It can be shown that $I_{21}(\nu, t)$ can be written as follows:

$$I_{21}(\nu, t) = I_{21}'(\nu, t) + I_{21}''(\nu, t) \quad , \tag{B.32}$$

where

$$I'_{21}(\nu, t) = -\frac{1}{\nu^2}\frac{1}{2\pi}\int_{-\infty}^{\infty}\frac{e^{-\sigma^2\omega^2/2}}{1+\omega^2\tau^2}e^{j\omega\tau}\,d\omega \quad , \tag{B.33}$$

$$I''_{21}(\nu, t) = -\tau\frac{\partial}{\partial t}I'_{21}(\nu, t) \quad . \tag{B.34}$$

Following the similar procedure as before, Eq. (B.33) can be transformed into the following form:

$$I'_{21}(\nu, t) = -\sqrt{\frac{\pi}{2}}\frac{1}{\nu^2\tau}\frac{1}{\sigma}\int_{-\infty}^{\infty}e^{-(t-\alpha)^2/2\sigma^2}e^{-|\alpha|/\tau}\,d\alpha \quad . \tag{B.35}$$

$I''_{21}(\nu, t)$ can be evaluated by making use of Eqs. (B.33) and (B.34).

It can be shown that $I'_1(\nu, t)$ as given by Eq.(B.28) may be expressed in the following form:

$$I'_1(\nu, t) = \frac{\pi}{2}\frac{1}{\nu\tau}e^{\sigma^2/2\tau^2} \quad x$$

$$x\left[-\left\{1+\operatorname{erf}\frac{1}{\sqrt{2}}\left(\frac{t}{\sigma}+\frac{\sigma}{\tau}\right)\right\}e^{t/\tau}\right.$$

$$\left.+\left\{1-\operatorname{erf}\frac{1}{\sqrt{2}}\left(\frac{t}{\sigma}+\frac{\sigma}{\tau}\right)\right\}e^{t/\tau}\right] \quad , \tag{B.36}$$

where the error function is defined as follows

$$\operatorname{erf} x = \frac{2}{\sqrt{\pi}}\int_0^x e^{-t^2}\,dt \quad . \tag{B.37}$$

After using Eqs. (B.36) and (B.29), $I_1''(\nu, t)$ is obtained as in the following

$$I_1''(\nu, t) = \frac{\pi}{2} \frac{1}{\nu\tau} \left[\frac{2}{\sqrt{2}} \frac{\tau}{\sigma} e^{-t^2/2\sigma^2} - e^{-\sigma^2/2\tau^2} \left\{ \left(1 + \operatorname{erf} \frac{1}{\sqrt{2}} \left(\frac{t}{\sigma} - \frac{\sigma}{\tau}\right)\right) e^{-t/\tau} + \left(1 - \operatorname{erf} \frac{1}{\sqrt{2}} \left(\frac{t}{\sigma} + \frac{\sigma}{\tau}\right)\right) e^{t/\tau} \right\} \right] . \quad \text{(B.38)}$$

Introducing Eqs. (B.38) and (B.36) into Eq. (B.23), we obtain the following expression for $I_1(\nu, t)$:

$$I_1(\nu, t) = \frac{\pi}{\nu\sigma} \left[-\frac{\sigma}{\tau} e^{\sigma^2/2\tau^2} \left\{ 1 + \operatorname{erf} \frac{1}{\sqrt{2}} \left(\frac{t}{\sigma} - \frac{\sigma}{\tau}\right) \right\} e^{-t/\tau} + \frac{1}{\sqrt{2}} e^{-t^2/2\sigma^2} \right] . \quad \text{(B.39)}$$

$I_{21}'(\nu, t)$ as given by Eq. (B.35) can be evaluated in closed form and is given by:

$$I_{21}'(\nu, t) = -\frac{\pi}{2} \frac{1}{\nu^2\tau} e^{\sigma^2/2\tau^2} \left[\left\{ 1 + \operatorname{erf} \frac{1}{\sqrt{2}} \left(\frac{t}{\sigma} - \frac{\sigma}{\tau}\right) \right\} e^{-t/\tau} + \left\{ 1 - \operatorname{erf} \frac{1}{\sqrt{2}} \left(\frac{t}{\sigma} + \frac{\sigma}{\tau}\right) \right\} e^{t/\tau} \right] . \quad \text{(B.40)}$$

After using Eqs. (B.34) and (B.40) $I_{21}''(\nu, t)$ is obtained as follows:

$$I_{21}''(\nu, t) = \frac{\pi}{2} \frac{1}{\nu^2\tau} e^{\sigma^2/2\tau^2} \left[-\left\{ 1 + \operatorname{erf} \frac{1}{\sqrt{2}} \left(\frac{t}{\sigma} - \frac{\sigma}{\tau}\right) \right\} e^{-t/\tau} + \left\{ 1 - \operatorname{erf} \frac{1}{\sqrt{2}} \left(\frac{t}{\sigma} + \frac{\sigma}{\tau}\right) \right\} e^{t/\tau} \right] . \quad \text{(B.41)}$$

By making use of Eqs. (B.40), (B.41) and (B.32) we obtain:

$$I_{21}(\nu, t) = -\pi \frac{1}{\nu^2 \tau} e^{\sigma^2/2\tau^2} \left\{ 1 + \operatorname{erf} \frac{1}{\sqrt{2}} \left(\frac{t}{\sigma} - \frac{\sigma}{\tau} \right) \right\} e^{-t/\tau} \quad . \tag{B.42}$$

Introducing Eq. (B.42) into Eq. (B.30) we obtain:

$$I_2(\nu, t) = \frac{\pi}{\sigma \nu} \cdot \frac{\sigma}{\nu \tau} e^{\sigma^2/2\tau^2} \left[- \left\{ 1 + \operatorname{erf} \frac{1}{\sqrt{2}} \left(\frac{t}{\sigma} - \frac{\sigma}{\tau} \right) \right\} e^{-t/\tau} + \right.$$

$$\left. + \left\{ 1 + \operatorname{erf} \frac{1}{2} \left(\frac{t - \tau\nu}{\sigma} - \frac{\sigma}{\tau} \right) \right\} e^{-\frac{t-\tau\nu}{\tau}} \right] \quad . \tag{B.43}$$

After introducing Eqs. (B.42) and (B.43) into Eq. (B.20) we finally obtain the following:

$$I(\nu, t) = \frac{\pi}{\nu\sigma} \left[\frac{1}{\sqrt{2}} e^{-t^2/2\sigma^2} - \frac{\sigma}{\tau} \left(1 + \frac{1}{\nu} \right) \left\{ 1 + \operatorname{erf} \frac{1}{\sqrt{2}} \left(\frac{t}{\sigma} - \frac{\sigma}{\tau} \right) \right\} e^{-t/\tau} e^{\sigma^2/2\tau^2} \right.$$

$$\left. + \frac{\sigma}{\nu\tau} e^{\sigma^2/2\tau^2} \left\{ 1 + \operatorname{erf} \frac{1}{\sqrt{2}} \left(\frac{t - \tau\nu}{\sigma} - \frac{\sigma}{\tau} \right) \right\} e^{-\frac{t-\tau\nu}{\tau}} \right] . \tag{B.44}$$

Changing ν to ν' in Eq. (B.44) we obtain:

$$I(\nu', t) = \frac{\pi}{\nu'\sigma} \left[\frac{1}{\sqrt{2}} e^{-t^2/2\sigma^2} - \frac{\sigma}{\tau} \left(1 + \frac{1}{\nu'} \right) \left\{ 1 + \operatorname{erf} \frac{1}{\sqrt{2}} \left(\frac{t}{\sigma} - \frac{\sigma}{\tau} \right) \right\} e^{-t/\tau} e^{\sigma^2/2\tau^2} \right.$$

$$\left. + \frac{\sigma}{\nu'\tau} e^{\sigma^2/2\tau^2} \left\{ 1 + \operatorname{erf} \frac{1}{\sqrt{2}} \left(\frac{t - \tau\nu'}{\sigma} - \frac{\sigma}{\tau} \right) \right\} e^{-\frac{t-\tau\nu'}{\tau}} \right] . \tag{B.45}$$

Thus we obtain the following expression for $I(\nu, t) + I(\nu', t)$:

$$I(\nu, t) + I(\nu', t) = \frac{\pi}{\sigma} \left[\frac{1}{\sqrt{2}} \left(\frac{1}{\nu} + \frac{1}{\nu'} \right) e^{-t^2/2\sigma^2} \right.$$

$$- \frac{\sigma}{\tau} e^{-t/\tau} \; e^{\sigma^2/2\tau^2} \left\{ 1 + \operatorname{erf} \frac{1}{\sqrt{2}} \left(\frac{t}{\sigma} - \frac{\sigma}{\tau} \right) \right\} \left(\frac{\nu+1}{2} + \frac{\nu'+1}{\nu'^2} \right)$$

$$+ \frac{\sigma}{\tau} e^{\sigma^2/2\tau^2} \left\{ \left(1 + \operatorname{erf} \frac{1}{\sqrt{2}} \left(\frac{t-\nu\tau}{\sigma} - \frac{\sigma}{\tau} \right) \right) \frac{e^{-\frac{t-\nu\tau}{\tau}}}{\nu^2} \right.$$

$$\left. + \left(1 + \operatorname{erf} \frac{1}{\sqrt{2}} \left(\frac{t-\nu'\tau}{\sigma} - \frac{\sigma}{\tau} \right) \right) \frac{e^{-\frac{t-\nu'\tau}{\tau}}}{\nu'^2} \right\} \Bigg] \qquad \text{(B.46)}$$

Introducing Eq. (B.40) into Eq. (B.17) we obtain the following expression for the far field waveform produced by the antenna:

$$e_\theta(\theta, t) = \frac{\pi}{\psi} \sqrt{\frac{\pi}{2}} \sin\theta \left[\frac{1}{\sqrt{2}} \left(\frac{1}{\nu} + \frac{1}{\nu'} \right) e^{-t^2/2\sigma^2} \right.$$

$$- \frac{\sigma}{\tau} e^{-t/\tau} \; e^{\sigma^2/2\tau^2} \left\{ 1 + \operatorname{erf} \frac{1}{\sqrt{2}} \left(\frac{t}{\sigma} - \frac{\sigma}{\tau} \right) \right\} \left(\frac{\nu+1}{\nu^2} + \frac{\nu'+1}{\nu'^2} \right)$$

$$+ \frac{\sigma}{\tau} e^{\sigma^2/2\tau^2} \left\{ 1 + \operatorname{erf} \frac{1}{\sqrt{2}} \left(\frac{t-\nu\tau}{\sigma} - \frac{\sigma}{\tau} \right) \right\} \frac{e^{-\frac{t-\nu\tau}{\tau}}}{\nu^2}$$

$$\left. + \frac{\sigma}{\tau} e^{\sigma^2/2\tau^2} \left\{ 1 + \operatorname{erf} \frac{1}{\sqrt{2}} \left(\frac{t-\nu'\tau}{\sigma} - \frac{\sigma}{\tau} \right) \right\} \frac{e^{-\frac{t-\nu'\tau}{\tau}}}{\nu'^2} \right] , \qquad \text{(B.47)}$$

where,

$$\nu = 1 + \cos\theta ,$$

$$\nu' = 1 - \cos\theta ,$$

In the direction $\theta = \pi/2$, $\nu = \nu' = 1$ and we obtain from Eq. (B.47):

$$e_\theta\left(\frac{\pi}{2}, t\right) = \frac{\pi}{\psi}\sqrt{2\pi}\left[\frac{e^{-t^2/2\sigma^2}}{\sqrt{2}}\right.$$

$$- \frac{2\sigma}{\tau} e^{\sigma^2/2\tau^2}\left\{1 + \operatorname{erf}\frac{1}{\sqrt{2}}\left(\frac{t}{\sigma} - \frac{\sigma}{\tau}\right)\right\} e^{-t/\tau}$$

$$\left. + \frac{\sigma}{\tau} e^{\sigma^2/2\tau^2}\left\{1 + \operatorname{erf}\frac{1}{\sqrt{2}}\left(\frac{t-\tau}{\sigma}\right) - \frac{\sigma}{\tau}\right)\right\} e^{-\frac{t-\tau}{\tau}}\right] . \quad \text{(B.48)}$$

At time $t = 0$ the Eq. (B.47) reduces to the following:

$$e_\theta(\theta, 0) = \frac{\pi}{\psi}\sqrt{\frac{\pi}{2}} \sin\theta\left[\frac{1}{\sqrt{2}}\left(\frac{1}{\nu} + \frac{1}{\nu'}\right)\right.$$

$$- \frac{\sigma}{\tau} e^{\sigma^2/2\tau^2}\left\{1 - \operatorname{erf}\frac{\sigma}{\sqrt{2}\tau}\right\}\left(\frac{\nu+1}{\nu^2} + \frac{\nu'+1}{\nu'^2}\right)$$

$$+ \frac{\sigma}{\tau} e^{\sigma^2/2\tau^2}\left\{1 - \operatorname{erf}\frac{1}{\sqrt{2}}\left(\frac{\nu\tau}{\sigma} + \frac{\sigma}{\tau}\right)\right\}\frac{e^{\nu}}{\nu^2}$$

$$\left. + \frac{\sigma}{\tau} e^{\sigma^2/2\tau^2}\left\{1 - \operatorname{erf}\frac{1}{\sqrt{2}}\left(\frac{\nu'\tau}{\sigma} + \frac{\sigma}{\tau}\right)\right\}\frac{e^{\nu'}}{\nu'^2}\right] \quad . \quad \text{(B.49)}$$

The broadside field produced by the antenna at time $t = 0$ is obtained by setting $\theta = \pi/2$ and $\nu = \nu' = 1$ in Eq. (B.48) and is given by:

$$e_\theta\left(\frac{\pi}{2}, 0\right) = \frac{\pi}{\psi}\sqrt{2\pi}\left[\frac{1}{\sqrt{2}} - \frac{2\sigma}{\tau} e^{\sigma^2/2\tau^2}\left\{1 - \operatorname{erf}\left(\frac{\sigma}{\sqrt{2}\tau}\right)\right\}\right.$$

$$\left. + \frac{\sigma}{\tau} e^{\frac{\sigma^2}{2\tau^2}+1}\left\{1 - \operatorname{erf}\frac{1}{\sqrt{2}}\left(\frac{\tau}{\sigma} + \frac{\sigma}{\tau}\right)\right\}\right] \quad . \quad \text{(B.50)}$$

For both large positive and negative time, i.e., $t \gg \tau$, and $\tau > \sigma$, it can be shown that Eq. (B.48) can be approximated by the following:

$$e_\theta\left(\frac{\pi}{2}, t\right) \sim \frac{\pi\sqrt{2\pi}}{\psi} \left[\frac{e^{-t^2/2\sigma^2}}{\sqrt{2}} + \frac{\sigma}{\tau} e^{\sigma^2/2\tau^2} \left\{ 1 + \operatorname{erf} \frac{t}{2\sigma} \right\} (e-2) \right] e^{-t/\tau} . \qquad (B.51)$$

$|t| \gg \tau$

$|t| \gg \tau, \ \tau > \sigma$

It can be seen from Eq. (B.50) that $e_\theta(\pi/2, t) \longrightarrow 0$ as $t \longrightarrow \infty$ which is as it should be.

It can be seen from Eqs. (B.47) and (B.48) that the radiated waveform is different from Gaussian and also that it is a function of the parameter σ/τ. It is thus anticipated that the radiated pulse shape will strongly depend on the ratio of the input pulse width to the transit time on the antenna.

6. TIME DEPENDENT CURRENT DISTRIBUTION i(z, t)

In some cases it may be of interest to know explicitly the time dependent current distribution on the Gaussian pulse excited loaded antenna. The current distribution on the antenna excited by a harmonically time dependent unit slice generator is given by Eq. (B.10). For a Gaussian input signal of the form given by Eqs. (B.4) and (B.5), the time dependent current distribution on the antenna is obtained by using the following relations:

$$i(z, t) = \frac{1}{2\pi} \int_{-\infty}^{\infty} \tilde{I}(z, \omega) \tilde{V}(\omega) e^{j\omega t} \, d\omega \ , \qquad (B.52)$$

where $\tilde{I}(z, \omega)$ and $\tilde{V}(\omega)$ are given by Eqs. (B.10) and (B.5) respectively. The integral in Eq. (B.52) can be evaluated in closed form in a manner discussed in Section 5. The final expression for the time dependent current distribution is given by the following:

$$i(z,t) = \frac{\pi\sqrt{2\pi}}{\eta_o \psi}\left[1 - \frac{|z|}{L}\right] \quad x$$

$$x \left[\frac{e^{-(t-|z|/c)^2/2\sigma^2}}{\sqrt{2}} - \right.$$

$$\left. - \frac{\sigma}{\tau}\, e^{\sigma^2/2\tau^2}\left\{1 + \operatorname{erf}\frac{1}{\sqrt{2}}\left(\frac{t - z/c}{\sigma}\right)\right\} \quad e^{-\frac{t-|z|/c}{\tau}}\right] . \qquad \text{(B.53)}$$

The input current $i(0,t)$ on the antenna when excited by an input signal of the form $V(t) = e^{-t^2/2\sigma^2}$ is given by:

$$i(0,t) = \frac{\pi\sqrt{2\pi}}{\eta_o \psi}\left[\frac{e^{-t^2/2\sigma^2}}{\sqrt{2}} - \frac{\sigma}{\tau}\, e^{\sigma^2/2\sigma^2}\left\{1 + \operatorname{erf}\frac{1}{\sqrt{2}}\left(\frac{t}{\sigma} - \frac{\sigma}{\tau}\right)\right\} e^{-t/\tau}\right] . \qquad \text{(B.54)}$$

7. NUMERICAL RESULTS

In this section we discuss some of the selected results obtained by numerical computation of the waveform expressions derived in section 5. Figs. B-1 and B-2 show $e_\theta(\frac{\pi}{2}, t)$ vs t for $\sigma = 1.0$ ns and $\sigma = 0.471$ ns respectively and for two different values of the parameter ψ. In both cases the transit time on the antenna is $\tau = 3.33$ ns. The corresponding values of $e_\theta(\frac{\pi}{2}, t)$ obtained by direct numerical investigation are also shown in the same figures for comparison.

The direct numerical investigation of the problem has been discussed in a Appendix A. However, it is appropriate here to give a very brief outline of the numerical method. In this method, at first, the current distribution $\tilde{I}(z, \omega)$ on the harmonically excited loaded antenna is obtained by numerically solving an appropriate form of Hallen's integral equation. The transfer function $\tilde{f}_\theta(\theta, \omega)$ of the antenna and

the spectral density $\tilde{e}_\theta(\theta, \omega)$ of the radiated waveform are then obtained by numerically evaluating Eq. (6) with the help of fast Fourier inversion technique.

The results shown in Figs. B-1 and B-2 indicate that the agreement between the analytical and numerical solutions may be considered to be satisfactory. In particular, in the main pulse region the two results agree very well.

Figs. B-3 and B-4 show the radiated waveforms obtained from Eq. (B.47) for three different values of θ and for $\sigma = 1$ ns, and $\sigma = 0.471$ ns. The transit time on the antenna is $\tau = 3.33$ ns.

8: CONCLUSION

In the above we have developed analytic expressions for the waveforms radiated by a resistively loaded linear antenna excited by Gaussian pulse. The antenna is assumed to be loaded such that it sustains a pure traveling wave of current. The analytic results have been compared with those obtained by direct numerical means. The general agreement between the two results has been found to be satisfactory. It is thus concluded that the various expressions given above may be used to study the behavior of waveforms radiated by a resistively loaded linear antenna excited by a Gaussian pulse.

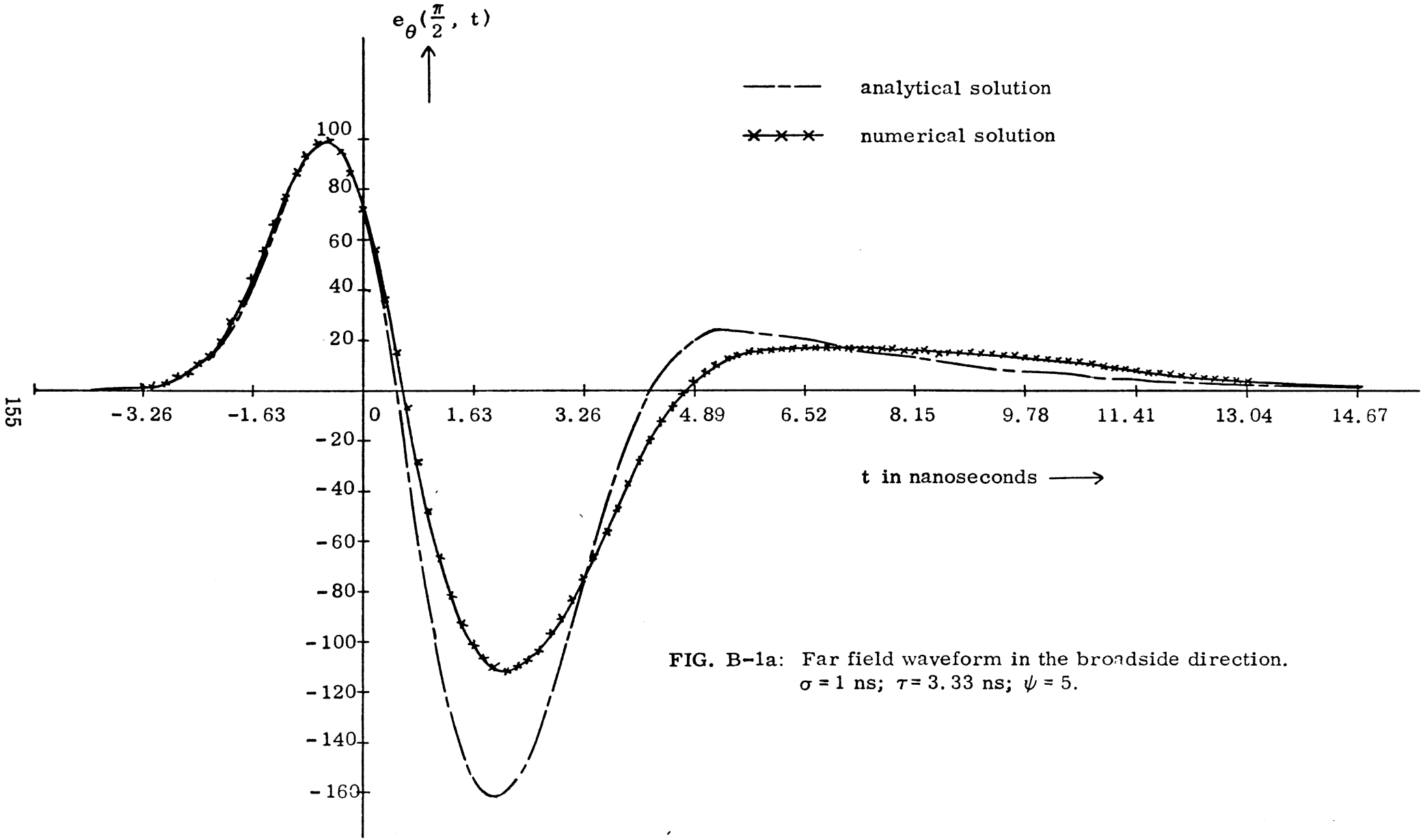

FIG. B-1a: Far field waveform in the broadside direction.
$\sigma = 1$ ns; $\tau = 3.33$ ns; $\psi = 5$.

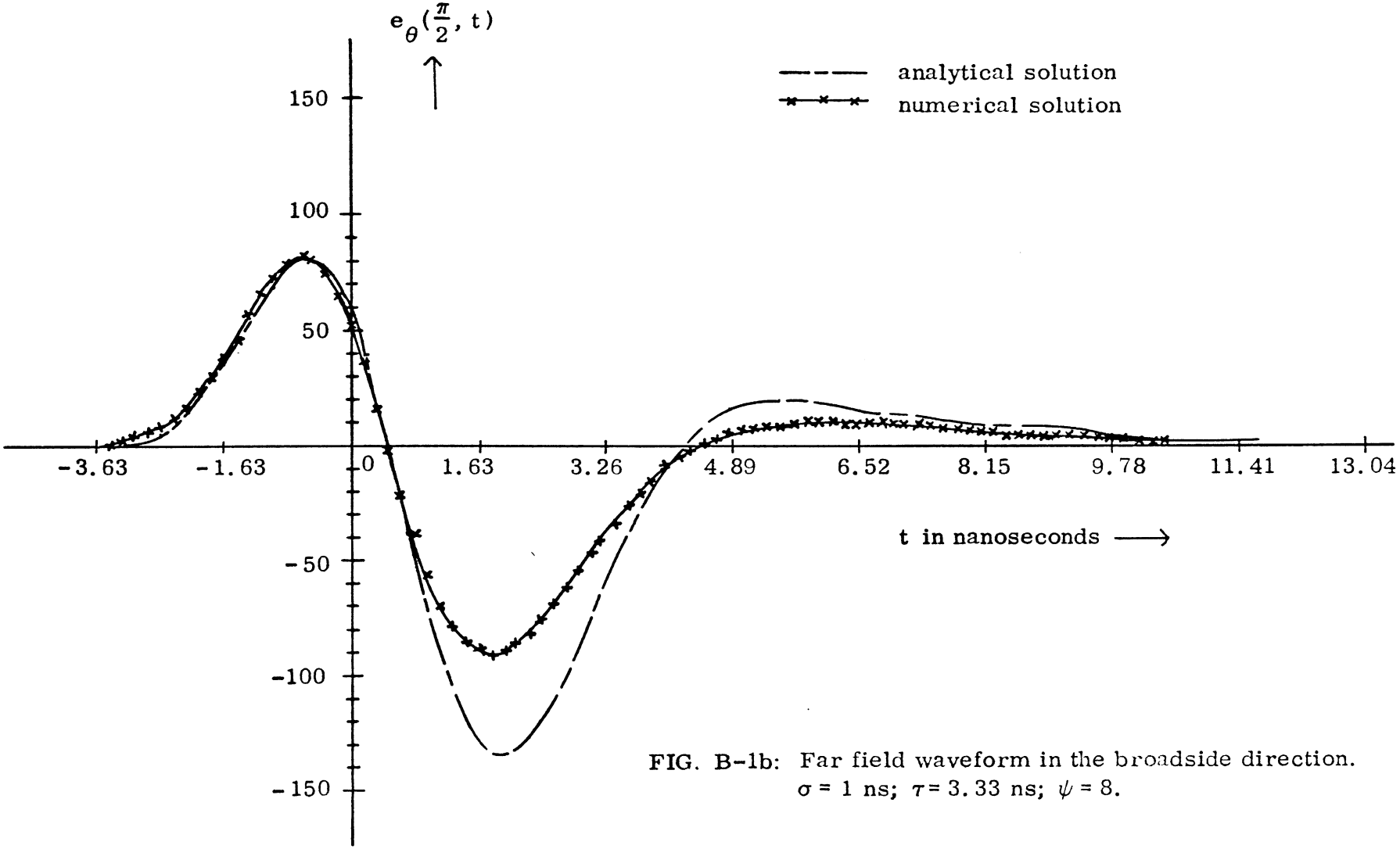

FIG. B-1b: Far field waveform in the broadside direction.
σ = 1 ns; τ = 3.33 ns; ψ = 8.

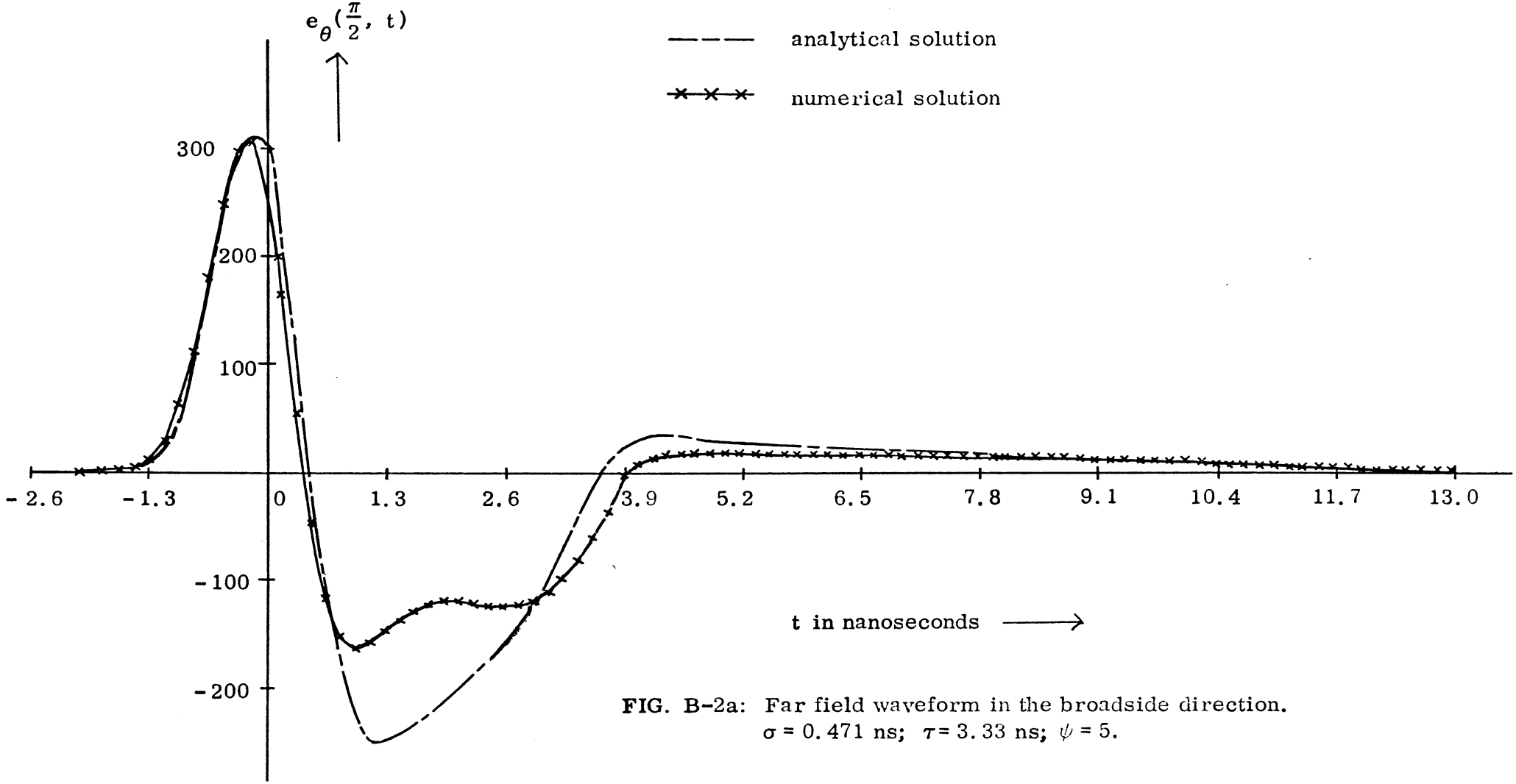

FIG. B-2a: Far field waveform in the broadside direction.
$\sigma = 0.471$ ns; $\tau = 3.33$ ns; $\psi = 5$.

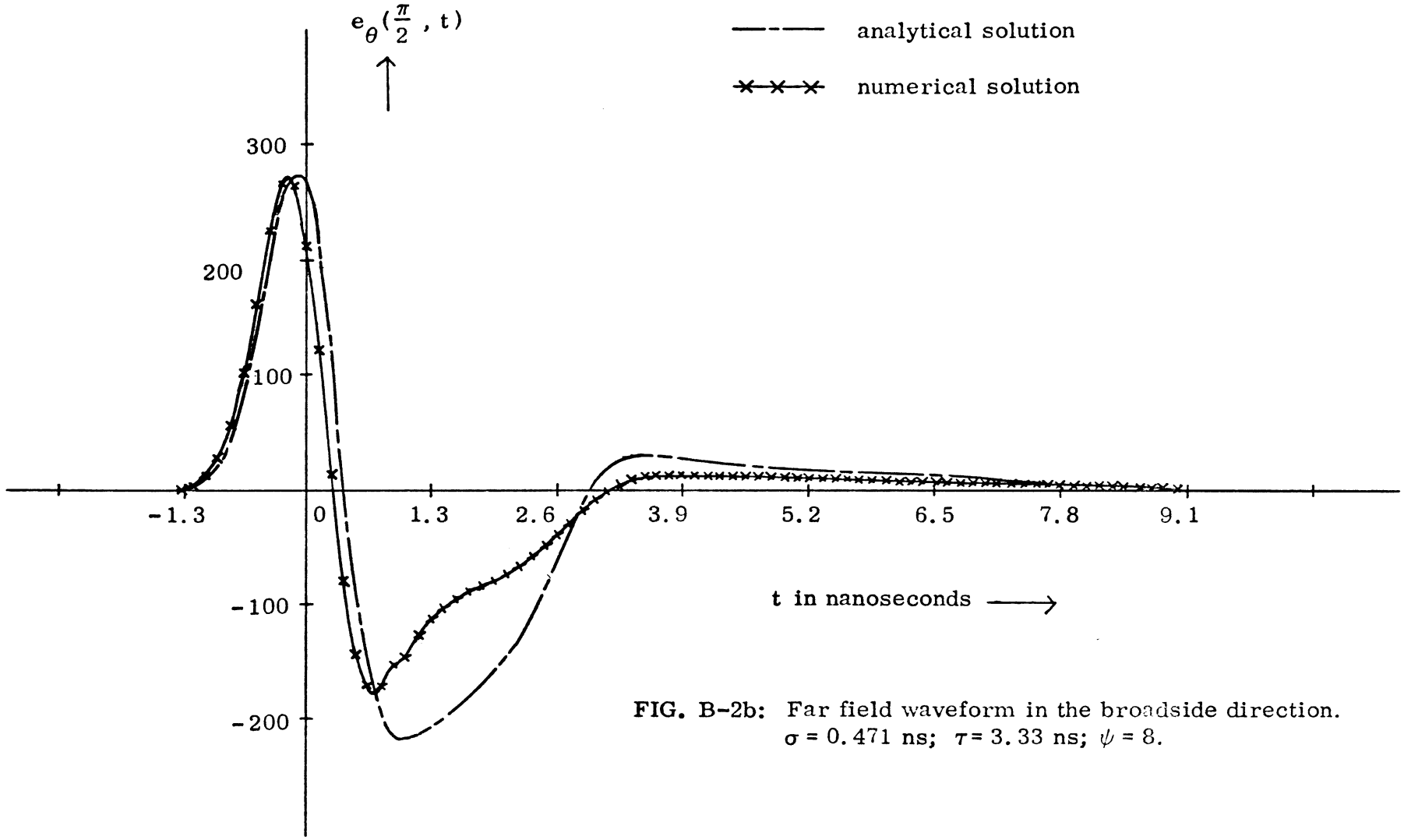

FIG. B-2b: Far field waveform in the broadside direction. $\sigma = 0.471$ ns; $\tau = 3.33$ ns; $\psi = 8$.

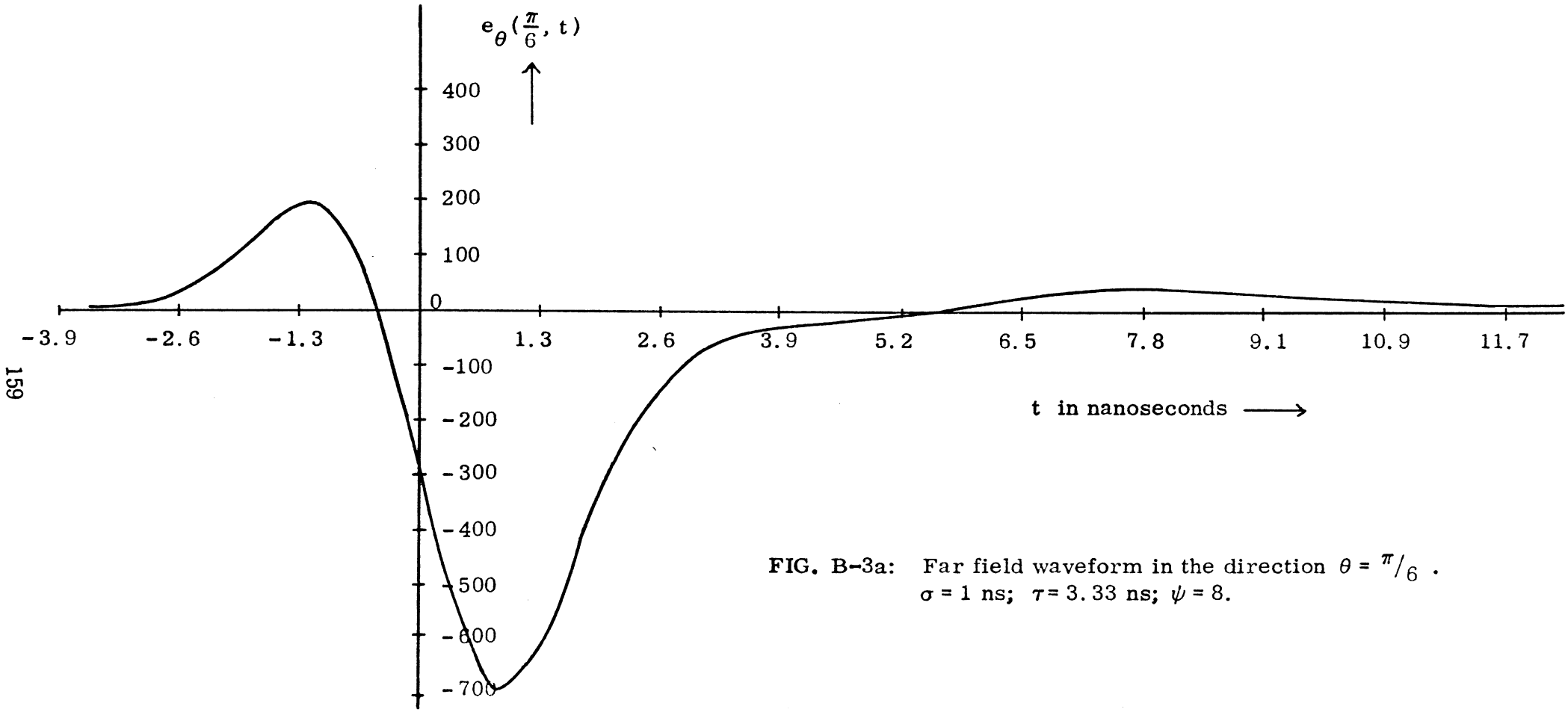

FIG. B-3a: Far field waveform in the direction $\theta = {}^{\pi}/_{6}$.
$\sigma = 1$ ns; $\tau = 3.33$ ns; $\psi = 8$.

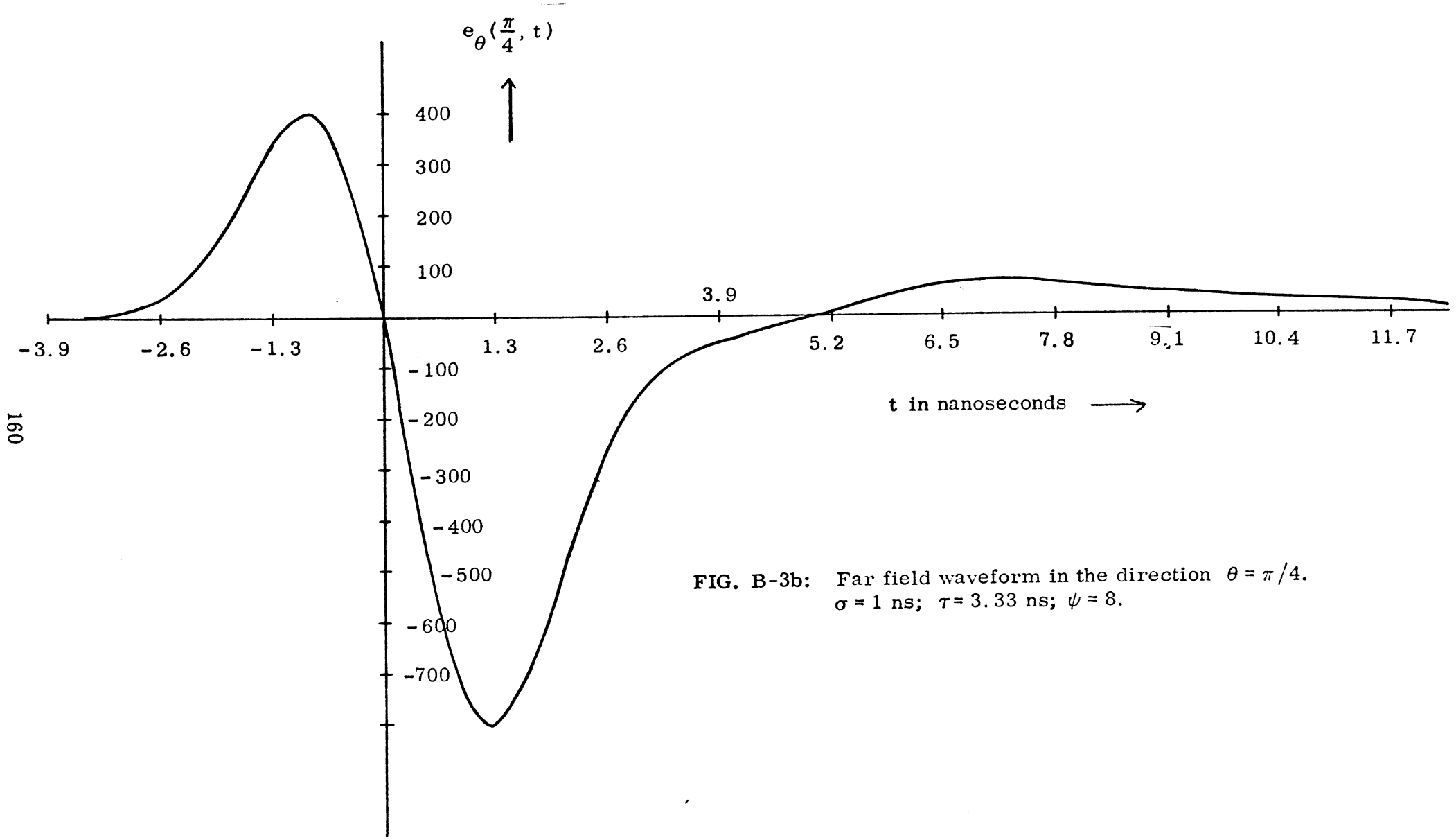

FIG. B-3b: Far field waveform in the direction $\theta = \pi/4$. $\sigma = 1$ ns; $\tau = 3.33$ ns; $\psi = 8$.

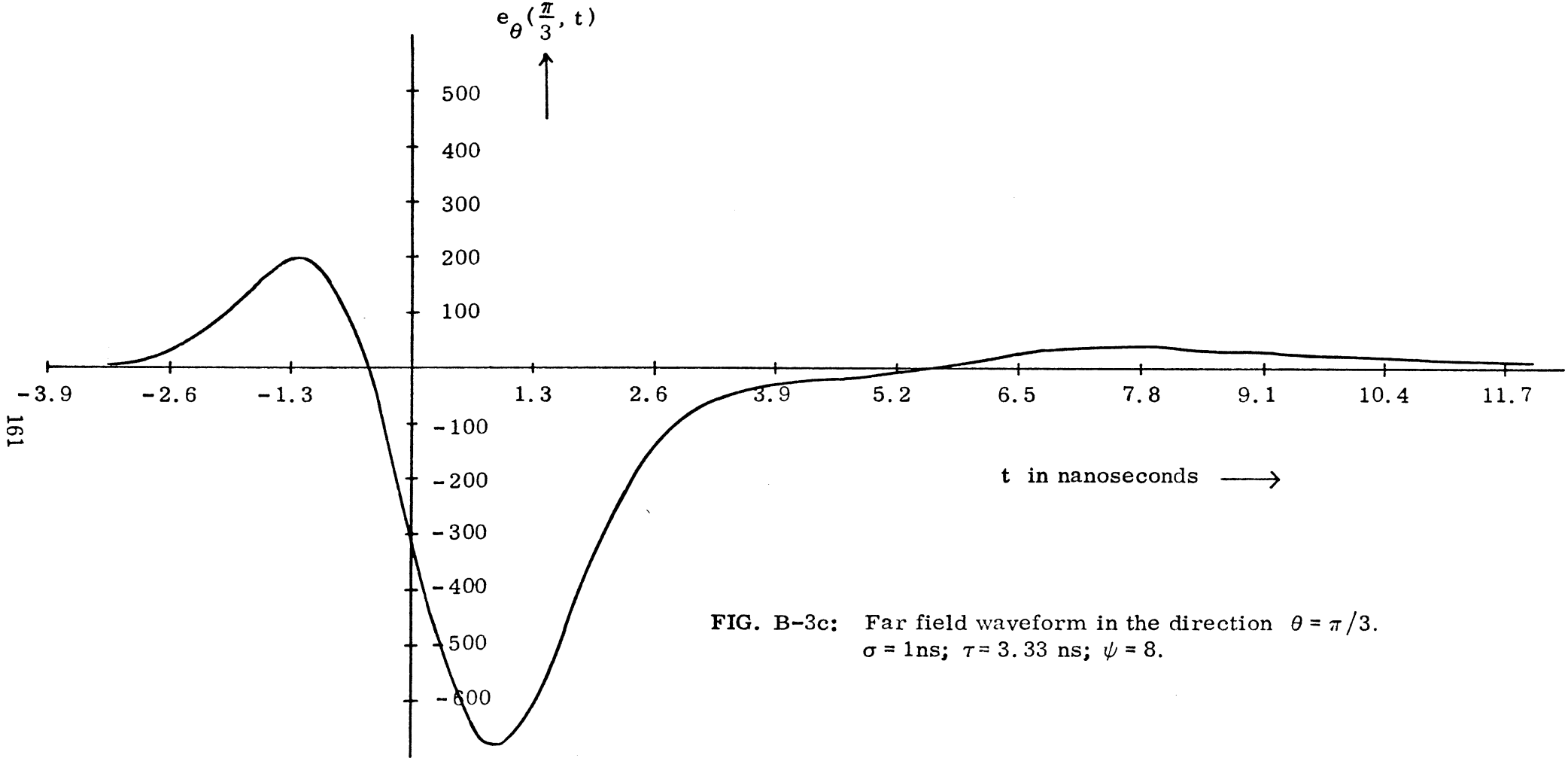

FIG. B-3c: Far field waveform in the direction $\theta = \pi/3$. $\sigma = 1$ns; $\tau = 3.33$ ns; $\psi = 8$.

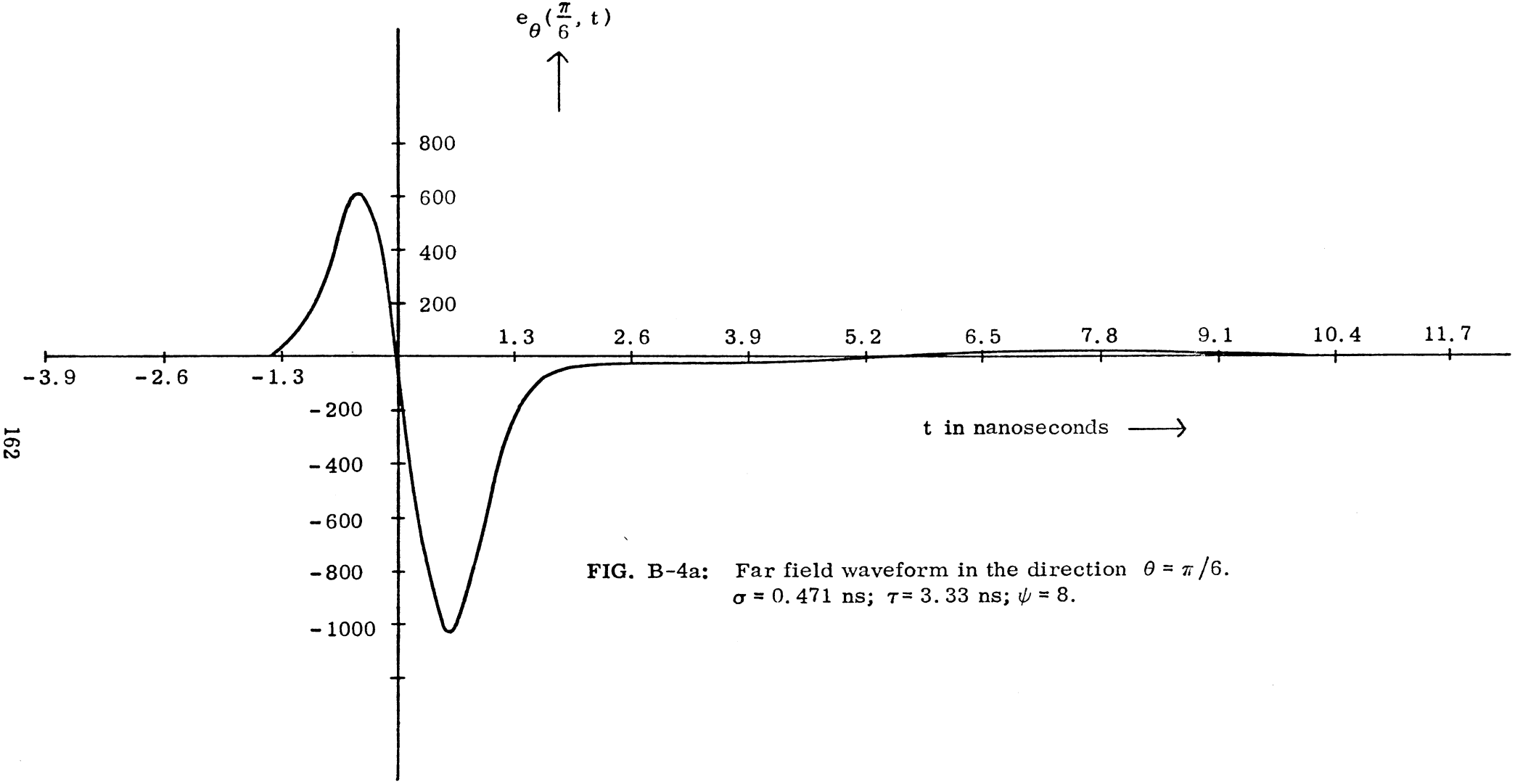

FIG. B-4a: Far field waveform in the direction $\theta = \pi/6$. $\sigma = 0.471$ ns; $\tau = 3.33$ ns; $\psi = 8$.

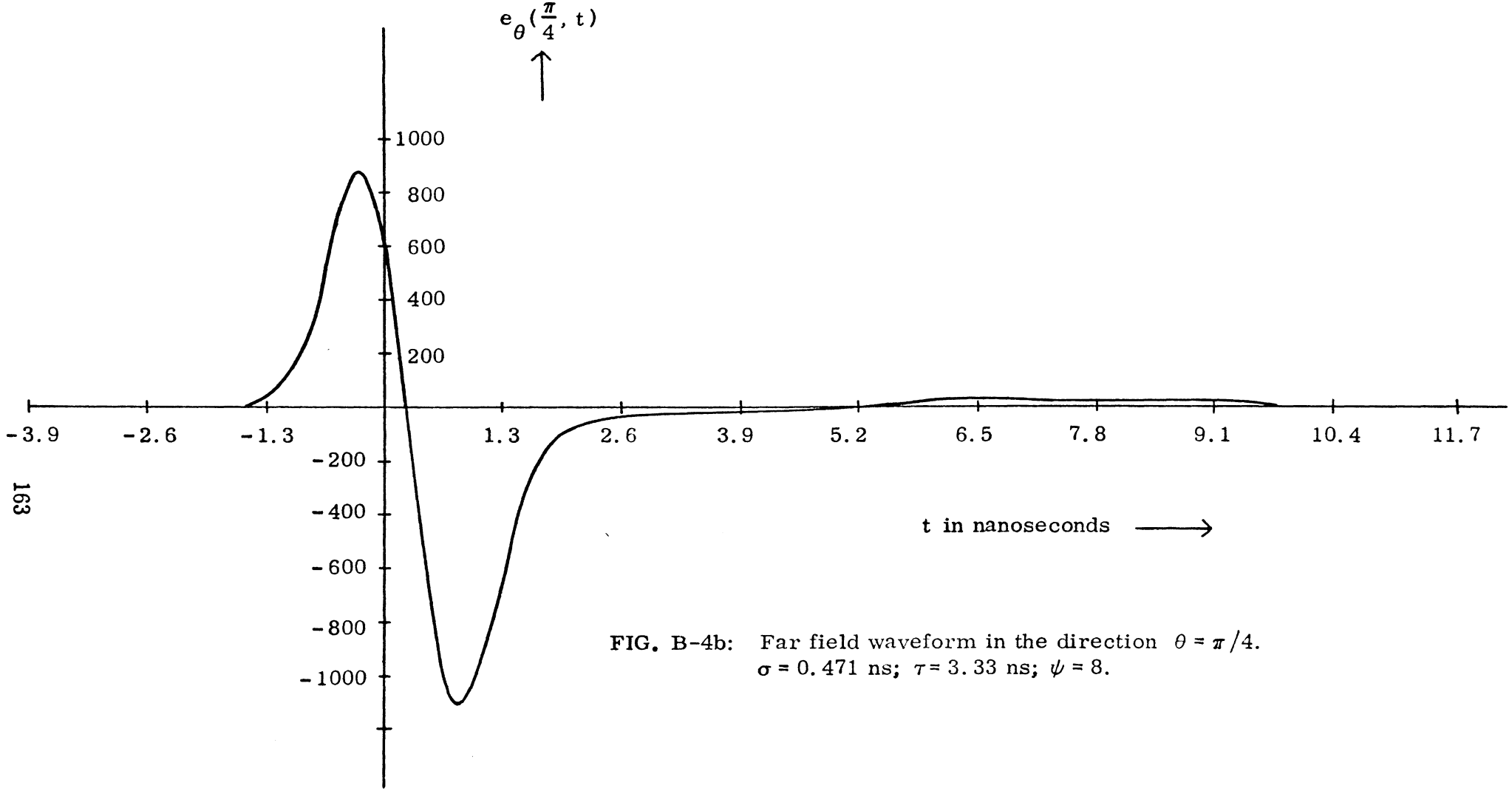

FIG. B-4b: Far field waveform in the direction $\theta = \pi/4$.
$\sigma = 0.471$ ns; $\tau = 3.33$ ns; $\psi = 8$.

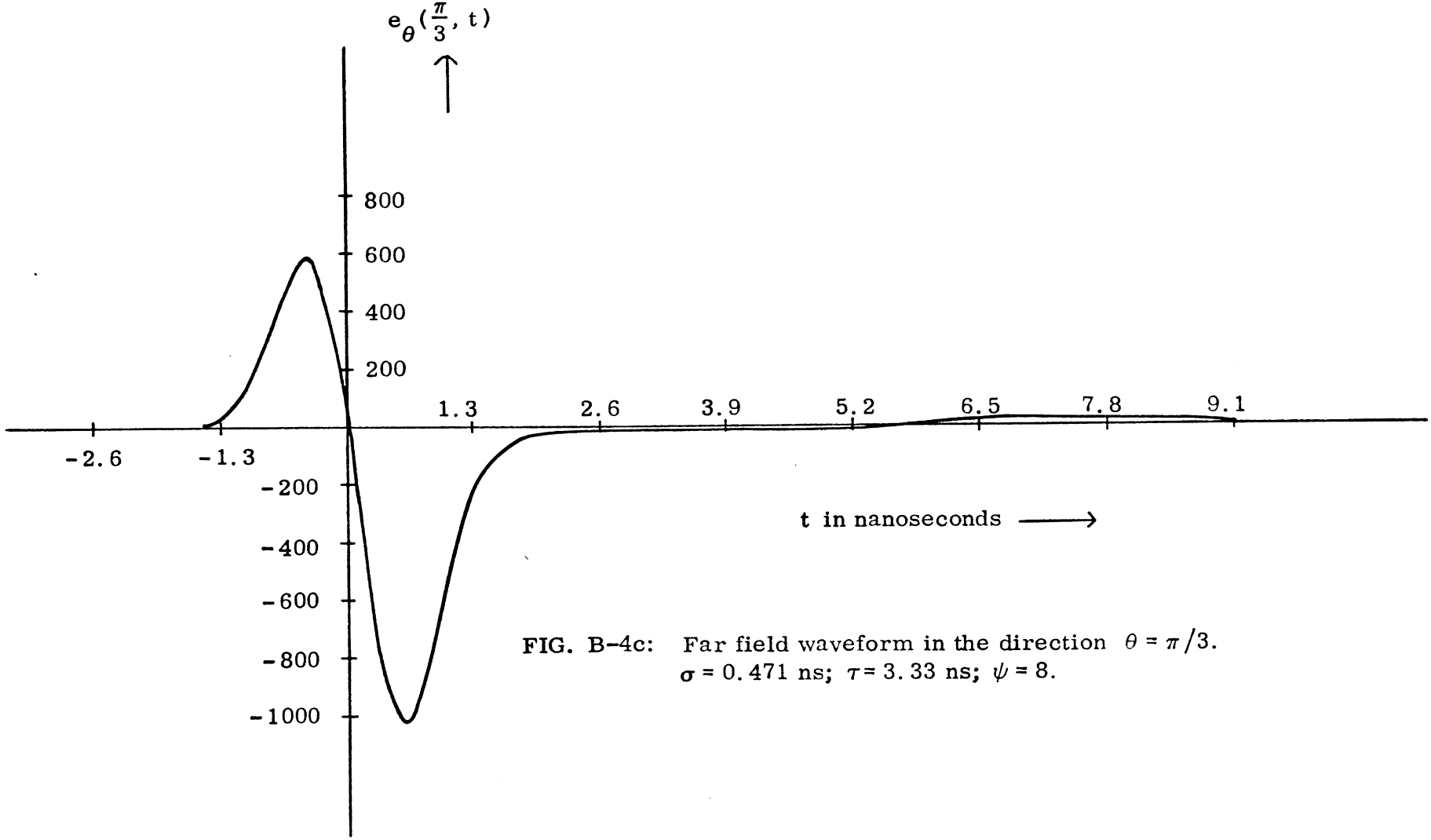

FIG. B-4c: Far field waveform in the direction $\theta = \pi/3$.
$\sigma = 0.471$ ns; $\tau = 3.33$ ns; $\psi = 8$.

REFERENCES

1. Baum, C. E., (October 1968), AFWL EMP 1-4, Vol. 4, SSN-65, Some Limiting Low-Frequency Characteristics of a Pulse-Radiation Antenna.

2. Baum, C. E., (January 1969), AFWL EMP 1-5, Vol. 5, SSN-69, Design of a Pulse-Radiating Dipole Antenna as Related to High-Frequency and Low-Frequency Limits.

3. Wu, T. T. and R. W. P. King, (1964), The Cylindrical Antenna with Non-Reflecting Resistive Loading, IEEE Trans., AP-13, No. 3, pp. 369-373.

4. Baum, C. E., (1970), Resistively Loaded Radiating Dipole Based on a Transmission Line Model for the Antenna, AFWL EMP 1-6, Vol. 6, SSN-81, pp. 1-27.

5. Wu, T. T., (1961), Transient Response of a Dipole Antenna, Journal of Math. Phys., Vol. 2, No. 6, pp. 892-894.

6. Morgan, S. P., (1962), Transient Response of a Dipole Antenna, Journal of Math. Phys., Vol. 3, No. 3, pp. 564-565.

7. Brundell, Per-Olof, (1960), Transient electromagnetic waves around a cylindrical transmitting antenna, Ericsson Technics, Vol. 16, No. 1, pp. 137-162.

8. Latham, R. M. and K. S. H. Lee, (1969), Pulse Radiation and Synthesis by an Infinite Cylindrical Antenna, AFWL 1-5, Vol. 5, SSN-73.

9a. Latham, R. M. and K. S. H. Lee, (1970), Radiation of an Infinite Cylindrical Antenna with Uniform Resistive Loading, AFWL EMP 1-6, Vol. 6, SSN-83.

9b. Latham, R. M. and K. S. H. Lee, (1970), Transient Properties of an Infinite Cylindrical Antenna, Radio Science, Vol. 5, No. 4, pp. 715-723.

9c. Marin, Lennart, (1970), Radiation from a Resistive Tubular Antenna Excited by a Step Voltage, AFWL EMP 1-8, Vol. 8, SSN-101.

10. Harrison, C. W. and R W. P. King, (1967), On the Transient Response of Infinite Cylindrical Antenna, IEEE Trans., AP-15, No. 2, pp. 301-302.

11. Bennett, C. L. and A. M. Auckenthaler, (1971), Transient and Time-Domain Solutions for Antennas and Scatterers, SRRC-RR-70-61, Sperry Rand Research Center, Sudbury, Massachusetts.

12. Schmitt, H. J., (1961), Transients in Cylindrical Antennae, Proc. IEE (London). Mimeograph No. 377E, April 1960, pp. 292-298.

13. Sayre, E. P., (1969), Transient Response of Wire Antennas and Scatterers, Technical Report TR-69-4, Electrical Engineering Department, Syracuse, New York.

14. Taylor, C. D. and T. H. Shumpert, (1971), Electromagnetic Pulse Generation by an Impedance Loaded Dipole Antenna, AFWL EMP 1-8, Vol. 8, SSN-104.

15. Shumpert, T. H., (1971), Some Theoretical-Numerical Procedures for the Study of the Impedance Loaded Dipole Antenna, AFWL EMP 1-8, Vol. 8, SSN-105.

16. Merewether, D. E., (1968), SSN-70, Transient Pulse Transmission Using Impedance Loaded Cylindrical Antennas.

17. Merewether, D. E., (1960), SSN-71, Transient EM Fields Near a Cylindrical Antenna Multiply Loaded with Lumped Resistors.

18. Shen, Liang-Chi and T. T. Wu, (1967), Cylindrical Antenna with Tapered Resistive Loading, Radio Science, Vol. 2 (new series), No. 2, pp. 191-201.

19. Mei, K. K., (1965), On the Integral Equations of Thin Wire Antennas, IEEE Trans., AP-14, No. 3, pp. 374-378.

20. Harrington, R. F., (1968), Field Computations by Moment Methods, The Macmillan Co., New York, Chapters 1, 4.

21. Shen, Liang-Chi, (1962), An Experimental Study of the Antenna with Non-Reflecting Resistive Loading, IEEE Trans., AP-15, No. 5, pp. 606-611.

22. King, R. W. P., C. W. Harrison and E. A. Aransen, (1966), The Imperfectly Conducting Cylindrical Transmitting Antenna: Numerical Results, IEEE Trans., AP-14, No. 5, pp. 535-542.

23. Taylor, C. D., (1968), Cylindrical Transmitting Antenna: Tapered Resistivity and Multiple Impedance Loadings, IEEE Trans., AP-16, No. 2, pp. 176-179.

24. Shen, L-C. and R. W. P. King, (1965), The Cylindrical Antenna with Non-Reflecting Resistive Loading, IEEE Trans., AP-13, p. 998.

25. Magnus, Wilhelm and Oberhettinger, (1949), Formulas and Theorems for the Special Functions of Mathematical Physics, Chelsea Publishing Co., New York, 11, p. 115.